The July Arctic front in North America from ECMWF ERA-40 and NCEP/NCAR reanalysis products

A Thesis Submitted to the Faculty of Graduate Studies
in Partial Fulfillment of the Requirements
for the Degree of

MASTER OF SCIENCE

Department
of Geography

University
of Ottawa
Ottawa, Ontario
Canada

Matthew Jared Ladd

Supervisor: Dr. Konrad Gajewski
Laboratory for Paleoclimatology and Climatology
Department of Geography, University of Ottawa

Committee Members:
Dr. Luke Copland
Department of Geography, University of Ottawa

Dr. Mike Sawada
Department of Geography, University of Ottawa

Table of Contents

List of Tables

List of Figures

List of Abbreviations

ACIA – Arctic Climate Impact Assessment

AMO – Atlantic Meridional Oscillation

AO – Arctic Oscillation

AVHRR – Advanced Very High Resolution Radiometer

cA – continental Arctic air

CAA – Canadian Arctic Archipelago

CAVM – Canadian Arctic Vegetation Mapping project

CDAS – Climate data assimilation system

cP – continental polar air

CPC – Climate Prediction Center (NOAA)

CDO – Climate Data Operators

CRU – Climate Research Unit at University of East Anglia in Norwich, UK

cT – continental tropical air

ENSO – El Niño Southern Oscillation

ECMWF – European Center For Medium Range Weather Forecasting

ERA-40 – European Reanalysis (40 year)

ERA-15 - European Reanalysis (15 year)

GCMs - Global climate models

GEOTIFF – Georeferenced Tagged Image File Format

GIMMS - Global Inventory Modeling and Mapping Studies

GRADS – Grid Analysis and Display System

GRIB – Gridded Binary Data Format

HDF5 - Hierarchical Data Format

hPa – Hectopascal (similar to milibar unit of pressure)

IPCC – Intergovernmental Panel on Climate Change

mA – maritime Arctic air

MASL – Meters above sea level

mP – maritime polar air

MSLP – Mean Sea Level Pressure

mT – maritime tropical air

NAO – North Atlantic Oscillation

NARR – North American Regional Reanalysis

NCEP-DOE II – National Center For Environmental Prediction Department of the Environment (2nd generation reanalysis)

NCEP/NCAR – National Center For Environmental Prediction / National Center For Atmospheric Research

NCDC – National Climatic Data Center (NOAA)

NCL – NCAR Command Language

NDVI – Normalized Difference Vegetation Index

NetCDF – Network Common Data Format

NOAA – National Oceanic and Atmospheric Administration

NNR – NCEP/NCAR Reanalysis

NSIDC – National Snow and Ice Data Center (NOAA)

NWP - numerical weather prediction

PDO – Pacific Decadal Oscillation

PNA – Pacific / North American Pattern

SOI – Southern Oscillation Index

U component – zonal wind

UCAR – University Corporation For Atmospheric Research

V component – meridional wind

VCDAT – Visual Climate Data Analysis and Tools

WDC-P – World Data Center For Paleoclimatology (NOAA)

Z – zulu or Universal Time Coordinate (GMT -5 in Eastern DST

Abstract

Boundaries between air masses, called frontal zones, have been associated with vegetation boundaries (Bryson, 1966; Hare and Ritchie, 1972). Using gridded climate reanalysis data, we analyze the air masses and frontal zones of North America. The position of the July Arctic front varies significantly through the period 1948-2007, with a mean position similar to that found by Bryson (1966). The variability of the front position can be associated with changes in the general circulation; when the AO and SOI are positive (negative), the position of the July Arctic front is further north (south). There is also more variability in the July Arctic front position in Eastern versus Western Canada. When the July Arctic front is north (south) of the mean position, the boreal forest and tundra vegetation is more (less) productive. There is some evidence that climate warming is only starting to shift the July Arctic front to the north.

Acknowledgements

I would like to thank my supervisor, Konrad Gajewski for all of his advice and support, and providing many interesting ideas and timely feedback on my work. Having such an excellent supervisor, ensured that my research was on track and that the thesis was feasible. My appreciation is extended to my committee members for their assistance during, and at the conclusion of my research. My thanks go to the members of the Laboratory for Paleontology and Climatology (LPC), and to the lab technicians for their encouragement and interesting discussions. It is a very professional group of people to work with on a daily basis. Thanks is extended to the National Science and Engineering Research Council (NSERC) and the Canadian Foundation For Climate and Atmospheric Science (CFCAS) funded Polar Climate Stability Network (PCSN), for the grants to support my research. It is due to these grants that I was able to finish in a timely fashion. A special mention is given to a former member of the lab, Brett O' Neil, who helped with the setup of the Linux computer and installed the climate software. I am very indebted for his help as it saved me a substantial amount of time. Also, thanks to the other graduate students I have met from the other labs in the department of Geography. Finally, I would like to thank my family and friends for their support. I leave you with the following quote: "The weather and climate is always interesting."

Matthew J Ladd, 2008

Chapter 1

1.0 Introduction

The purpose of this study is to examine the July air mass boundaries in North America, specifically the Arctic front from 1948 to 2007. The results are compared with previous studies that were completed in the 1960s and 1970s. The spatial and temporal variability of the July Arctic front will be examined in relation to atmospheric circulation patterns and vegetation productivity anomalies.

1.1 Arctic climate change and variability

The climate in the Arctic is changing rapidly, with most climate model projections showing a warming of several degrees by the end of this century (Arctic Climate Impact Assessment [ACIA], 2005). The warming is particularly significant at high latitudes relative to Northern Hemisphere trends, due to the positive feedbacks that amplify the warming (ACIA, 2005). An example of a positive feedback is the reduction of the summer sea ice in the Arctic, which can amplify the warming the following year (Serreze and Francis, 2006).

The climate of the Arctic has varied significantly on timescales ranging from millennial to interannual. Documenting the various scales of variability is difficult, however, as the instrumental record in the Arctic is often short. Proxy-climate data are therefore required for longer time-scale studies. Proxy-climate data such as tree rings, microfossils from lake sediment cores and ice cores allow for the past climate to be reconstructed with a high degree of accuracy.

In the 20th century, there has been significant warming in most of the Arctic region relative to the past few centuries (ACIA, 2005; IPCC, 2007). Over northern high latitudes, 20th century zonally averaged annual temperatures have shown an overall increase of 1^{o}C (Serreze and Barry, 2005). According to the ACIA (2005) there are some areas of the Arctic such as Baffin Island, northern Quebec and Labrador that are not showing an increase in temperatures, but a decrease instead. There are significant seasonal differences in current temperature trends. For example, there is evidence that northern Eurasia has cooled during the autumn and winter (Serreze and Barry, 2005). Parts of the central Canadian Arctic islands cooled during June, July, and August from 1964 to 2004 (Chapin *et al*, 2005).

1.2 Air masses and fronts

Studying climate changes and variability requires summarizing the state of the atmosphere in various ways. For example, interpolated maps of surface temperature can be used to show large-scale warming and cooling. One concept used to summarize the state of the atmosphere over large spatial scales is the *air mass*. An air mass is defined as a region of the atmosphere where properties such as temperature and humidity are relatively similar horizontally (Trewartha and Horn, 1980). Air masses are features of the atmosphere that result from air acquiring the characteristics of the underlying region if the air remains over the surface for a relatively long period of time. For example, over the Polar Regions the absence of daylight in winter, along with strong radiational cooling allows for the creation of an exceptionally cold and dry air mass (Serreze and Barry, 2005). The transitions between air masses, where the spatial gradient is greater than within the air mass itself, are called frontal zones. There is evidence that the structure and location of the major vegetation formations of the earth are determined by air masses and, that the boundaries between biomes (ecotones) are associated with frontal zones (Bryson, 1966; Hare and Ritchie, 1972).

Because the air masses are created through interaction with the surface, seasonal changes in the surface energy balance affect their strength and extent. In July, the main air masses affecting North America are maritime tropical (mT), continental tropical (cT), maritime polar (mP), and continental polar (cP) (Figure 1). The two major air mass boundaries are the Arctic front (dashed grey line in Figure 1), separating the cP air north of the front from the mP and mT air masses to the south of the front and the Pacific front (dashed orange line in Figure 1) which separates mP and cT west of the front from mT air east of the front. In Godske *et al* (1957) this Pacific front was called the Atlantic Polar Front since it was the boundary between mP and mT air, merging with the Trade front over the Western USA, separating cT from mT air. Bryson (1966) has a reference to Maritime Arctic (mA) air however, this is not shown in newer air mass interpretations such as Trewartha and Horn (1980) and Oliver and Fairbridge

(1987). In older meteorology texts such as Hewson and Longley (1944) and Peterson (1956) there is no mention of mA air.

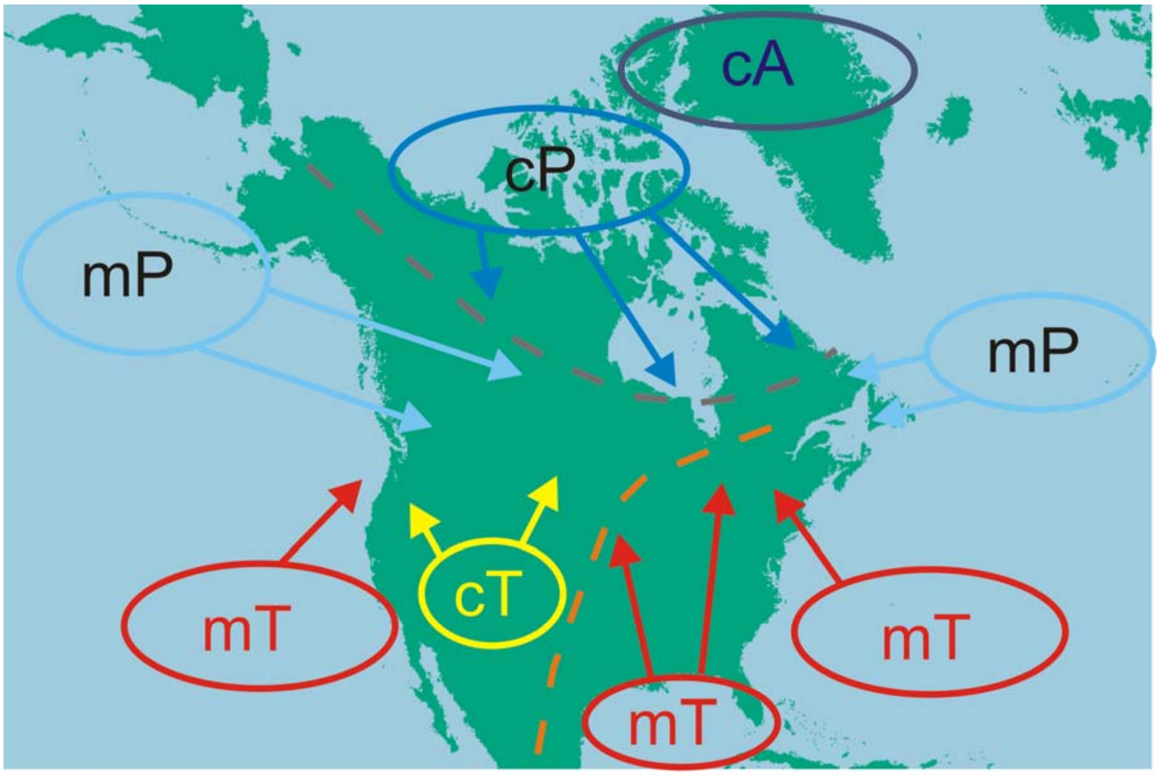

Figure 1. July air masses and frontal boundaries in North America adapted from Bryson (1966) and Oliver and Fairbridge (1987).

1.3 Definition of the Arctic front

The Arctic front is defined as the semi-permanent, discontinuous front between the cold Arctic air mass and the intermediate Polar air mass, bounded in the south by the Polar Front (Oliver and Fairbridge, 1987). The polar front extends up to the 500 mb level (approximately 5550 metres above sea level [MASL]), whereas the Arctic front is identified in the boundary layer, extending to one or two kilometers above the surface (Palmen and Newton, 1969). True cA air does not exist during the summer in North America, except over Greenland and the ice caps of the Canadian Arctic (Bryson, 1966; Trewartha and Horn, 1980). Therefore the summer Arctic front could be defined as the boundary between continental Polar (cP) and maritime Polar (mP) air masses.

According to Reed and Kunkel (1960), the Arctic front is a feature that is separate from the polar front and found only during the summer. Even if both fronts were located at the same latitude, they are separate because of their extent in the atmosphere. The definition from Oliver and Fairbridge (1987) supports the idea that the Arctic and Polar fronts are separate features. Barry (1967) found a winter Arctic front at 850 mb level (approximately 1650 MASL) but not at the surface. It is likely that a winter Arctic front exists but is weaker and more difficult to locate than the summer Arctic front. According to Sereze *et al* (2001), "*It nevertheless seems that despite a fairly ample literature, there is as yet no universally accepted view as to what truly distinguishes 'Arctic'' from 'Polar' fronts*". In this paper the term Arctic front will be used to be consistent with the literature. The winter Arctic front would be the boundary between cA and cP air (Figure 2). Willis and Grice (1977) examined the existence of a winter Arctic front in Alaska and found that the change in the position of the Arctic front in Alaska was directly related to the position and movement of low pressure systems in the Gulf of Alaska.

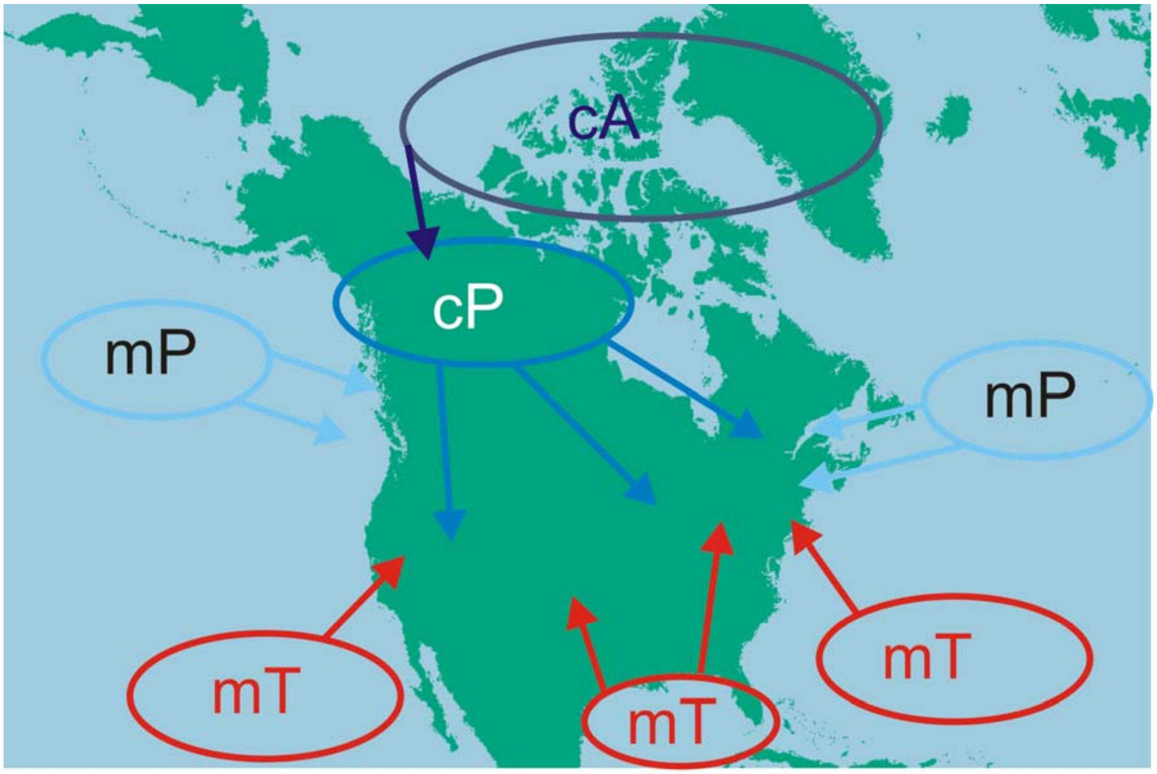

Figure 2. January air masses and frontal boundaries in North America adapted from Bryson (1966) and Oliver and Fairbridge (1987).

1.4 Wind streamlines

Locations of the major air masses and the resulting air mass boundaries can be identified by creating maps of wind streamlines (Figure 3). A streamline is a line tangent to the instantaneous motion at each point of the velocity vector (Barry and Carleton, 2001). The streamlines may be coloured to indicate their magnitude. Streamlines can converge into or diverge from centers of inflow and outflow known as “singular points” (Barry and Carleton, 2001). The air mass boundaries can be more easily identified with streamlines than with wind vectors because the length of each streamline is not determined by the magnitude of the wind vector. Streamline maps can be produced using software such as the Grid Analysis and Display System (GRADS; Doty, 2001) using the GRADS scripting language (GRADS user guide; Doty, 1995). In previous studies such as Bryson (1966) and Wendland and Bryson (1981), the streamlines were hand-drawn.

1.5 Previous studies

A classic study was that of Bryson (1966), who identified the major air mass boundaries in North America from streamline maps. These maps (July streamlines shown in Figure 3) were based on the frequency distributions of air masses using data from 1948 to 1957, collected at 120 stations throughout North America and a trajectory analysis of the source of the streamlines. He suggested a strong relation between the major vegetation transitions and frontal zones. In particular, he concluded that the northern edge of the boreal forest coincides closely with the confluence zone between Pacific and Arctic air masses in July, as depicted in his streamline maps. He also concluded that the modal position of the summer Arctic front is closely positioned to that obtained in previous studies such as Reed and Kunkel (1960). Finally, using the partial collectives method, a mixture model approach, (Essenwanger, 1976; Viau *et al*, 2002), he showed that stations near the July Arctic front should have a multi-modal distribution of July maximum temperatures because of the different air masses present.

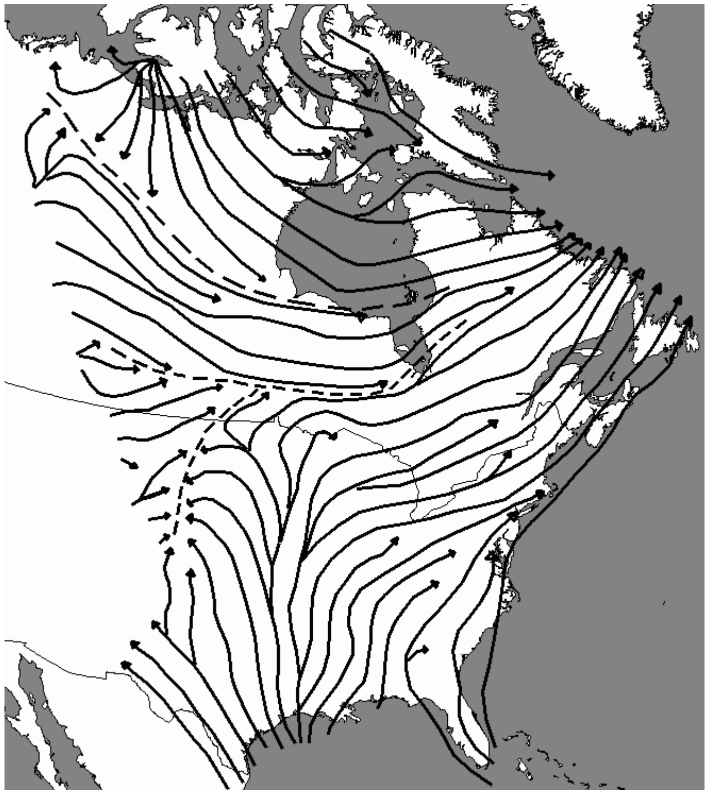

Figure 3. July streamline map (adapted from Bryson, 1966).

In addition to the method of streamline confluence there are several other methods to locate a frontal boundary such as the Arctic front. These methods have been applied to the analysis of the Eurasian summer Arctic front. Krebs and Barry (1970) determined the median position of the Eurasian Arctic Front using station data from 1952 to 1956 and the maximum frequency of fronts derived from daily July sea level pressure (SLP) plots. The front was defined as a meridional gradient of 1000-500 mb thickness of greater than 100m per 10º of latitude, which results in a difference in temperature of roughly 1ºC per 2.5º of latitude (Krebs and Barry, 1970).

Several studies have examined the front in North America in the upper atmosphere, specifically at the 850 mb level. Serreze *et al.* (2001) studied the

Arctic frontal boundary in Alaska using parameters such as the vertical component of relative vorticity, a thermal front parameter from the surface to the 850 mb level, the convergence of q-vectors, wet bulb temperature, wind shear, and the height of the tropopause to identify the front. Barry (1967) identified the seasonal location of the Arctic front in North America for January, April, July, and October, where the study focused on the front at the 850 mb level. The July position of the 850 mb front for 1961 to 1965 is mostly over the southern Canadian Arctic Archipelago (CAA) and much further to the north than the front at the surface, except for July 1964 (Barry, 1967).

1.6 The Arctic front and climate change

The position of the July Arctic front has varied in time, as a consequence of climate variations. Ritchie and Hare, (1971) suggest that during the mid-Holocene period the July Arctic front was well north of its present position, as boreal forest occupied the Tuktoyaktuk Peninsula. This may be a partial analogue of the future, as there has been warming over the past century in the Arctic causing a rapid decline in sea ice, shorter duration of snow cover, receding glaciers, and changes in the distribution of vegetation (ACIA, 2005 and IPCC, 2007). It is possible that the Arctic front may shift slightly to the north during this warming climate.

1.7 Influence of vegetation and other controls on the Arctic front

It has been shown that the position of the July Arctic front is close to that of tree line (Bryson, 1966; Barry, 1967; Krebs and Barry, 1970). Ritchie and Hare (1971) demonstrated the median position of the present day summer Arctic front is located about 300 km south of tree line in most of North America except Alaska.

In western Canada tree line is very narrow, whereas in eastern Canada, the tundra-boreal forest transition is much wider (Bryson, 1966; Barry, 1967; Payette, 1983; Timoney, 1992). The implication of this is that the wide vegetation transition in eastern Canada may be due to a large variability in July Arctic front positions (Barry, 1967). Also, the elevation changes are different in eastern versus western Canada. Previous studies such as Bryson (1966) do not extend the front east of Hudson Bay due to the presence of several different air masses. The front position in this region was described as “problematic” by Reed and Kunkel (1960). In addition, Serreze and Barry (2005) found the summer Arctic frontal zone over Eastern North America to be not well expressed. In the Western regions, specifically Alaska, Yukon and western NWT, there is a strong heating contrast between the ice-covered ocean and the snow-free land, in addition to coastal topography, which may help develop and anchor the front (Reed and Kunkel, 1960; Lynch *et al*, 2001).

The influence of vegetation on the position of the July Arctic front occurs because of differences in energy balance across vegetation transitions, and these may aid in the determination the location of Arctic front (Hare and Richie, 1972; Pielke and Vidale, 1995). The boreal forest absorbs more solar radiation than tundra, which is often snow-covered into early July. Thus there is a difference in heating across the vegetation boundary which could lead to small-scale circulations (Pielke and Vidale, 1995; Figure 4). However, Beringer *et al*, (2001) conclude that these surface energy balance contrasts are not likely to determine the preferred position of the Arctic front. Thus it is unlikely that the vegetation transitions could control the position of the Arctic front, and most of the evidence shows that tree line is mostly a response to the position of the summer Arctic front (Serreze and Barry, 2005). The energy balance across the vegetation transitions is important. It is likely that surface energy exchanges along tree line could enhance climate warming (Lafleur and Rose, 1995; Beringer *et al*, 2005).

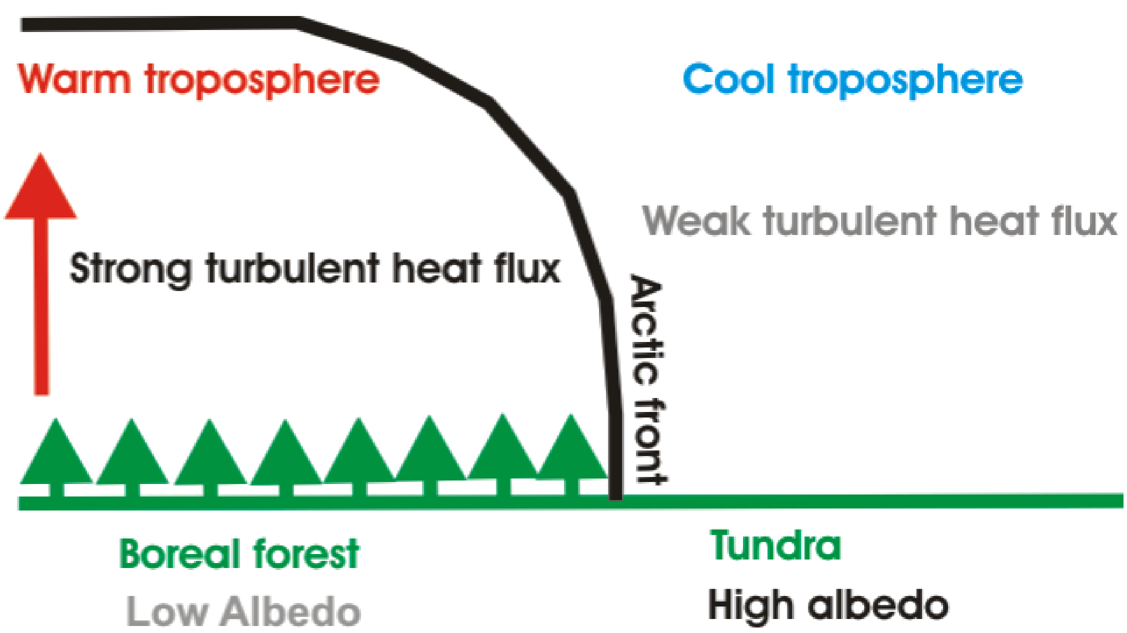

Figure 4. Arctic front caused by differences in heat flux across the boreal forest-tundra boundary (adapted from Pielke and Vidale, 1995 and MacDonald et al, 2004).

1.8 Scope of study

The study area encompasses an area of North America with boundaries of 170°W to 40°W longitude and 20°N to 90°N latitude (Figure 4). In this region, the major features of the general circulation are the subtropical highs in the NE Pacific Ocean and the Western Atlantic Ocean and weak subpolar lows. The temporal range of this study is 1948 to 2007, for which data are available, with particular focus on 1958 to 2002, as explained below.

Figure 5. Study area for July air mass boundaries and the Arctic front.

1.9 Climatology of Northern Canada

In northern Canada and the adjacent oceans, the summer mean sea level pressure (MSLP) maps include lower MSLP near Baffin Island and higher MSLP over the Beaufort Sea (Serreze *et al,* 1993). Slightly lower MSLP tends to dominate the central Arctic region in the summer (Serreze and Barry, 2005). Synoptic features are not as well defined during winter (Barry and Carleton, 2001). Mesoscale effects are evident, especially along coastal regions of the Canadian Arctic Archipelago. This results in a poor estimation of summer surface air temperatures in the region from synoptic station data unless mesoscale effects are accounted for (Atkinson and Gajewski, 2002). There is a temperature inversion present, but it is much shallower and weaker than during the winter (Atkinson, 2000; Serreze and Barry, 2005). There is a higher frequency of cloud cover, especially over the Arctic Ocean and precipitation is significantly higher over most regions of the Arctic than in the winter (Orvig, 1970; Serreze and Barry, 2005).

1.10 Objectives

This study presents July streamline maps using gridded climate data, and identifies the location of the major frontal zones for the period of study. As such, it updates older studies by analyzing these fronts using gridded data rather than station data. In addition, the data source covers a longer period of analysis than Bryson (1966) used and is related to atmospheric circulation patterns and vegetation. The July Arctic front is identified for each year starting in 1948 (1958) and ending in 2007 (2002) from NNR (ERA-40), using the method of wind streamline confluence and the source of streamlines. The period of 1948 to 1957 is also examined for comparison with the results of Bryson (1966).

Second, the variability of the position of the front for 1948-2007 (derived from NNR) and 1958-2002 (derived from ERA-40) will be shown along with the ranges of the front position for 10 year intervals. This will help identify trends in the front position in relation to climate changes. The spatial variability of the front will be examined by determining the latitudinal position of the front for a given year across 10° longitude intervals. The temporal variability of the front will be examined by averaging the latitudinal position of the front across all longitudes then examining the interannual variability.

Third, the relationship between the atmospheric circulation patterns such as the Arctic Oscillation (AO) and Southern Oscillation Index (SOI) and the position of the front will be examined. Other teleconnections were examined (Chapter 2.6.2) but not statistically significant in relation to the front position. The AO is defined as the oscillation in atmospheric mass between mid and high latitudes (Thompson and Wallace, 2000). The SOI is the difference in pressure between Tahiti and Darwin, Australia and a component of El Niño (Trenberth, 1997). The July Arctic front position is compared to time series of the AO and SOI data to examine the connection between them. The July Arctic front is a synoptic feature and synoptic features are part of the general atmospheric circulation so any changes in the circulation should be reflected in changes of the position of the front.

Finally, the link between the productivity of the vegetation and the front will be examined. Using anomalies of the July Arctic front position and NDVI data we can examine if warmer (cooler) air masses cause vegetation to be more (less) productive. Since vegetation transitions are associated with transitions in air masses, it is expected that when the front is north (south) of the mean position, the productivity of the vegetation should be higher (lower), because of a warmer and moister (cooler and drier) air mass present. This means that there should be a higher frequency of positive (negative) NDVI anomalies (greater than 50%) when the July Arctic front is north (south) of the mean position.

This document is in the format of a thesis by article therefore Chapter 2 is a discussion of the data and methods, Chapter 3 presents the results of this study, in the form of a paper to be submitted to a journal, and Chapter 4 is a summary of the thesis, followed by references and appendices.

Chapter 2

2.0 Data and Methods

2.1 Introduction

Gridded climate data has five dimensions (Institute of Global Environment and Society, 2008): latitude, longitude, level of the atmosphere, time, and the variable of interest. The multidimensional nature of the data can make it challenging to visualize and process. Therefore graphical formats are needed to display variables such as temperature, pressure, precipitation, wind, etc. Some of the most widely used gridded climate data in the atmospheric research community are the reanalysis products.

2.2 Reanalysis Product

This study uses gridded climate reanalysis products rather than climate station data. Station data could be used to verify air mass boundaries, although at high latitudes stations tend to be sparse, with many missing observations. The advantage of using reanalysis “data” is the consistency of observations due to the fixed climate model used to to develop the reanalysis product (Uppala *et al*, 2005).

The major data sources of this study are the European Center for Medium Range Weather Forecasting European Reanalysis-40 (ECMWF, 2008; Uppala *et* *al*, 2005) and the National Center For Environmental Prediction (NCEP) / National Center For Atmospheric Research (NOAA 2008a; Kalnay *et al*, 1996; Kistler *et al*, 2001), hereafter referred to as NNR. Other reanalysis products examined, such as the North American Regional Reanalysis (NARR) (Mesinger, 2006), are described in Appendix F.

Reanalysis products are produced using a climate data assimilation system (CDAS) and a large volume of re-processed climate observations. The products are essentially a new analysis of the atmosphere using historical climate data and a fixed data assimilation system, incorporating more observations (Barry and Carleton, 2001). The sources of climate data are surface observations from land and ship, ocean buoys, and upper air observations from radiosondes and rawinsondes (weather balloons with instruments attached), aircraft, and satellites that provide the raw data, which is incorporated into the CDAS (Barry and Carleton, 2001). The CDAS consists of the processing of observed data, interpolation, initialization, numerical forecast, and post-processing (Kanamitsu, 1989). A major part of the CDAS is a climate model which has a certain number of levels in the atmosphere (usually 30-60) and a specific resolution, which is essentially the distance between grid points given in either degrees or kilometers (Kistler *et al*, 2001).

2.2.1. National Center for Environmental Prediction (NCEP) / National Center for Atmospheric Research (NCAR) Reanalysis

The NNR (R-1; Kalnay *et al*, 1996; Kistler *et al*, 2001) is a 2.5º gridded dataset produced four times daily (00Z, 06Z, 12Z and 18Z) by the National Oceanic and Atmospheric Administration (NOAA) / Oceanic and Atmospheric Research (OAR) / Earth Systems Research Laboratory – Physical Sciences Division (ESRL PSD) at Boulder, Colorado and spans the period from 1948 to present. Prior to this time upper air observational networks were sparse. This is the dataset that is most frequently used and cited in climate studies because it has a large number of climate variables and covers a longer period of record than other reanalysis products. The monthly mean data (1948–2007) for this study were obtained from the NCEP/ NCAR Reanalysis Project at:

http://www.cdc.noaa.gov/cdc/reanalysis/reanalysis.shtml.

2.2.2. European Center For Medium Range Weather Forecasting (ECMWF) European Reanalysis (ERA-40)

The ERA-40 is the reanalysis completed by the European Centre for Medium-Range Weather Forecasts (ECMWF), Reading, UK, and contains results for September 1957 to August 2002 using conventional observations and satellite-derived data. The 2.5° gridded analyses are produced four times daily at 00Z, 06Z, 12Z and 18Z. It is provided by the ECMWF from their web site at http://data.ecmwf.int/data/d/era40_daily/. For a detailed description of the ERA-40 product see Uppala *et al,* (2005). There is also available a shorter reanalysis

(ERA-15) covering the period from 1979 to 1993 available at http://data.ecmwf.int/data/d/era15/.

2.3 Data Quality and Consistency

Uppala *et al* (2005) provide a detailed description of the ERA-40 reanalysis product. The ERA-40 improves on the NNR product by including more satellite data such as Special Sensor Microwave Imager (SSM/I) data for winds starting in 1987 (Uppala *et al*, 2005). Reanalysis products were compared in Sterl (2004) and surface air temperature of the ERA, NCEP and CRU were compared in Simmons *et al,* (2004). Most of the problems with certain variables are over extreme high latitudes and over regions with high topography and extreme heating, as described by Serreze *et al* (2001). The ERA-40 provides a better estimate of precipitation over the Arctic Basin than the NNR; the NNR overestimated summer convective precipitation over the high latitudes because of increased evaporation and hence moisture in the atmosphere (Serreze *et al*, 2005). The wind component data are reliable except where wind speed is underestimated in areas of high wind speed (ECMWF, 2004).

The ERA-40 reanalysis was completed in the early part of this decade. Although the reanalysis has gridded fields starting as early as 1957, the reanalysis product becomes more reliable with the introduction of satellite data in the 1970s. Specific years of the reanalysis had improvements because of the inclusion of more data (Table 1). Changes in the climate should be interpreted carefully when examining specific years such as 1979 where new observations were incorporated into the data assimilation system (Sterl, 2004).

Table 1. Improvements to the ERA-40 observing system from 1958 to 2002 (adapted from Uppala *et al*, 2005).

1973	The introduction of data from aircraft and the vertical temperature radiometer.
1979	Additional satellites such as the Tiros Operational Vertical Sounder.
1987	The addition of the Special Sensor Microwave Imager.
1991 and 1995	The addition of the ESA remote sensing satellites.
1998	The addition of the Advanced Microwave Sounding Unit.

2.4 Formats

The large size of the database and the complex nature of the data require an organized approach to data management. This can be addressed by extracting only the variables, years, and months required. The common data formats are gridded binary (GRIB) and network common data format (NetCDF) data, which are the most efficient formats for storage and transmission. GRIB files will have a file extension of either .grib or .grb. NetCDF files will have a file extension of .nc. One benefit of the NetCDF format is that it can be easily visualized in ESRI ArcGIS 9.2 software. Another multidimensional format is Hierarchical Data Format (HDF5), which is used by earth observing satellites to store data (UCAR, 2007).

2.5 Software

Software to read and process these data are widely available, most of which run only in the Unix or Linux operating systems. A selection of the programs used in this study is listed in Appendix H. An example of such a program is the Grid Analysis and Display System (GRADS) (Doty, 2001) developed at the National Atmospheric and Oceanic Administration (NOAA). With such a program, one or more atmospheric variables can be visualized by setting certain dimensions to be fixed such as time and height. Longitude and latitude are allowed to vary in order to select the area of interest unless values at a specific point are required.

2.6 Additional Datasets

2.6.1. Global Inventory Modeling and Mapping Studies (GIMMS) Advanced Very High Resolution Radiometer (AVHRR) Normalized Difference Vegetation Index (NDVI)

In order to examine changes in vegetation productivity in relation to the front, the Global Inventory Modeling and Mapping Studies data set (Pinzon *et al*, 2005; Tucker *et al*, 2004; Tucker *et al*, 2005) was acquired. The GIMMS data set is a remotely sensed Normalized Difference Vegetation Index product available at http://glcf.umiacs.umd.edu/data/gimms/index.shtml for the period from 1981 to 2003. The data set is derived from imagery obtained from the AVHRR instrument onboard the NOAA satellite series 7, 9, 11, 14, 16 and 17 and has been corrected for calibration, view geometry, volcanic aerosols, and other effects not related to vegetation change (Global Land Cover Facility, 2008).

2.6.2. Teleconnection data

"The term 'teleconnection pattern' refers to a recurring and persistent, large-scale pattern of pressure and circulation anomalies that spans vast geographical areas" (NOAA, 2008b). The major teleconnection patterns, including the Arctic Oscillation (AO), North Atlantic Oscillation (NAO), El Niño Southern Oscillation (ENSO), Pacific Decadal Oscillation (PDO), and the Pacific North American (PNA) pattern are described in Barnston and Livezey (1987). In addition there is the Atlantic Meriodional Oscillation (AMO), which has been linked to decadal changes in hurricane activity (Barry and Carleton, 2001). The state of ENSO is analyzed with the southern oscillation index (SOI), the pressure difference between Darwin, Australia and Tahiti, and the sea surface temperature anomalies in the Niño 3.4 region (Trenberth, 1997).

These teleconnection data are available on a monthly, seasonal, and annual timescale from the NOAA World Data Center for Paleoclimatology. In some cases estimates of the annual indexes extend back over one thousand years, derived using tree-ring chronologies. For this thesis SOI (CRU, 2004a) and AO (JISAO, 2004), Niño 3.4 (NCAR, 2008), NAO (CRU, 2004b), PDO (JISAO, 2000), and PNA (NOAA, 2008c) data were acquired. Additional teleconnection data can be obtained from the sites listed at http://www.cdc.noaa.gov/ClimateIndices/List/.

2.7 Methods

The main steps used in this study are as follows. Each of these steps is described in detail in the subsequent sections.

1. Data collection and mapping
   1.1. Acquire the reanalysis data (ERA-40 and NNR).
   1.2. Calculate monthly means (ERA-40 only).
   1.3. Create mean July streamline maps using a Grads script for all years of the reanalysis and groups of years.
   1.4. Import the streamline maps into ESRI ArcGIS (ESRI, 2006) and plot the July fronts.
2. Analysis of temporal variability
   2.1. Create a spreadsheet with the quantitative July Arctic front data and statistics, which can be used to create time series plots and maps with the ranges of front positions. This allows for a determination of how the position of the July Arctic front is changing through time.
   2.2. Relate the July Arctic front position to the atmospheric circulation data such as the July AO and SOI.
   2.3. Evaluate the July Arctic front positions derived from NNR vs ERA-40
   2.4. Compare the July Arctic front position for 1948-1957 with the position of the front as found by Bryson (1966)
3. Comparison of frontal zone position to vegetation indices
   3.1. Acquire NDVI data and calculate NDVI anomalies for July of each year (1981 to 2003).

3.2. Import NDVI data into ArcGIS with July Arctic front positions for each year.

3.3. Create polygon shapefiles in ArcGIS bounded by the July Arctic front position for a given year and the long term mean position.

3.4. These polygons will be used to calculate the frequency of NDVI anomalies (using Hawths Tools; Appendix H) in order to determine how the position of the July Arctic front is related to changes in vegetation productivity.

2.7.1. Acquire selected variables from the reanalysis products

- The ERA-40 product was acquired by selecting specific variables for a specific month (July) for all years (1958-2002) and downloading daily data from the ECMWF data server at http://data.ecmwf.int/data/d/era40_daily/. The specific variables in this case are the zonal (u) and meridional (v) 10m (surface) wind components are necessary in order to create the streamline maps. Monthly means and long term monthly mean were not available for download therefore were calculated from the daily data. Other variables were acquired as necessary.
- The NNR required less preparation since the monthly means were available for download at: http://www.cdc.noaa.gov/cdc/reanalysis/reanalysis.shtml, although it was still necessary to calculate the long term monthly means. NNR wind

component data used were at the 1000 mb level of the atmosphere, which is roughly comparable to the 10 m wind data from ERA-40.

2.7.2. Overview of the process to calculate the wind monthly means from ERA-40

- The creation of monthly means required selecting out the individual years from the July monthly file for all years and then calculating the mean for each monthly file using Climate Data Operators (CDO; Max Planck Institute for Meteorology, 2006) software (Appendix H).
- A final step to make the grib files readable by Grads is to create the control files (these describe the structure of the grib data) using grib2ctl (Ebisuzaki, 2006) and then gribmap to associate the grib file with the control file by creating an index file.
- Since CDO, grib2ctl, and gribmap (part of the Grads package) are each command line programs designed to run under the Unix/Linux operating system, a series of scripts were developed (Appendix H) to output the code necessary to process a large number of files.
- There is a script to generate the code for the following tasks: select the years using CDO (selyears_era40.awk), calculate the monthly means (ymonmean_era40.awk) using CDO, create a list of the grib files (listgrib.sh), and to process the grib files (from the list generated from listgrib.sh) using grib2ctl and gribmap
- A standardized file convention naming scheme was used to facilitate programming, In this case file names were: jan_windcomp10m_1958-

2002.grib , feb_windcomp10m_1958-2002.grib, etc.

- The grib files should be quickly loaded and plotted with XConv software (British Atmospheric Data Center, 2006) (Appendix H) to ensure the correctness of the data.
- The details of the steps are as follows:
  - Run the script "selyears_era40.awk" (Appendix H) as follows: awk -f selyears_era40.awk selyears.txt > outputcdo.sh). The specific years can be modified by editing selyears.txt. The names and locations of the input and output files can be modified by editing selyears_era40.awk. Simply paste the code from outputcdo.sh into a terminal window and the files are created: jan_windcomp10m_1958.grib, jan_windcomp10m_1959.grib, feb_windcomp10m_1958.grib, feb_windcomp10m_1959.grib, etc.
- There are two methods for obtaining the monthly mean values, either using CDO to output the file or using GRADS when the data files only need to be plotted.
  - Run the script "ymonmean_era40.awk" (Appendix H) as follows: awk -f ymonmean_era40.awk selyears.txt > outputcdo.sh. This will output the Climate Data Operators code necessary to generate the monthly mean file for each month of every year. The specific years can be modified by editing selyears.txt. The names and locations of the input and output files can be modified by editing ymonmean_era40.awk. Simply paste the code from outputcdo.sh

into a terminal window and the files are created: jan_mean_windcomp10m_1958.grib, etc.

  - Use GRADS to calculate the monthly mean with the following commands:

    Define varname = ave(var,t=start,t=end)

    Define u10ave = ave(u10,t=1,t=124)

    Define v10ave = ave(v10,t=1,t=124)

- Now it is necessary to create the control (.ctl) and index (.idx) files so that the files can be read in GRADS. A sample control file is shown in Appendix F. It is possible to create a control file is using XConv software but the program does not allow for batch creation of control files and it occasionally has problems with very large files.
  - Xconv will create a .dat file rather than an .idx file. The .idx files are binary but the .ctl files can be edited, which is useful in case a field name needs to be modified. The .ctl file is unique to a specific grib file.
  - The script listgrb.sh (Appendix H) will create a list of the grib files (gribfiles.txt). Then run process_all.awk (Appendix H) to create the code (awkoutput.sh) that is required to output the control and index files using grib2ctl and gribmap (Appendix H). This code should be pasted into a terminal window rather than being run as a shell script: awk -f process_all.awk gribfiles.txt > awkoutput.sh

2.7.3. Creation of mean July wind streamline maps in GRADS

- Streamline maps were created using ERA-40 gridded 10 m wind component data using GRADS software (Appendix H). The streamline maps are used to determine the air mass boundaries and the location of the July Arctic front.
- For July there are 124 time steps (4x daily x 31 days). The variables are then simply plotted using the display (d) command. It is possible to create both streamline and wind vector maps in GRADS.
    - After starting GRADS, type open <full path to grib file>.
    - Enter "query file" to get the variable names for the wind components.
    - To create a streamline map enter "set gxout stream". For a vector map, enter "set gxout vector". The default projection is latlon. To change to a north polar stereographic projection enter "set mproj nps".
    - Set the latitude/longitude of the map using "set lat 20 90" and "set lon -170 -40", for a study area from 20ºN to 90ºN and 170ºW to 40ºW. The map units can also be set.
    - To create the streamline map enter:

      "d uwnd;vwnd;mag(uwnd,vwnd)" where uwnd is the name of the zonal wind component and vwnd is the name of the meridional wind component.
    - To output the map as an image enter "printim filename.png x800

y600 white". The map will be 800 x 600 pixels with a white background in png format. It is possible to further customize the map by setting the title of the map, including a legend (using the GRADS script cbar.gs), etc.

- A GRADS script (.gs) was created to automate the production of mean wind component maps for July of every year. This script is monmean_windcomp10m_july.gs (Appendix H). Another script was created to output plots using the NNR. Plots created by the script are shown in Appendix A.

2.7.4. Plotting the July fronts in ArcGIS from streamline maps

- Although the streamline maps show the air mass boundaries and fronts, it is necessary to bring these into ArcGIS in order to plot the position of the fronts, from which a quantitative analysis can be completed. The steps are as follows:
  - Create a line shapefile for each year of reanalysis (set coordinate system to WGS 84).
  - Open North America map and open streamline map from Grads (image in GIF format).
  - Georeference the streamline map to the North American map (save Georeferencing information so that it can be loaded quickly for subsequent streamline maps).
  - Add the line shapefile for same year as the streamline map.

- Use the editing tool in ArcGIS to start editing the shapefile.
- Trace a line where the frontal boundary should be located and consider the following points:
    - Find the confluence of streamlines, essentially where streamlines with a northerly and southerly component meet.
    - If there is space between the confluence of these streamlines, plot the front about half way between the confluence of streamlines.
    - If there is a curl because of a synoptic feature such as low pressure try to smooth it out.
    - Stop plotting if the front turns back on itself.
    - Plot the front from West to East.
    - It is not necessary to connect a front that is discontinuous.
    - It is not necessary to extend the front beyond 170ºW / 50ºW or beyond land.
    - If frontal position is unclear do not plot it or plot a shorter front.
    - Use ERA-40 position of front if NNR position is unclear (or vice-versa). There are some unavoidable minor positional errors because fronts are hand drawn and due to the georeferencing involved.

2.7.5. Quantify the July Arctic front position through time

- It was necessary to determine the latitudinal position of the July Arctic front for each year at 10° longitude increments. The steps are as follows:
  - o Calculate the distance between points on a line using Hawths GIS tools.
  - o Create a spreadsheet of values (Appendix D).
  - o Create time series plots by longitude with a trend line and loess smoothing using a statistical package (Chapter 3).
  - o Calculate the statistics on position by longitude (mean, median, mode, minimum, maximum, range, standard deviation; Appendix D).
  - o Determine the range of front positions for groups of years (1948-1957, 1958-1967, 1968-1977, 1978-1987, 1988-1997, 1998-2007; Chapter 3).

2.7.6. Provide a qualitative description of the July Arctic front position in relation to synoptic patterns

- The reason for this step is that quantitative data alone do not show how the July Arctic front fits into the overall synoptic pattern. The steps are as follows:
  - o Open the ArcGIS map document with the July Arctic frontal position from each year overlain with the corresponding streamline map.
  - o A qualitative description of the frontal boundary position and the

synoptic pattern from streamline maps for July of each year was completed (Appendix B).

2.7.7. Determine the relationship of the July Arctic front to the Arctic Oscillation and Southern Oscillation Index

- Here the goal is to relate the atmospheric circulation patterns to the July Arctic front position. The patterns with the highest correlations were the AO and the SOI. The steps are as follows:
    - Import the July AO and SOI data (Appendix F).
    - Rank the July Arctic frontal boundary position anomalies from greatest positive to negative (Appendix F).
    - Compare these anomalies to the AO and SOI indexes (Chapter 3).
    - Calculate correlations and create time series plots (Chapter 3).

2.7.8. Comparing the front positions derived from ERA-40 versus NNR

- The purpose of this step is to compare the ERA-40 and NNR derived July Arctic front positions to identify differences between them. The analysis steps are as follows:
    - Calculate the mean front position for each year over all longitudes from 160°W to 60°W for both NCEP and ERA positions of front (Appendix B).
    - Create a time series plot of the difference in position (Chapter 3).

2.7.9. Comparing NCEP/NCAR position of the front for 1948-1957 with the position determined by Bryson (1966)

- The purpose of this step is to map the July Arctic front using the same years as Bryson (1966), but with gridded rather than station data. The steps are as follows:
    - This required the creation of a mean July streamline map for 1948 to 1957 and comparing it to the streamline map produced by Bryson (1966) (Appendix G).
    - The mean positions of the front were also compared both quantitatively and qualitatively.
    - Although the actual streamline map was produced using GRADS, the averaging of July wind component data was performed in ArcGIS using the raster calculator.
    - In order to create a mean of the wind component data in ArcGIS it is necessary to use the NetCDF to raster tool on each U and V component data file for all years of the period.
    - Then the rasters are averaged using the raster calculator. Finally, the rasters are converted back to NetCDF and then U and V component NetCDF files are combined for each of the years in the period using XConv software. The averaging could also be done using CDO software (Appendix H) on a linux machine.

2.7.10. Creation of July mean NDVI anomaly maps using GIMMS AVHRR NDVI data

- Mean July NDVI anomaly maps were not available so it was necessary to create them using ArcGIS. The steps are as follows:
    - Acquire GIMMS AVHRR NDVI data.
    - Open each file in ArcGIS and export as GEOTIFF to get the scaled NDVI values.
    - Open files in ArcGIS (there are 2 files for July of each year, 15a for the first half of July and 15b for the second half of July).
    - Calculate the monthly mean for each year using the raster calculator.
    - Calculate the long term mean for July 1981 to 2003.
    - Calculate the NDVI anomalies for each year using Raster calculator: subtract the July long term mean from the July monthly mean for each year 1981-2003.
    - Reclass anomaly values into 4 classes (these are NDVI values scaled by 1000 – actual values range from -1 to 1):
        - 1000 to -500
        - 500 to 0
        - 0 to 500
        - 500 to 1000

2.7.11. Creating the polygons used to analyse the NDVI anomalies between the July Arctic front position for a given year and the long term mean position

- The purpose of this step was to create the study areas for vegetation productivity analysis in relation to the July Arctic front position. The steps are as follows:
    - Open the July NDVI anomaly raster and corresponding Arctic front shapefile (derived from ERA-40) for a given year and the long term mean NDVI raster created in the previous method.
    - The long term mean front position is either the position calculated from the individual years of the front in the Excel spreadsheet (only 10º longitude intervals) or the mean interpreted from the long term mean streamline map in GRADS.
    - Determine the number of polygons in the area between the front for a given year and the long term mean front.
    - Create the polygon shapefiles and give them meaningful names.
    - Repeat this process using the July Arctic front position (derived from NNR) shapefiles.

2.7.12. Determining NDVI anomalies from GIMMS AVHRR data and position of July Arctic front relative to long term mean

- This was the final step in the procedure to investigate if there is a higher frequency of positive (negative) NDVI anomalies when the July Arctic front is north (south) of the long term mean position, establishing a relationship between the front position and the productivity of the vegetation. The steps are as follows:
  - Run the thematic raster summary tool in Hawths Tools to get values for the NDVI anomalies (positive or negative) for the raster areas clipped by the polygons for July of a specific year (Figure 3).
  - For each polygon this tool summarizes the frequency of occurrence of cells in each category in the thematic raster layer (Beyer, 2004).
  - Create a spreadsheet of July NDVI anomaly frequencies for all polygons of all NDVI years (1981-2003) from both ERA-40 and NNR derived July Arctic front positions.

Chapter 3

3.0 Results

The North American July Arctic front during 1948 to 2007

Abstract

Boundaries between air masses, called frontal zones, have been associated with vegetation boundaries (Bryson, 1966; Hare and Ritchie, 1972). Using gridded climate reanalysis data, we analyze the air masses and frontal zones of North America. The position of the July Arctic front varies significantly through the period 1948-2007, with a mean position similar to that found by Bryson (1966). The variability of the front position can be associated with changes in the general circulation; when the AO and SOI are positive (negative), the position of the July Arctic front is further north (south). There is also more variability in the July Arctic front position in Eastern versus Western Canada. When the July Arctic front is north (south) of the mean position, the boreal forest and tundra vegetation is more (less) productive. There is some evidence that climate warming is only starting to shift the July Arctic front to the north.

Introduction

The purpose of this study is to examine the July air mass boundaries in North America, specifically the Arctic front. The results are compared with previous studies that were done in the 1960s and 1970s. The spatial and temporal variability of the July Arctic front is examined in relation to atmospheric circulation patterns and vegetation productivity anomalies.

An air mass is a region where atmospheric properties such temperature and humidity are relatively homogeneous (Trewartha and Horn, 1980). This homogeneity results from air above a region acquiring surface characteristics over a relatively long period of time. For example, over the Polar Regions the absence of daylight in winter, along with strong radiational cooling allows for the creation of an exceptionally cold and dry air mass, called Continental Arctic (cA) (Serreze and Barry, 2005). Air masses undergo transformations when they move over a different surface, such as cold Arctic air moving over warmer ocean water. The transitions between air masses, where the spatial gradient is greater than within the air mass itself, are termed frontal zones. Frontal zones are important in climate research since they reflect the major synoptic features of the general atmospheric circulation. There is evidence that the structure and location of the major vegetation formations of the earth (biomes) are determined in part by air mass characteristics and the transitions between biomes are associated with frontal zones (Bryson, 1966; Hare and Ritchie, 1972).

Air masses are created through interaction with the surface, where seasonal changes in the surface energy balance affect the strength and extent of the air masses (Trewartha and Horn, 1980). In July, the main air masses affecting North America are maritime tropical (mT), continental tropical (cT), maritime polar (mP), and continental polar (cP). The two major air mass boundaries are the Arctic front, separating the cP air north of the front from the mP and mT air masses to the south and the Pacific front, separating mP and cT west of the front from mT air east of the front.

One of the most significant air mass boundaries is the Arctic front, which according to Reed and Kunkel (1960) is a feature found only during the summer and is a separate feature from the polar front. However, several studies such as Barry (1967) and Willis and Grice (1977) have shown the existence of a winter Arctic front. The definitions of the Arctic and Polar front are ambiguous according to Serreze *et al* (2001): *"It nevertheless seems that despite a fairly ample literature, there is as yet no universally accepted view as to what truly distinguishes 'Arctic' from 'Polar' fronts"*. In this paper the term Arctic front will be used, consistent with previous literature. The Arctic front is defined as the semi-permanent, discontinuous front between the cold Arctic air mass and the intermediate Polar air mass, bounded in the south by the Polar Front (Oliver and Fairbridge, 1987). This is the definition of the winter Arctic front since true cA air does not exist during the summer in North America, except over Greenland and the ice caps of the Canadian Arctic (Bryson, 1966; Trewartha and Horn, 1980). Therefore the summer Arctic front can be defined as the boundary between continental Polar (cP) and maritime Polar (mP) air masses. The polar front extends up to the 500 mb level (approximately 5550 metres above sea level

[MASL]); whereas the Arctic front is identified in the boundary layer, up to one or two kilometers above the surface (Palmen and Newton, 1969).

Synoptic patterns and the resulting air mass boundaries can be analyzed by creating maps of wind streamlines. A streamline is a line tangent to the instantaneous motion at each point (Barry and Carleton, 2001). The streamlines are coloured to indicate their magnitude. Streamlines are constructed from the velocity vectors and can converge into or diverge from centers of inflow and outflow known as “singular points” (Barry and Carleton, 2001). The air mass boundaries can be more easily identified with streamlines than with wind vectors because the length of each streamline is not determined by the magnitude of the wind vector. Streamline maps can be produced using software such as the Grid Analysis and Display System (GRADS) (Doty, 2001) using the GRADS scripting language (Doty, 1995).

Air mass boundaries can be analyzed by creating maps of wind streamlines. A classic study of air mass distributions in North America was that of Bryson (1966), who produced streamline maps based on the frequency distributions of air masses, using data from 1948 to 1957 collected at 120 stations throughout North America. The two methods used were the partial collectives method, a mixture model approach, (Essenwanger, 1976; Viau *et al*, 2002) and trajectory analysis of the source of the streamlines. Bryson (1966) identified the major air mass boundaries in North America and suggested a strong relation between the major vegetation transitions and frontal zones. For example, the northern edge of the boreal forest coincides closely with the confluence zone between Pacific and Arctic air masses in July, as depicted in his streamline maps. The modal position of the summer Arctic front in his analysis was closely positioned to previous studies such as Reed and Kunkel (1960). In previous studies such as Bryson (1966) and Wendland and Bryson (1981), the streamlines were hand drawn.

In addition to the analysis of streamline confluence there are other methods to locate a frontal boundary. Stations near the front should have a multi-modal distribution of July maximum temperatures because of the different air masses present. Another method is the "frequency of fronts" method, which was applied to the analysis of the Eurasian summer Arctic front by Krebs and Barry (1970). They determined the median position of the Eurasian Arctic Front using station data from 1952 to 1956 and the maximum frequency of fronts derived from daily July sea level pressure (SLP) plots. The front was defined as a meridional gradient of 1000-500 mb thickness of greater than 100m per 10º of latitude, which results in a difference of roughly 1ºC per 2.5º of latitude.

Although the above studies examined the surface Arctic front, others have examined the front in North America in the upper atmosphere, specifically at the 850 mb level (approximately 1650 MASL). Any analysis above this level will be too high to identify the front. Barry (1967) identified the seasonal location of the Arctic front at the 850 mb level in North America for January, April, July, and October. The July position of the 850mb front for 1961 to 1965 is mostly over the southern Canadian Arctic Archipelago and much further to the north than the front at the surface. Serreze *et al* (2001) focus on the Arctic frontal boundary in

Alaska, using parameters such as the vertical component of relative vorticity, a thermal front parameter from the surface to the 850 mb level, the convergence of q-vectors, wet bulb temperature, wind shear, and the height of the tropopause to identify the front.

The structure and nature of the vegetation has some impact on the position of the July Arctic front, as differences in energy balance across vegetation transitions may influence the location of the frontal zone (Hare and Richie,1972; Pielke and Vidale, 1995). The boreal forest absorbs more solar radiation (low albedo) in contrast to the tundra, which reflects more solar radiation (high albedo), and is often snow-covered into early July. This results in a difference of heating across the boundary which could lead to small scale circulations, the result of significantly greater turbulent heat fluxes over the boreal forest versus the tundra, causing a synoptic front (Pielke and Vidale, 1995). However, Beringer *et al*. (2001) conclude that these surface energy balance contrasts are not significant enough to control the position of the Arctic front. Most of the evidence shows that the location of tree line is mostly a response to the position of the summer Arctic front (Serreze and Barry, 2005).

In Eastern Canada, the tundra-boreal forest transition is wider than western North America (Bryson, 1966; Barry, 1967; Payette, 1983; Timoney, 1992). The implication is that the wide vegetation transition in Eastern North America may be due to the larger north-south variability of July Arctic front positions (Barry, 1967). Previous studies such as Bryson (1966) do not extend the front east of Hudson Bay and the frontal position in this region was described as “problematic” by Reed and Kunkel (1960). In addition, more recent work by Serreze and Barry (2005) found the summer Arctic frontal zone over this region to be poorly expressed.

In Alaska, the Yukon and western NWT, there is a strong heating contrast between the ice-covered ocean and the snow-free land, in addition to coastal topography, which may help develop and anchor the front (Reed and Kunkel, 1960; Lynch *et al*, 2001). The July Arctic front in this region is similar to the Eurasian July Arctic front, which exhibits less north-south variability, because of the strong land-ocean contrast.

In this study we analyze the July air masses and frontal zones in North America using gridded climate data. Previous studies of these air masses, such as Bryson (1966), were completed in the 1960s when available climate data were sparsely distributed and computers and software were limited, so much analysis was done by hand. The increased computing resources and availability of more data, including reanalysis products, permit a more detailed analysis of the variability of the frontal zone and its relation to the major vegetation zones. We identify the July Arctic and Pacific fronts for each year of the reanalysis periods (both ERA-40 and NNR) using the wind streamline confluence method. In this way, the variability of the position of the front for 1948 to 2007 will be shown, along with the mean values for certain averaging periods. Using this approach, we can investigate the question of whether the latitudinal position of the July Arctic front is more variable in Eastern versus Western North America.

Next, the relationship between the atmospheric circulation patterns such as the Arctic Oscillation and Southern Oscillation Index and the position of the front will be examined. The front is a synoptic feature and these are part of the general atmospheric circulation so any changes in the circulation should be reflected in changes of the position of the front.

Finally, the link between the productivity of the vegetation and the major air mass distributions will be examined using the relation between the frontal zones and Normalized Difference Vegetation Index gridded datasets. Since vegetation transitions are associated with transitions between air masses (Bryson, 1966), it is expected that when the front is North (South) of the mean position, the productivity of the vegetation in the anomalous region should be greater (lower), because of a warmer (cooler) air mass present. This study provides a method to analyze large-scale climate change impacts on vegetation.

Data & Methods

The data used in this study are the ECMWF ERA-40 and NCEP/NCAR reanalysis products, both of which supply a uniformly-derived dataset of the three-dimensional structure of the atmosphere. Other datasets used include teleconnection time series from various sources and Advanced Very High Resolution radiometer (AVHRR) Global Inventory Modeling and Mapping Studies (GIMMS) Normalized Difference Vegetation Index (NDVI) data. The availability of these data permits objective analysis of the interannual variability of the Arctic front in relation to vegetation and climate changes.

The NCEP/NCAR reanalysis (R-1; Kalnay *et al*, 1996; Kistler *et al*, 2001) is a 2.5 degree gridded dataset produced four times daily at 00Z, 06Z, 12Z and 18Z by the National Oceanic and Atmospheric Administration (NOAA) / Oceanic and Atmospheric Research (OAR) / Earth Systems Research Laboratory – Physical Sciences Division (ESRL PSD) at Boulder, Colorado and spans the period from 1948 to present. Monthly mean u and v wind component data (1948–2007) for this study were obtained from the NCEP/ NCAR Reanalysis Project.

The ERA-40 reanalysis (Uppala *et al*, 2005) is a 2.5° gridded dataset completed by the European Centre for Medium-Range Weather Forecasts (ECMWF) and contains results for September 1957 to August 2002. The analyses are produced four times daily at 00Z, 06Z, 12Z and 18Z. Monthly mean u and v wind component data (1958–2002) for this study were obtained from the ECMWF data server.

Time series of the Southern Oscillation index (SOI) (Ropelewski and Jones, 1987) were obtained from the Climate Research Unit at the University of East Anglia, Norwich, UK. Data for the Arctic Oscillation (AO) (Trenberth and Paolino, 1980; Thompson and Wallace, 2000) were obtained from the Joint Institute for the Study of the Atmosphere and Ocean (JISAO; University of Washington and the National Oceanic and Atmospheric Administration).

In order to examine changes in vegetation productivity in relation to the air mass distributions, the GIMMS data set (Pinzon *et al*, 2005; Tucker *et al*, 2004; Tucker *et al*, 2005) was used. This is a NDVI product available for the period 1981 to 2003. The data have been corrected for calibration, view geometry, volcanic aerosols, and other effects not related to vegetation, and are derived from imagery obtained from the AVHRR instrument onboard the NOAA satellite series 7, 9, 11, 14, 16 and 17 (Global Land Cover Facility, 2008).

Surface (10 metre; from ERA-40) or 1000 mb (from NNR) wind component data were used to create mean streamline maps for July of each year using the Grid Analysis and Display System (Doty, 2001). The mean streamline map for July of all available years, the long term mean for 1958-2002, and groups of years (10 year intervals) were plotted, derived from both NNR and ERA-40 products. The location of the July Arctic and Pacific front was plotted based on a visual examination of the streamline confluence, and the July Arctic front latitudinal position extracted at 10° longitude intervals. The mean latitudinal position of the front was compared to the July AO and SOI values. Finally, GIMMS NDVI anomaly data were overlain on the Arctic front position from July of each year. The frequency distributions of the NDVI anomalies were extracted from polygons north and south of the position of the Arctic front for the particular year in relation to the long-term mean position, establishing a relationship between the front position and the vegetation productivity.

Results

The mean July streamline maps for the years 1958 to 2007, when both NNR and ERA-40 have data (Figures 6, 7) show the main synoptic features of North America during the summer. The two subtopical high pressure systems are visible, and there is also high pressure over the Beaufort Sea and low pressure systems over Northern Quebec and Baffin Island. Although there are some differences in the streamline maps of the two analyses (below), overall they are broadly similar.

To permit comparison of this analysis with the results of Bryson (1966), a map using NNR data from the years 1948-1957, the same years used in the older study was prepared (Figure 8). The major confluence zone across Canada is located further to the north in the 1948-1957 map than in the 1958-2007 map, but again, the major synoptic features are similar in both maps. This confluence zone is seen in all analyses, including older ones mapped by Reed (1960) and Bryson (1966), where they are comparably located in the Mackenzie region (Figure 9).

The boundary between the air masses formed by the two subtropical highs is called the Pacific front. The Pacific front separates mT from Continental Tropical (cT) air and mP from mT air further north. In some years mP air can extend as far east as central Quebec. The position of the Pacific front in July averaged for the years 1958 to 2002 derived from the NNR extends from Mexico into the Great Plains, where there is a bend to the east in central Canada (Figure 9). The Pacific front ends over Quebec where it is south of the Arctic front. The position of the July Pacific front derived from ERA-40 is slightly to the south and west of the position derived from NNR.

The July Arctic front separates Continental Polar (cP) air from Maritime Polar (mP) and Maritime Tropical (mT) air (Figure 7). The July Arctic front extends across the Northern Boreal region of North America reaching its most southerly latitude in Northern Ontario. The Arctic front position derived from the NNR for 1948-1957 (blue line in Figure 9) is further to the north in Central and Eastern Canada for the 1948-1957 period versus the NNR derived 1958-2002 period (yellow line in Figure 9). The NNR derived July Arctic front (gold line) is almost completely within the modal frontal location of Bryson (1966) (hatched area in Figure 9) and close to Bryson's mean position for 1948-1957 (light purple line in Figure 9). It is also close to the July Arctic front position identified by Reed (1960) except over Ontario and Quebec (dark purple line in Figure 9).

The location of the July Arctic front depends on the prevailing synoptic conditions over the course of the summer. There is considerable spatial (west to east) and temporal variability of the latitude of the July Arctic front (Figure 10), but no obvious temporal trend for the mean latitudinal position averaged across all longitudes.

The temporal variability was analyzed by plotting the latitudinal position of the front where it intersects every ten degrees of longitude for every July (Figure 11 and 12), as well as averaged over all longitudes. A smoothed time series plot of the mean July Arctic front position as a function of longitude shows less temporal variability between 140° W to 160° W (Figure 11). Although there is no temporal trend at the far eastern and western longitudes, there is a suggestion of a slight southward (northward) trend in west-central (east-central) Canada from 110° W to 130° W (70° W to 90° W).

The spatial variability was quantified by computing the standard deviation of the latitude, where the front intersects a given longitude, for all years of the reanalysis period. There is a higher standard deviation in Eastern North America than in the west (Table 3). Over Alaska and the Yukon, the front is close to the Arctic coast and shows much less north-south variability in position (Figure 11).

There is an interesting trend in the change in the mean July Arctic front position (by longitude) through time. At 160^{o} W the mean position of the front shows increasing latitude through time, although the slope of the regression is overly influenced by two years in the 1960s when the front was quite far south (Figure 12). At 150^{o} W the mean position of the front shows almost no change in latitude (Figure 12). At 140^{o} W and 130^{o} W there is a trend for strongly decreasing latitude and at 120^{o} W and 110^{o} W the decreasing trend is slight (Figure 12). At 100^{o} W and 90^{o} W there is almost no change in latitude (Figure 12). At 80 ^{o} W and 70^{o} W there is a trend for slightly increasing latitude, and finally at 60^{o} W there is a trend for strongly decreasing latitude (Figure 12). When averaged over all longitudes, there is a slight decreasing slope through time, but this value is not statistically significant (Table 2). In several of the longtudes where the overall trend is southward through time, there is an increase in the last few years (e.g., 110^{o} W, 100^{o} W. 140^{o} W; overall average; Figure 12). The only trend that is statistically significant at the 95% confidence level is the southward trend of the front position at 130^{o} W (Table 2).

The range in the location of the mean monthly July Arctic front position for several decadal averaging periods is shown in Figure 13. The range of values is lower in Alaska in most decades than across Canada. In Eastern and Central Canada the range of values is larger. There is similarity between the periods

1948-1957 (Figure 13a) and 1958-1967 (Figure 13b), and between 1968-1977 (Figure 13c) and 1978-1987 (Figure 13d). There is greater difference between 1988-1997 (Figure 13e) and 1998-2007 (Figure 13f) since the range of front positions in the latter period is narrower and further to the north. The mean position averaged across all longitudes (Table 4) varies by only about two degrees over the period of 1948 to 2007, which shows significant variability.

The position of the Pacific front is less variable than that of the Arctic front especially south of 40° N (Figure 14). In July of most of the years the front curves toward the Northeast in the Northern Plains. This is consistent with the streamline maps showing mP air from the Pacific penetrating well eastward into Ontario and during some years, as far east as Central Quebec.

Changes in the location of the frontal zones and extent of the major air masses are a reflection of changes in the general circulation. One method to summarize this is by relating the position of the front to the major teleconnection patterns. Atmospheric teleconnections are described in Barnston and Livezey (1987) and include the Arctic Oscillation (AO) (Thompson and Wallace, 1998) and the Southern Oscillation Index (SOI) (Ropelewski and Jones, 1987), should be associated with changes in the location of the frontal boundaries as these are defined by variations in the strength of the circulation, which also affects the location of the frontal positions. The SOI is a component of the El Niño Southern Oscillation (ENSO), along with sea surface temperature anomalies in the Niño 3.4 region, bounded by 120° W to 170° W and 5° S to 5° N (Trenberth, 1997). In this study the front position was examined in relation to the AO and SOI since these teleconnections had the most significant correlations with the front position anomaly through time (Table 5). Correlations with other teleconnections such as the Pacific Decadal Oscillation (PDO) (Mantua and Hare, 2002), North Atlantic Oscillation (NAO) (Hurrell, 1995), and the Pacific / North American (PNA) (NOAA, 2008c) pattern were not significant at the 95 % confidence interval (Table 5).

When the SOI is negative (positive) the front is often further south (north) (Figure 15-16). When the AO is negative (positive) the front is often further south (north) (Figure 17-18). The association between the mean July Arctic front position was stronger with the AO (figure 19) than the SOI (Figure 16). The five years (July 1954, 1967, 1989, 1964, 1981) with the largest positive mean latitude anomalies were all months when the AO was significantly positive and they were also all months when the SOI was positive, except for 1967 (neutral SOI). The five months (July 1972, 1987, 1977, 1950, 1996) with the largest negative mean latitude anomalies were all months when the AO was significantly negative, except for July 1996 (positive AO) and they were also all months when the SOI was negative, except for July 1950 (no data) and 1996 (positive SOI).

The impact on these atmospheric teleconnections is shown in diagrams of the front position relative to the long term mean. In July 1968 (Figure 19a) and July 1993 (Figure 19d) the front was mostly south of the mean position. In July 1970 (Figure 19b) the front was close to the mean position. Finally, in July 1989 (Figure 19c) the front was well north of the mean position.

To study the relationship of the frontal zones with the vegetation, we located the position of the July Arctic front on a map of the NDVI for each year between 1981 and 2001, the years where the NDVI dataset overlaps with the NNR and ERA-40 and a front could be identified. For each year, polygons were identified by overlaying the Arctic front position of that year with the mean position, and noting areas north or south of the mean. The frequency of NDVI anomalies was computed for all areas north or south of the mean for each year of the NDVI product using front positions derived from both NNR and ERA-40. If the front was north (south) of the long term mean position then the polygon extended south (north) from the front to the long term mean front.

The map of July 1993 (Figure 20c) is an example where the association between the air mass and the primary productivity of the vegetation is particularly striking. In that year, the Arctic front was located well to the south of the mean position in much of western Canada, and was located north of the position in Quebec and Labrador, and this seems to be associated with a higher frequency of negative and positive NDVI anomalies respectively. Figure 20a shows July 1985 when the Arctic front was located near the mean position, and there seems to be generally more positive anomalies to the south of this position than to the north. In July 1989, the front was located to the north of the mean across all longitudes, and in that month much of northern Canada had positive NDVI anomalies (Figure 20b). In 1999, the situation was similar to that of 1993 (Figure 20d). In this year, the boreal forest had negative NDVI anomalies in the region where the front was to the south of the mean position, but the tundra was relatively productive.

The results for the total of all areas north and south of the mean July Arctic front position (derived from both NNR and ERA-40) are summarized in Table 6. There is a higher frequency (greater than 50%) of positive (negative) vegetation productivity anomalies for all areas north (south) of the mean July Arctic front position as would be expected (Table 6). The results for the change in NDVI anomaly frequency from polygons based on the Arctic front position derived from NNR for July 1981 to July 2003 are shown in time series plots (Figures 21 and 22). The time series plots for ERA-40 show similar results (not shown).

Although the location of the July Arctic front derived from ERA-40 is slightly further to the south of the position derived from NNR, in most years, the locations are comparable (Figure 23). This may be due to the observations used in the model to produce the reanalysis products. More likely it is due to the underestimation of wind speed in areas of higher wind speed (ECMWF, 2004), which was also an issue in the previous ERA-15 reanalysis for 1979 to 1993 (Sterl and Komen, 1998). Mean July streamline plots derived from ERA-40 produced show lower wind speeds in areas of high wind speed compared to the NNR streamline plots. It is possible that the weaker circulation modeled by the ERA-40 results in a southward displaced position of the July Arctic front.

Discussion

In this study, July air mass boundaries in North America were studied through the analysis of surface wind streamline maps derived from NNR and ERA-40 products. Synoptic features such as the subtropical highs and subpolar lows are visible on the mean plots. The position of both the July Arctic and Pacific fronts was plotted using the streamline confluence method.

There is high interannual variability in the position of the July Arctic front over Central and Eastern Canada. Some of the extreme positions of the July Arctic front occurred in July 1989 (Figure 19c) and 1993 (Figure 19d). In July 1989 the front was significantly far to the north and much shorter, possibly due to the strongly positive AO and SOI. In July 1992 and 1993 the front was significantly far to the south, except over Alaska and Quebec. 1992 was slightly cooler globally due to the eruption of Mount Pinatubo in 1991 (Hansen *et al*, 1992), showing that cooler conditions are associated with a front position further to the south. The changes in the position of the Arctic front when averaged over a decade are less significant but in cooler periods such as 1968-1977 (Figure 13c), the front is generally located more to the south than warmer periods such as 1998-2007 (Figure 13f).

The spatial variability of the Arctic front, quantified as the standard deviation of the latitudinal position of the front at longitudinal intervals from 160 to 60ºW for the period of 1948 to 2007, is greater in Eastern than Western North America. Over Alaska the variability of July Arctic front positions is small. This is consistent with a study by Lynch *et al,* (2001) which concluded that the front over

Alaska is anchored by topography such as the Brooks Range and the land-sea contrast. There is almost as much variability in the position of the Arctic frontal zone over Central Canada as in Quebec. Over Central and Eastern Canada the land/sea contrast is less important, except near Hudson Bay. There are some topographic influences on the vegetation transition zone in Quebec and in Central Canada, which were noted by Barry (1967) and Timoney (1992). Although the large range of front positions in Central and Eastern Canada may be due to the wide vegetation transition, it could also be due to the variability of synoptic features such as the Baffin low. In years where this low pressure is further to the northwest, the front has more of a SW to NE orientation. Consequently, when the low is further to the southeast over Quebec, the front has a more zonal orientation. Bryson (1966) noted that there were more air masses present in Quebec in July than over North Central Canada, which was his reasoning for not extending the front into Quebec. The air masses present over Quebec in July are mT, mP, cP, and possibly mA, which is likely cA air from the ice caps of Baffin Island, modified by its passage over the Hudson Strait. Over North Central Canada the only air masses present in July are cP and mP.

Our composite map (Figure 9) shows that the 1948-1957 position of the July Arctic front (derived from NNR) is slightly further to the north than Bryson’s position for the same period. Therefore it is possible that Bryson’s mean July Arctic front may have been positioned too far to the south in this region or the position derived from reanalysis data is too far north. Several of the years, especially 1954 and 1957, have frontal positions that are much further north, which contributes to a mean position that is further to the north. Only a few years such as July 1948 and 1950 had a front position located further to the south. The position of the July Arctic front found by Reed (1960) is different from that of Bryson but closer to the position found in this study, except to the east of Manitoba, where it is further south.

Atmospheric teleconnections contribute to the changes in the July Arctic front position. The most significant teleconnection patterns in relation to the July Arctic front are the AO and the SOI; the relationship between the July Arctic front position and other teleconnection patterns such as the PNA was less significant. One reason for the low correlation and significance of the PNA with the July Arctic front position is that the PNA pattern is present in every month except June and July (Barry and Carleton, 2001). A possible reason for the low correlation and significance of the front position with the PDO and NAO is that the centers of action for these patterns are located over the oceans. The July Arctic front is slightly further to the north (south) with the positive (negative) Arctic Oscillation and positive (negative) Southern Oscillation Index. A positive (negative) SOI is usually associated with La Niña (El Niño) conditions. A negative SOI may allow for a more meridional long wave pattern over North America (Barry and Carleton, 2001), causing the July Arctic front position to be located to the south. The significant negative correlation with sea surface temperatures (SSTs) in the Niño 3.4 region means that when the front is further north (south), SSTs in the Niño 3.4 region are colder (warmer) than normal.

July 1968, 1970, and 1989 illustrate particular synoptic situations that are the reflection of one or more atmospheric teleconnections. When the Beaufort high is strong, such as in 1968 (July AO index was negative; Figure 19a), the front is further to the south in central Canada than when the feature is weak as in 1970 (July AO index was positive; Figure 19b). A strong Beaufort high is implicated in the record minimum sea ice extent for the Arctic that occurred in September 2007 (Levinson and Lawrimore, 2008). A negative AO, such as occurred in July 1968, usually allows cooler air to penetrate further south into the mid-latitudes of North America (Hurrell, 1995), and we would therefore expect the July Arctic front to be located further to the south. One of the most northerly positions of the July Arctic front occurred in 1989 (Figure 19c), when the AO was strongly positive and the SOI was also positive.

Bryson (1966) and Hare and Ritchie (1972) noted the close association of the position of the July Arctic front with the transition between the major biomes. However, this association does not explain possible causal mechanisms; for example, the type of air mass should affect the actual primary productivity of the vegetation. The relationship between air mass and biome boundaries is not always precise as there are local climate effects such as colder bodies of water and topographic changes that can modify the boundaries of a biome. For example, a change in topography results in a sharp vegetation transition from Boreal forest to tundra in the region to the NE of Great Slave Lake (Timoney, 1992).

The position of the July Arctic front, and hence the type of air mass present, affects the primary productivity of the vegetation. The air mass present in other months leading up to July (such as May and June) could also affect the vegetation since there are lags in the climate-vegetation response. A cooler and drier (warmer and moister) air mass in the spring/early summer could reduce (increase) July vegetation productivity. The results of July could also apply to other months such as June and August. When the July Arctic front is located further to the north there are warmer and moister air masses (mP, mT) present that cause the tundra to be more productive. Conversely, when the July Arctic front is further to the south there are cooler air masses (cP) that cause the boreal forest to be less productive. This is evident in the trend of increasing frequency of positive (negative) NDVI anomalies, when the front is further to the north (south) (Figure 21 and 22). Both the frequency of NDVI anomalies obtained when using NRR and ERA-40 derived July Arctic front positions show a similar result of vegetation productivity (Table 4).

A study by Verbyla (2008) showed the tundra to become more productive whereas the boreal forest became less productive in a warming climate. This is illustrated in NDVI anomaly maps for certain years such as July 1989 (Figure 20b). One question that remains to be answered is to what degree the July Arctic front controls the position of tree line or vice–versa (Pielke and Vidale, 1995), and this could be answered through modeling studies where a regional atmosphere-ocean general circulation model is coupled with a vegetation model. If the July Arctic front is controlled by vegetation transitions to some degree, then it is possible we have yet to see the northward shift of the Arctic front until the tree line shifts north. However, the lag in the shift of the boreal forest northward relative to climatic warming could be a few hundred years (MacDonald *et al*, 2004).

The July Arctic front is roughly located along the Northern edge of the Boreal forest as was found by Bryson (1966). The mean position of the front for 1948-1957 derived from NNR is situated at the northern edge of Bryson's modal frontal zone. It should be noted that Bryson's mean position is located slightly far to the south to be considered "along the Northern edge of the Boreal forest". However, the close similarity of our results to Bryson's (1966) is striking, given that the Bryson study was completed over 40 years ago, with limited climate station data and hand drawn streamlines. The front has been extended into Quebec and the position found by the authors is reasonable given the streamline maps, the synoptic controls on the front, and the position of tree line.

It has been shown that climate warming has a significant impact on temperature and precipitation, especially at the high latitudes (ACIA, 2005 and IPCC, 2007). With climate warming there should be a slight shift northward of air mass boundaries such as the Arctic front. The climate warming has shifted the front slightly north in eastern and central Canada but this is accompanied by a larger shift of the front further south at 130º W and 140º W. This oscillation has resulted in little overall change in the mean position of the July Arctic front until very recently. From this study the mean position of the July Arctic front shows very little change as derived from the NNR (ERA-40) for the period 1958-2002.

There is a slight northward shift over Manitoba, but a slight southward shift in most other locations. More importantly, there is a northward shift of the front in the last part of the period visible in the loess smoothed time series plots (Figure 11). This demonstrates that we may start to see the northward shift of the front in the warming climate, perhaps during the next 50 to 100 years. However, the results should be interpreted with caution because of the length of the record and because changes in front position for most of the longitudes were not statistically significant at the 95% confidence level.

It is uncertain how climate warming impacts the Pacific front although mT air from the south could penetrate further north but not much further to the west. To the extent that the front is determined by the production of cT air over the deserts of southwestern United States and northwestern Mexico, warmer conditions could produce even more cT air and shift the frontal zone to the east. There is the topographic control of the Rocky Mountains which anchors the front in the south central USA, not allowing it to shift much further to the west. There are some years with the front with a bend to the NW rather than the NE. These are years where it is likely the mP air did not penetrate nearly as far east, possibly due to the strength and position of the NE Pacific subtropical high.

This study is an update upon the work of Bryson (1966) by providing the mean streamline maps for July with updated air mass boundaries using gridded climate data, examining the geographic and temporal variability of the July Arctic front, and relating the position of the July Arctic front to atmospheric circulation patterns and vegetation productivity anomalies. Future work would examine other summer months such as June and August for North America using the higher resolution North American Regional Reanalysis for the source of wind component data. The same work should be completed for the July Arctic front in Eurasia, which is similar to the front in North America.

Acknowledgements

This study was funded by the Natural Sciences and Engineering Research Council (NSERC) and the Polar Climate Stability Network (PCSN) project funded by the Canadian Foundation for Climate and Atmospheric Sciences (CFCAS).

Table 2. Results for linear regression fit to July Arctic front position by longitude.

Longitude	Equation (y =)	Std error of slope	R^2	P-value
160	-29.25 + 0.05x	1.15	0.1	0.09
150	62.16 + 0.003x	1.83	0.001	0.86
140	147.20 - 0.04x	0.83	0.04	0.24
130	198.50 - 0.07x	0.94	0.21	0.002
120	207.90 - 0.07x	0.44	0.05	0.14
110	247.50 - 0.10x	0.35	0.05	0.14
100	120.80 - 0.03x	0.40	0.007	0.57
90	109.10 - 0.03x	0.46	0.007	0.59
80	-14.78 + 0.03x	0.52	0.01	0.47
70	-10.52 + 0.03x	0.48	0.01	0.53
60	102.30 - 0.03x	1.61	0.04	0.27
60 to 160	145.30 – 0.04x	0.78	0.05	0.13

Table 3. Standard deviations of the latitude of the July Arctic front position for various longitudes. Period of record is 1958 to 2002.

Standard deviation	Longitude (^{o}W)								
	150	**140**	**130**	**120**	**110**	**100**	**90**	**80**	**70**
NNR	1.5	1.6	2.8	3.6	5.1	5.3	5.2	4.8	4.3
ERA-40	1.3	2.8	2.8	1.9	4.4	5.6	5.0	4.4	3.9

Table 4. Mean (averaged across all longitudes) July Arctic front position (derived from NNR and ERA-40) for ranges of years.

Period	Mean frontal position (°N) [NNR]	Mean frontal position (°N) [ERA]
1948-1957	61.3	N/A
1958-1967	59.6	61.2
1968-1977	60.0	59.3
1978-1987	61.1	59.0
1988-1997	59.4	59.1
1998-2007	60.1	N/A
1958-2002	**60.1**	**59.7**
1948-2007	**60.3**	**N/A**

Table 5. Correlations of July Arctic front position anomaly for 1958 to 2002 (derived from ERA-40) with atmospheric teleconnection data for July

	anomaly	AO	SOI	Niño34	NAO	PDO	PNA
Pearson Correlation	1	.45	.44	-.30	.23	-.17	-.02
Sig. (2-tailed)		.002	.026	.046	.119	.272	.886
N	45	44	45	45	45	45	45

Table 6. NDVI anomalies for areas north and south of mean July Arctic front position for July 1981-2003.

July	Total polygons	N or S of mean	Negative	Positive	Freq neg	Freq pos
All years (ERA-40)	51	South	249183	227155	52.3%	47.7%
	49	North	218612	333364	39.6%	60.4%
All years (NNR)	34	South	328565	279867	54.0%	46.0%
	42	North	177157	202421	46.7%	53.3%

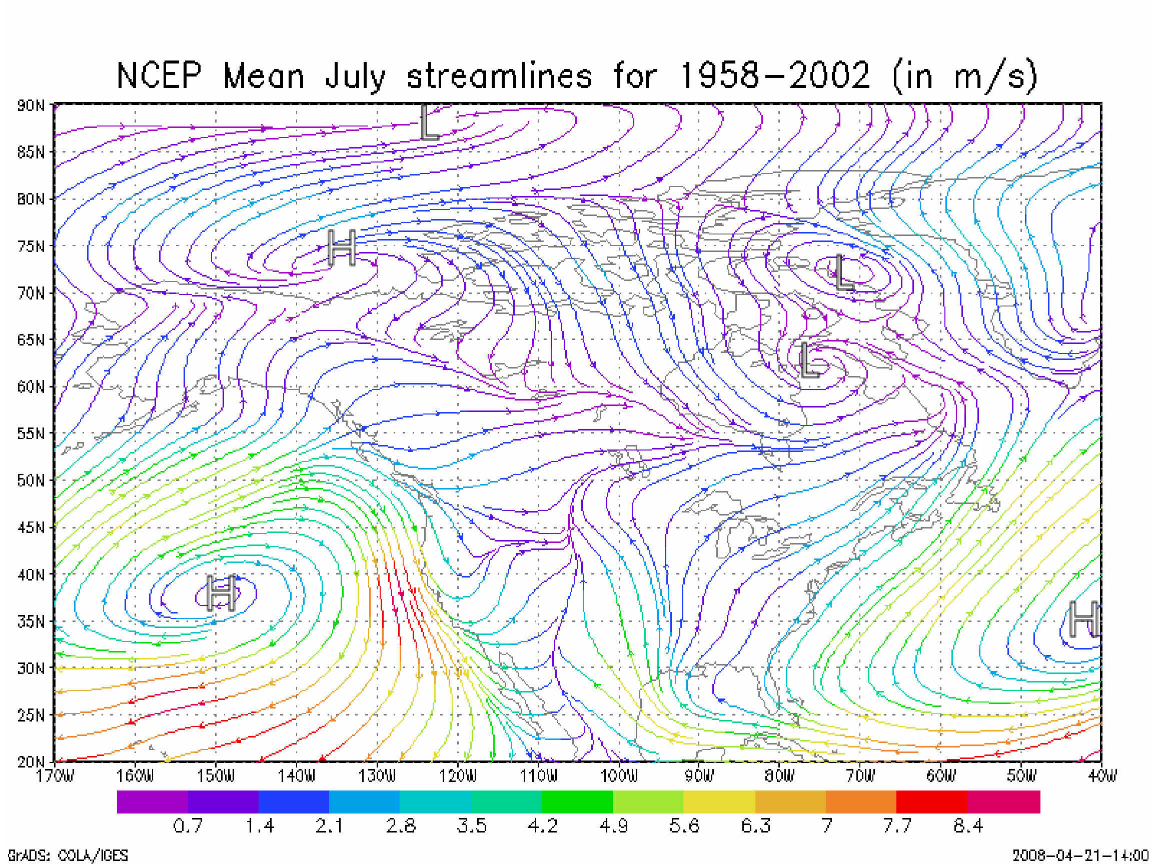

Figure 6. Mean 10m (surface) streamlines for July 1958-2002 derived from NNR with estimated positions of semi-permanent low and high pressure systems.

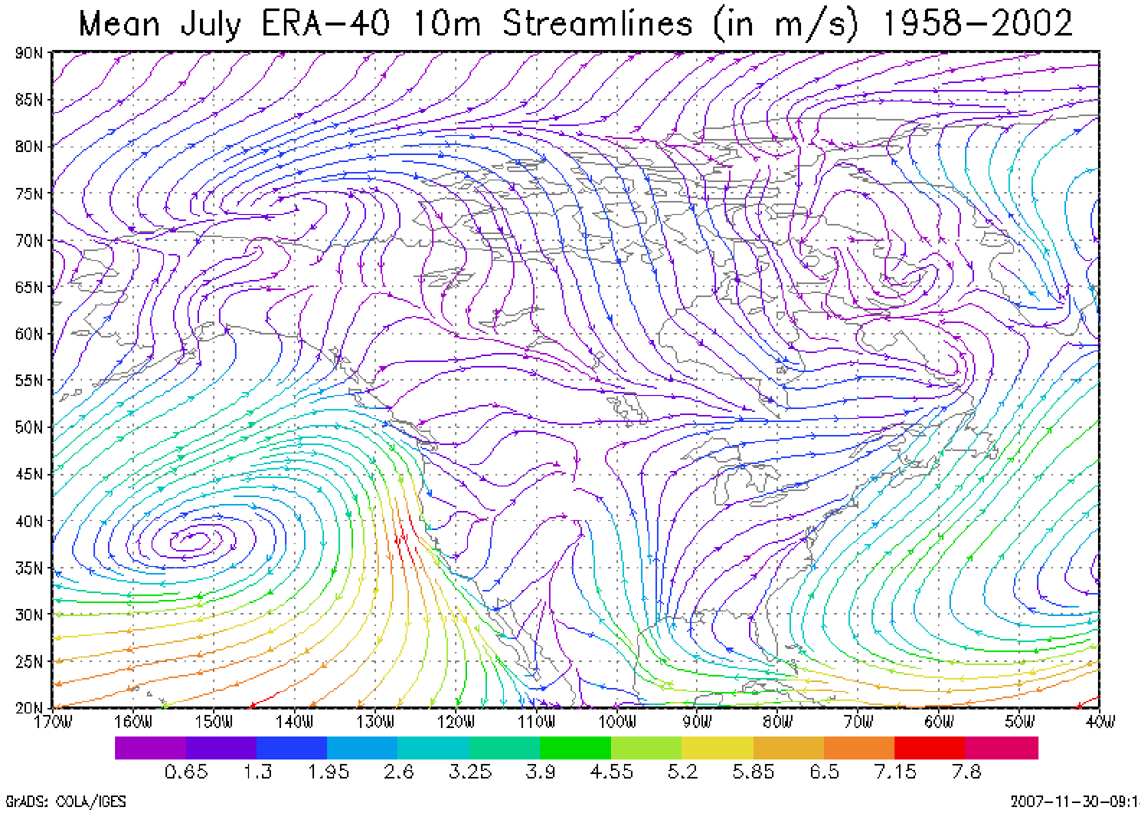

Figure 7. Mean 10m (surface) streamlines for July 1958-2002 derived from ERA-40.

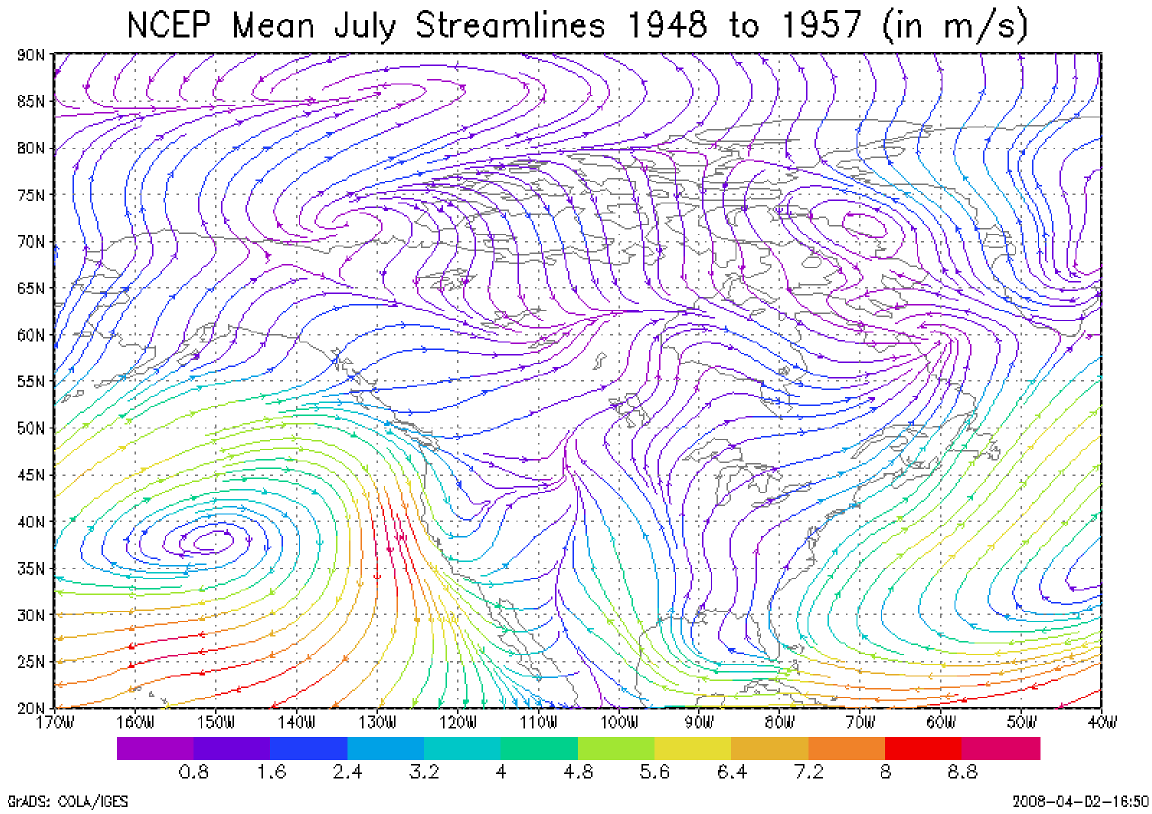

Figure 8. Mean 10m (surface) streamlines for July 1948-1957 derived from NNR.

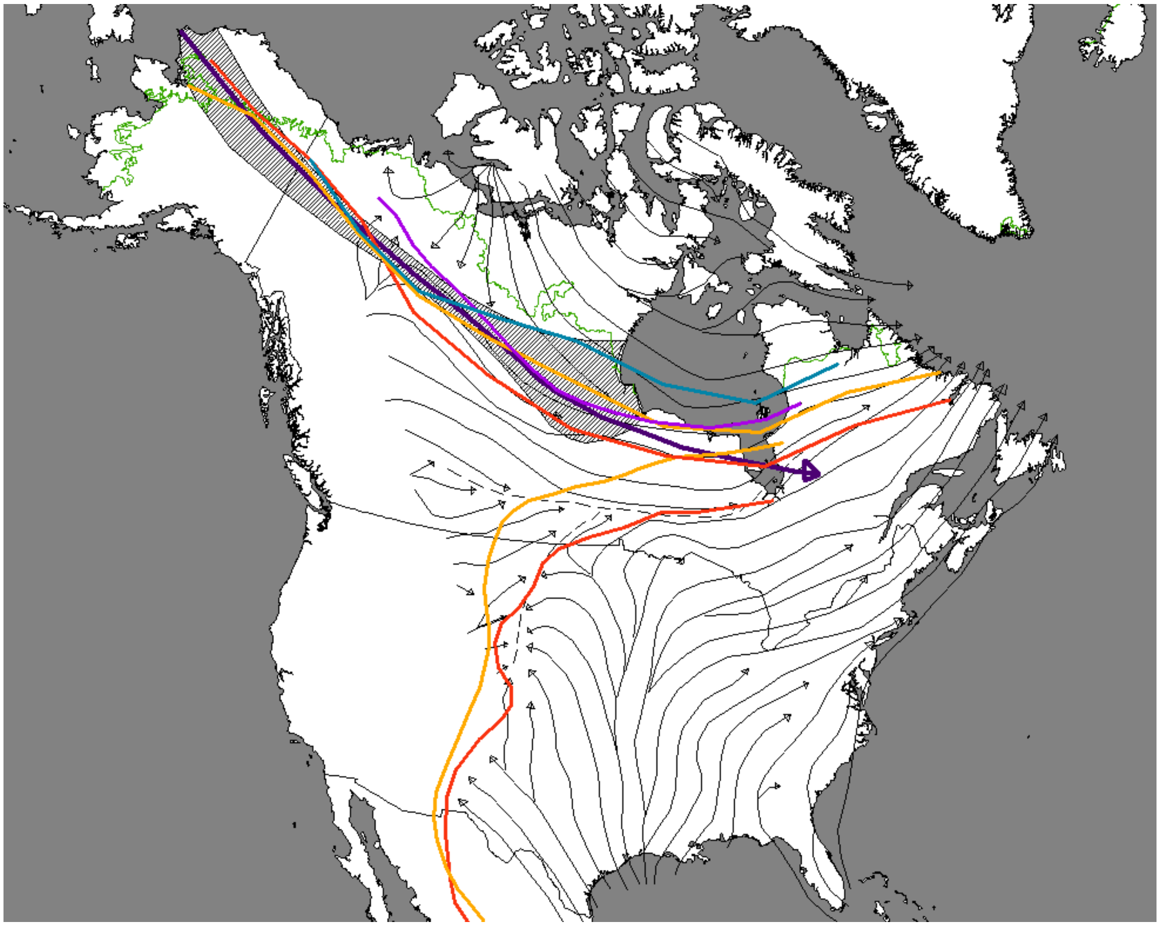

Figure 9. July Streamlines for 1948-1957 (adapted from Bryson, 1966) with frontal positions and tree line overlain. The hatched area depicts the modal July Arctic frontal zone as found by Bryson (1966). Green line – tree line from the CAVM project (CAVM team, 2003). Light purple line – mean position of the July Arctic front for 1948-1957 as found by Bryson (1966). Dark purple line – mean position of the July Arctic front as found by Reed (1960). Blue line – mean position of the July Arctic front for 1948-1957 derived from NNR. Gold lines – mean position of the July Arctic and Pacific fronts for 1958-2002 derived from NNR. Red lines - mean position of the July Arctic and Pacific fronts for 1958-2002 derived from ERA-40.

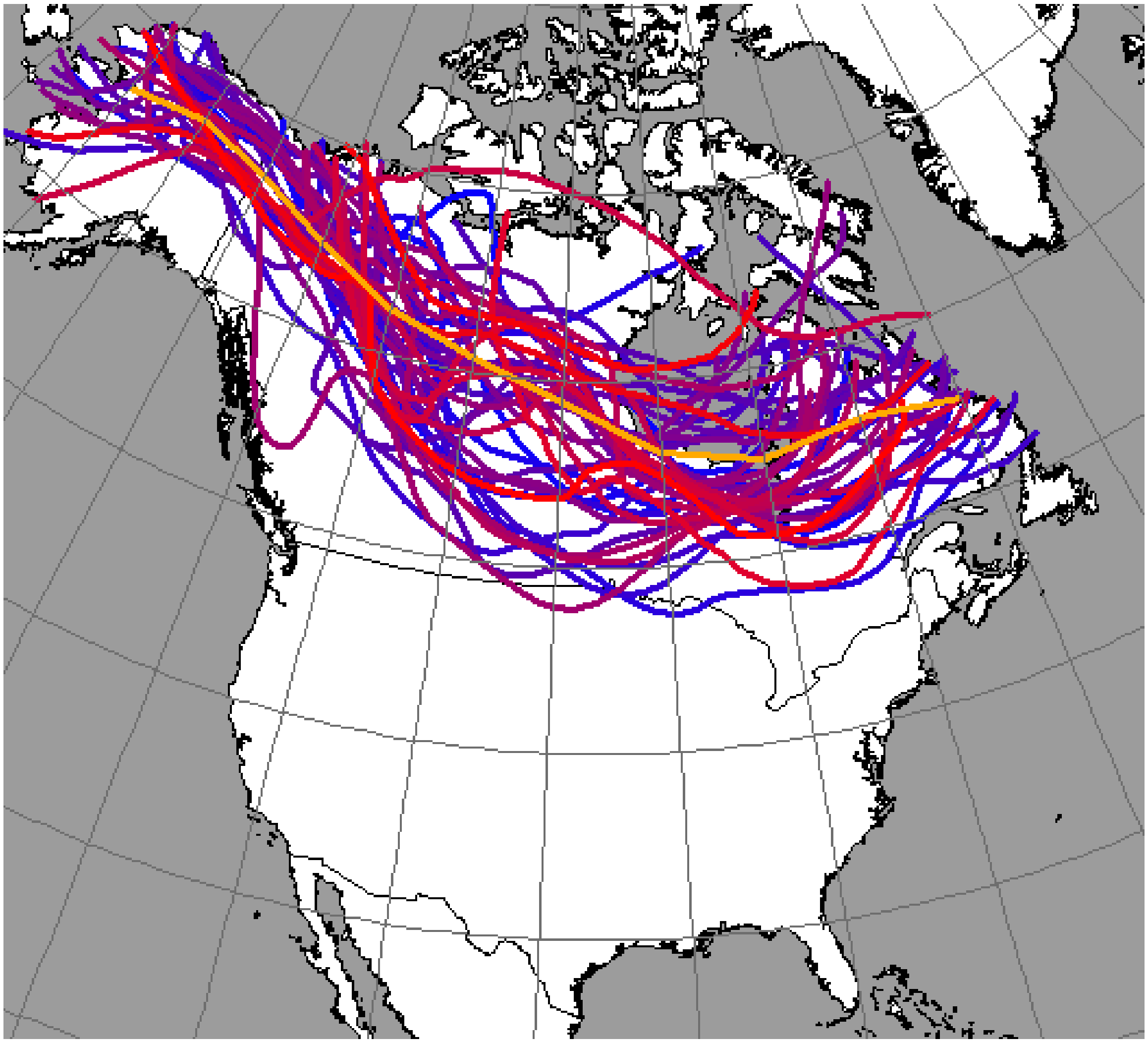

Figure 10. Position of July Arctic front for 1958-2002 derived from NNR; colours are from bright red (1958) to blue (2002), 1958-2002 mean is orange line.

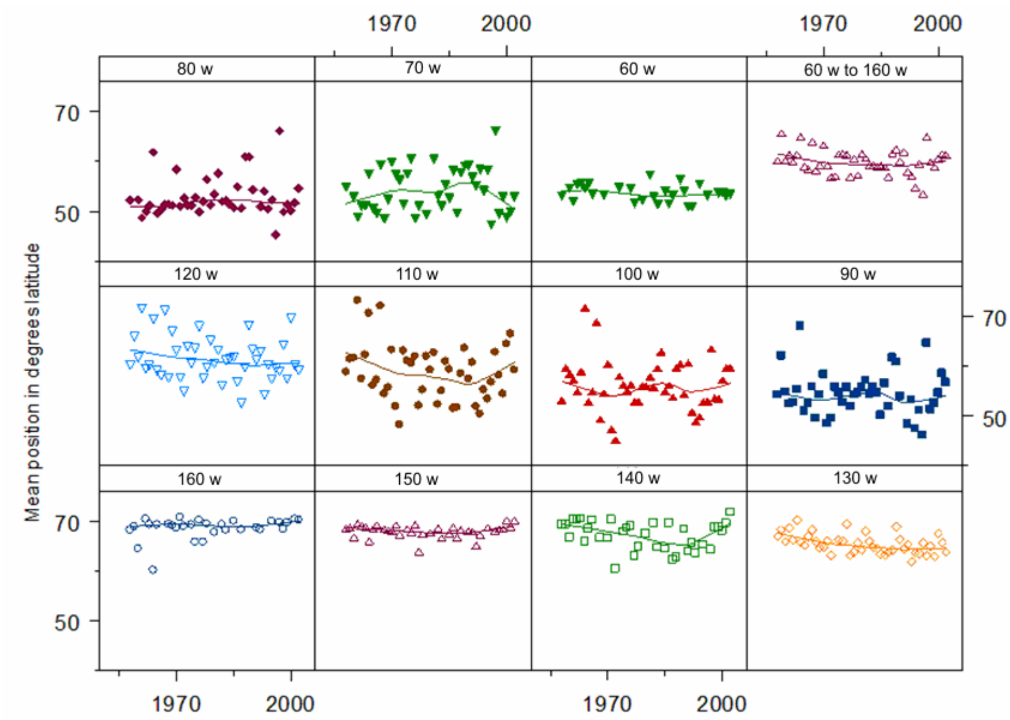

Figure 11. Mean position (loess smoothed) of July Arctic front for 1958-2002 (derived from ERA-40) at 10º longitude intervals (60°W - 60°W).

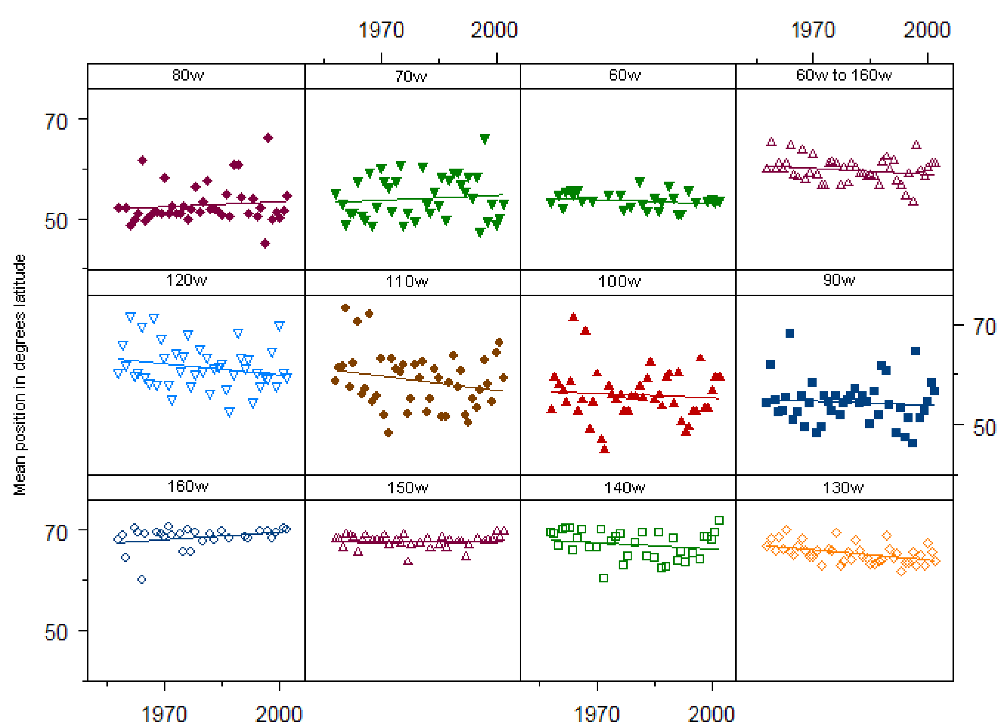

Figure 12. Mean position (trend) of July Arctic front for 1958-2002 (derived from ERA-40) at 10º longitude intervals (60°W - 160°W).

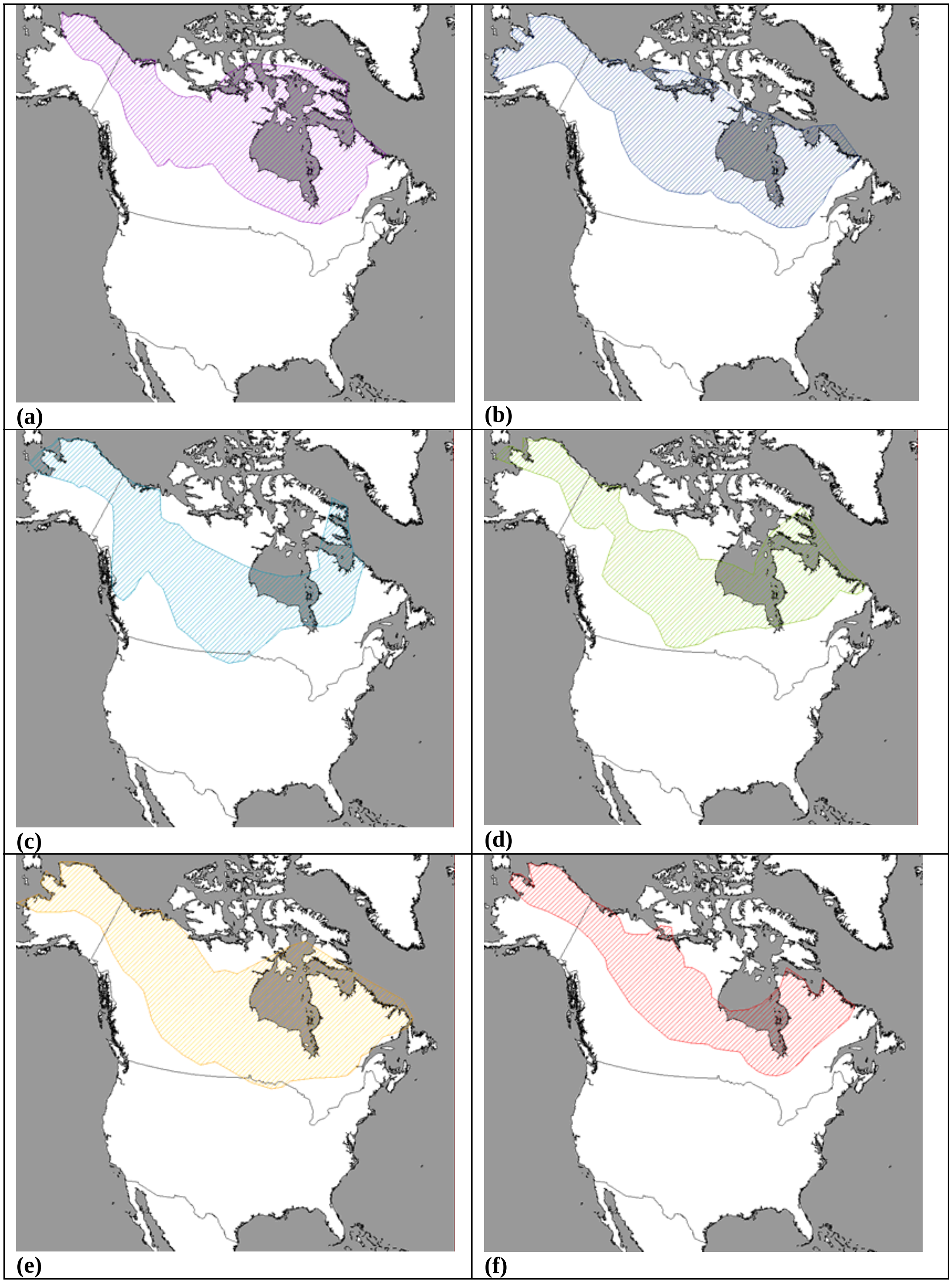

Figure 13. Range of July Arctic front positions are shown for (a) 1948-1957 (hatched purple area), (b) 1958-1967 (hatched dark blue area), (c) 1968-1977 (hatched blue area), (d) 1978-1987 (hatched green area), (e) 1988-1997 (hatched orange area) and (f) 1998-2007 (hatched red area).

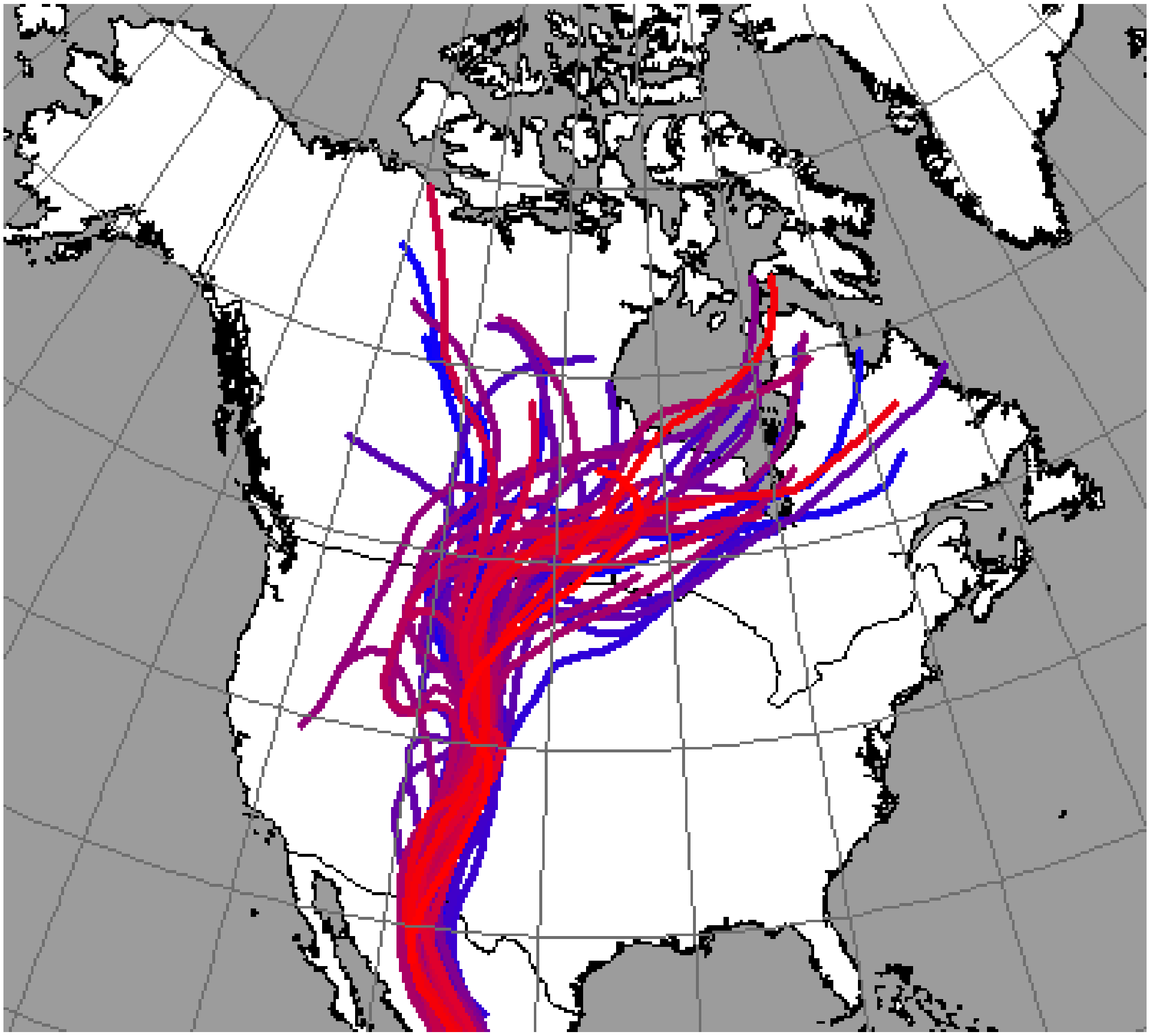

Figure 14. Position of July Pacific front for 1958-2002 derived from NNR; colours are from bright red (1958) to blue (2002).

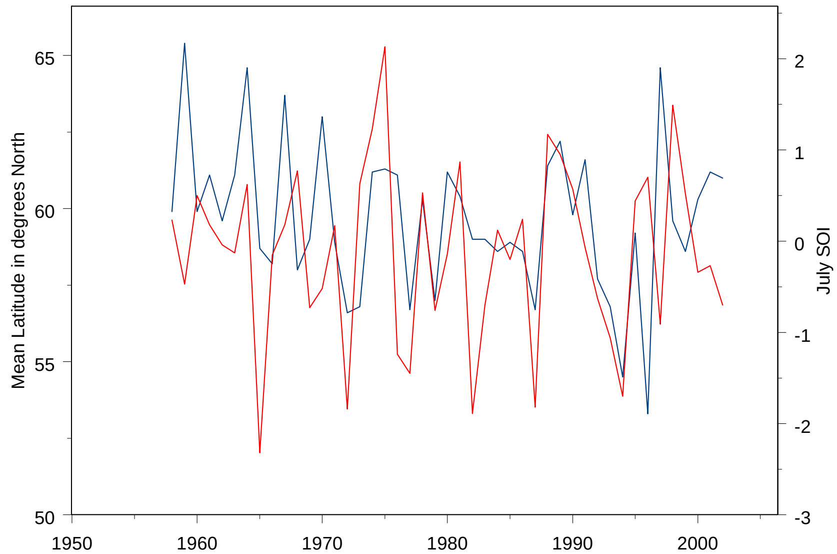

Figure 15. Average latitudinal position of the July Arctic front (in °N) 1948-2007 derived from ERA (blue) compared to the July SOI (red).

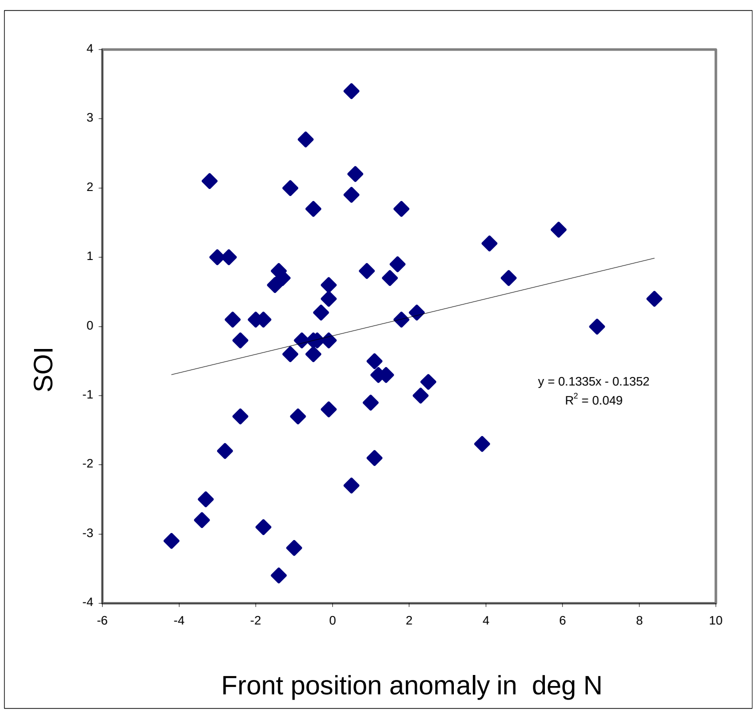

Figure 16. July Arctic front position anomaly (in °N) versus July SOI.

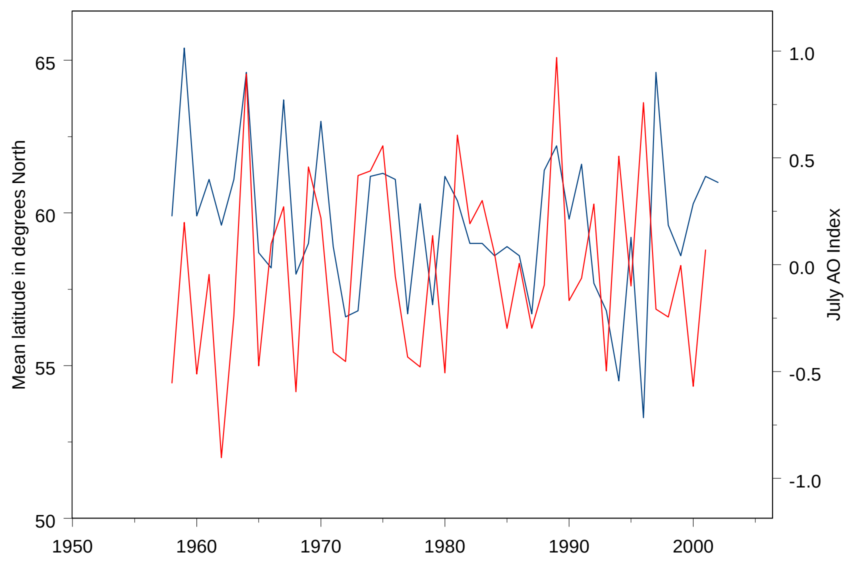

Figure 17. Latitudinal position of the July Arctic front (in °N) 1948-2007 derived from ERA (blue) compared to the July AO (red).

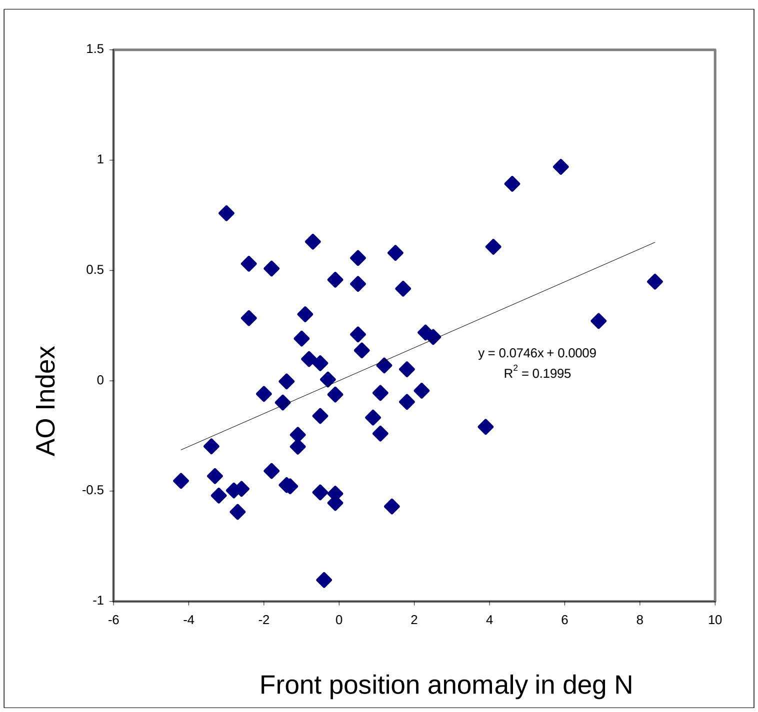

Figure 18. July Arctic front position anomaly (in °N) versus July AO Index.

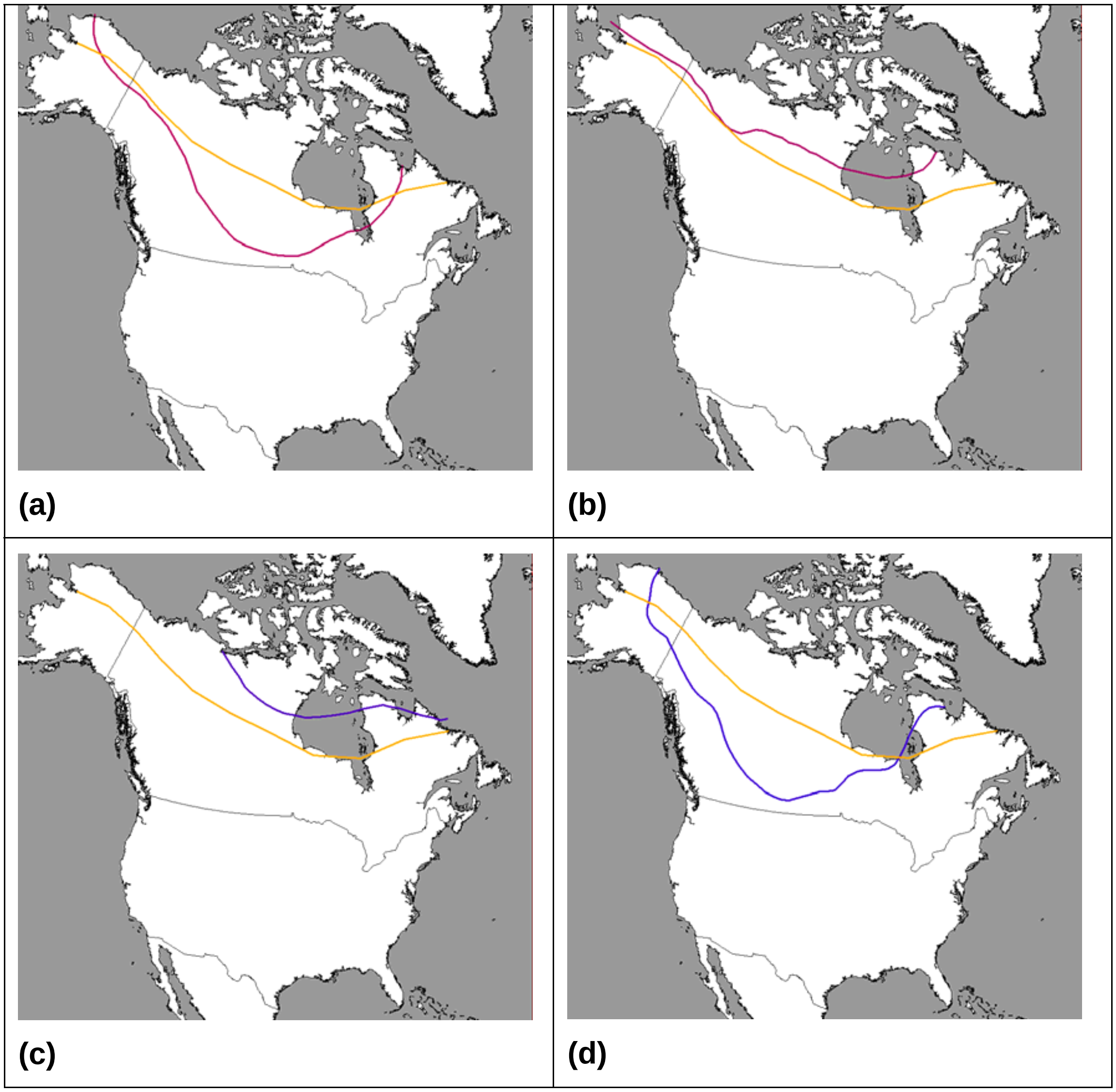

Figure 19. Position of July Arctic front for (a) 1968 (dark red), (b) 1970 (dark red), (c) 1989 (purple), and (d) 1993 (purple) compared to long term mean position (orange) (both derived from NNR).

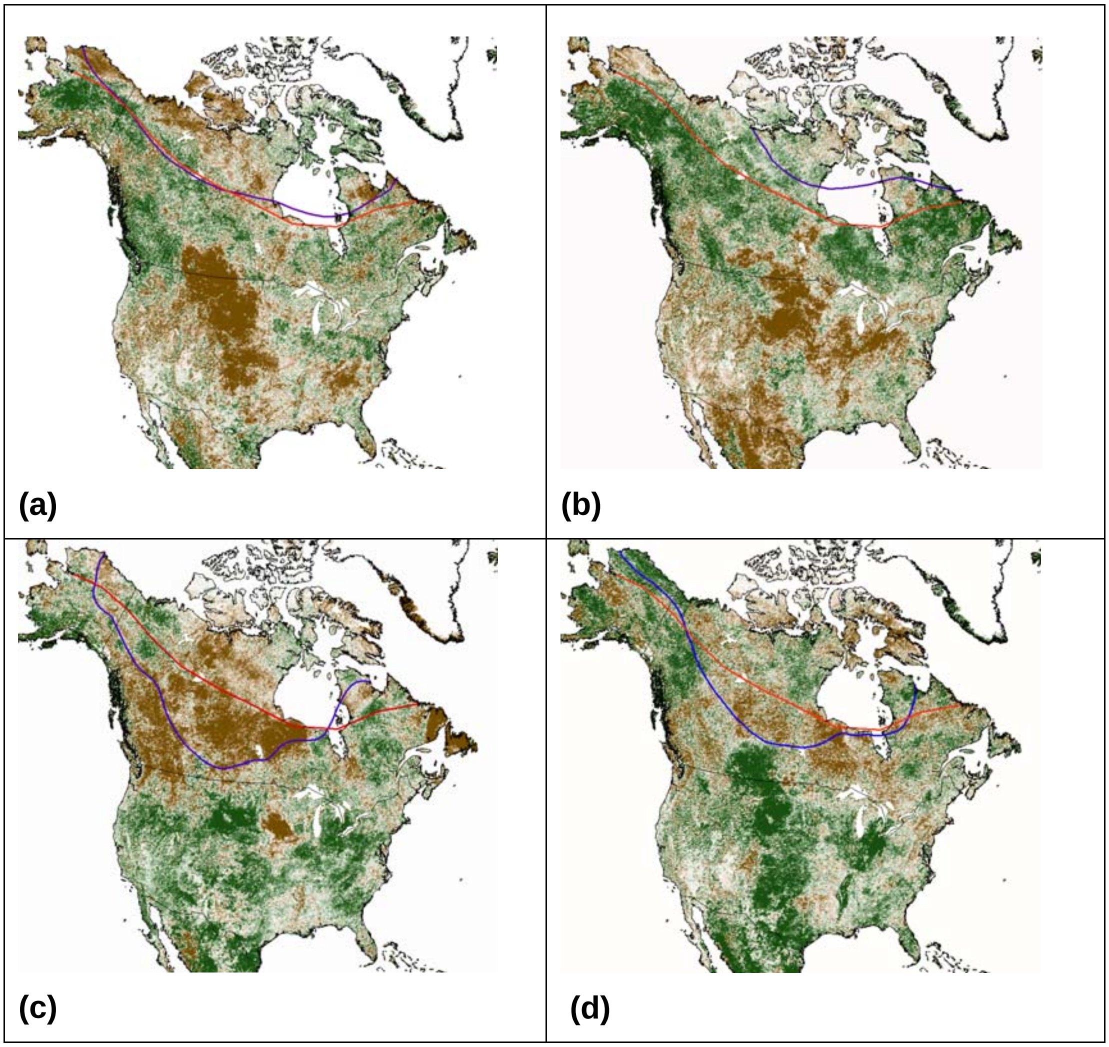

Figure 20. NDVI vegetation anomaly map (relative to July 1981-2003 mean) for (a) July 1985 front position (purple line), (b) July 1989 front position (purple line), (c) July 1993 front position (purple line), (d) July 1999 front position (blue line) and long term mean position (red line). Anomalies are dark green representing the largest positive anomalies (most productive) to brown representing the largest negative anomalies (least productive). White areas represent an anomaly of zero.

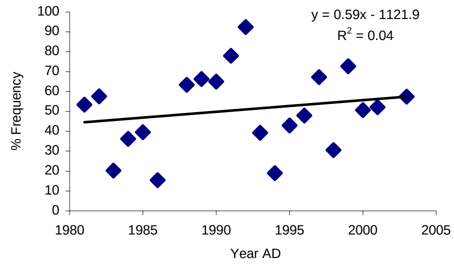	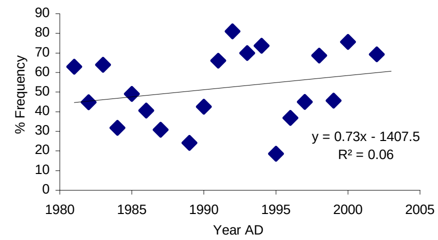
Figure 21. Percent frequency of positive NDVI anomalies of polygons north of NNR derived mean front for each year (p=0.40).	**Figure 22**. Percent frequency of negative NDVI anomalies of polygons south of NNR derived mean front for each year (p=0.28).

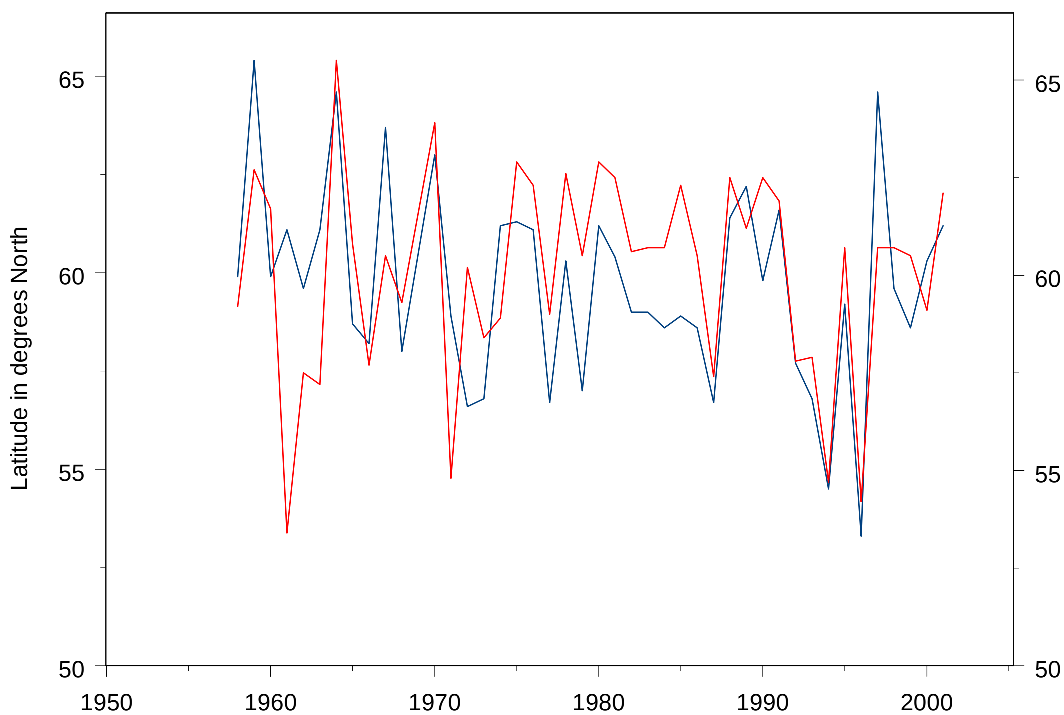

Figure 23. Time series of mean July Arctic front position in °N (averaged across 10º longitude intervals) derived from NNR (red) versus ERA-40 (dark blue).

Chapter 4

4.0 Thesis Summary

In this study, maps of July air mass boundaries in North America have been analyzed through the production of mean surface wind streamline maps in GRADS using data derived from NNR and ERA-40 products. The position of both the July Arctic and Pacific fronts was plotted using the streamline confluence method and analyzed both quantitatively and qualitatively. Finally the front position was compared to both atmospheric teleconnection patterns and the vegetation productivity anomalies derived from NDVI data.

The July Arctic front for the period of 1958 to 2002 is generally located along the northern edge of the Boreal forest and is similarly positioned to that of Bryson (1966) for 1948-1957. This is remarkable, given that Bryson's (1966) study was completed over 40 years ago, with limited climate station data and hand drawn streamlines. However, our analysis of the 1948 to 1957 July Arctic front position (derived from NNR) is further to the north than Bryson's (1966) position. Therefore it is possible that his July Arctic front position may have been located too far to the south. It is also possible that the position of the front derived from reanalysis data may be too far to the north. Finally, the position of the July Arctic front derived from ERA-40 is slightly further to the south of the position derived from NNR (Figure 24), most likely due to the underestimation of wind speeds in areas of high wind speed by the ERA-40 model.

The north-south variability of the front was examined both spatially (East-West) and temporally (individual years, 10 year periods, and all years of both reanalysis products). The spatial variability of the Arctic front, quantified as the standard deviation of the latitudinal position of the front at longitudinal intervals for the period of 1948 to 2007, is greater in Eastern/Central versus Western North America. There is a trend toward a more narrow (wider) range of July Arctic front positions in Western (Central/Eastern) North America. The temporal variability is not as clear since the interannual variability of the front position is large yet the mean position of the front from 1958 to 2002 shows almost no systematic change. This may be due to oscillation in frontal position shifts depending on the longitude, although only the trend at 130º W is significant.

There is significant interannual variability in the position of the July Arctic front. The July Arctic front is slightly further to the north (south) when the Arctic Oscillation and Southern Oscillation are both positive (negative). The weaker and more meridional atmospheric circulation when the AO and SOI are negative may cause the front position to be further to the south than normal. Other atmospheric teleconnection such as the NAO, PDO, and PNA were not significantly correlated with the July Arctic front position.

The position of the July Arctic front, and hence the type of air mass present, affects the primary productivity of the vegetation, with a higher frequency of less (more) productive vegetation when the front is further to the south (north), because of a cooler (warmer) air mass present. There is a slight trend for an increasing frequency of positive (negative) anomalies when the front is to the north (south) of the long-term mean position. This was shown with NDVI anomaly maps for July (selected years) with the front positions shown and the time series of NDVI frequencies for the areas of interest. There is likely some relationship between the air masses in spring months and the July vegetation productivity anomalies because of lags in the response of vegetation to climate. The frequency of NDVI anomalies should be tested with a Monte Carlo simulation to determine if the frequency of these anomalies is not simply random variation.

Although the position of the July Arctic front has changed very little in the past 50 years, we would expect some shift northward in the next 50 to 100 years. The trend with the Pacific front is less clear although a shift slightly north where the front is not topographically anchored could be expected. This analysis should be completed for other summer months in North America using a higher resolution gridded reanalysis product such as NARR. The front in Eurasia should be examined as well since it is likely controlled to a greater degree by land-ocean contrast.

References

ACIA. 2005. Arctic Climate Impact Assessment. Cambridge University Press: Cambridge.

Atkinson, D.E. 2000. Modeling July Mean Temperatures on the Fosheim Peninsula, Ellesmere Island. Chapter I.1.3 of Environmental Response to Climate Change in the Canadian High Arctic, Michelle Garneau (ed), Geological Survey of Canada Bulletin 529: Ottawa.

Atkinson, D.E. and Gajewski, K. 2002. High-resolution estimation of surface air temperature in the Canadian Arctic Archipelago. Journal of Climate 15(24): 3601-3614.

Barnston, A.G. and Livezey, R.E. 1987. Classification, seasonality and persistence of low-frequency atmospheric circulation patterns. Monthly Weather Review 115: 1083-1126.

Barry, R.G. 1967. Seasonal Location of the Arctic Front over North America. Geographical Bulletin 9 (2): 79-95.

Barry, R.G., and Carleton, A.M., 2001. Synoptic and dynamic climatology. Routledge: New York.

Beringer, J., Chapin III, F. S., Thompson, C.C., and McGuire, D.A. 2005. Surface energy exchanges along a tundra-forest transition and feedbacks to climate. Agricultural and Forest Meteorology 131: 143-161.

Beringer, J., Tapper, N. J., McHugh, I., Chapin III, F. S., Lynch, A. H., Serreze, M. C., and Slater, A., 2001. Impact of arctic tree line on synoptic climate. Geophysical Research Letters 28: 4247-4250.

Beyer, H. L. 2004. Hawth's Analysis Tools for ArcGIS. Available from http://www.spatialecology.com/htools.

British Atmospheric Data Center. 2006. Xconv: Release 1.91. Available from http://badc.nerc.ac.uk/help/software/xconv/.

Bryson, R.A., 1966: Air masses, streamlines, and the boreal forest. Geographical Review 8: 228-269.

CAVM Team. 2003. Circumpolar Arctic Vegetation Map. Scale 1:7,500,000. Conservation of Arctic Flora and Fauna (CAFF) Map No. 1. U.S. Fish and Wildlife Service, Anchorage, Alaska.

Chapin III, F.S., Sturm, M., Serreze, M.C., McFadden, J.P., Key, J.R., Lloyd, A.H., McGuire, A.D., Rupp, T.S., Lynch, A.H., Schimel, J.P., Beringer, J., Chapman, W.L., Epstein, E.H., Euskirchen, E.S., Hinzman, L.D., Jia, G., Ping, C.-L., Tape, K.D., Thompson, C.D.C., Walker, D.A., and Welker, J.M. 2005. Role of Land-Surface Changes in Arctic Summer Warming. Science 310: 657-660.

Climate Research Unit at University of East Anglia. 2004a. Southern Oscillation Index (SOI) data. Available from http://www.cru.uea.ac.uk/cru/data/soi.htm.

Climate Research Unit at University of East Anglia. 2004b. North Atlantic Oscillation (NAO) data. Available from http://www.cru.uea.ac.uk/cru/data/nao.htm.

Doty, B. 2001. Grid Analysis and Display System (GRADS): Release 1.8SL11. Center for Ocean-Land-Atmosphere Studies, Institute for Global Environment and Society. Available from http://www.iges.org/GRADS.

Doty, B. 1995. Grid Analysis and Display System (GRADS) User Guide. Retrieved March 15, 2007 from ftp://GRADS.iges.org/GRADS/beta/doc/gadoc151.pdf.

Ebisuzaki, W. 2006. grib2ctl script. National Oceanic and Atmospheric Administration. Available from http://www.cpc.ncep.noaa.gov/products/wesley/grib2ctl.html.

ECMWF. 2008. ECMWF 40 Years Re-Analysis, daily fields. Available from http://data.ecmwf.int/data/d/era40_daily/

ECMWF. 2004. ERA-40: ECMWF 45-year reanalysis of the global atmosphere and surface conditions 1957–2002 in European Center For Medium Range Weather Forecasting Newsletter 101 – Summer/Autumn 2004. Retrieved October 17, 2008, from http://www.ecmwf.int/publications/newsletters/pdf/101.pdf.

Environmental Systems Research Institute (ESRI). 2006. ArcGIS: Release 9.2 SP1. Redlands, California, USA.

Essenwanger, O.M. 1976. Applied Statistics in Atmospheric Science. Elsevier: Amsterdam.

Fritts, H.E., 1991. Reconstructing large-scale climatic patterns from tree-ring data. University of Arizona Press: Tucson.

Fritts, H.E., 1976. Tree rings and climate. Academic Press: London.

Global Land Cover Facility. 2008. GLCF: Global Inventory Modeling and Mapping Studies. Retrieved August 20, 2008, from http://glcf.umiacs.umd.edu/data/gimms/index.shtml.

Godske, C. L., Bergeron, T., Bjerknes, J., and Bungaard, R. 1957. Dynamic Meteorology and Weather Forecasting. American Meteorological Society: Boston.

Hansen, J., Lacis, A., Ruedy R. and Sato, M. 1992. Potential climate impact of Mount Pinatubo eruption. Geophysical Research Letters 19(2): 215–218.

Hare, F.C. and Ritchie, J.C. 1972. The Boreal Bioclimates. Geographical Review: 60(3): 333-365.

Hewson, E.W. and Longley, R.W. 1944. Meteorology, theoretical and applied. Wiley: New York.

Hurrell, J. W. 1995. Decadal Trends in the North Atlantic Oscillation: Regional Temperatures and Precipitation. Science 5224: 676-679.

Institute of Global Environment and Society. No year. GrADS-DODS-SERVER. Retrieved August 12, 2008, from http://www.iges.org/grads/gds/.

IPCC, 2007: Climate Change 2007: The Physical Science Basis. Contribution of Working Group I to the Fourth Assessment Report of the Intergovernmental Panel on Climate Change [Solomon, S., D. Qin, M. Manning, Z. Chen, M. Marquis, K.B. Averyt, M.Tignor and H.L. Miller (eds.)]. Cambridge University Press, Cambridge, United Kingdom and New York, NY, USA.

Joint Institute for the Study of Atmosphere and Ocean at University of Washington. 2000. Pacific Decadal Oscillation (PDO). Available from http://jisao.washington.edu/pdo/

Joint Institute for the Study of Atmosphere and Ocean at University of Washington. 2004. Arctic Oscillation (AO). Available from http://www.jisao.washington.edu/ao/

Kalnay, E., Kanamitsu, M., Kistler, R., Collins, W., Deaven, D., Gandin, L., Iredell, M., Saha, S., White, G., Woollen, J., Zhu, Y., Leetmaa, A., Reynolds, B., Chelliah, M., Ebisuzaki, W., Higgins, W., Janowiak, J., Mo, K.C., Ropelewski, C., Wang, J., Jenne, R., and Joseph, D. 1996: The NCEP/NCAR 40-Year Reanalysis Project. Bulletin of the American Meteorological Society 77: 437-472.

Kanamitsu, M. 1989. Description of the NMC Global Data Assimilation and Forecast System. Weather and Forecasting 4: 335-342.

Kanamitsu, M., W. Ebisuzaki, J. Woollen, S. -. Yang, J. J. Hnilo, M. Fiorino, and G. L. Potter. 2002. NCEP-DOE AMIP-II reanalysis (R-2). Bulletin of the American Meteorological Society 83: 1631-1643.

Kistler, R., Kalnay, E., Collins, W., Saha, S., White, G., Woollen, J., Chelliah, M., Ebisuzaki, W., Kanamitsu, M., Kousky, V., van den Dool, H., Jenne, R., and Fiorino, M. 2001. The NCEP-NCAR 50-Year Reanalysis: Monthly Means CD-ROM and Documentation. Bulletin of the American Meteorological Society 82: 247-268.

Krebs, J.S. and Barry, R.G. 1970. The Arctic Front and the Tundra-Taiga Boundary in Eurasia. Geographical Review 60(4): 548-554.

Lafleur, P.M. and Rouse, W.R. 1995. Energy Partitioning at Tree line Forest and Tundra Sites and Its Sensitivity to Climate Change. Atmospheric-Ocean 33(1): 121-135.

Levinson, D.H. and Lawrimore, J.H. (eds). 2008. State of the climate in 2007. Bulletin of the American Meteorological Society 89(7): 1-179.

Lynch, A.H., Slater, A.G., and Serreze, M.C. 2001. The Alaskan Arctic Frontal Zone: Forcing by Oragraphy, Coastal Contrast, and the Boreal Forest. 2001. Journal of Climate 14: 4351-4362.

Mantua, N.J., and Hare, S.R. 2002. Pacific Decadal Oscillation (PDO). Journal of Oceanography 58: 35-44.

Max Planck Institute of Meteorology. 2006. Climate Data Operators (CDO): Release 1.0.7. Available from http://www.mpimet.mpg.de/fileadmin/software/cdo/

Mesinger, F. 2006. North American Regional Reanalysis. Bulletin of the American Meteorological Society 87(3): 343-360.

National Center For Atmospheric Research. 2008. Niño Region 3 and Niño Region 3.4 SST Indices. Available from http://www.cgd.ucar.edu/cas/catalog/climind/Niño_3_3.4_indices.html

National Oceanic and Atmospheric Administration. 2008a. Earth Systems Research Laboratory Physical Sciences Division - NCEP/NCAR Reanalysis. Available from http://www.cdc.noaa.gov/cdc/reanalysis/reanalysis.shtml

National Oceanic and Atmospheric Administration. 2008b. Climate Prediction Center- Pacific/North American (PNA). Retrieved: October 5, 2008, from http://www.cpc.noaa.gov/data/teledoc/teleintro.shtml

National Oceanic and Atmospheric Administration. 2008c. Climate Prediction Center- Pacific/North American (PNA). Retrieved: August 21, 2008, from http://www.cpc.ncep.noaa.gov/data/teledoc/pna.shtml.

Oliver. J.E. and Fairbridge, R.W. (eds). 1987. The Encyclopedia of Climatology. Van Nostrand Reinhold: New York.

Orvig, S (ed). 1970. Climates of the Polar Regions. Elsevier: New York.

Overpeck, J., Hughen, K., Hardy, D., Bradley, R., Case, R., Douglas, M., Finney, B., Gajewski, K., Jacoby, G., Jennings, A., Lamoureux, S., Lasca, A., MacDonald, G., Moore,J., Retelle, M., Smith, S., Wolfe, A. and Zielinski, G. 1997. Arctic Environmental Change of the Past Four Centuries. Science 278: 1251-1256.

Palmen, E. H. and C.W. Newton, 1969: Atmospheric circulation systems: Their structure and physical interpretation. Academic Press: New York.

Payette, S. 1983. The forest tundra and present tree lines of the northern Québec–Labrador peninsula. Nordicana 47: 3–23.

Peterson, S. 1956. Weather Analysis and Forecasting. McGraw-Hill: New York.

Pielke, R. A., and Vidale, P.L., 1995. The boreal forest and the polar front. Journal of Geophysical Research 100: 755-758.

Pinzon, J., Brown, M.E. and Tucker, C.J., 2005. Satellite time series correction of orbital drift artifacts using empirical mode decomposition. In: N. Huang (Editor), Hilbert-Huang Transform: Introduction and Applications, pp. 167-186.

Reed, R. J., 1960: Principal frontal zones of the Northern Hemisphere in winter and summer. Bulletin of the American Meteorological Society 41: 591-598.

Reed, R.J. and Kunkel, B.A. 1960. The Arctic Circulation in Summer. Journal of the Atmospheric Sciences 17: 489-506.

Ritchie, J.C. and Hare, F.K. 1971. Late-quaternary vegetation and climate near the Arctic tree line of Northwestern North America. Quaternary Research 1, 331-341.

Ropelewski, C.F. and Jones, P.D., 1987: An extension of the Tahiti-Darwin Southern Oscillation Index. Monthly Weather Review 115, 2161-2165.

Serreze, M. C., and Francis, J.A., 2006. The Arctic Amplification Debate. Climatic Change 76: 241-264.

Serreze, M. C., Barrett, A. P. and Lo, F. 2005: Northern high-latitude precipitation as depicted by atmospheric reanalyses and satellite retrievals. Monthly Weather Review 133: 3407-3430.

Serreze, M.C., and Barry, R.G. 2005. The Arctic Climate System. Cambridge: New York.

Serreze, M.C., Lynch, A. H., and Clark, M. P. 2001. The Arctic Frontal Zone as Seen in the NCEP-NCAR Reanalysis. Journal of Climate 14: 1550-1567.

Serreze, M.C., Box, J. E., Barry, R.G., and Walsh, J. E., 1993. Characteristics of Arctic Synoptic Activity, 1952-1989. Meteorology and Atmospheric Physics 51: 147-164.

Simmons, A. J., Jones, P. D., Bechtold, V. da Costa, Beljaars, A. C. M. , Kållberg, P. W., Saarinen, S., Uppala, S. M., Viterbo, P. and Wedi, N. 2004. Comparison of trends and low-frequency variability in CRU, ERA-40, and NCEP/NCAR analyses of surface air temperature. Journal of Geophysical Research 109.

Sterl, A., 2004. On the (In) Homogeneity of Reanalysis Products. Journal of Climate 17: 3866–3873.

Sterl, A. Komen, G. J. Cotton, P. D. Fifteen years of global wave hindcasts using winds from the European Centre for Medium-Range Weather Forecasts reanalysis: Validating the reanalyzed winds and assessing the wave climate. Journal of Geophysical Research 103(C3): 5477-5492.

Thompson, D. W. J. Wallace, J. M. 2000. Annular Modes in the Extratropical Circulation. Part I: Month-to-Month Variability. Journal of Climate 13(5): 1000-1016.

Thompson, D. W. J., and Wallace, J. M., 1998. The Arctic oscillation signature in the wintertime geopotential height and temperature fields. Geophysical Research Letters 25: 1297-1300.

Timoney, K.P., La Roi, G.H., Zoltai, S.C., Robinson, A.L. 1992. The high subarctic forest-tundra of northwestern Canada: Position, width, and vegetation gradients in relation to climate. Arctic 45(1): 1-9.

Trenberth, K.E., and Paolino, D.A. 1980. The Northern Hemisphere Sea-Level Pressure Data Set: Trends, Errors and Discontinuities. Monthly Weather Review 108: 855–872

Trenberth, K. E., 1997. The Definition of El Niño. Bulletin of the American Meteorological Society 78: 2771-2777.

Trewartha, G T. and Horn, L.H. 1980. An introduction to climate. McGraw-Hill.

Tucker, C.J., Pinzon, J. E. Brown, M. E., Slayback, D., Pak, E. W., Mahoney, R. , Vermote, E. and El Saleous, N. 2005. An Extended AVHRR 8-km NDVI Data Set Compatible with MODIS and SPOT Vegetation NDVI Data. International Journal of Remote Sensing 26(20): 4485-5598.

Tucker, C.J., Pinzon, J.E., and Brown M.E. 2004. Global Inventory Modeling and Mapping Studies, NA94apr15b.n11-VIg, 2.0, Global Land Cover Facility, University of Maryland, College Park, Maryland, 04/15/1994.

UCAR. 2007. NetCDF (network Common Data Form). Retrieved April 27, 2007, from http://www.unidata.ucar.edu/software/netcdf/

Uppala, S. M., KÅllberg, P. W. , Simmons, A. J., Andrae, U. ., Bechtold, V. Da Costa, Fiorino, M., Gibson, J. K., Haseler, J., Hernandez, A., Kelly, G. A., Li, X. , Onogi, K., Saarinen, S., Sokka, N., Allan, R. P., Andersson, E., Arpe, K., Balmaseda, M. A., Beljaars, A. C. M. , Van De Berg, L. , Bidlot, J., Bormann, N. , Caires, S., Chevallier, F., Dethof, A., Dragosavac, M., Fisher, M. , Fuentes, M., Hagemann, S., Hólm, E., Hoskins, B. J., Isaksen, L., Janssen, P. A. E. M., Jenne, R., Mcnally, A. P., Mahfouf, J.-F., Morcrette, J.-J., Rayner, N. A., Saunders, R. W., Simon, P., Sterl, A., Trenberth, K. E., Untch, A., Vasiljevic, D., Viterbo, P., and Woollen, J. 2005. The ERA-40 re-analysis. Quarterly Journal of the Royal Meteorological Society 131(612): 2961-3012.

Verbyla, D. 2008. The Greening and Browning of Alaska based on 1982-2003 satellite data. Global Ecology and Biogeography 17: 547-555.

Viau, A.E., Gajewski, K., Fines, P., Atkinson, A.E., and Sawada, M.C. 2002. Widespread evidence of 1500 yr climate variability in North America during the past 14000 yr. Geology 30(5): 455-458.

Wendland, W.A and Bryson, R.A. 1980. Northern hemisphere airstream regions. Monthly Weather Review 109: 255-270.

Willis, R.A., and G.K. Grice, 1977: The Wintertime Arctic Front and Its Effect on Fairbanks, Alaska. Monthly Weather Review 105: 78–85.

Appendix A – Mean North American July surface streamline maps derived from ERA-40 and NNR products

In this section, the mean surface streamline maps for July of each year of the NNR are compared with those of ERA-40. This allows us to examine the interannual variability of the July synoptic patterns. Only the years of 1958 to 2002 can be compared between the two reanalysis products. There are slight differences evident between the NNR and ERA-40 derived maps for July of each year but the overall synoptic patterns are the same. Several composite maps are shown for groups of years such as 1958 to 1967, in order to examine decadal climate patterns for July. In these maps the air mass boundaries along with the synoptic features such as the subtropical highs and subpolar lows present along with the Arctic and Pacific fronts. In the central region of Canada, there is often low pressure near Great Slave Lake. Other synoptic features seen in July are low pressure over/near or north of Ellesmere Island (close to the North Pole), over the central Canadian Arctic Archipelago, and in some years, low pressure over Manitoba, or high pressure over Hudson Bay or the Yukon/NWT coast. High pressure over the Beaufort is not present in July of every year. In some years, there is low pressure present, or it is displaced such that it is just outside the study area. In these years the flow over Alaska is mostly from the South/Southwest.

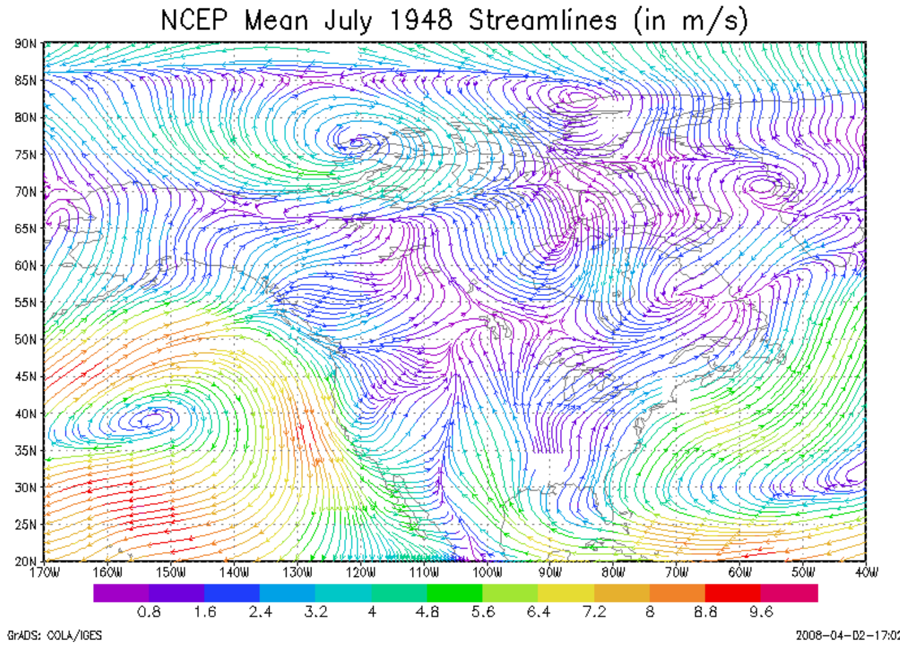

Figure A1. NCEP Mean July surface streamlines for 1948.

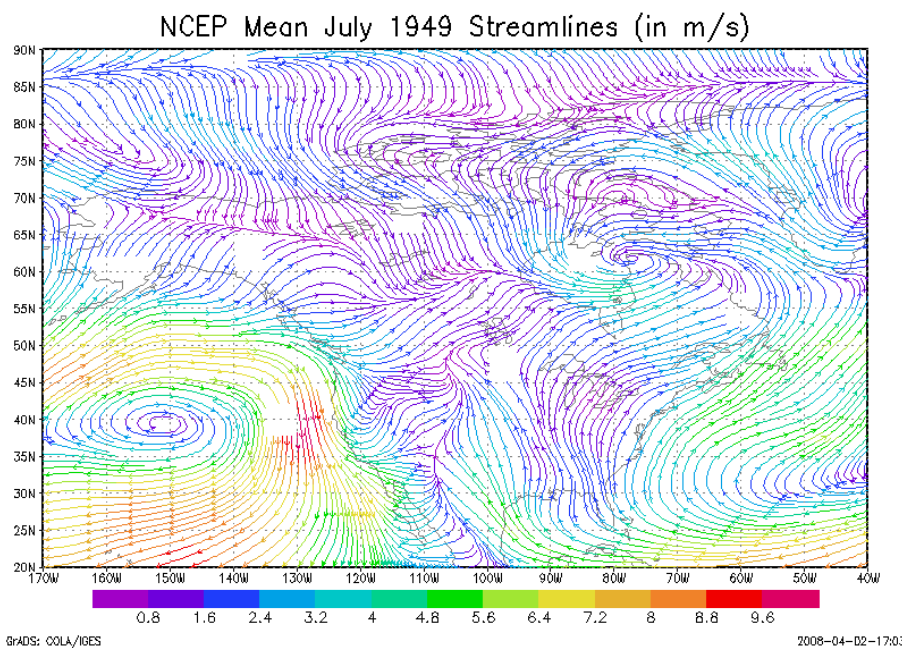

Figure A2. NCEP Mean July surface streamlines for 1949.

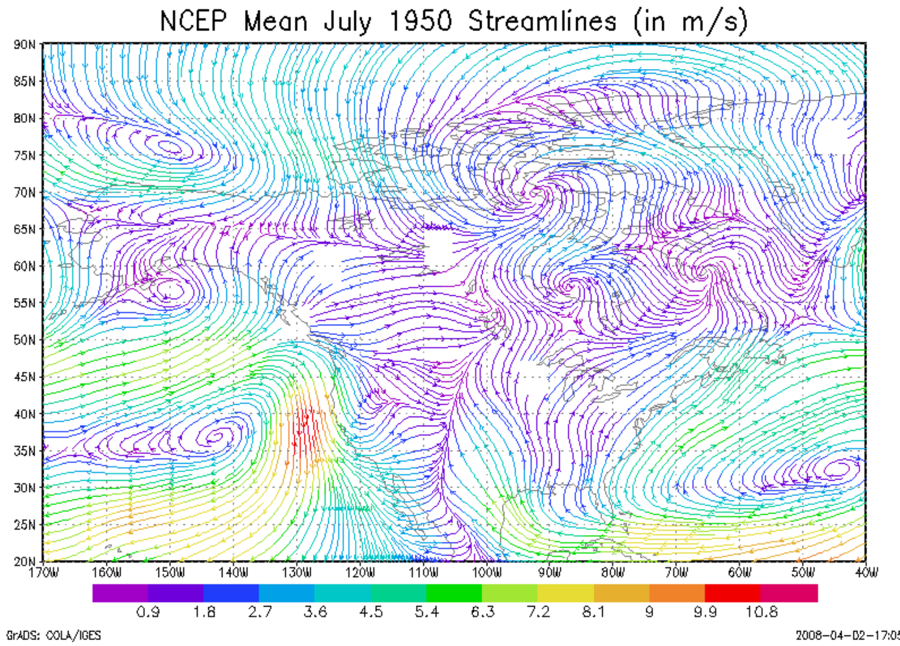

Figure A3. NCEP Mean July surface streamlines for 1950.

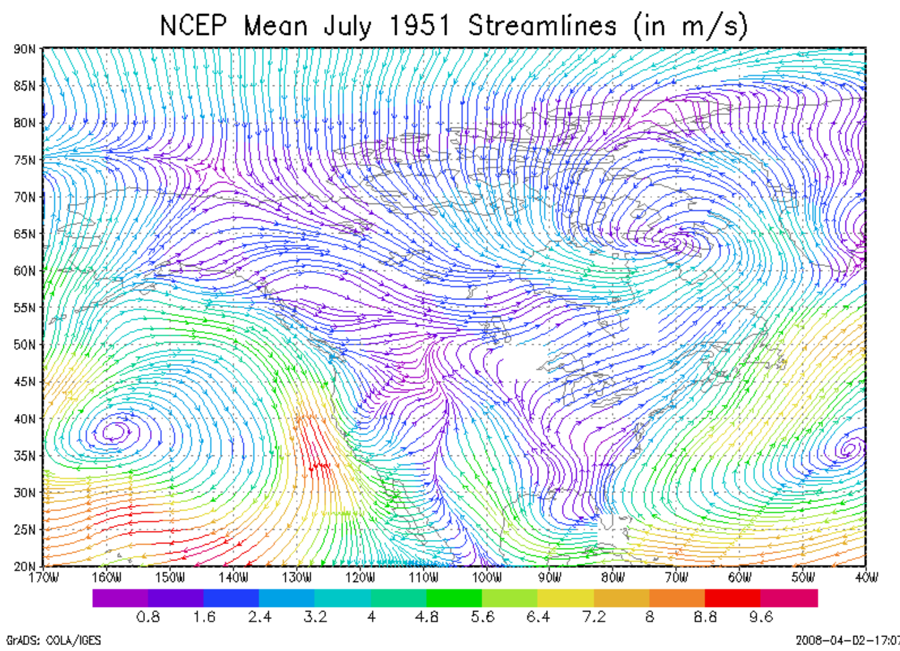

Figure A4. NCEP Mean July surface streamlines for 1951.

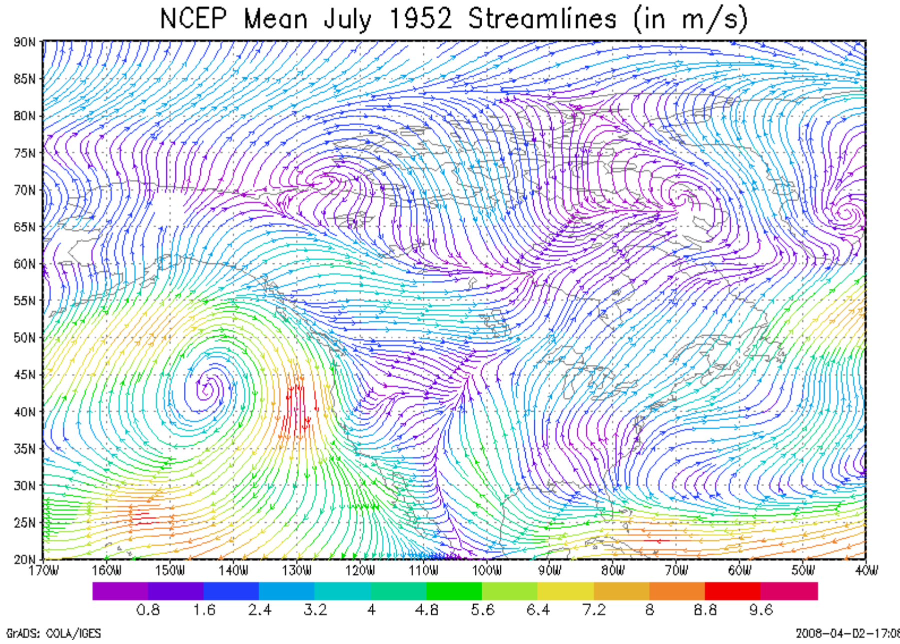

Figure A5. NCEP Mean July surface streamlines for 1952.

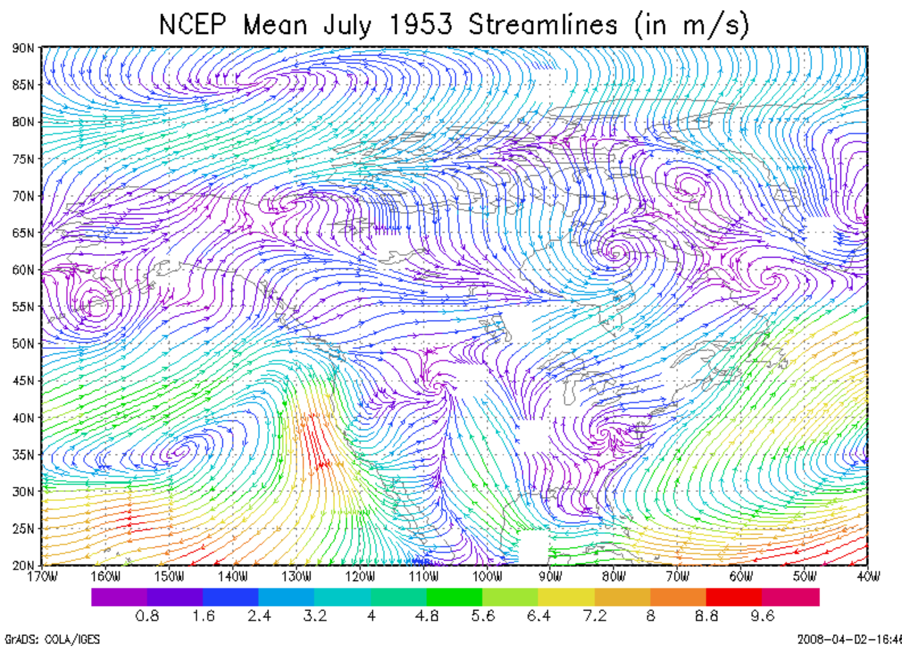

Figure A6. NCEP Mean July surface streamlines for 1953.

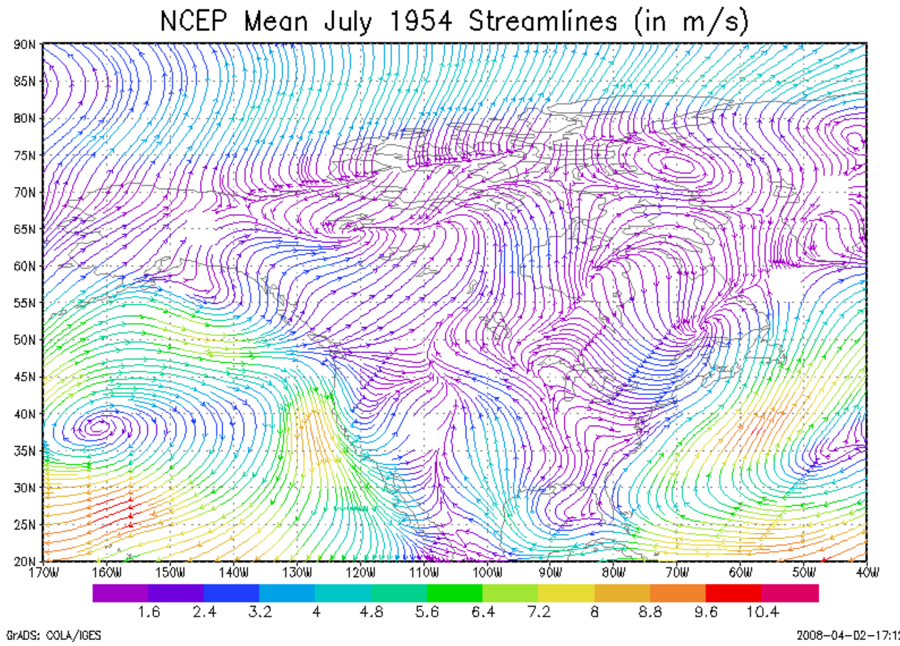

Figure A7. NCEP Mean July surface streamlines for 1954.

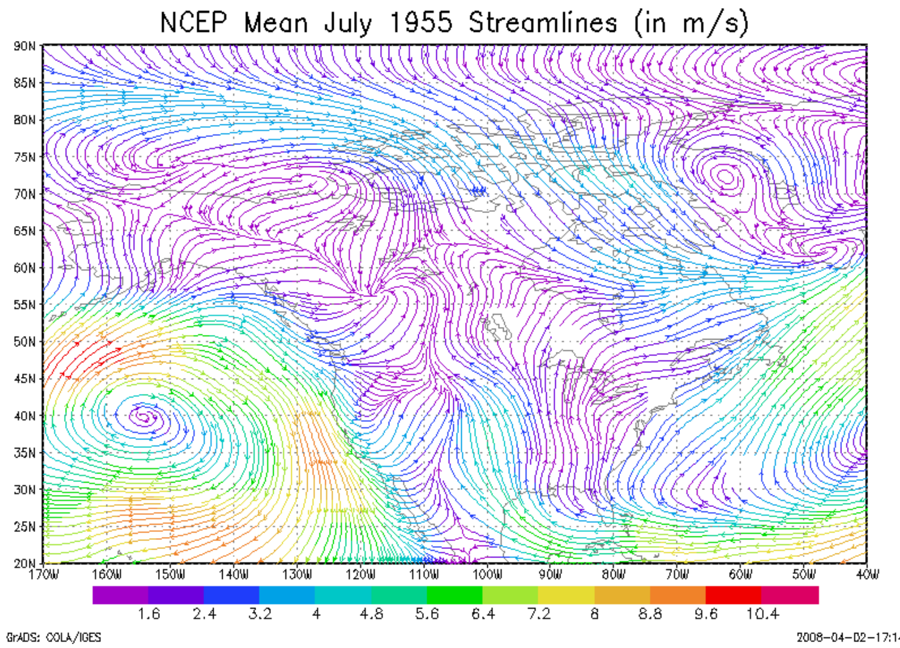

Figure A8. NCEP Mean July surface streamlines for 1955.

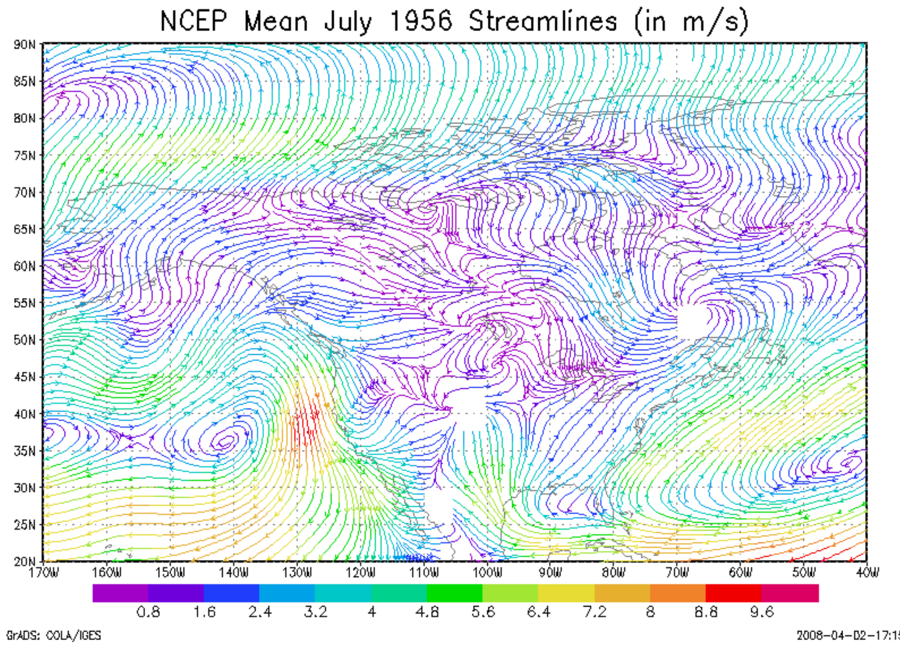

Figure A9. NCEP Mean July surface streamlines for 1956.

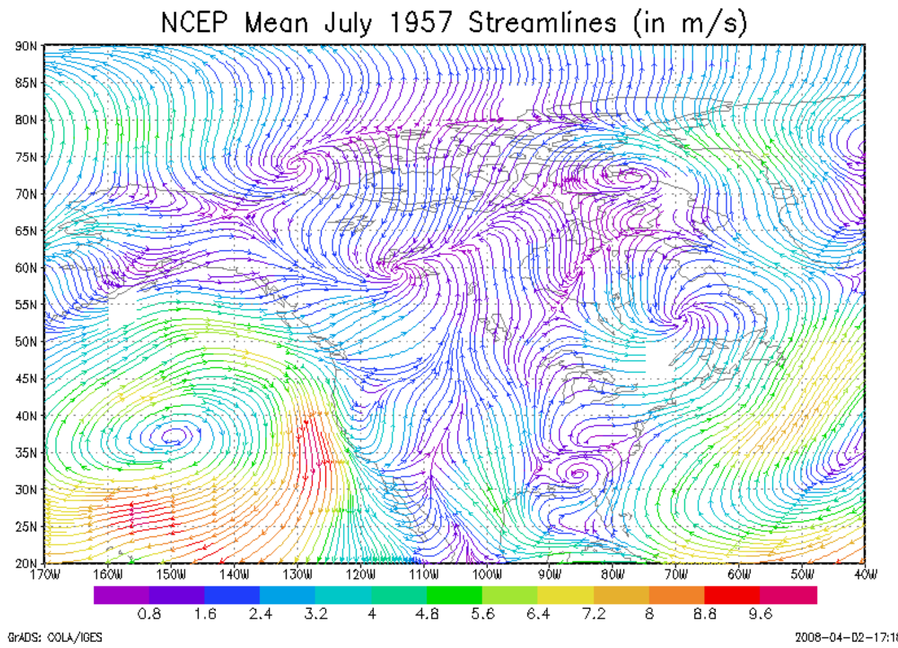

Figure A10. NCEP Mean July surface streamlines for 1957.

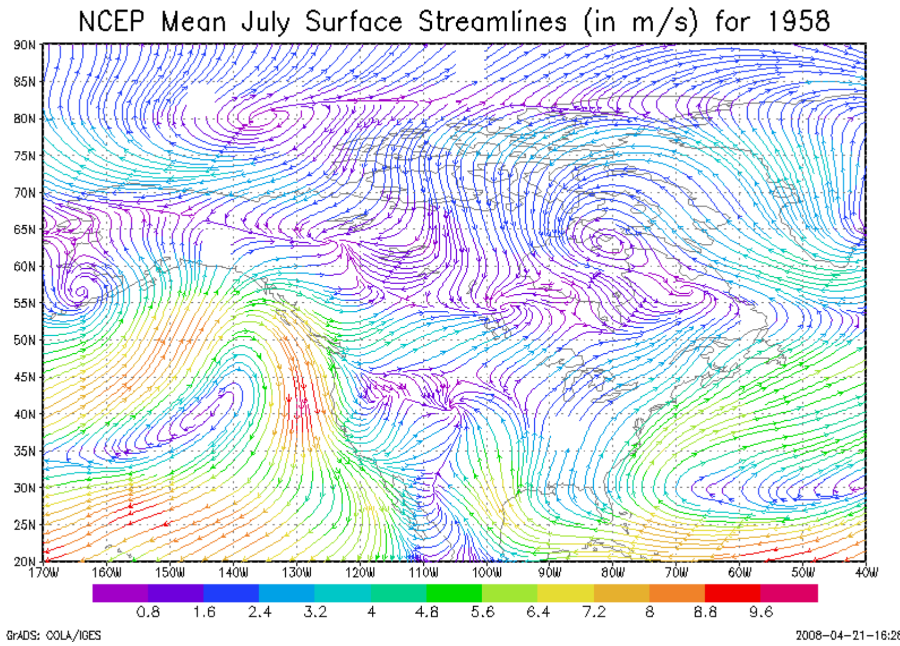

Figure A11. NCEP Mean July surface streamlines for 1958.

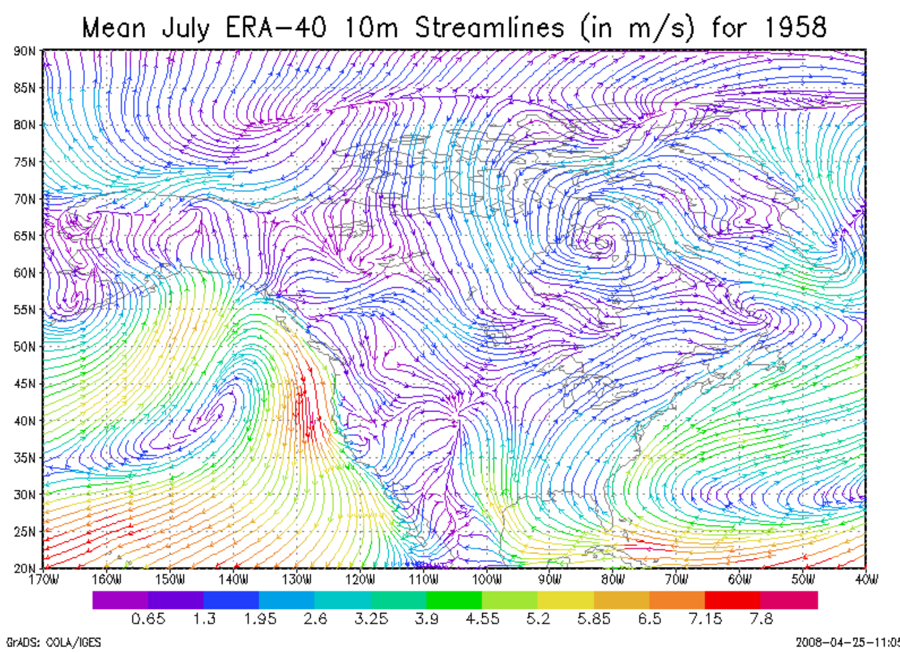

Figure A12. ERA-40 Mean July 10m streamlines for 1958.

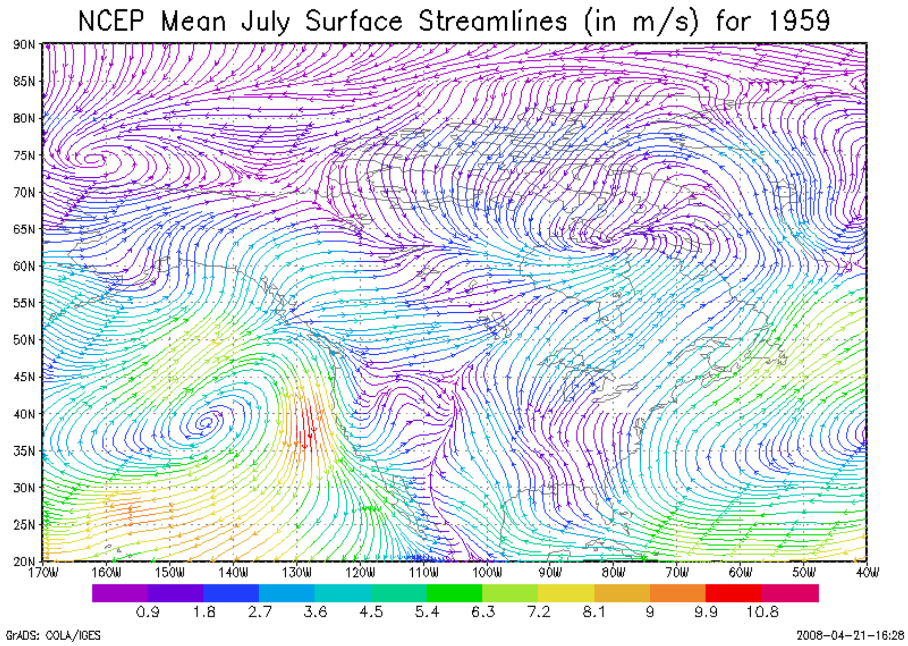

Figure A13. NCEP Mean July surface streamlines for 1959.

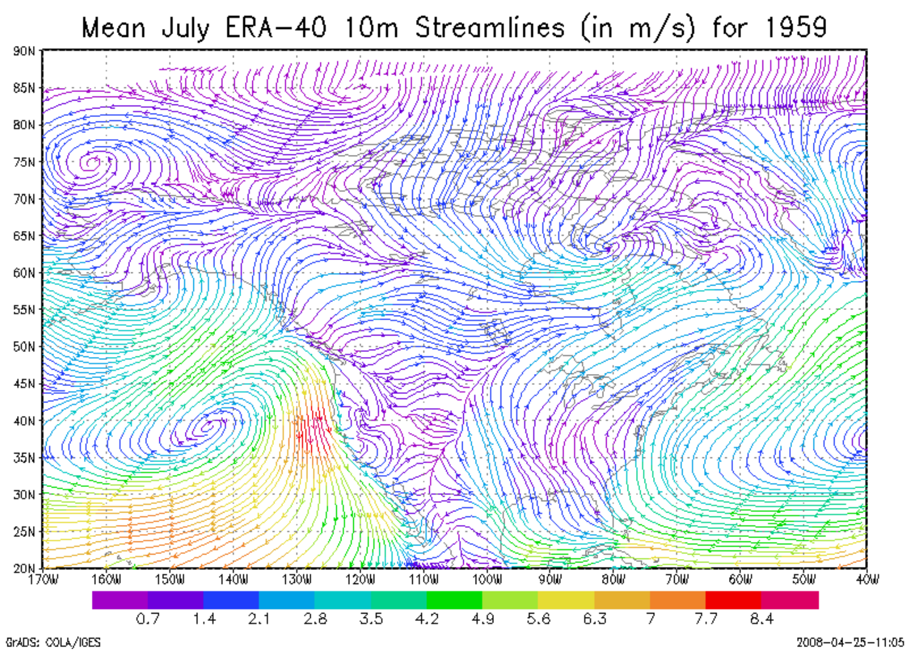

Figure A14. ERA-40 Mean July 10m streamlines for 1959.

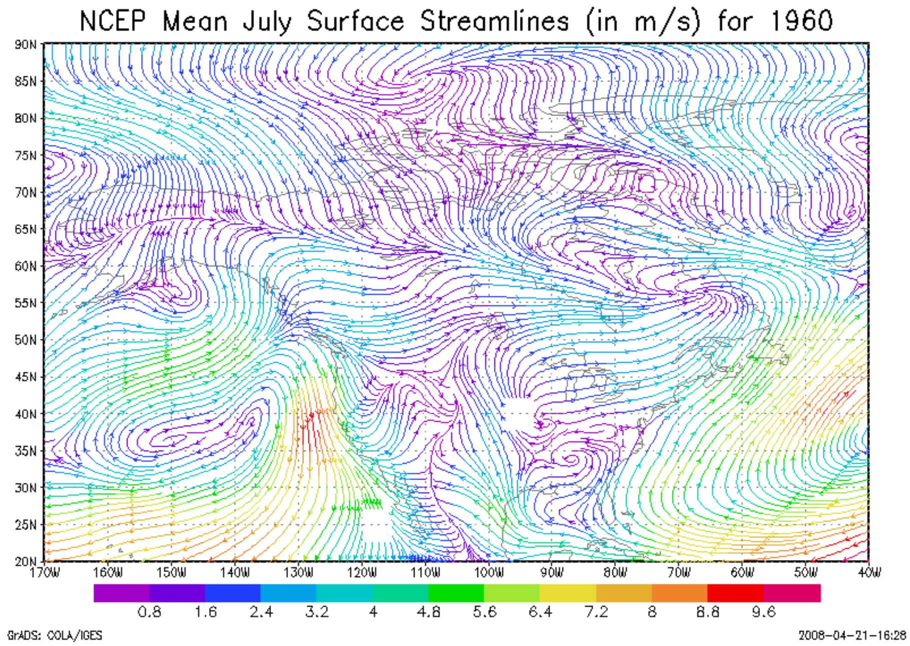

Figure A15. NCEP Mean July surface streamlines for 1960.

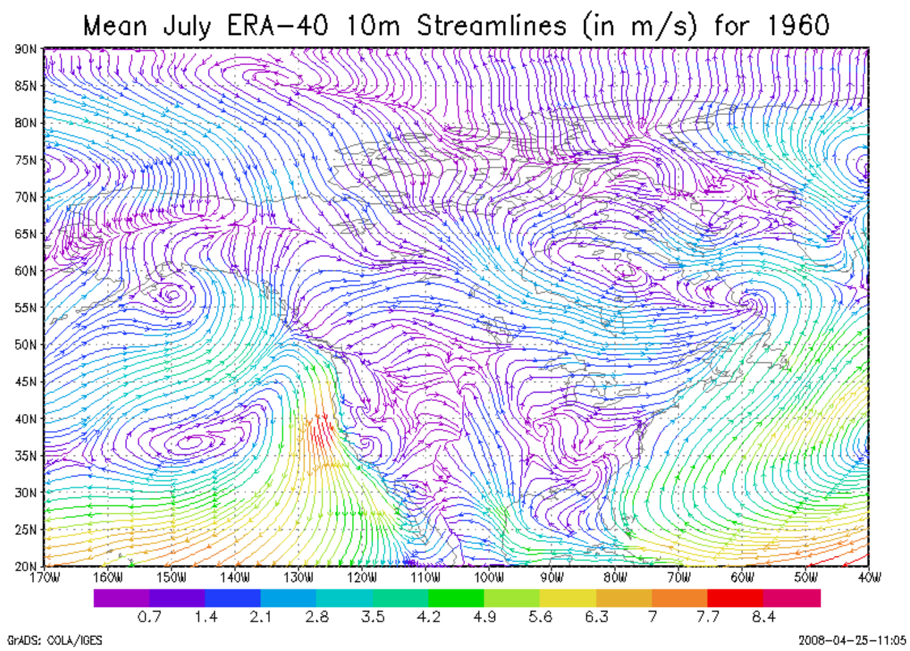

Figure A16. ERA-40 Mean July 10m streamlines for 1960.

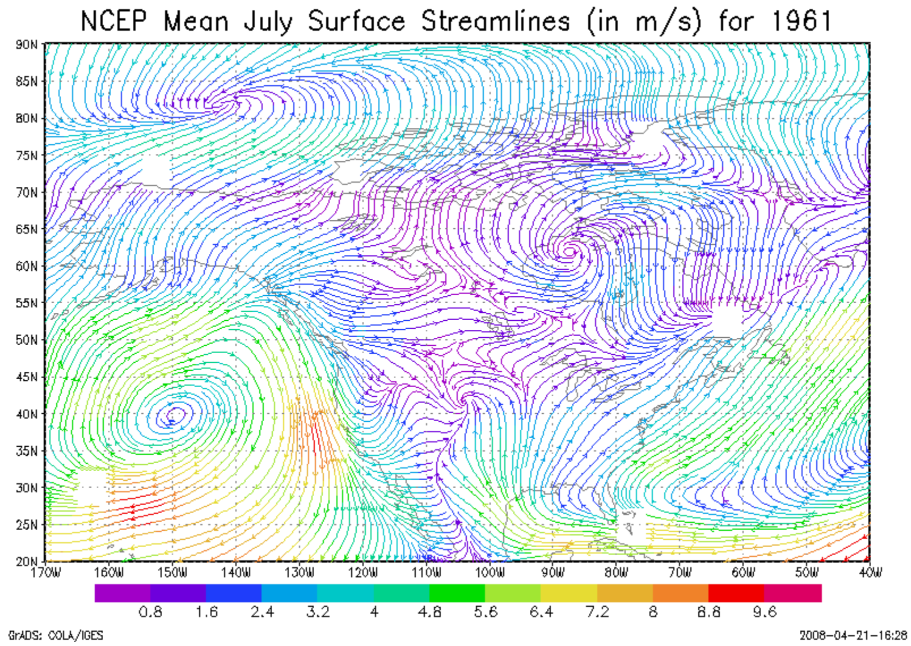

Figure A17. NCEP Mean July surface streamlines for 1961.

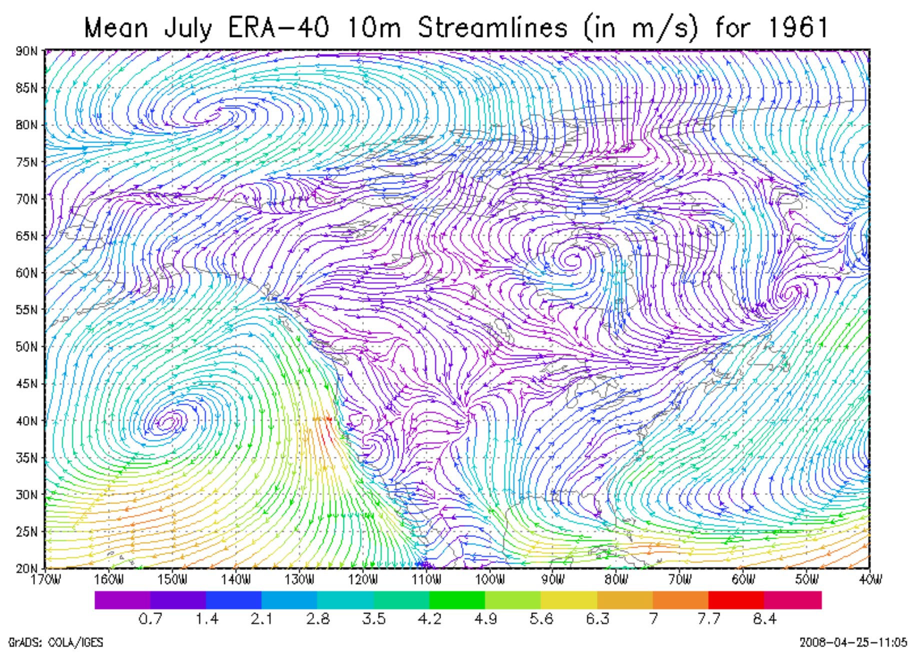

Figure A18. ERA-40 Mean July 10m streamlines for 1961.

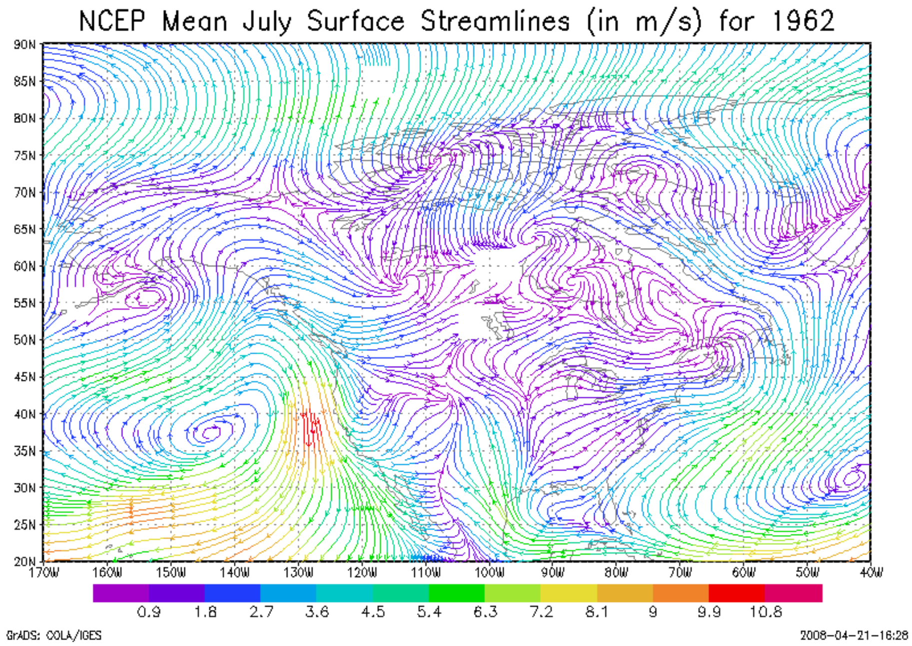

Figure A19. NCEP Mean July surface streamlines for 1962.

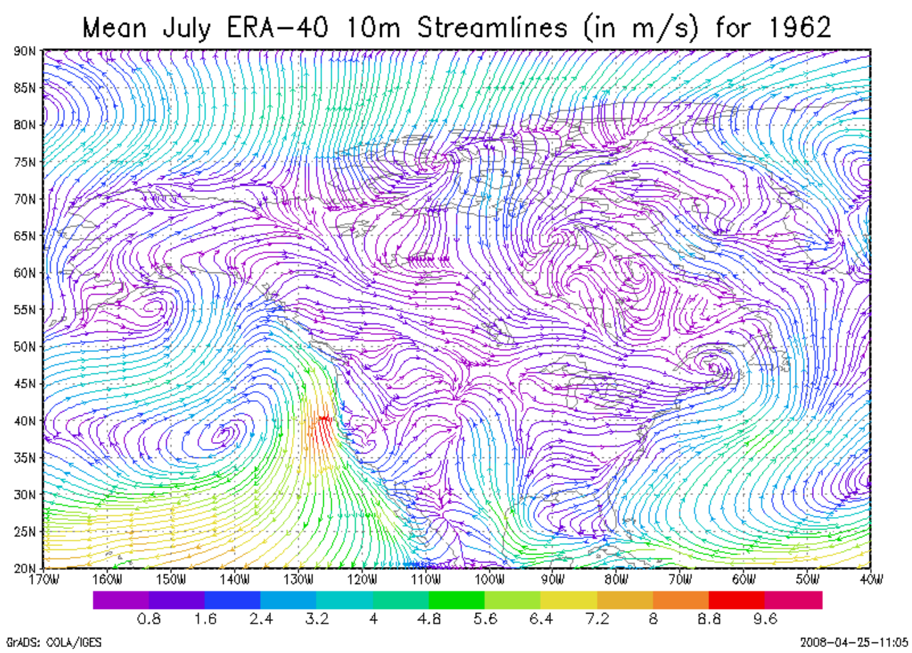

Figure A20. ERA-40 Mean July 10m streamlines for 1962.

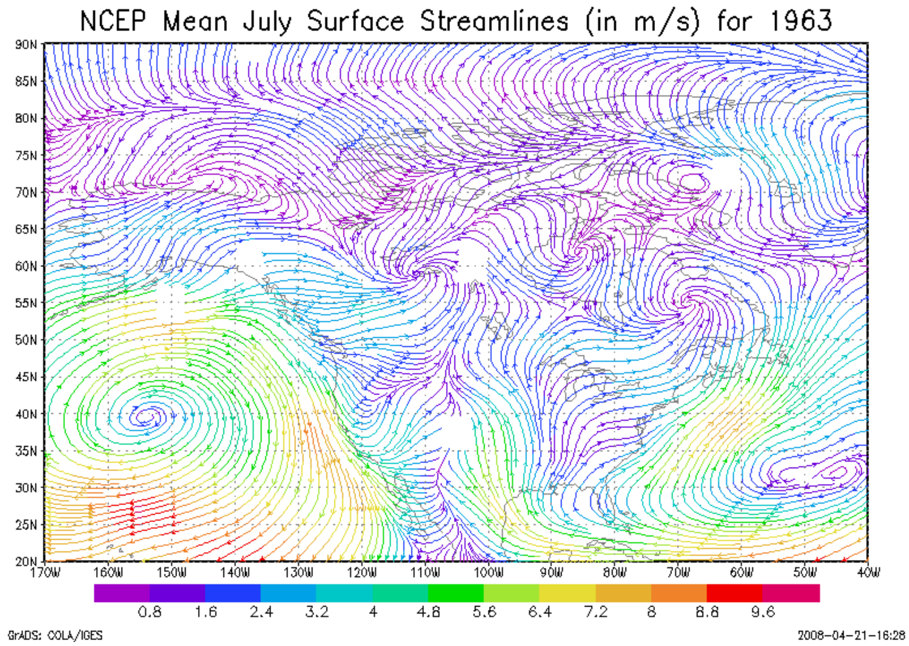

Figure A21. NCEP Mean July surface streamlines for 1963.

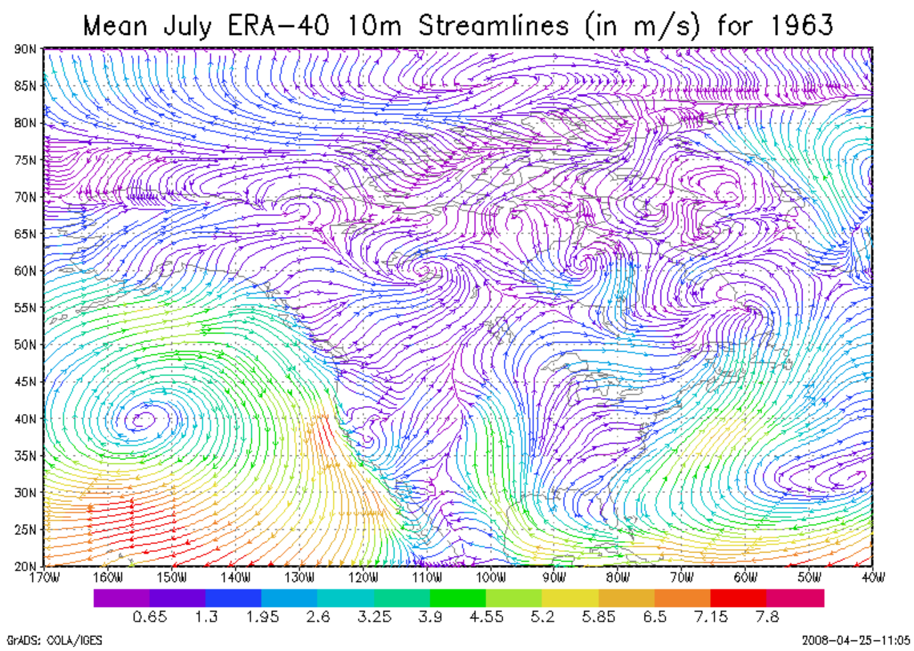

Figure A22. ERA-40 Mean July 10m streamlines for 1963.

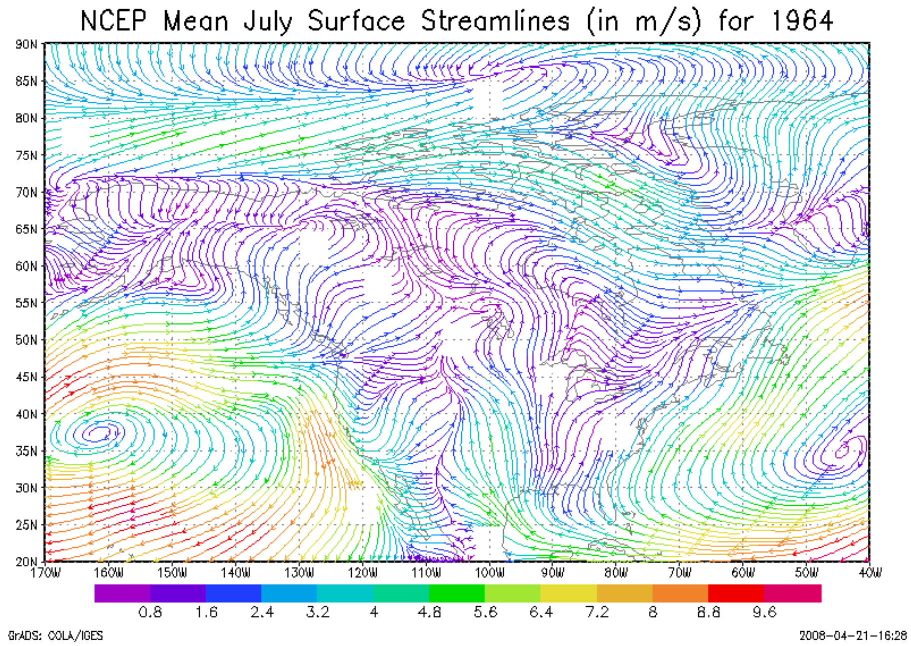

Figure A23. NCEP Mean July surface streamlines for 1964.

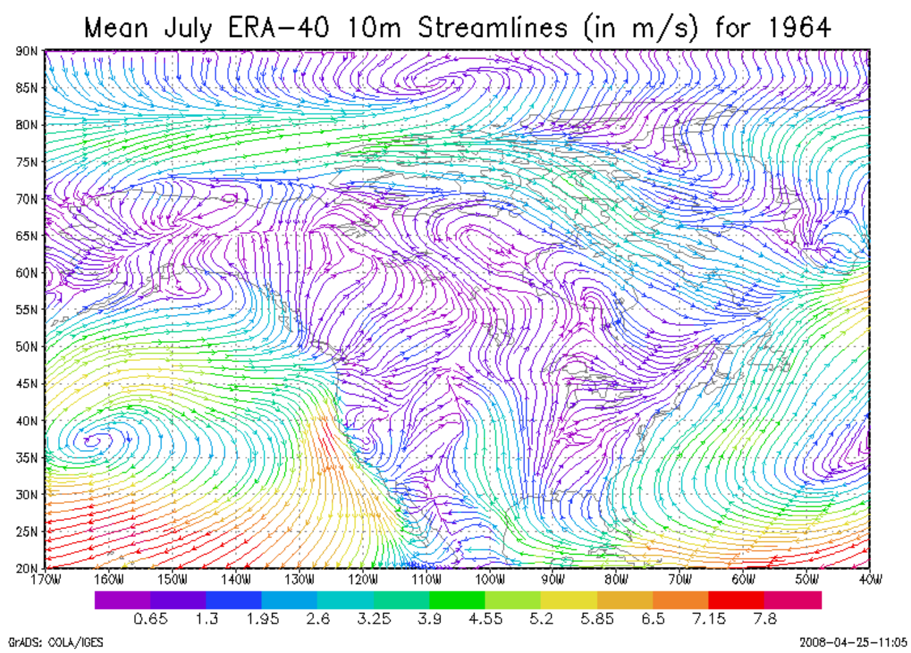

Figure A24. ERA-40 Mean July 10m streamlines for 1964.

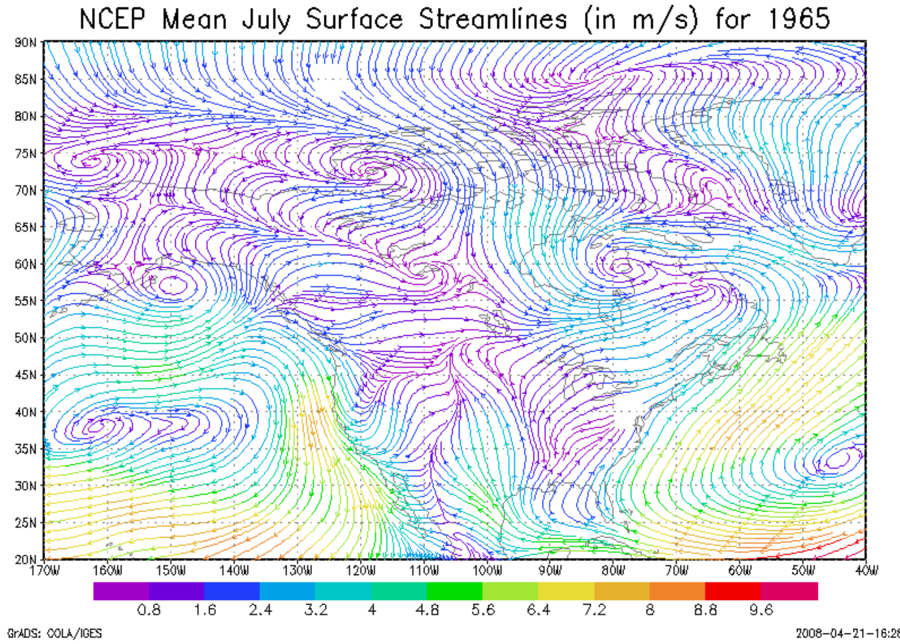

Figure A25. NCEP Mean July surface streamlines for 1965.

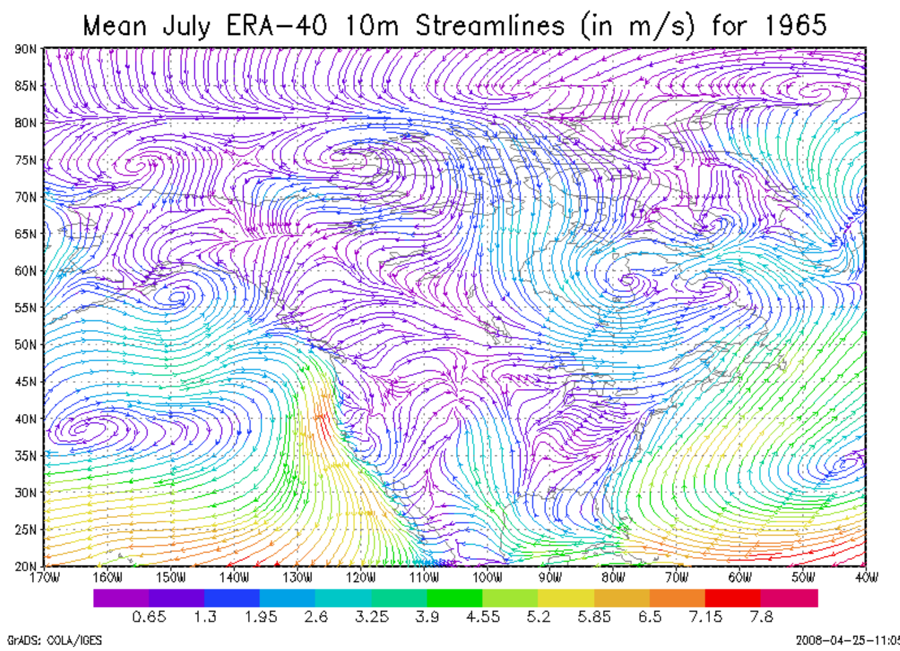

Figure A26. ERA-40 Mean July 10m streamlines for 1965.

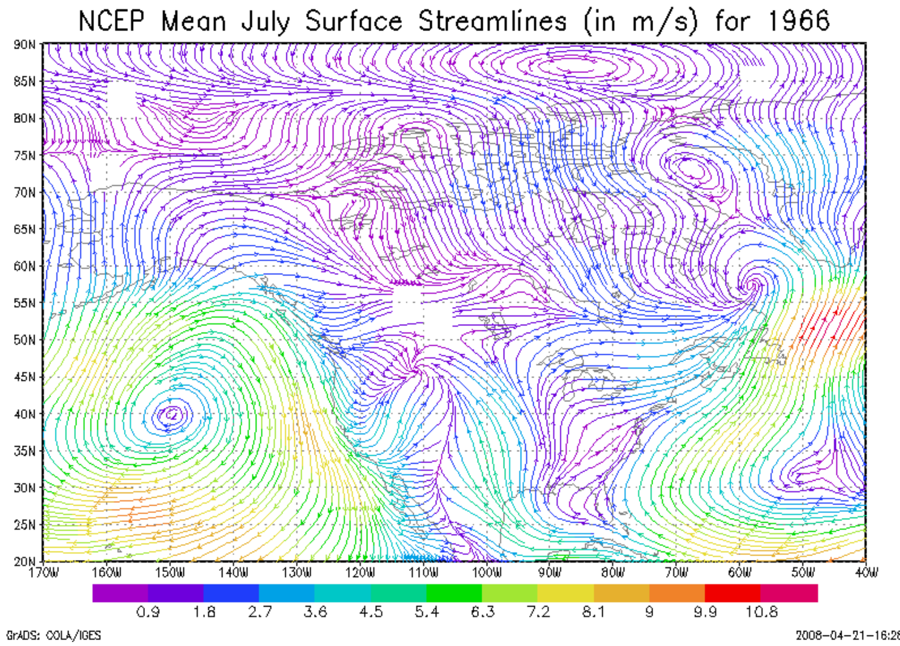

Figure A27. NCEP Mean July surface streamlines for 1966.

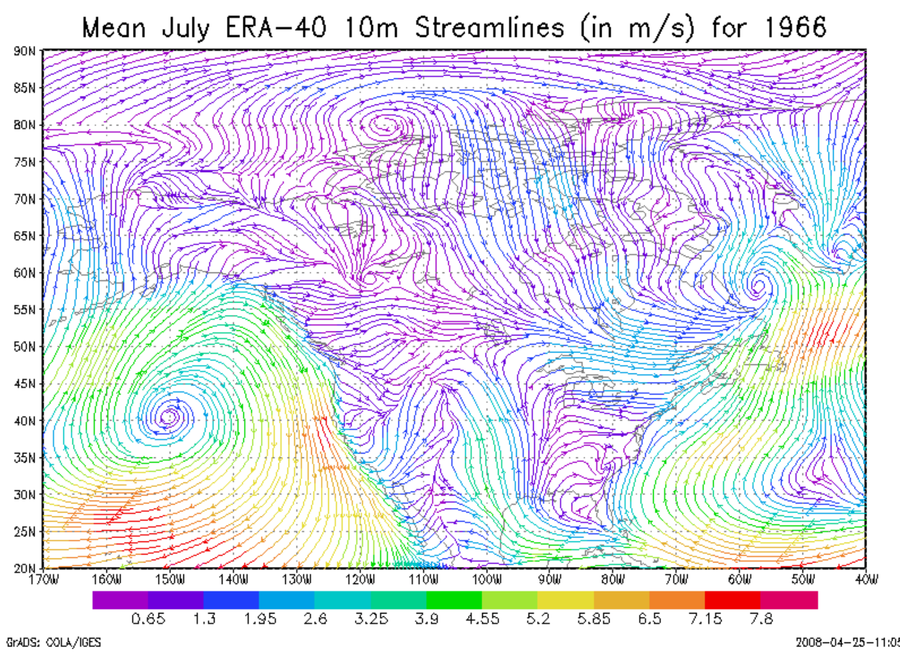

Figure A28. ERA-40 Mean July 10m streamlines for 1966.

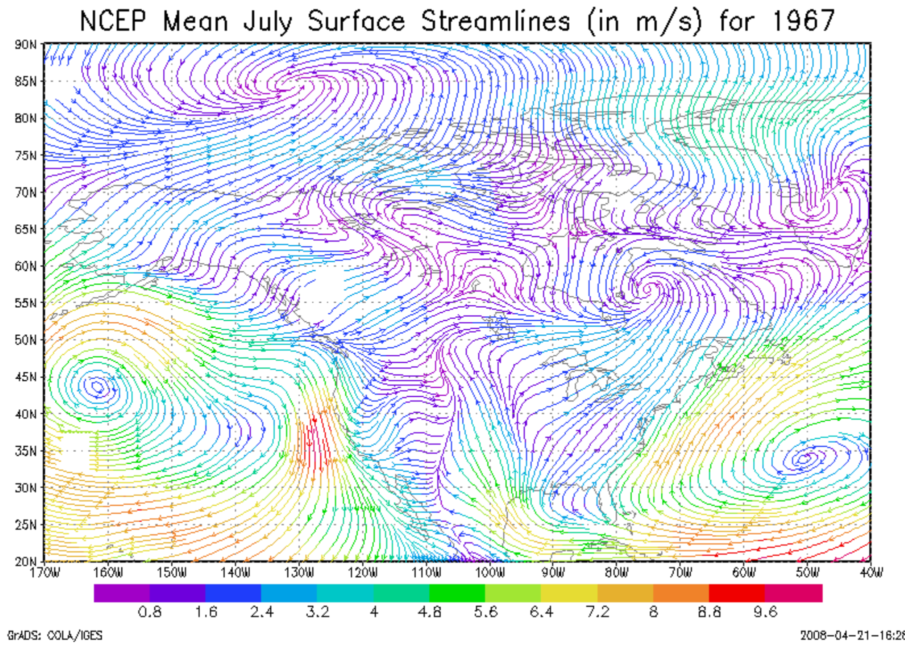

Figure A29. NCEP Mean July surface streamlines for 1967.

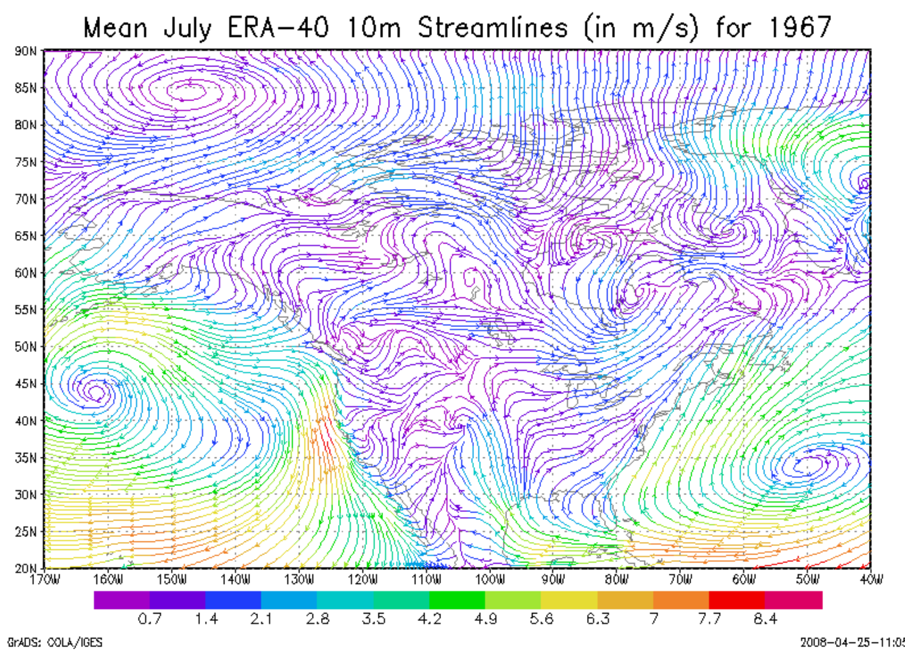

Figure A30. ERA-40 Mean July 10m streamlines for 1967.

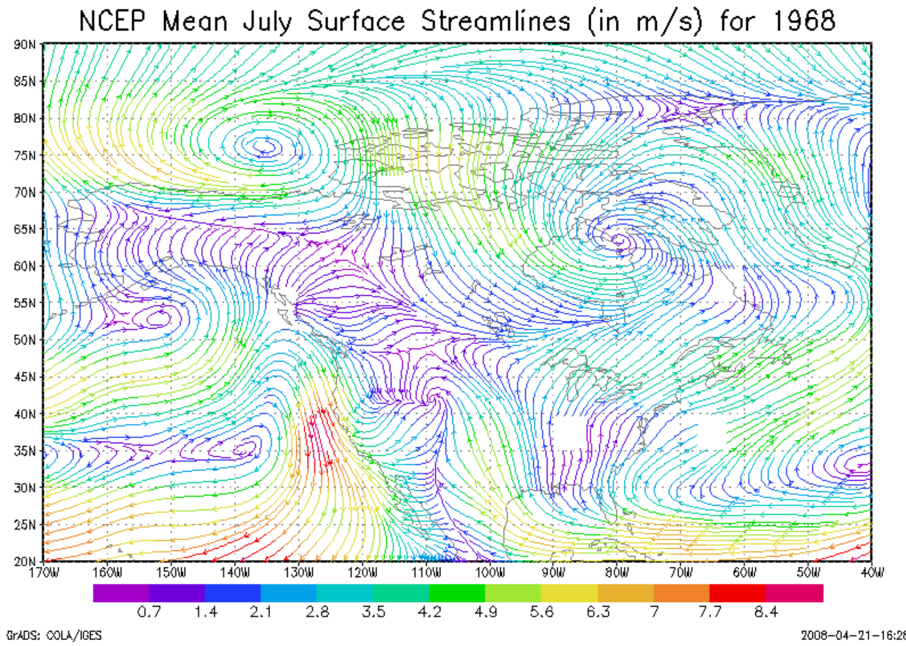

Figure A31. NCEP Mean July surface streamlines for 1968.

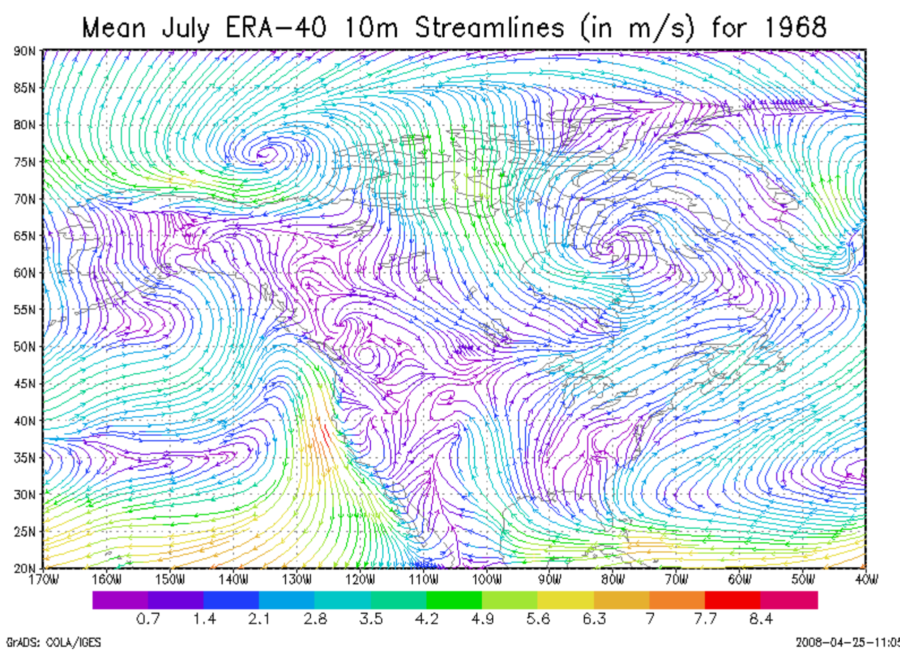

Figure A32. ERA-40 Mean July 10m streamlines for 1968.

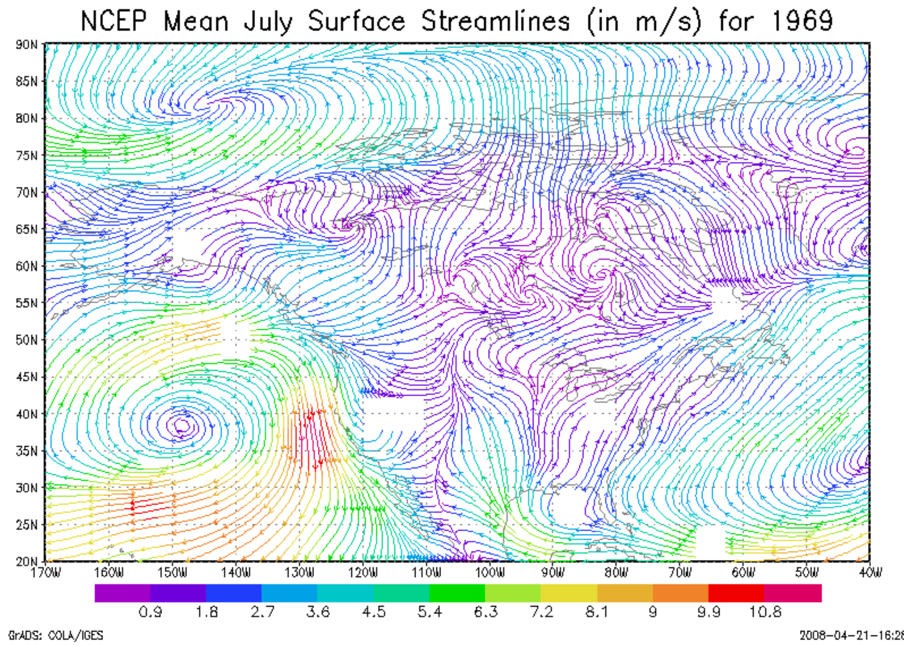

Figure A33. NCEP Mean July surface streamlines for 1969.

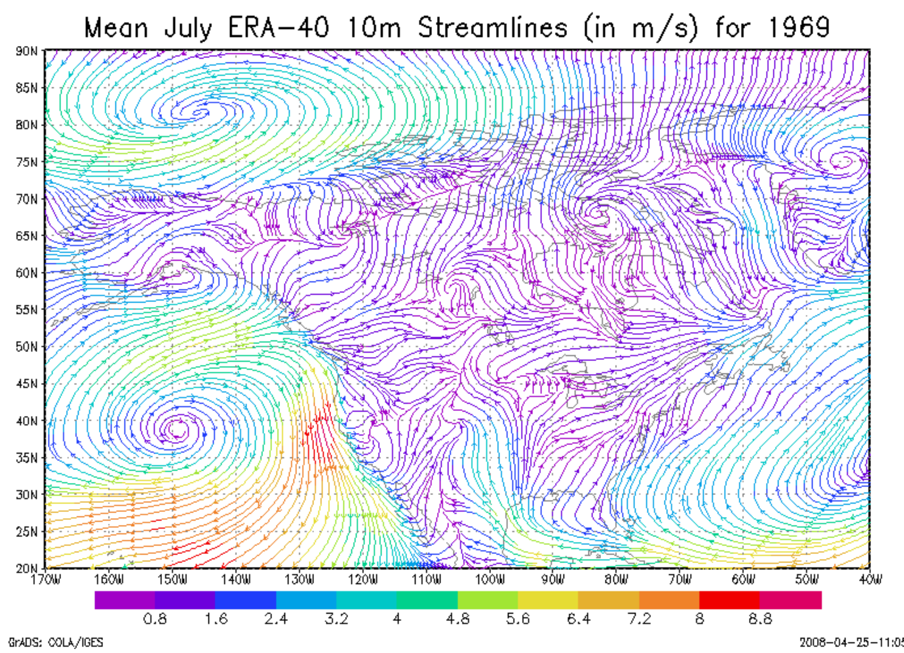

Figure A34. ERA-40 Mean July 10m streamlines for 1969.

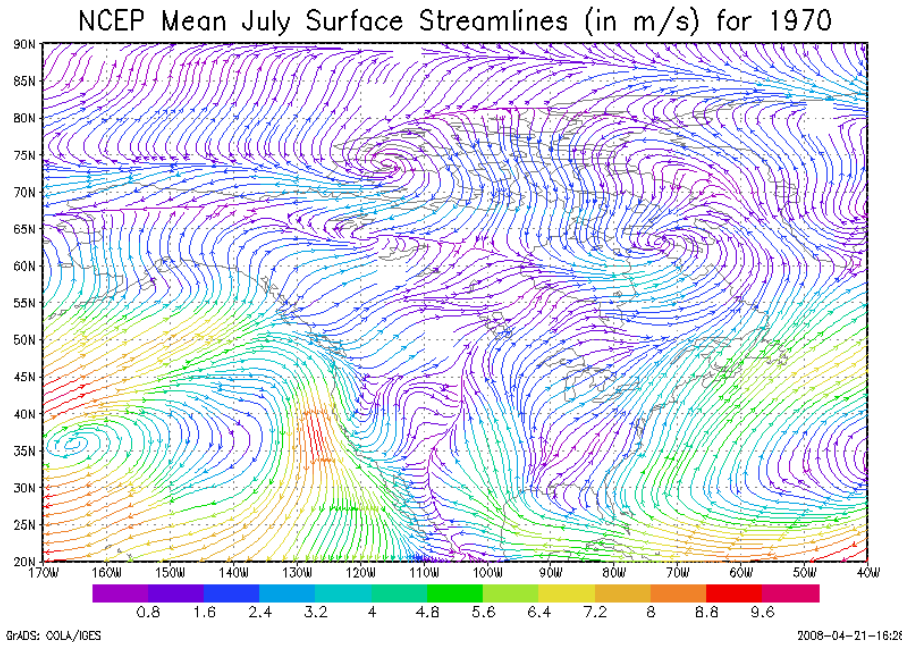

Figure A35. NCEP Mean July surface streamlines for 1970.

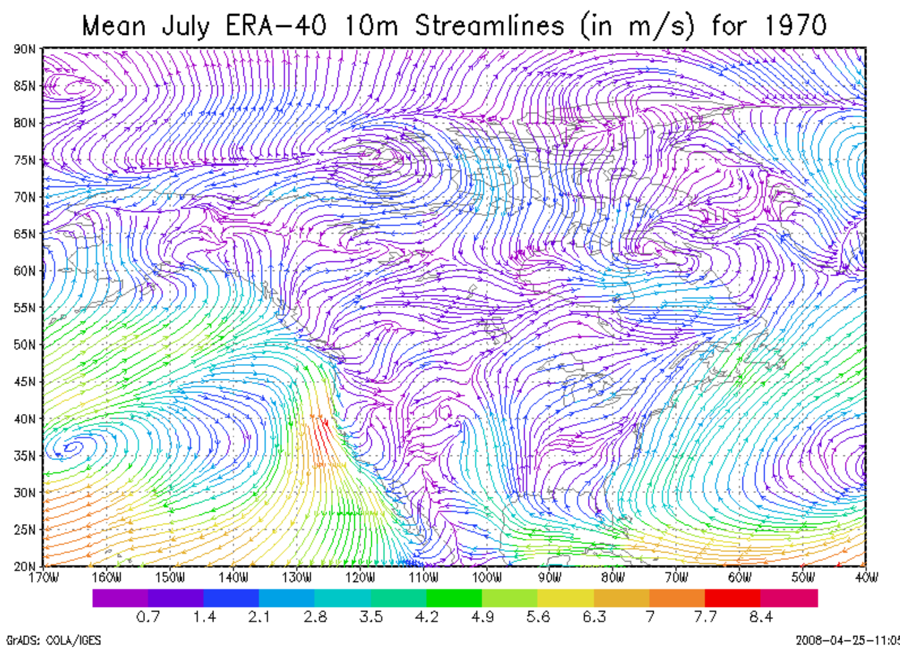

Figure A36. ERA-40 Mean July 10m streamlines for 1970.

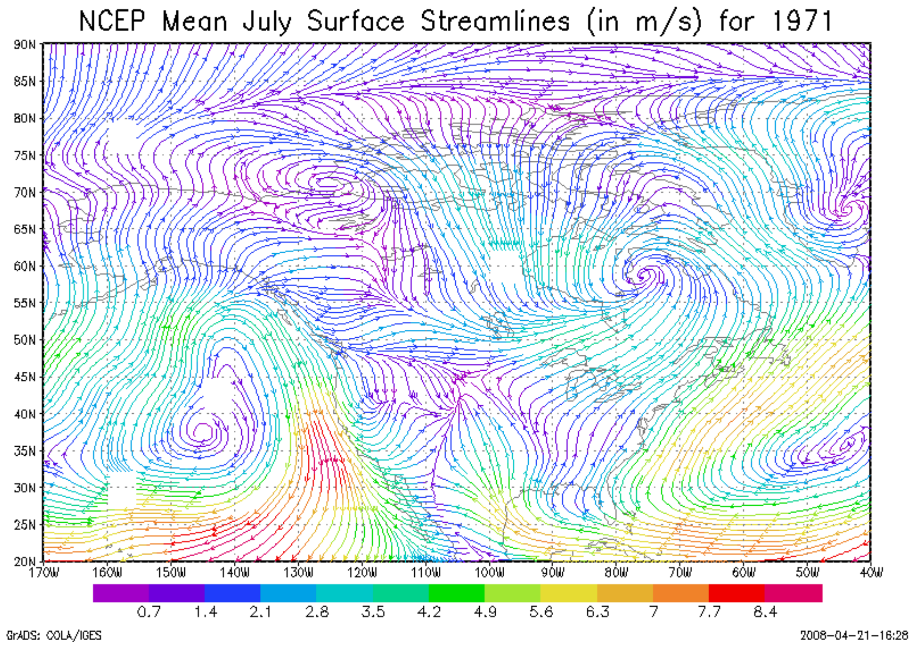

Figure A37. NCEP Mean July surface streamlines for 1971.

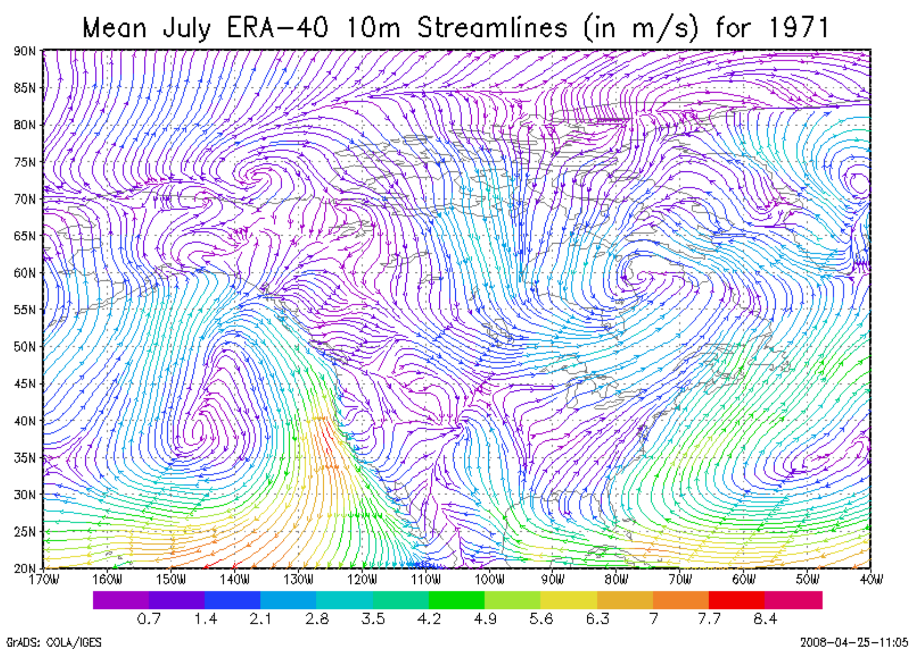

Figure A38. ERA-40 Mean July 10m streamlines for 1971.

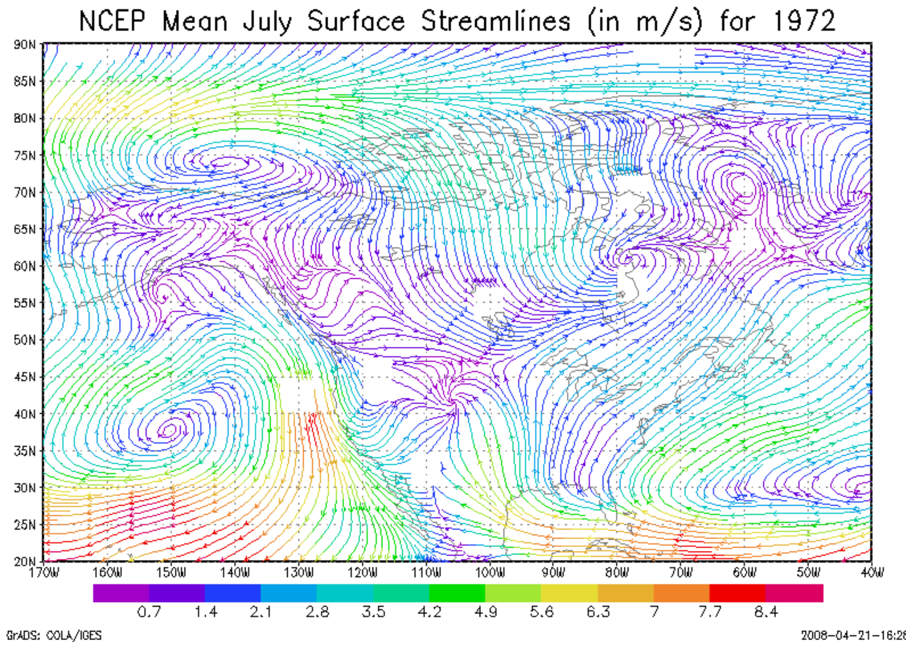

Figure A39. NCEP Mean July surface streamlines for 1972.

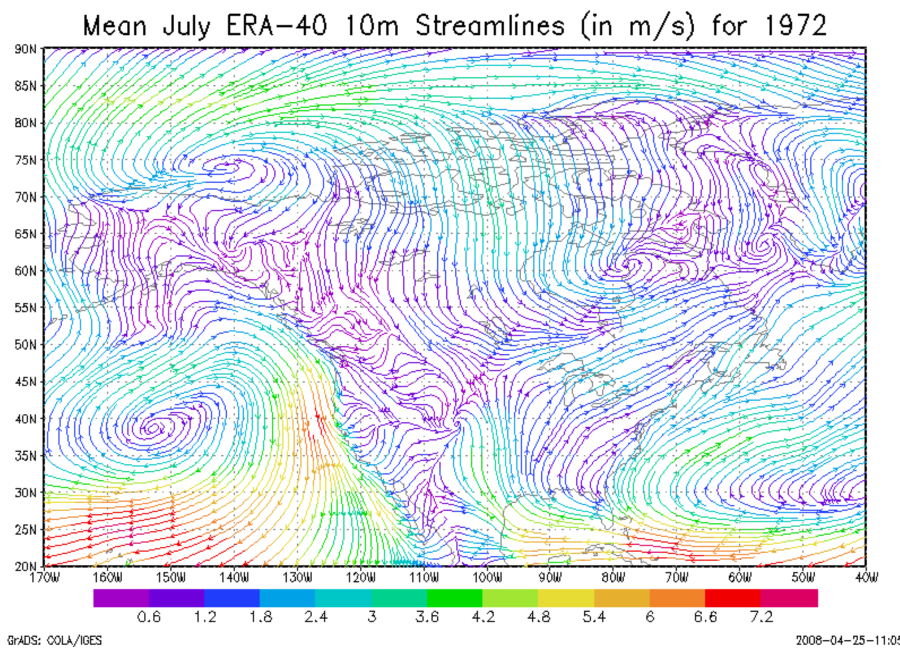

Figure A40. ERA-40 Mean July 10m streamlines for 1972.

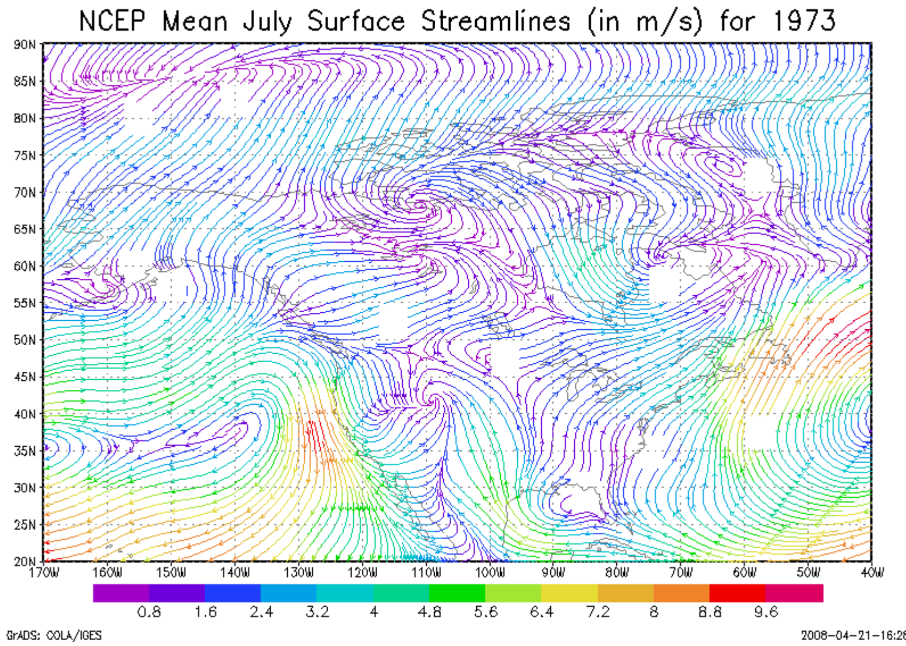

Figure A41. NCEP Mean July surface streamlines for 1973.

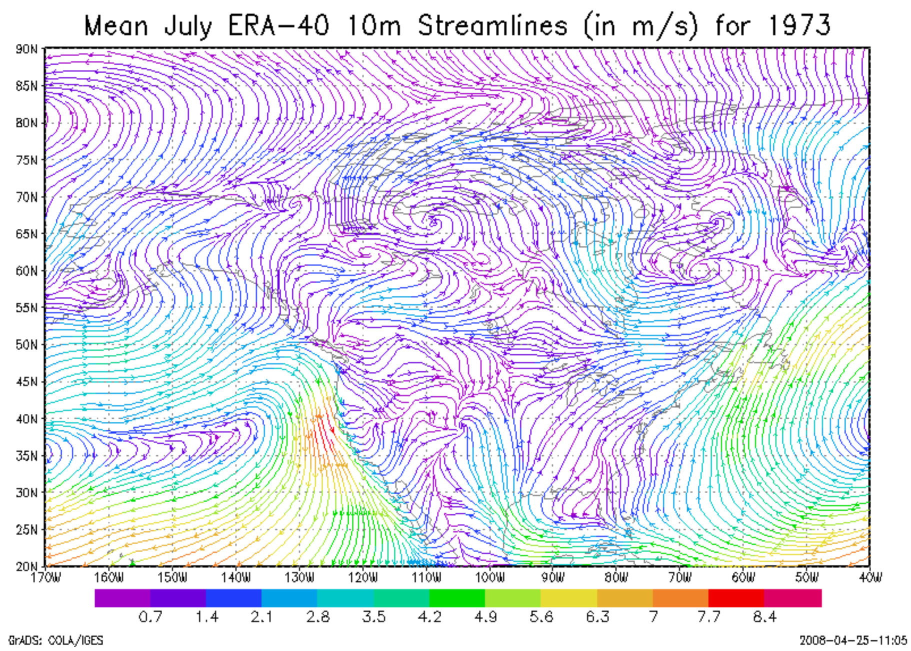

Figure A42. ERA-40 Mean July 10m streamlines for 1973.

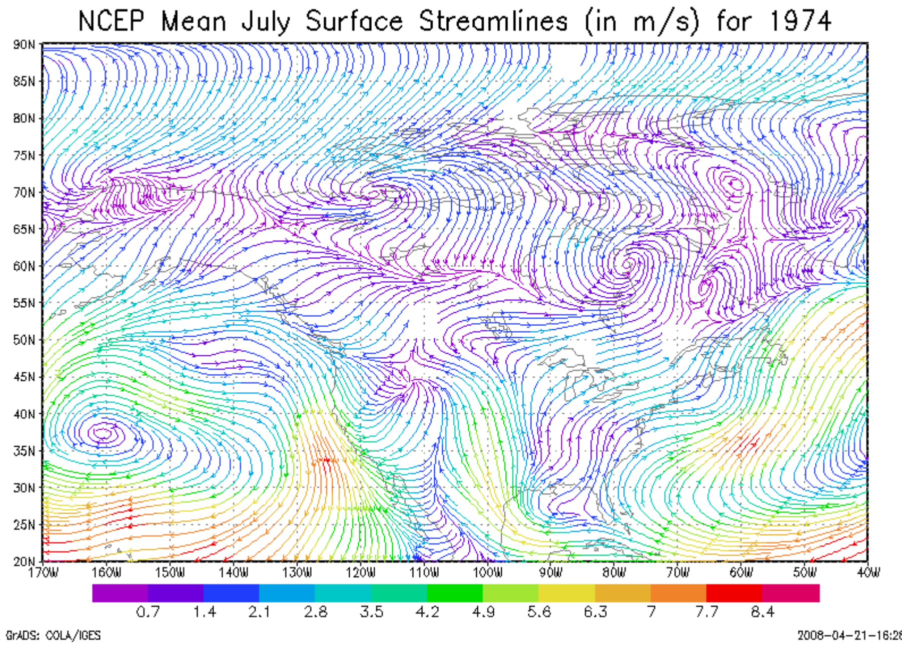

Figure A43. NCEP Mean July surface streamlines for 1974.

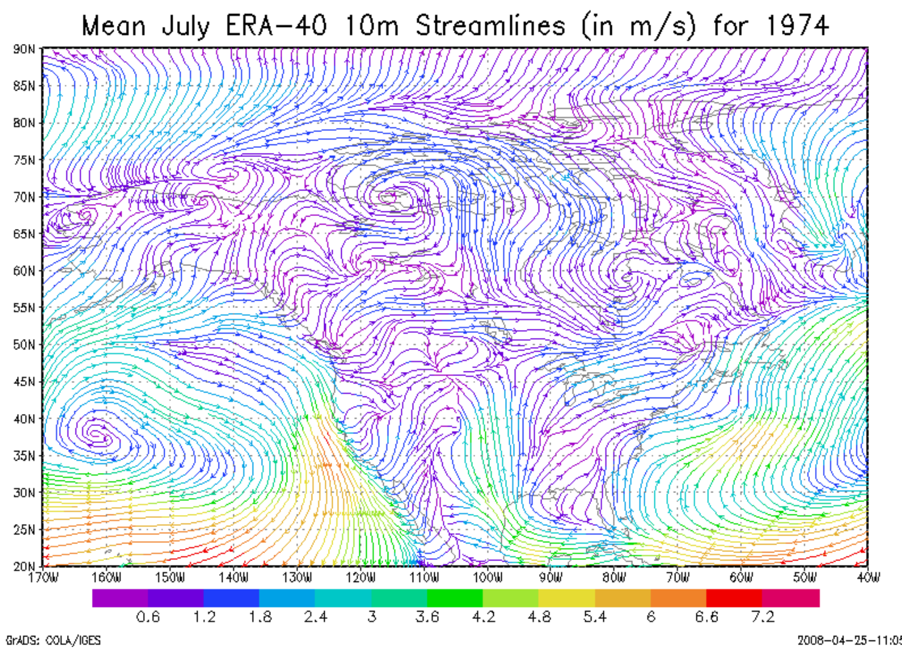

Figure A44. ERA-40 Mean July 10m streamlines for 1974.

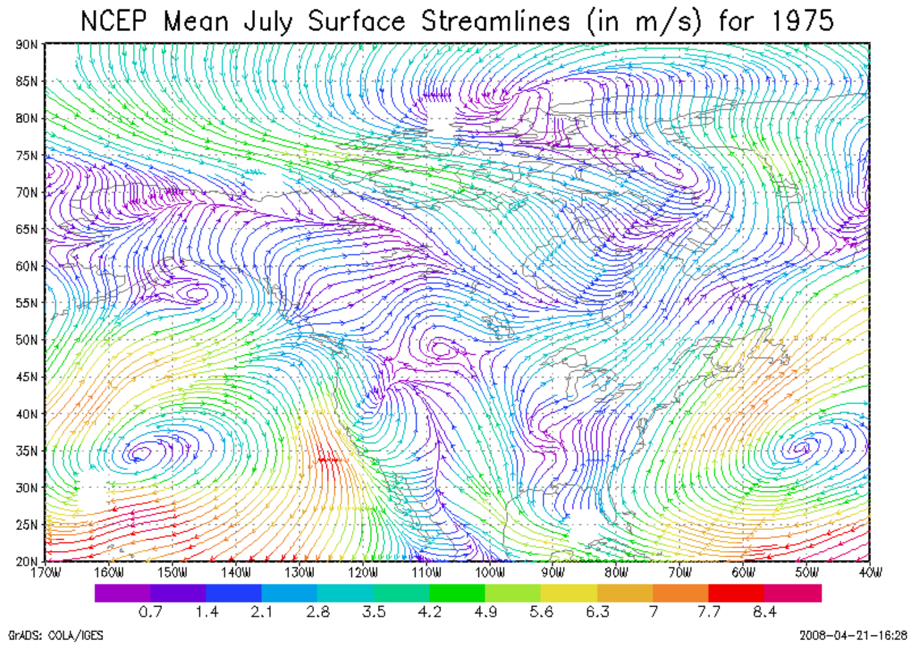

Figure A45. NCEP Mean July surface streamlines for 1975.

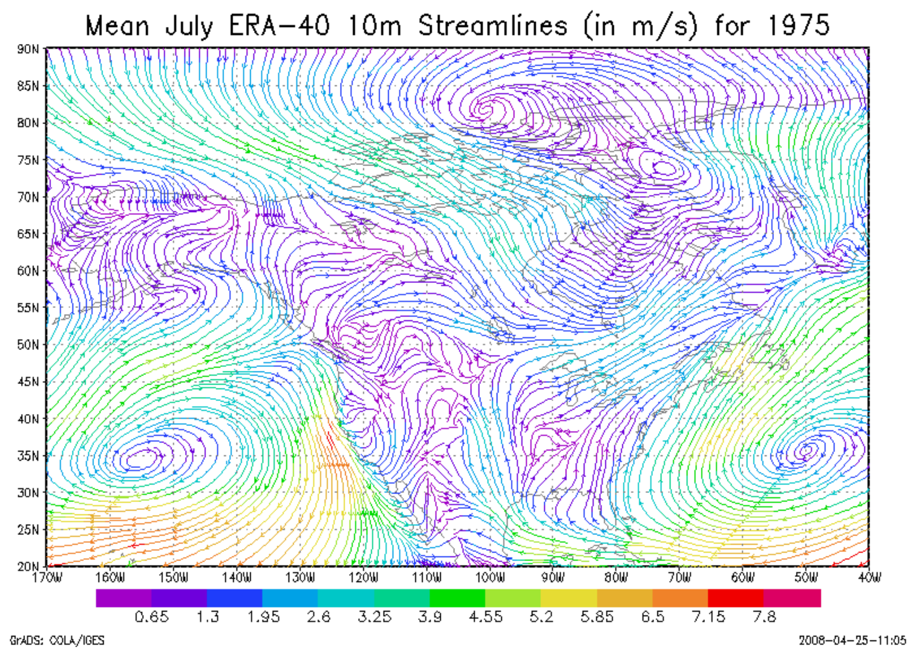

Figure A46. ERA-40 Mean July 10m streamlines for 1975.

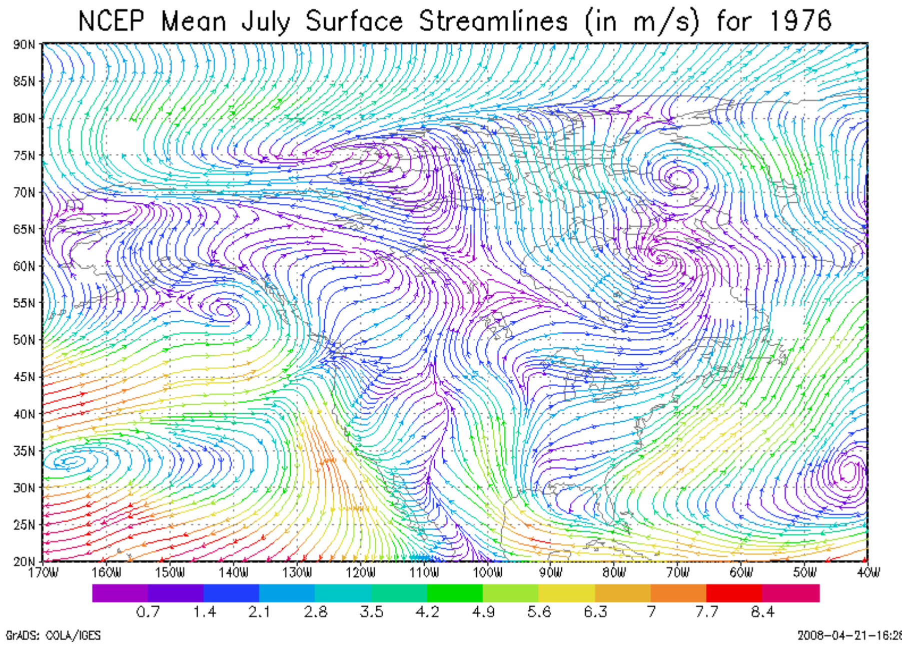

Figure A47. NCEP Mean July surface streamlines for 1976.

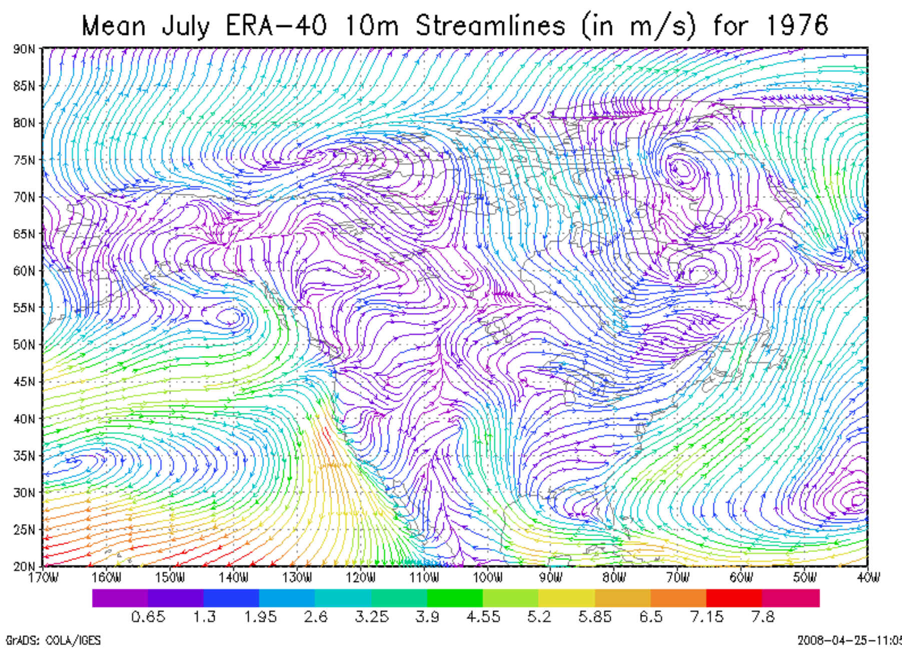

Figure A48. ERA-40 Mean July 10m streamlines for 1976.

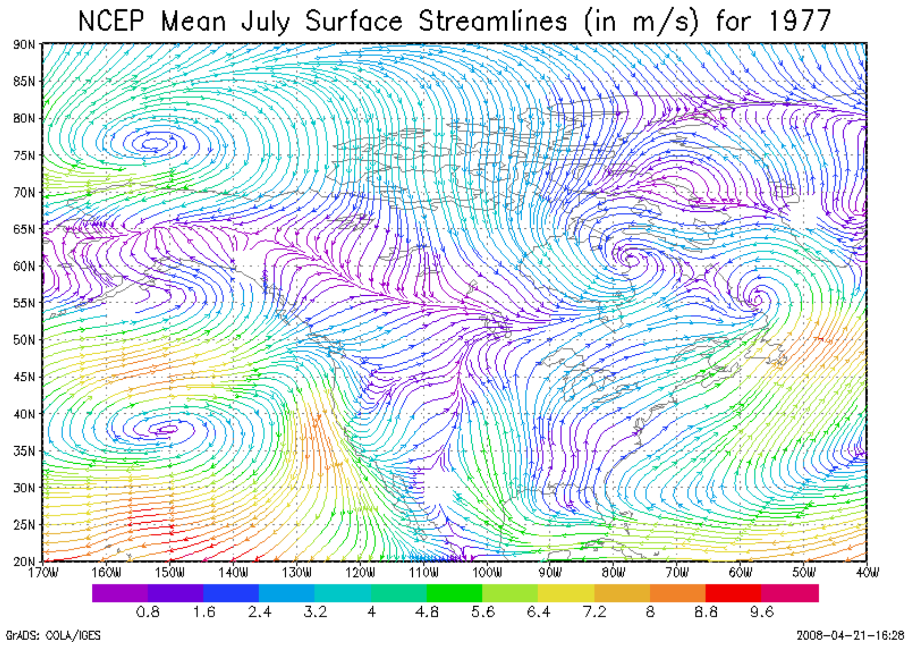

Figure A49. NCEP Mean July surface streamlines for 1977.

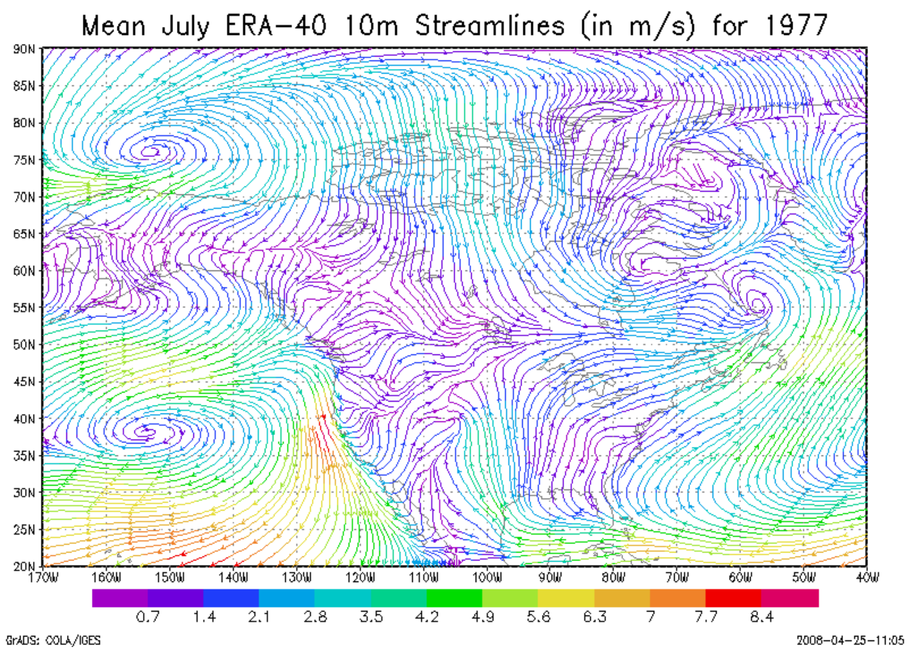

Figure A50. ERA-40 Mean July 10m streamlines for 1977.

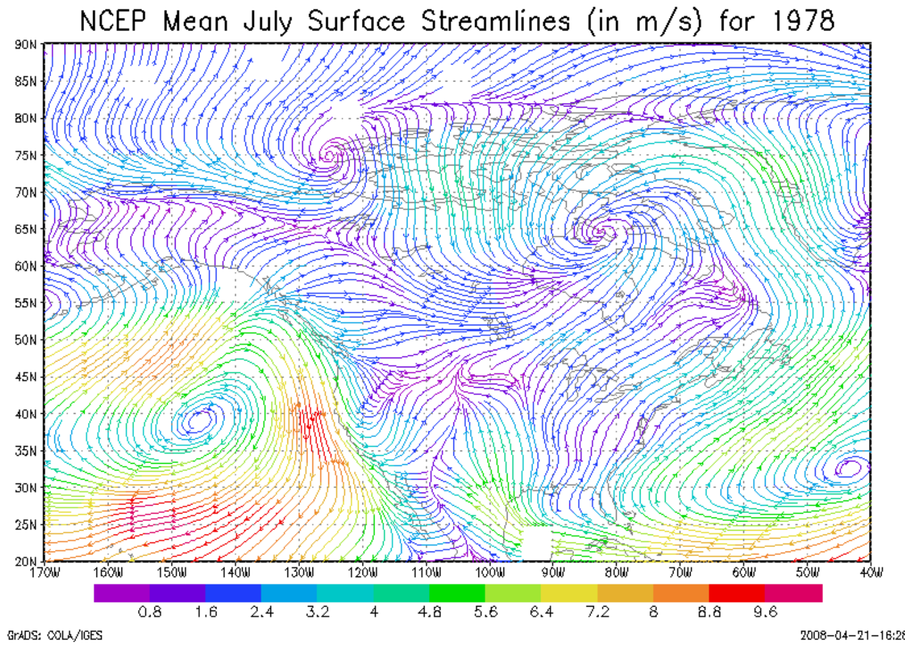

Figure A51. NCEP Mean July surface streamlines for 1978.

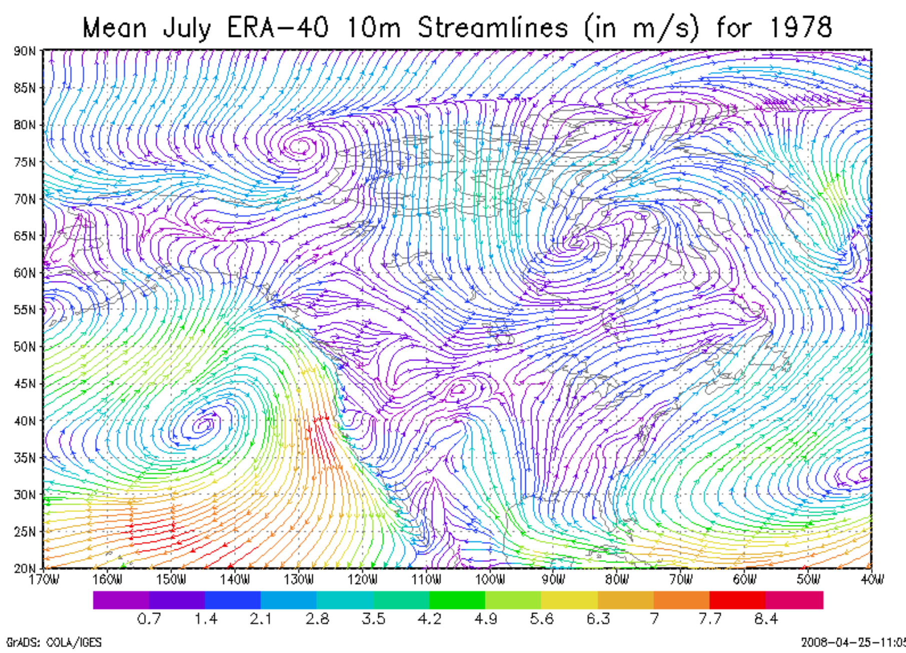

Figure A52. ERA-40 Mean July 10m streamlines for 1978.

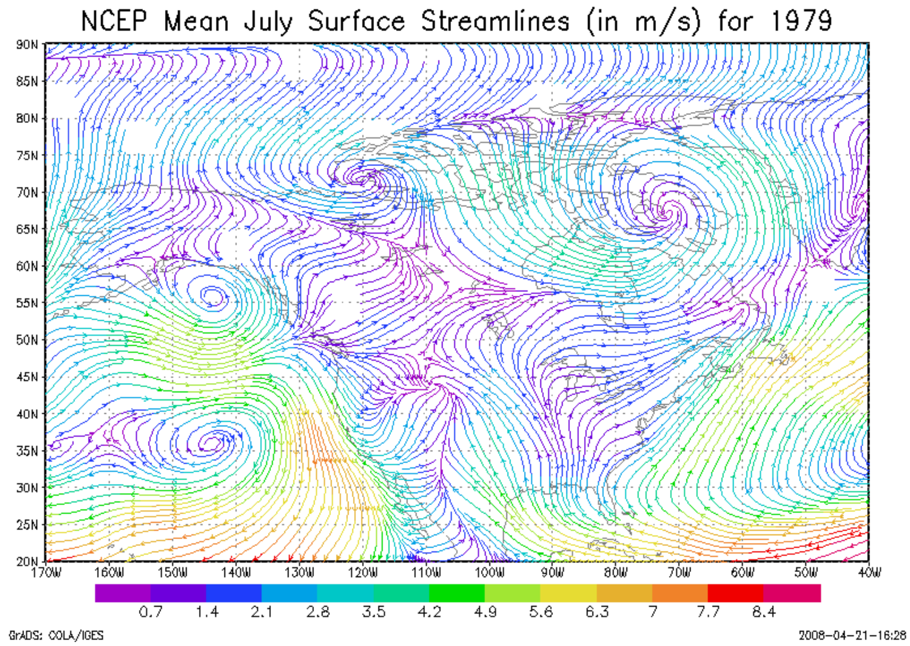

Figure A53. NCEP Mean July surface streamlines for 1979.

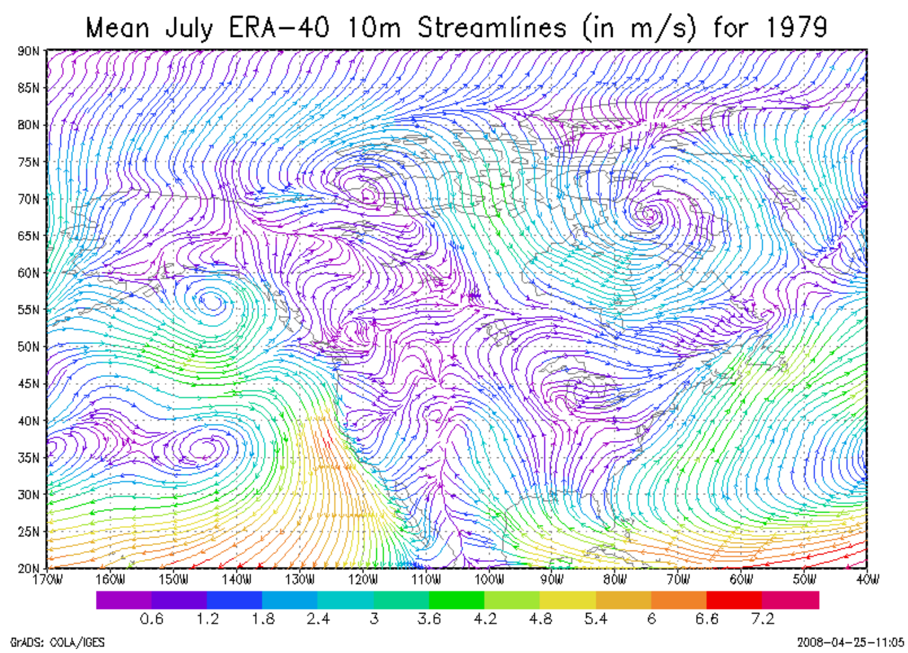

Figure A54. ERA-40 Mean July 10m streamlines for 1979.

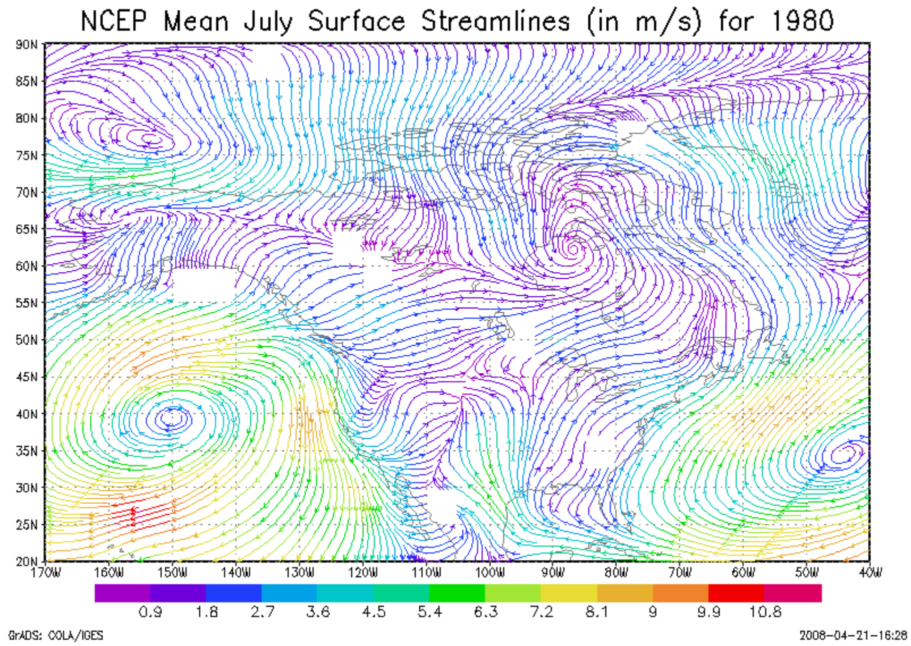

Figure A55. NCEP Mean July surface streamlines for 1980.

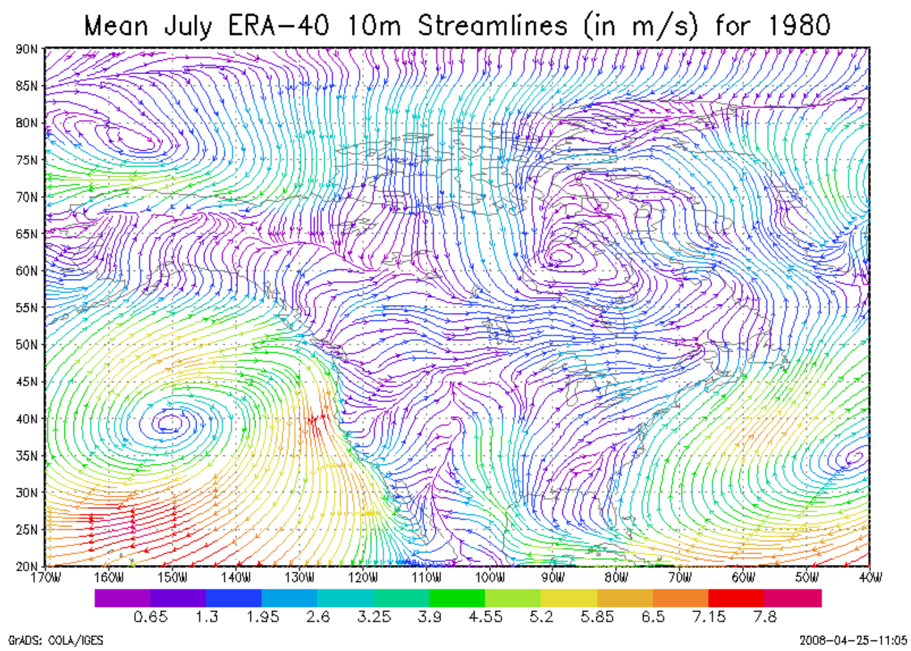

Figure A56. ERA-40 Mean July 10m streamlines for 1980.

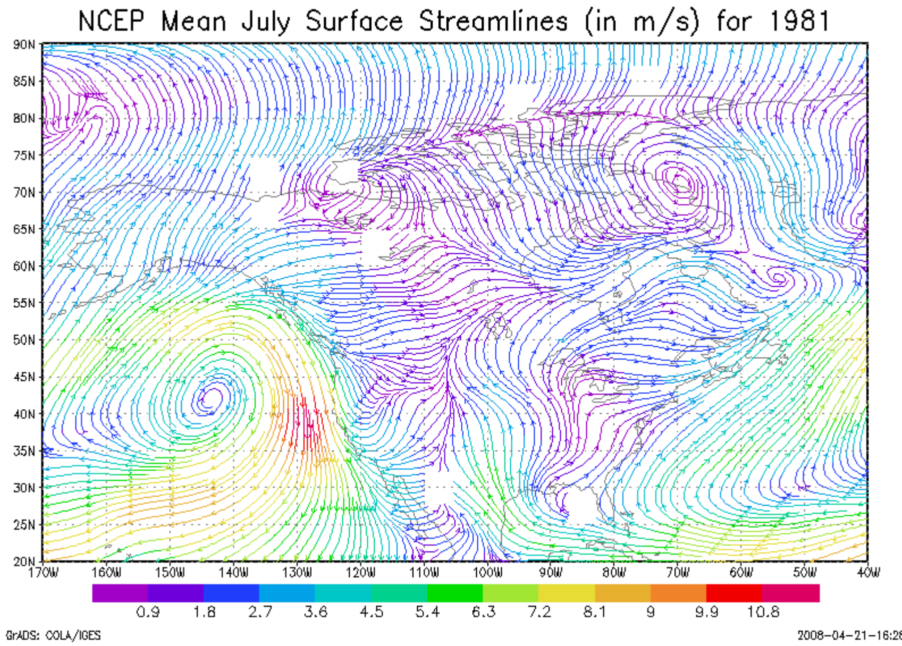

Figure A57. NCEP Mean July surface streamlines for 1981.

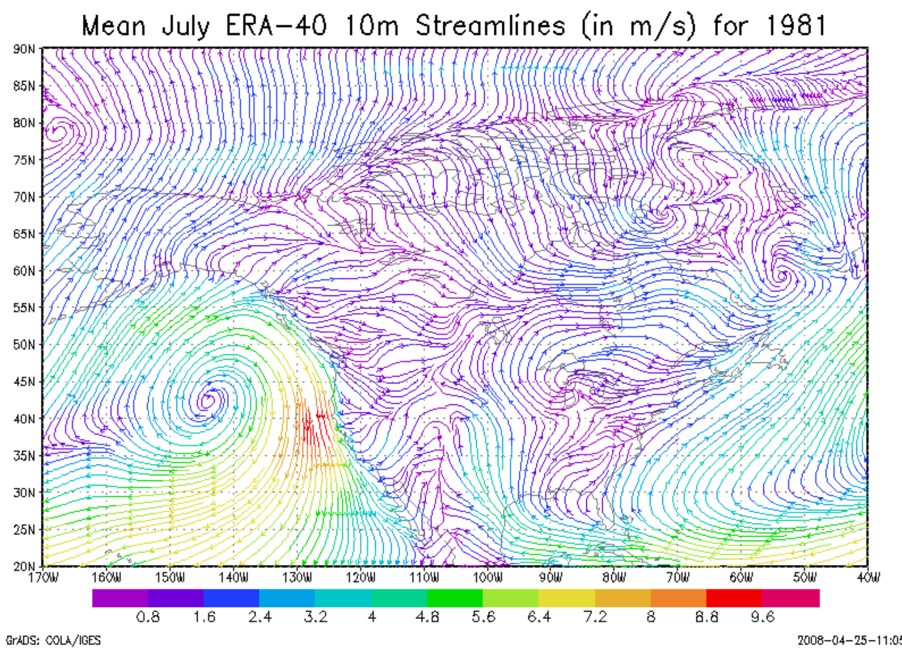

Figure A58. ERA-40 Mean July 10m streamlines for 1981.

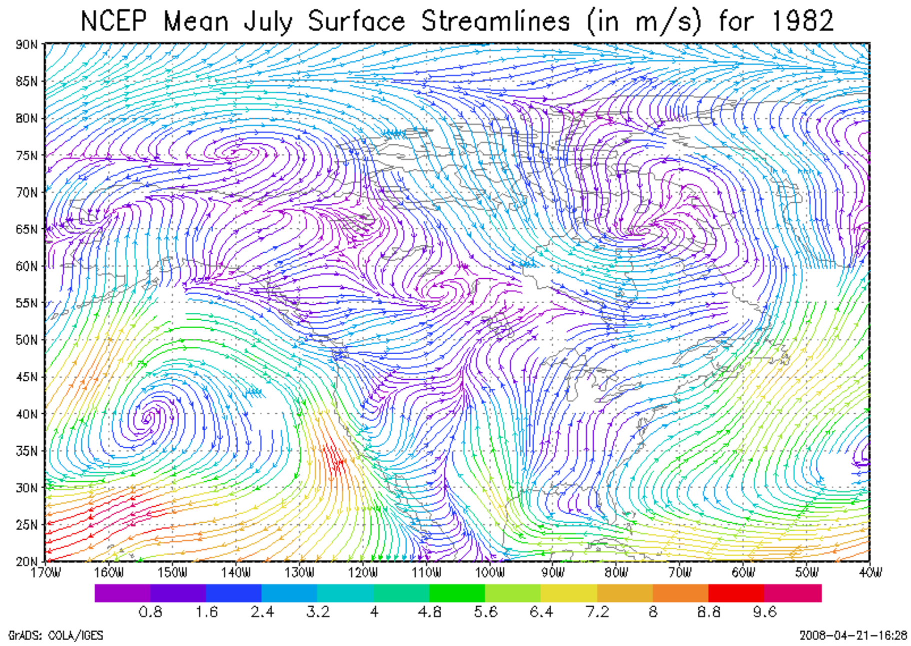

Figure A59. NCEP Mean July surface streamlines for 1982.

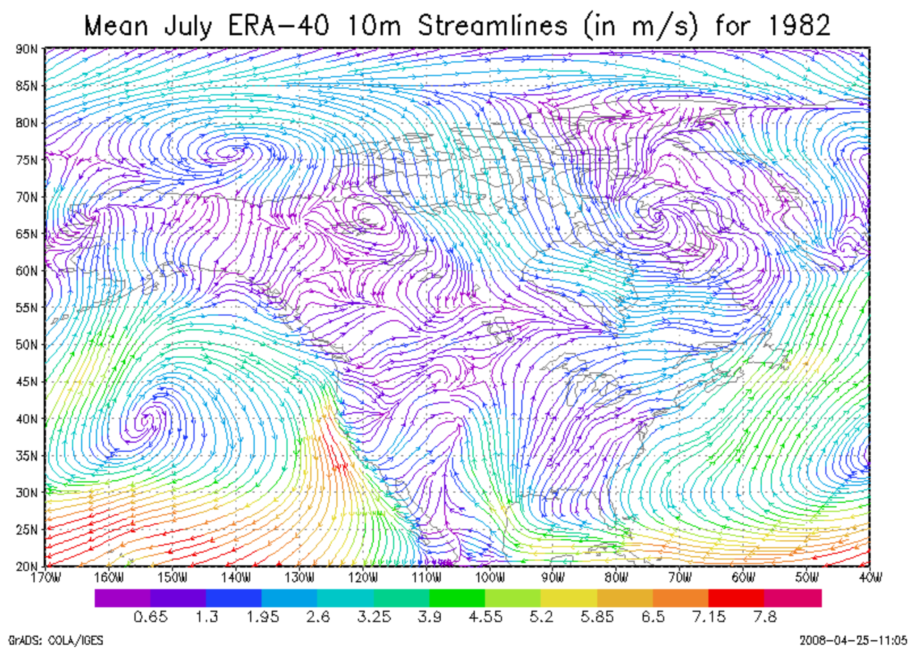

Figure A60, ERA-40 Mean July 10m streamlines for 1982.

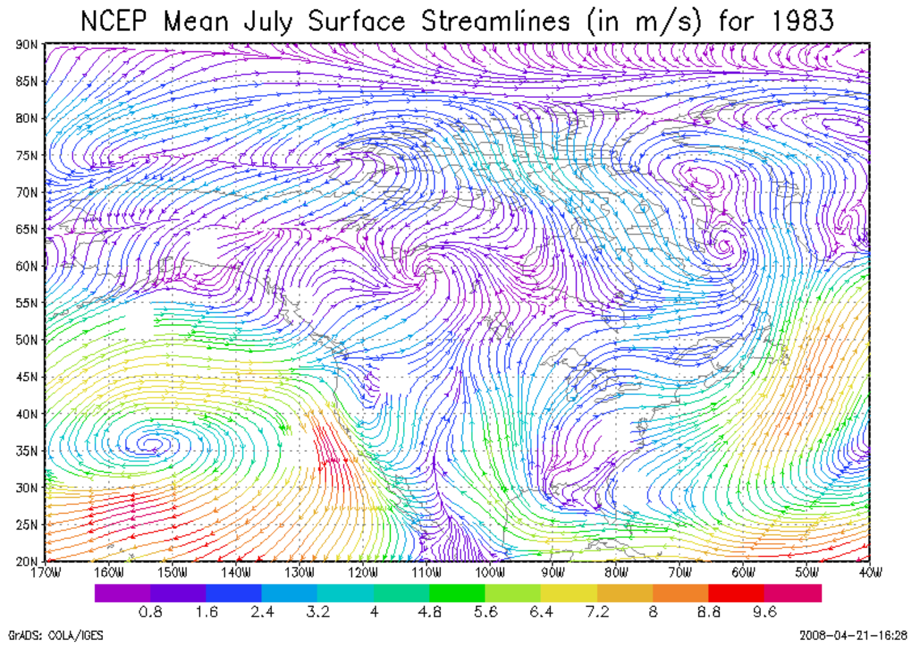

Figure A61. NCEP Mean July surface streamlines for 1983.

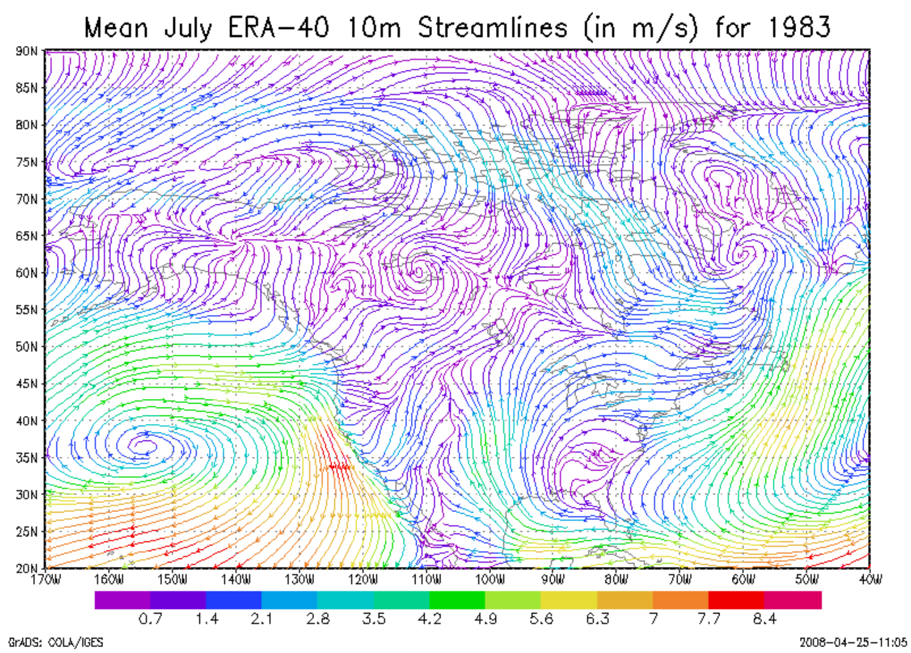

Figure A62. ERA-40 Mean July 10m streamlines for 1983.

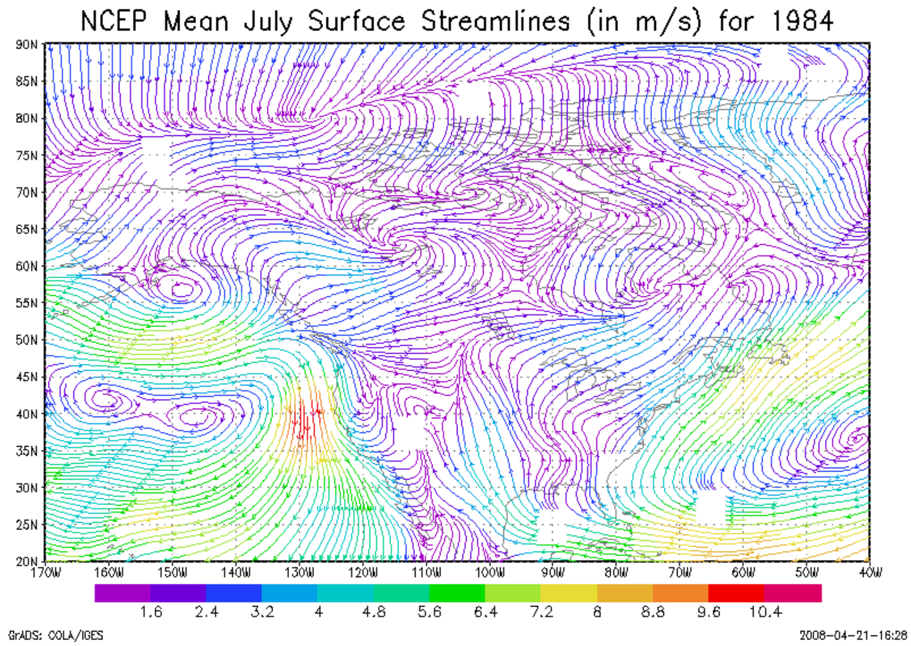

Figure A63. NCEP Mean July surface streamlines for 1984.

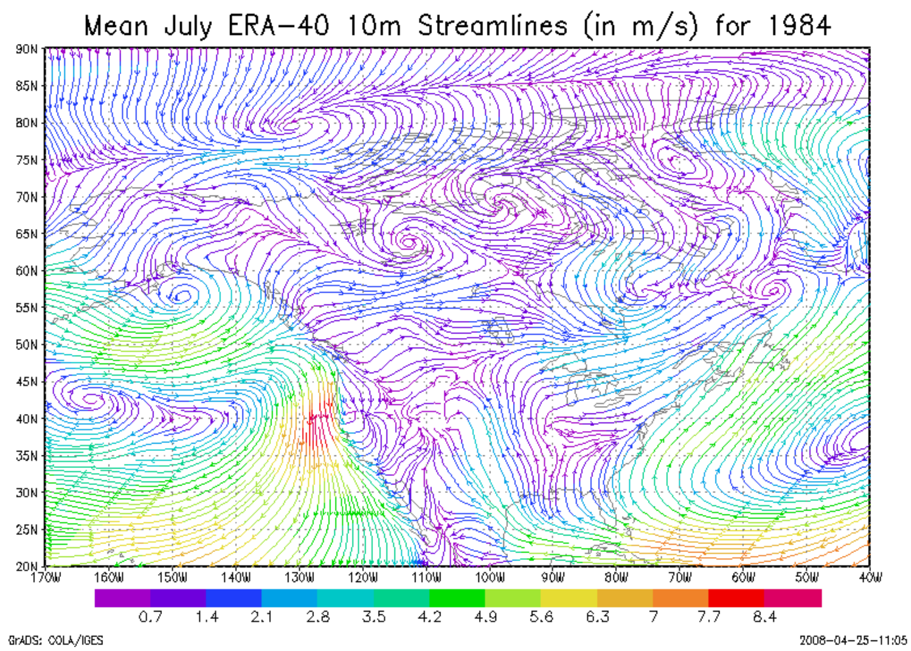

Figure A64, ERA-40 Mean July 10m streamlines for 1984.

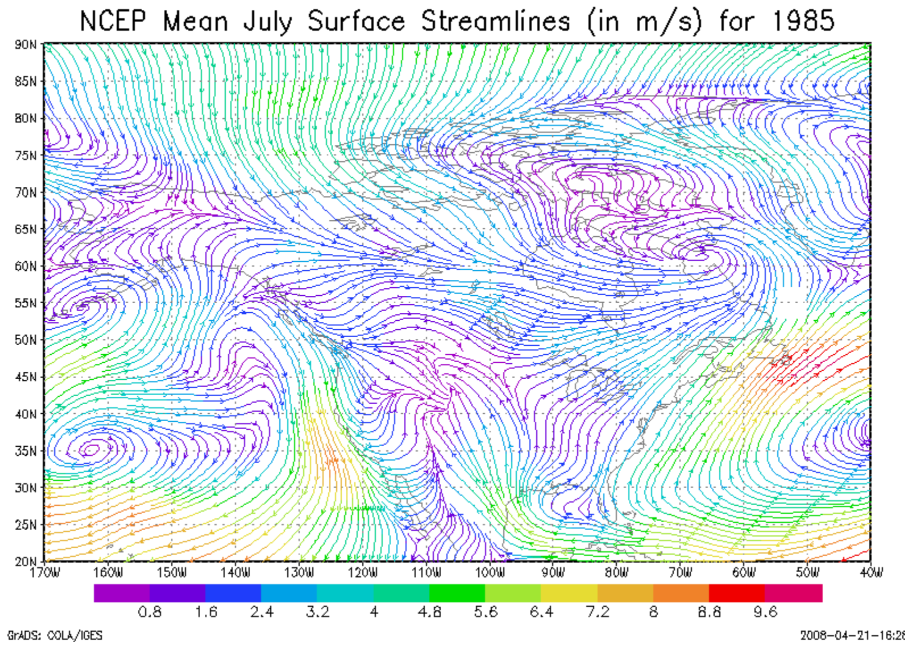

Figure A65. NCEP Mean July surface streamlines for 1985.

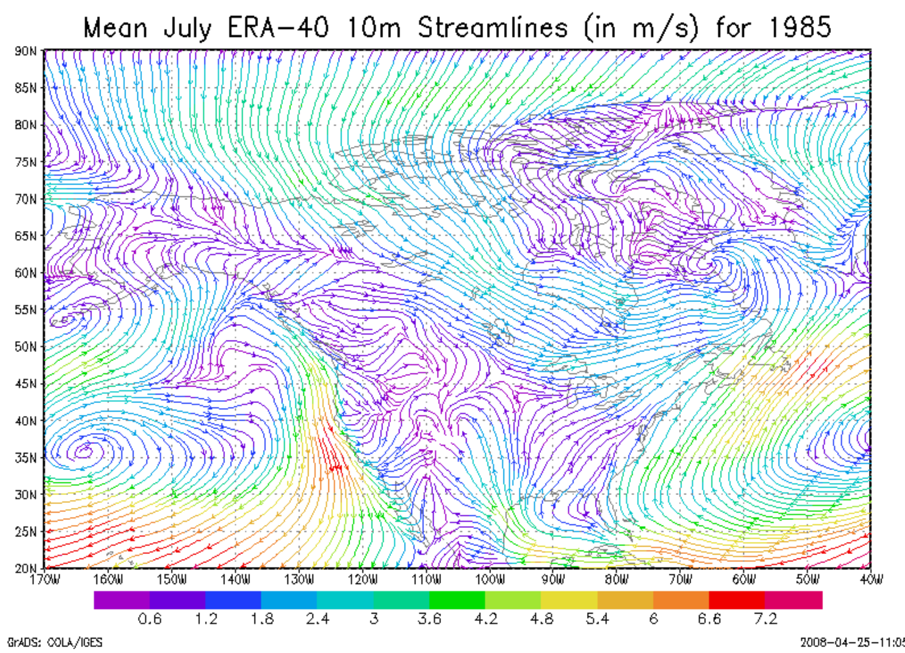

Figure A66. ERA-40 Mean July 10m streamlines for 1985.

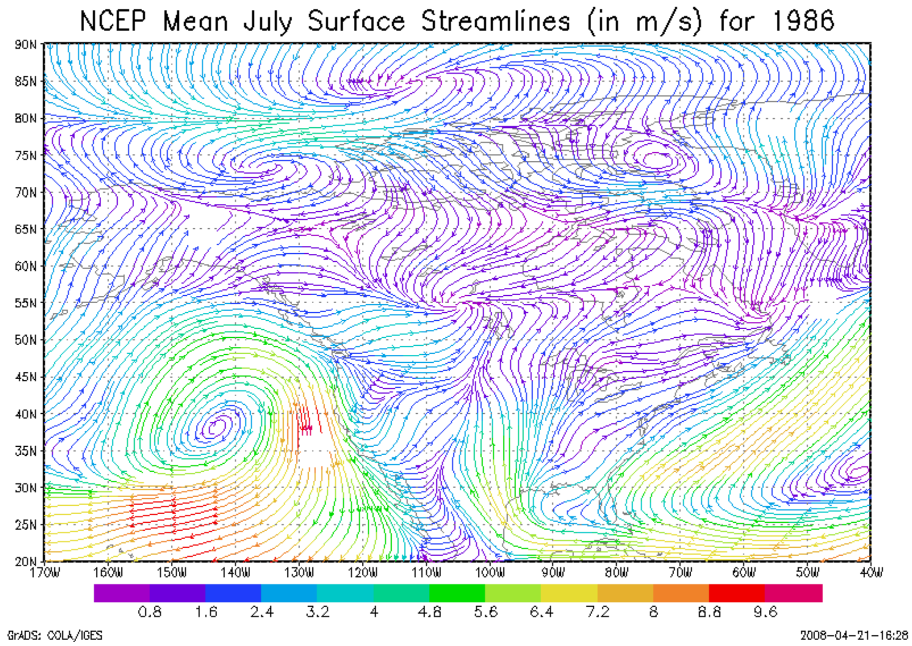

Figure A67. NCEP Mean July surface streamlines for 1986.

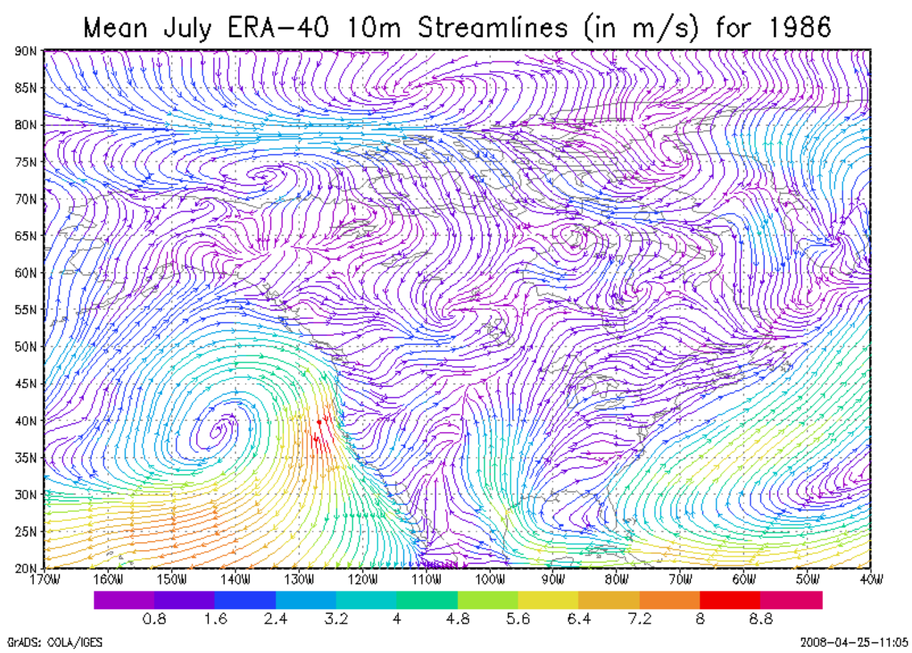

Figure A68. ERA-40 Mean July 10m streamlines for 1986.

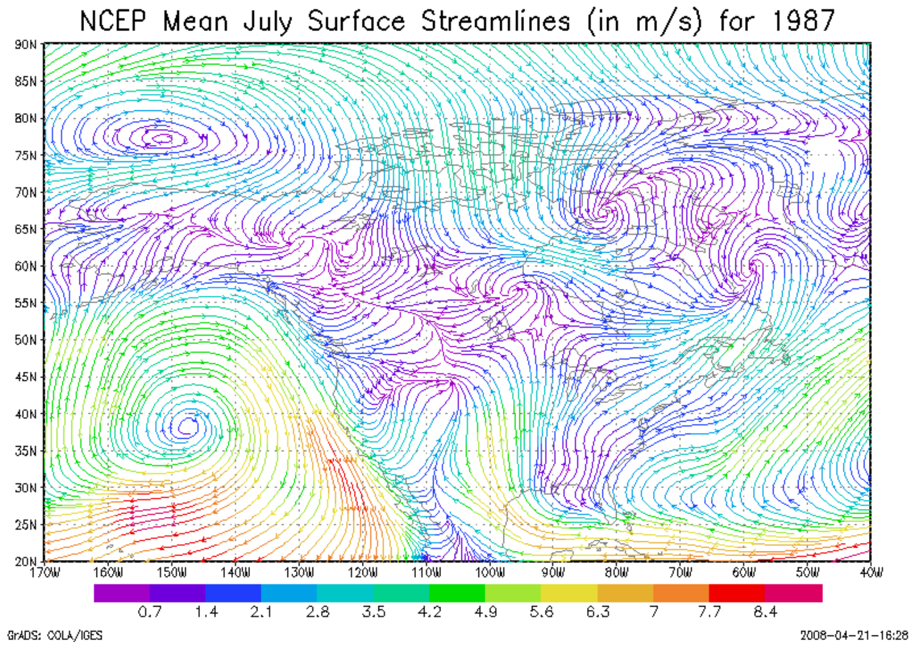

Figure A69. NCEP Mean July surface streamlines for 1987.

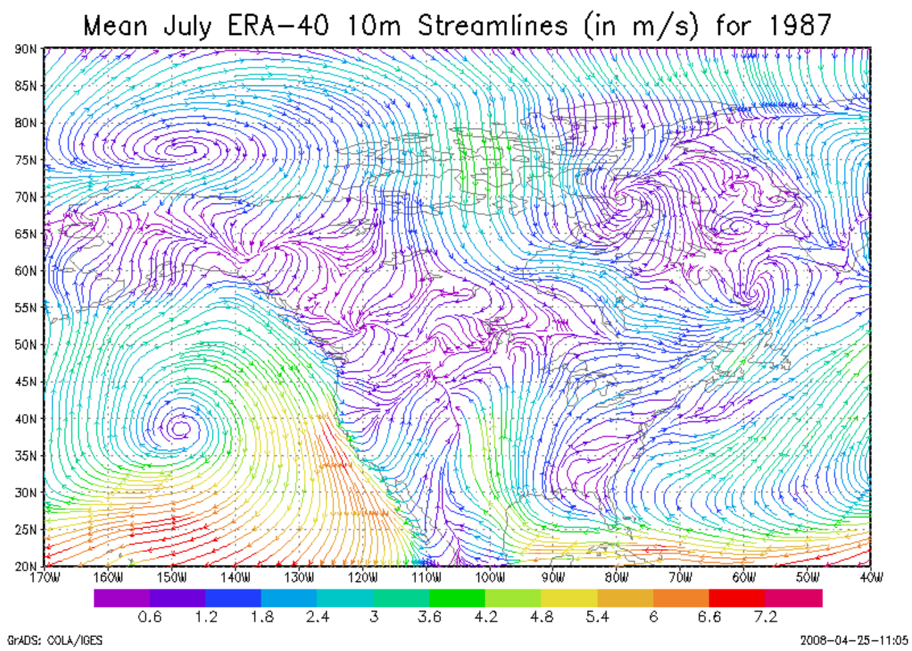

Figure A70. ERA-40 Mean July 10m streamlines for 1987.

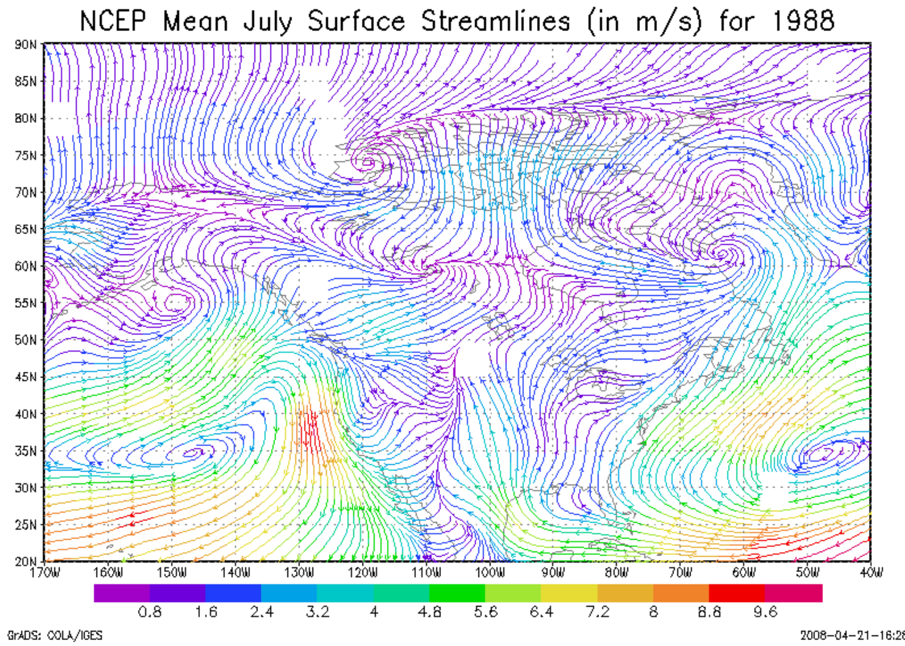

Figure A71. NCEP Mean July surface streamlines for 1988.

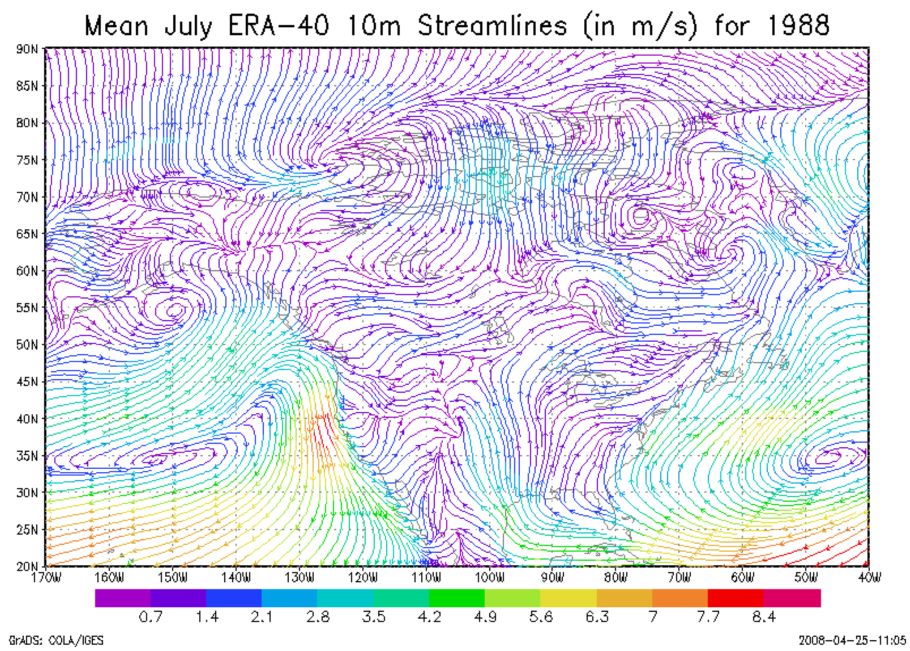

Figure A72. ERA-40 Mean July 10m streamlines for 1988.

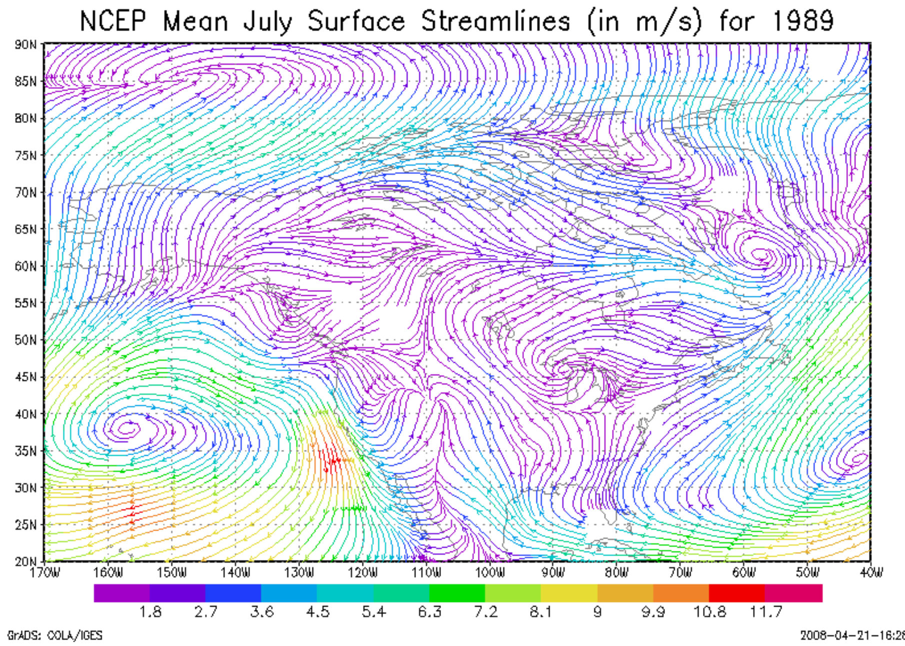

Figure A73. NCEP Mean July surface streamlines for 1989.

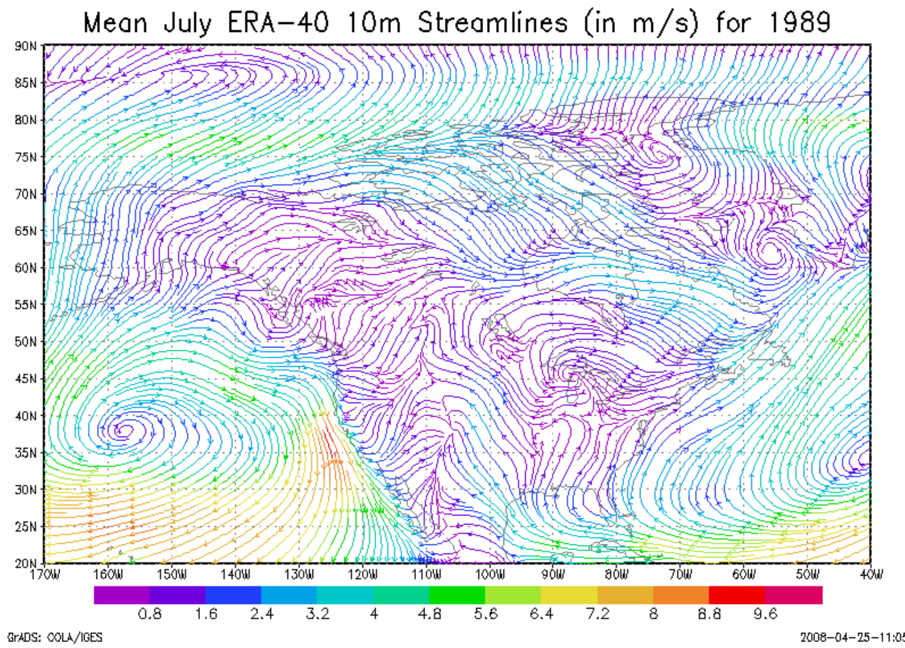

Figure A74. ERA-40 Mean July 10m streamlines for 1989.

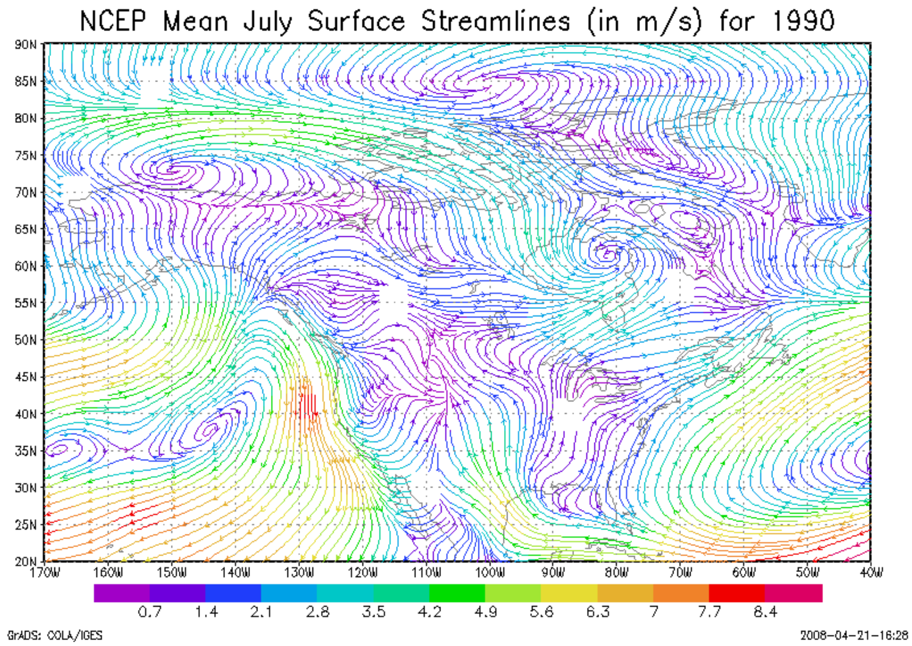

Figure A75. NCEP Mean July surface streamlines for 1990.

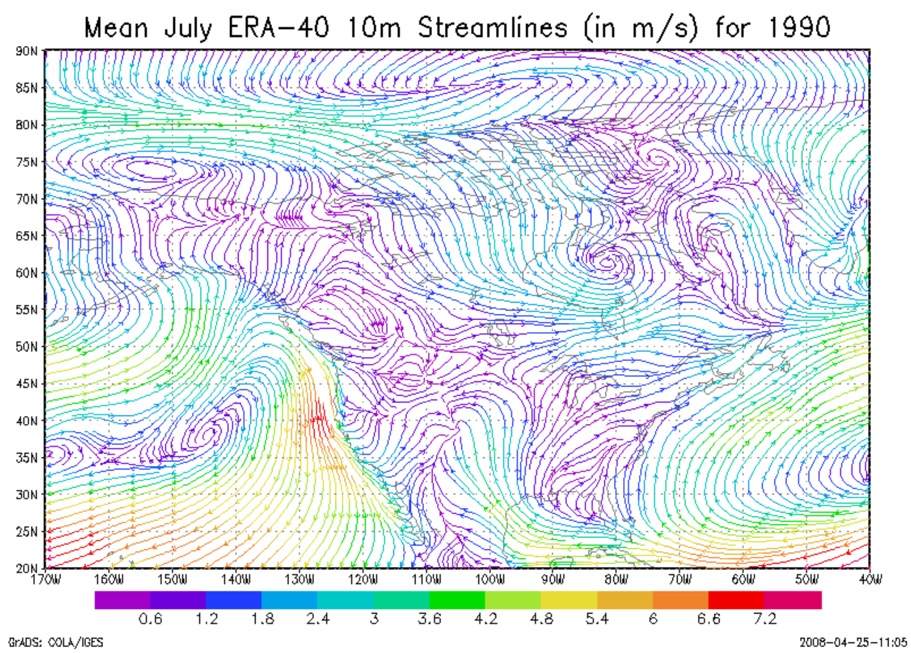

Figure A76. ERA-40 Mean July 10m streamlines for 1990.

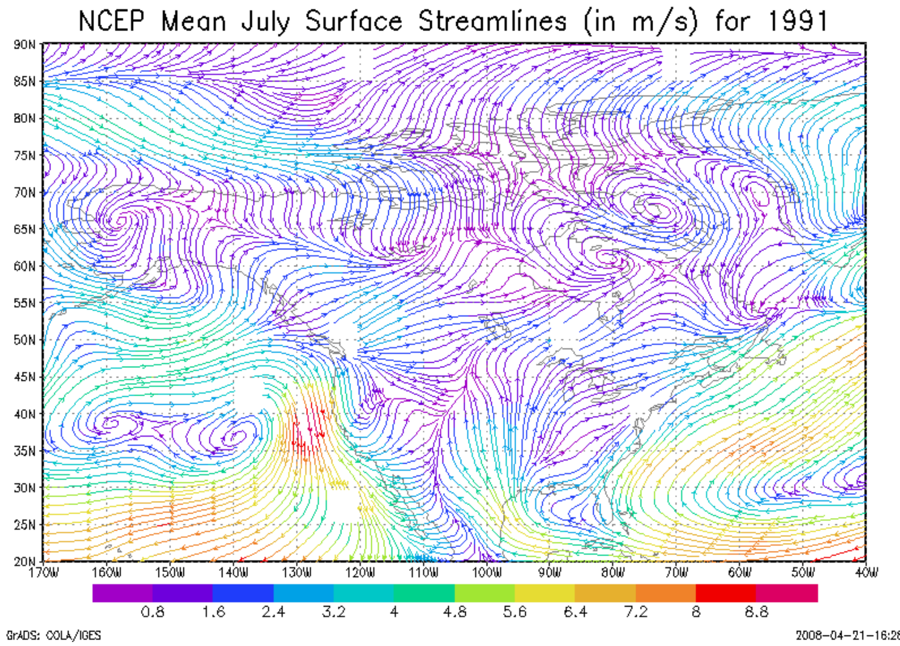

Figure A77. NCEP Mean July surface streamlines for 1991.

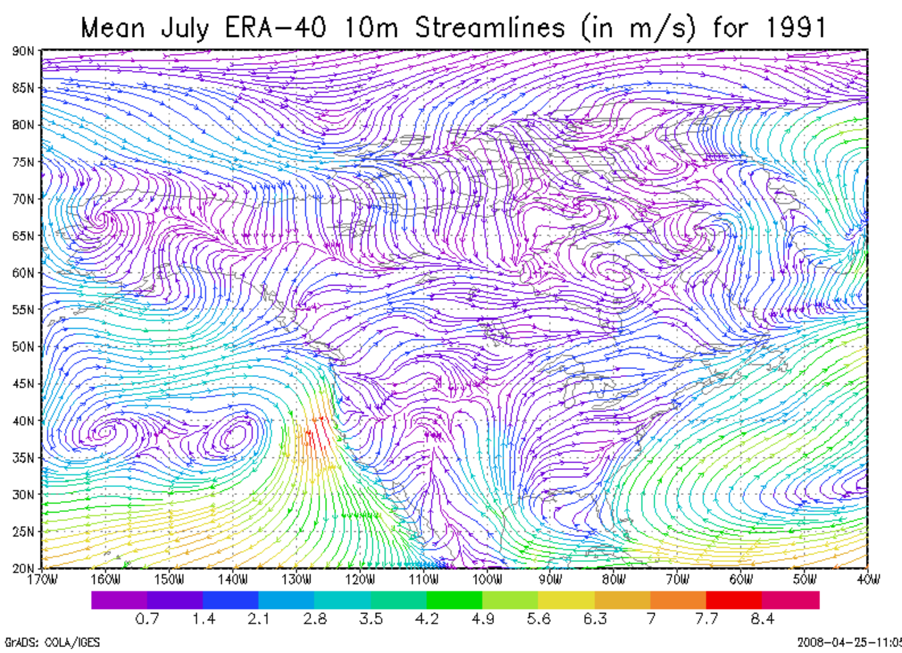

Figure A78. ERA-40 Mean July 10m streamlines for 1991.

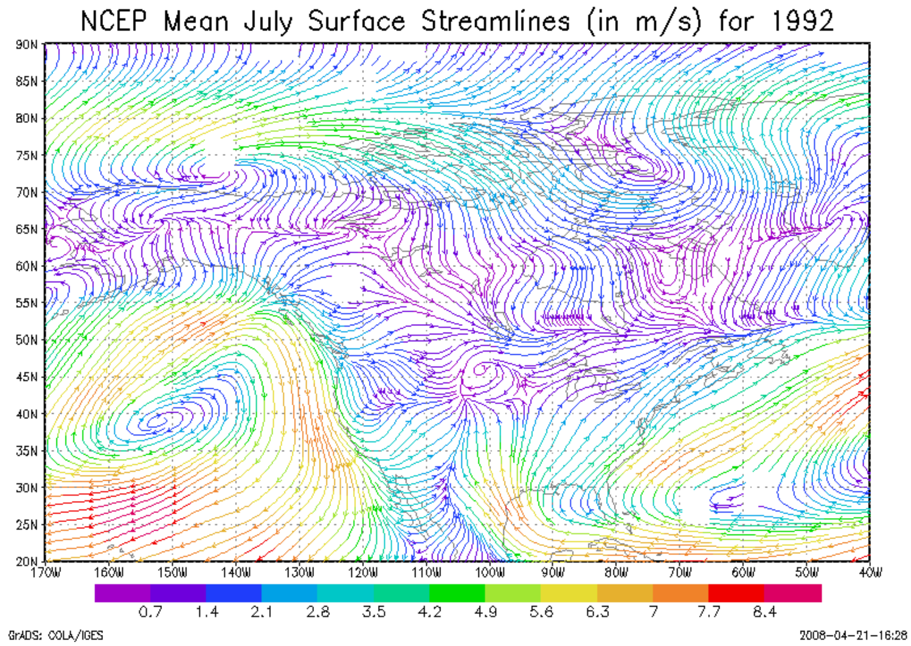

Figure A79. NCEP Mean July surface streamlines for 1992.

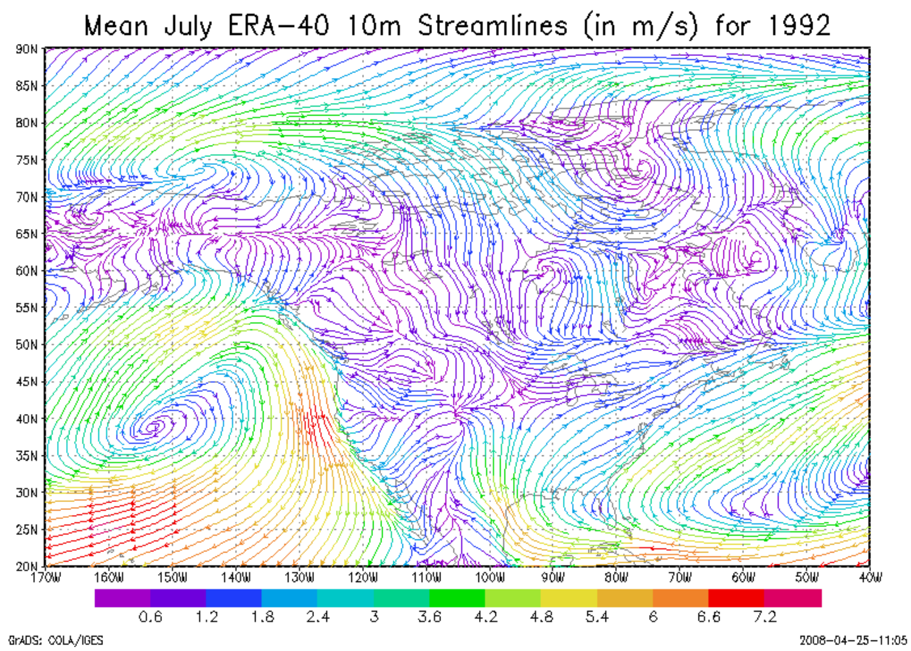

Figure A80. ERA-40 Mean July 10m streamlines for 1992.

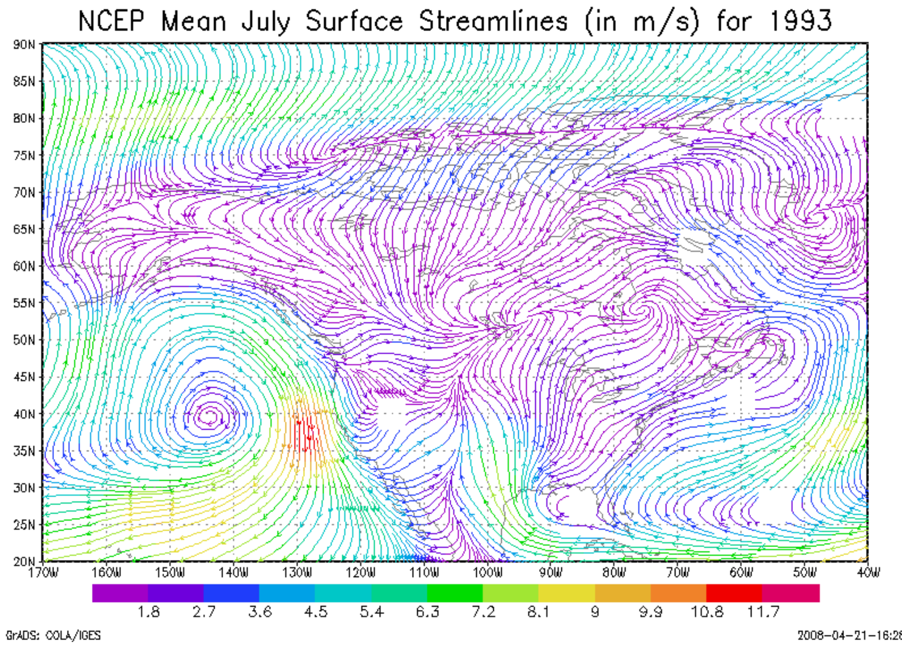

Figure A81. NCEP Mean July surface streamlines for 1993.

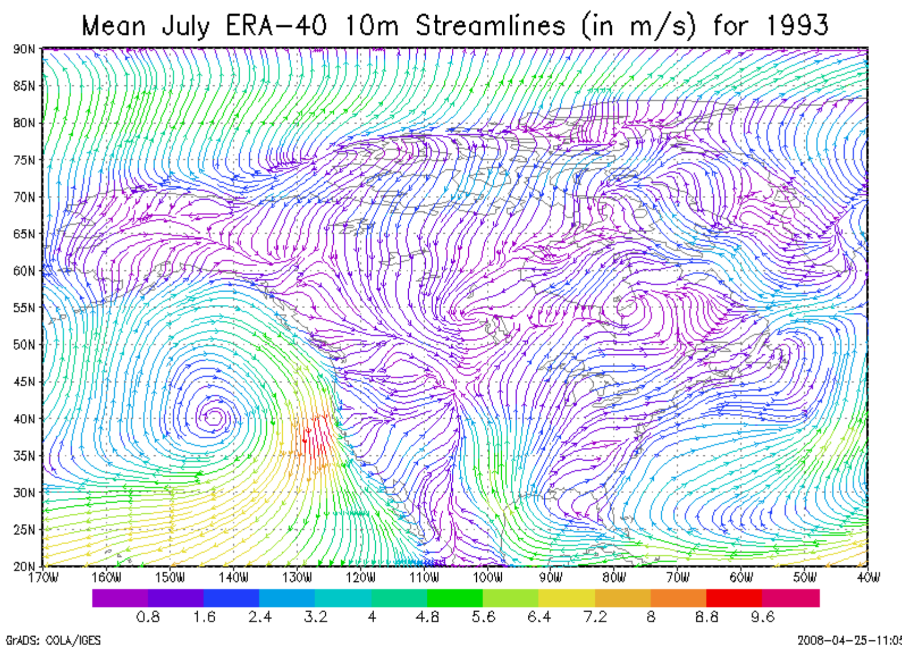

Figure A82. ERA-40 Mean July 10m streamlines for 1993.

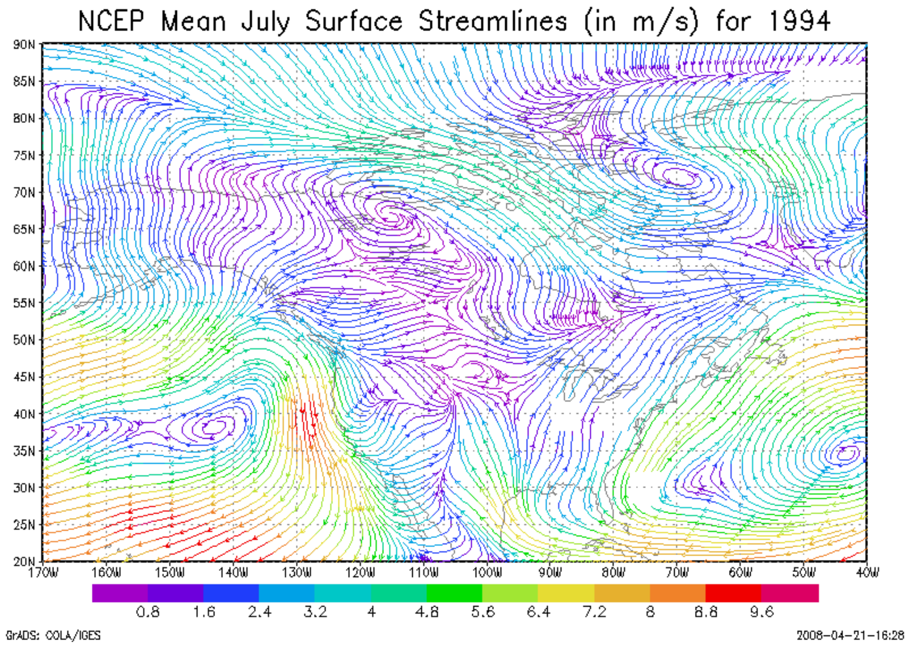

Figure A83. NCEP Mean July surface streamlines for 1994.

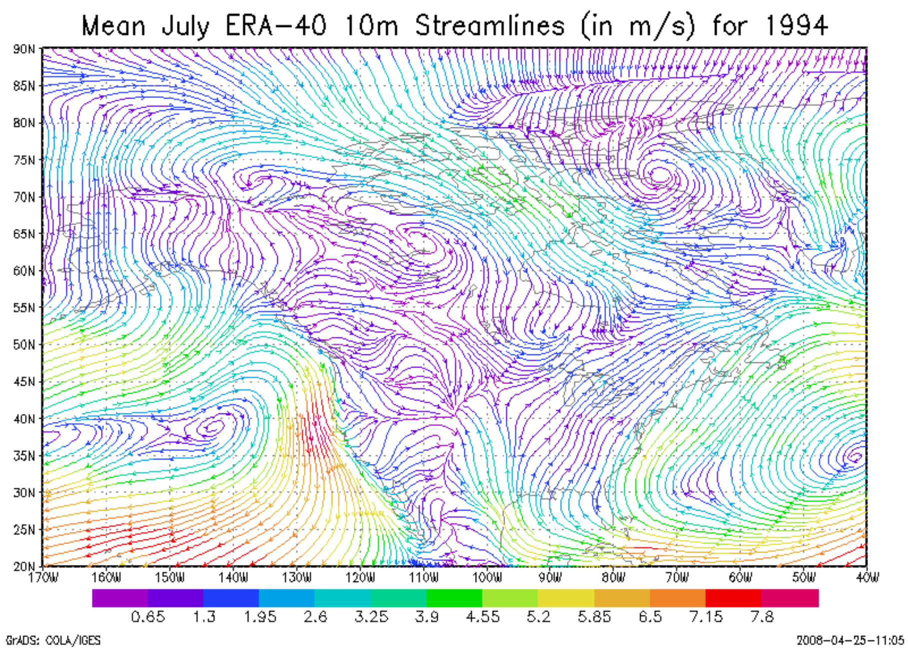

Figure A84. ERA-40 Mean July 10m streamlines for 1994.

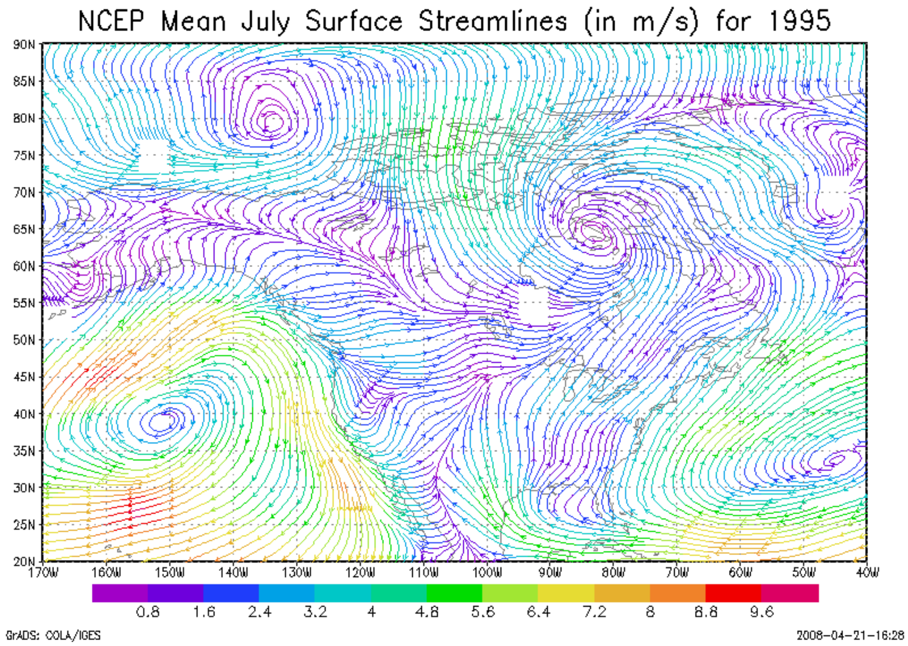

Figure A85. NCEP Mean July surface streamlines for 1995.

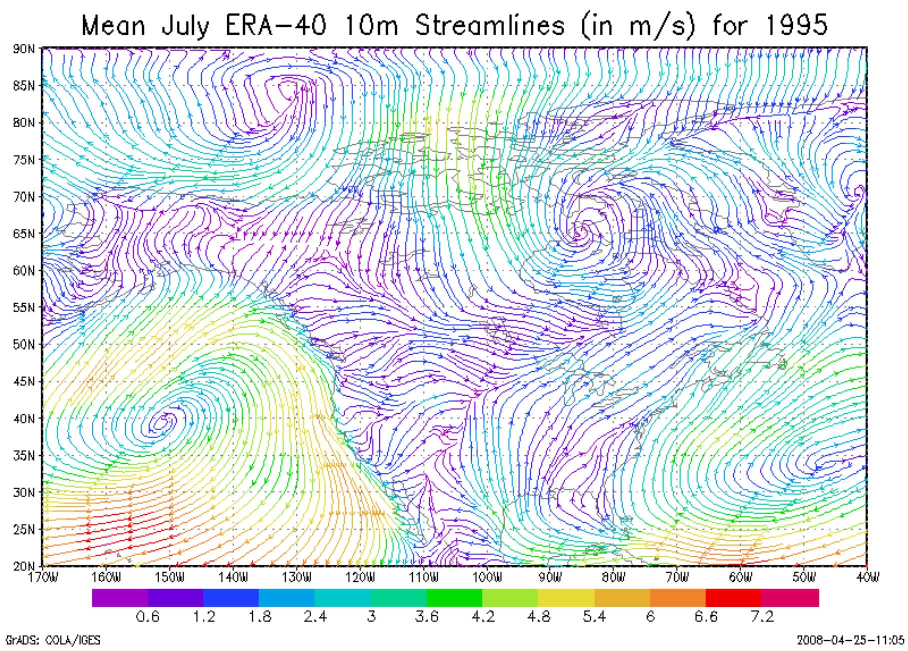

Figure A86. ERA-40 Mean July 10m streamlines for 1995.

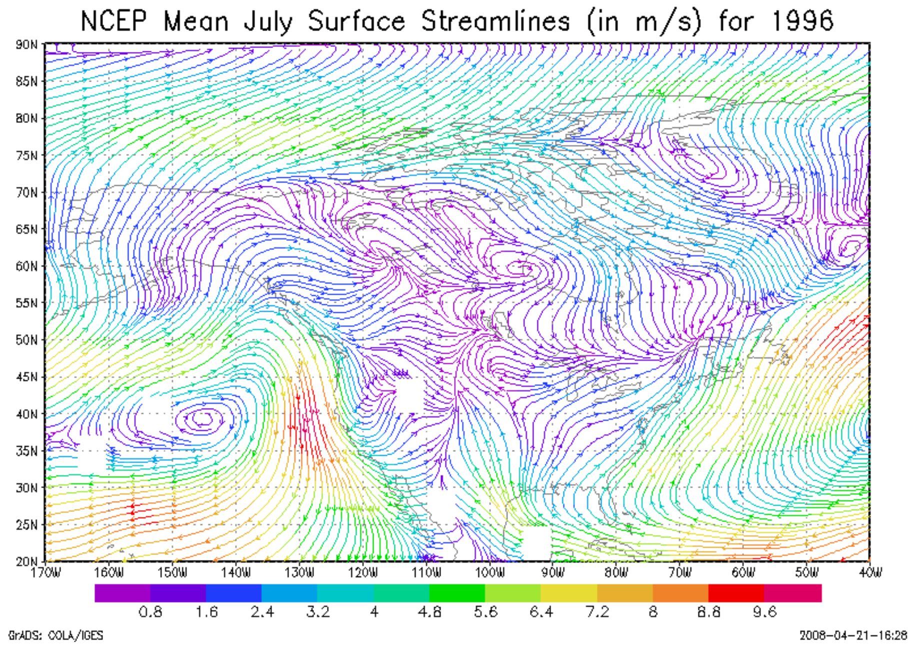

Figure A87. NCEP Mean July surface streamlines for 1996.

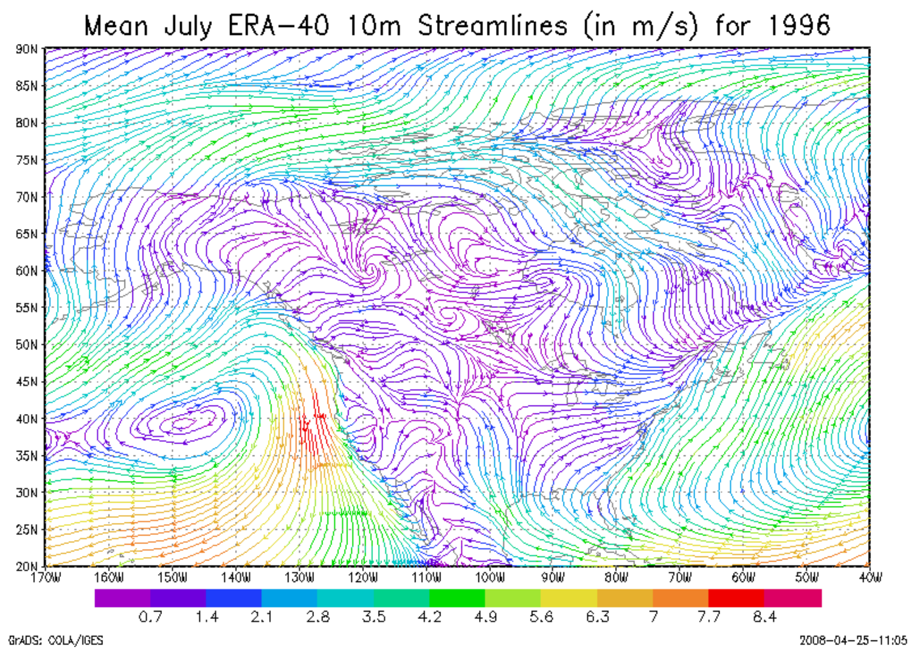

Figure A88. ERA-40 Mean July 10m streamlines for 1996.

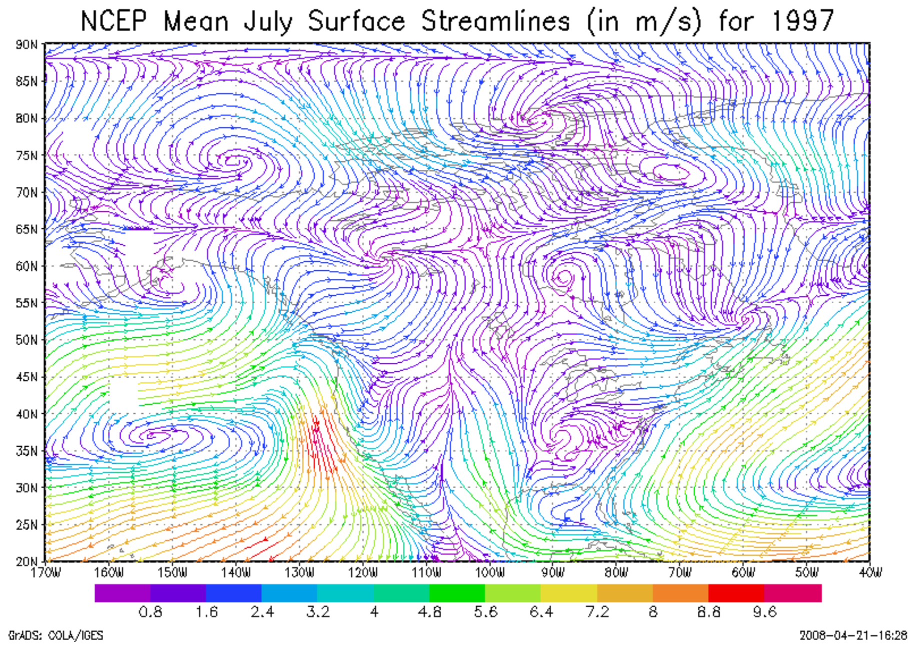

Figure A89. NCEP Mean July surface streamlines for 1997.

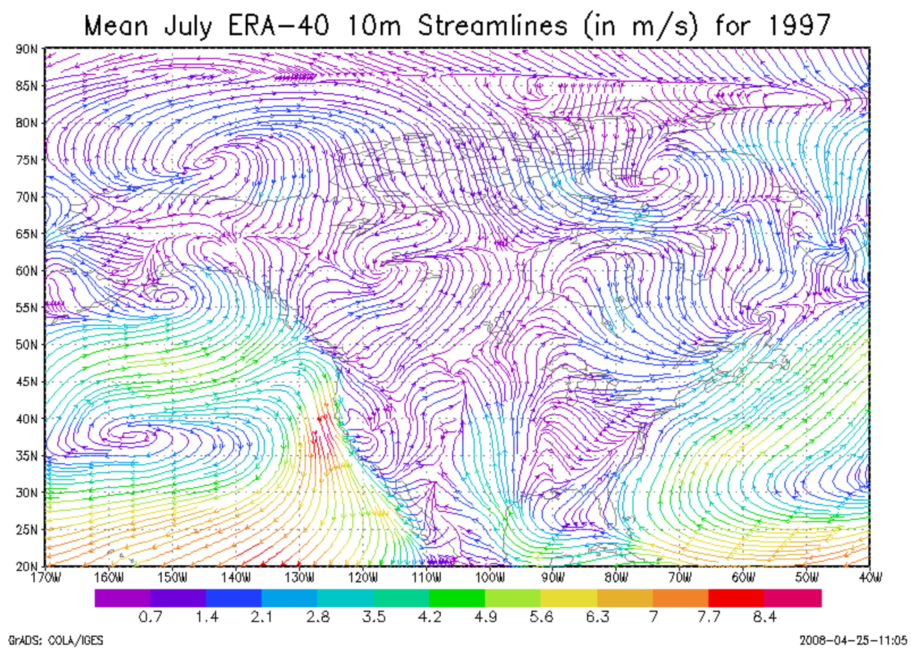

Figure A90. ERA-40 Mean July 10m streamlines for 1997.

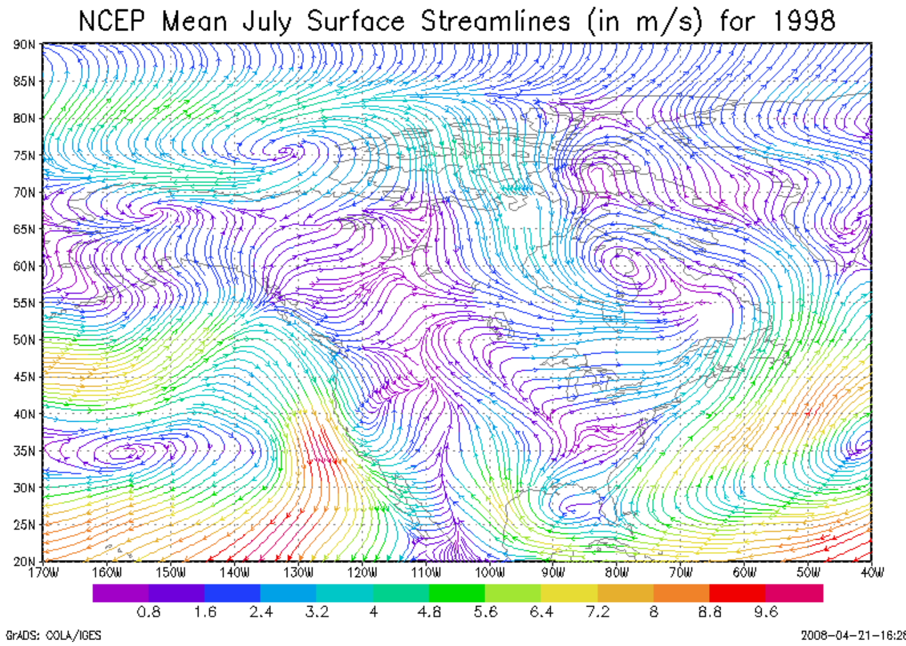

Figure A91. NCEP Mean July surface streamlines for 1998.

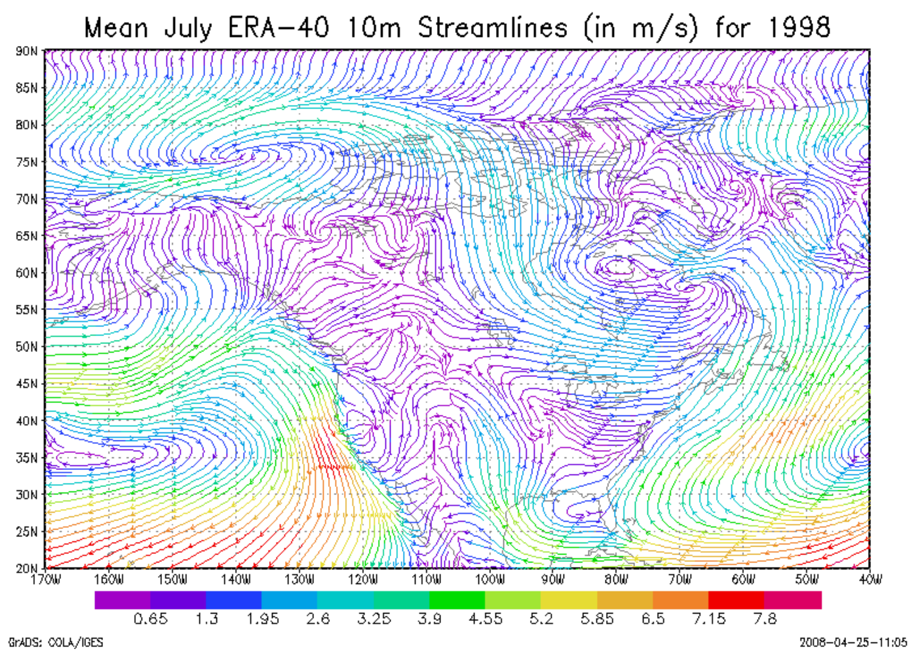

Figure A92. ERA-40 Mean July 10m streamlines for 1998.

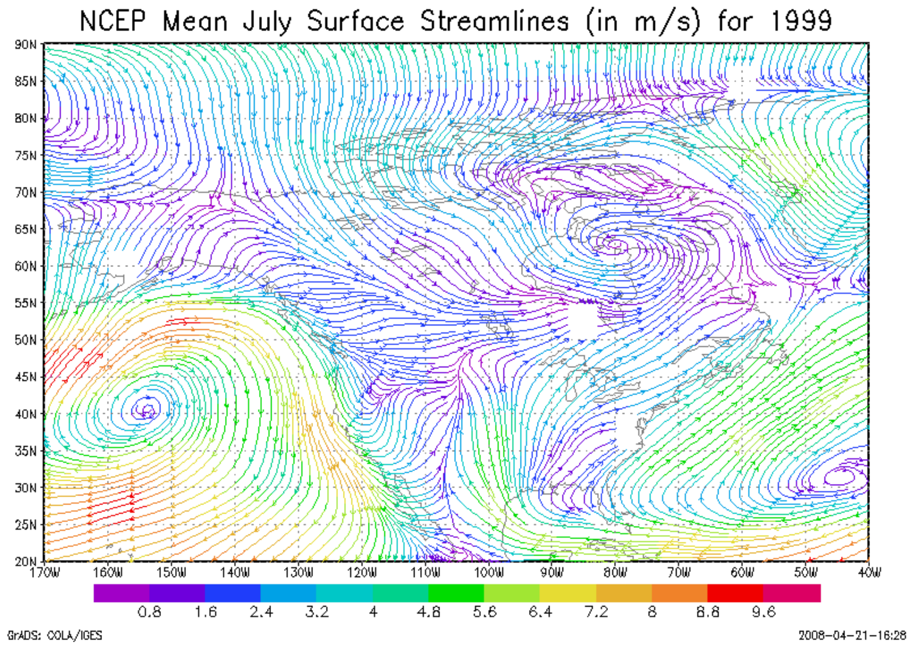

Figure A93. NCEP Mean July surface streamlines for 1999.

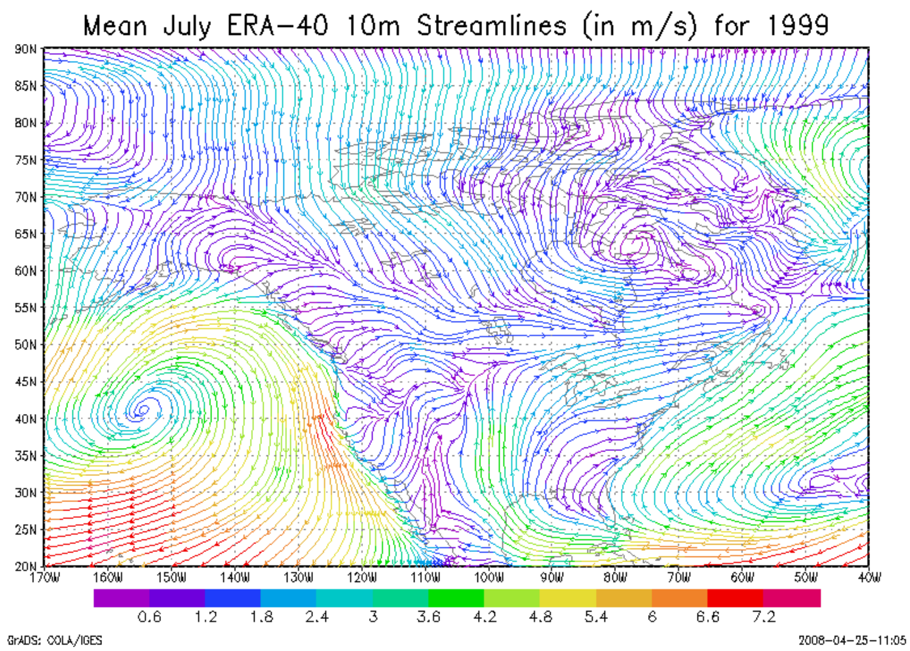

Figure A94. ERA-40 Mean July 10m streamlines for 1999.

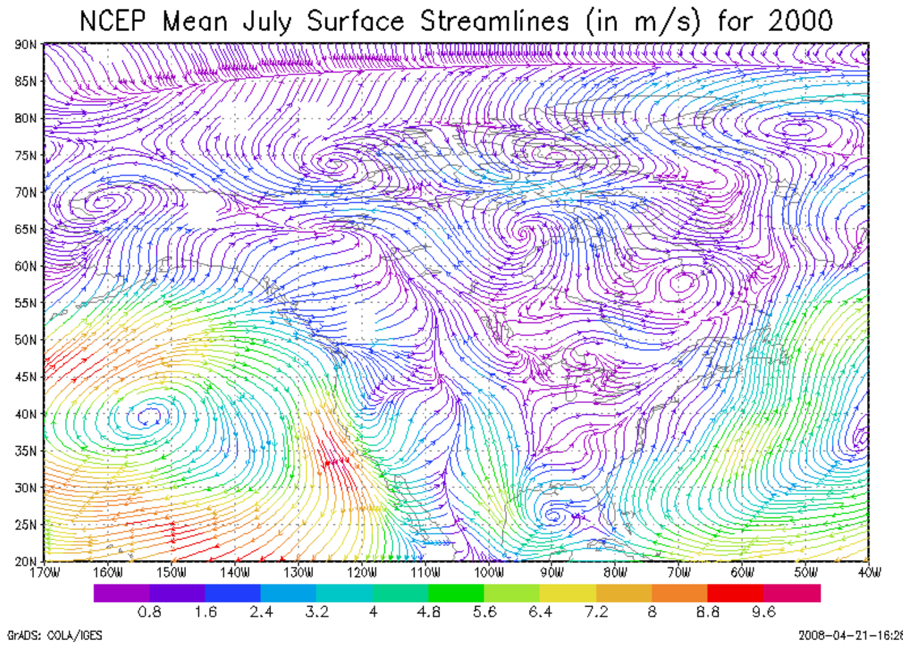

Figure A95. NCEP Mean July surface streamlines for 2000.

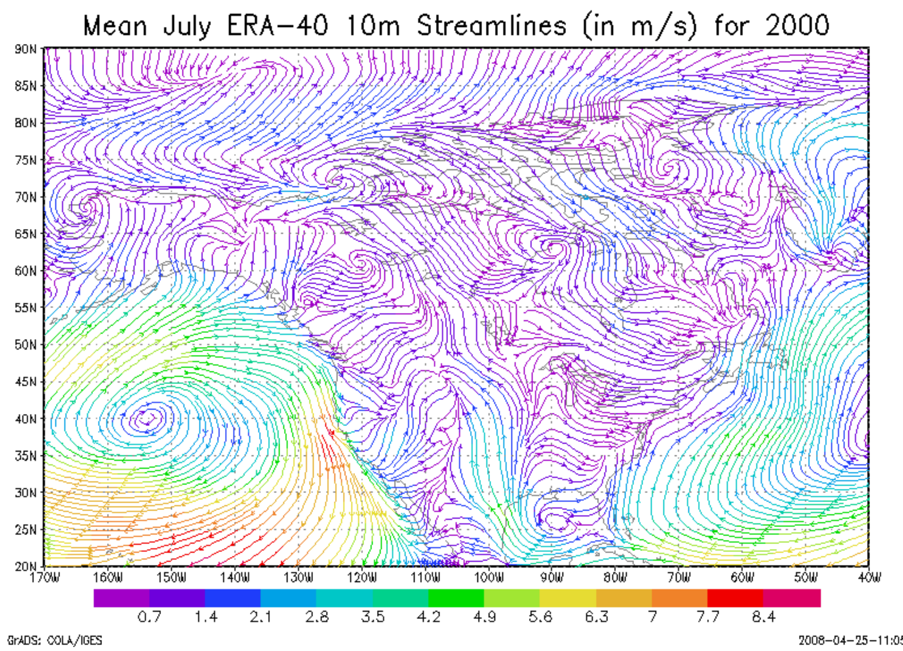

Figure A96. ERA-40 Mean July 10m streamlines for 2000.

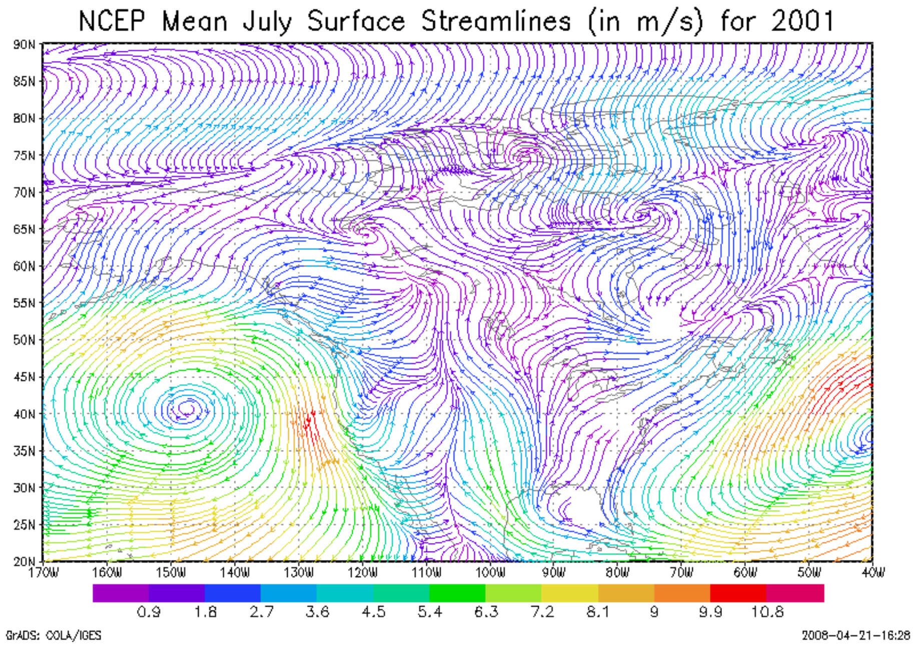

Figure A97. NCEP Mean July surface streamlines for 2001.

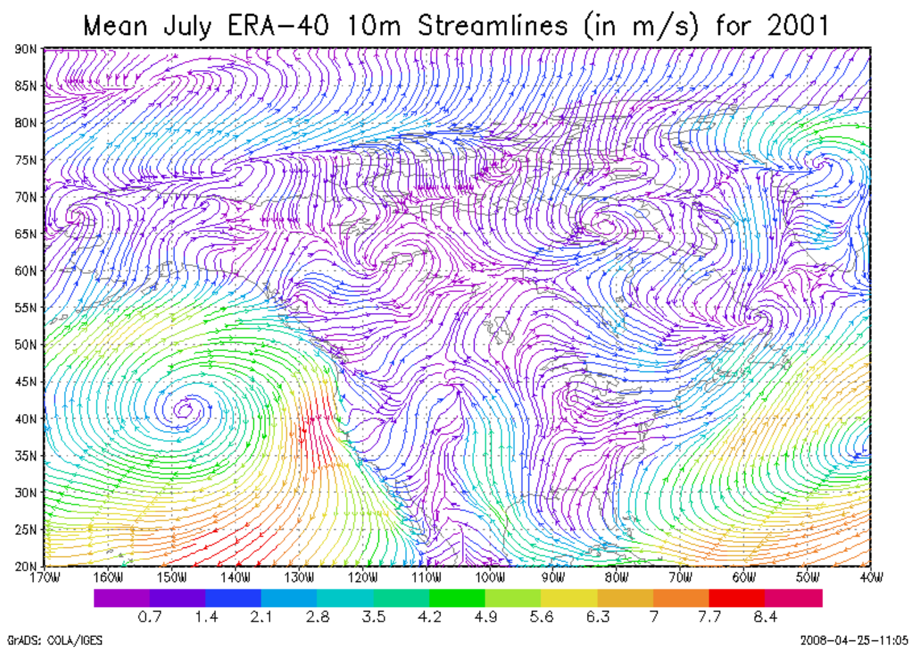

Figure A98. ERA-40 Mean July 10m streamlines for 2001.

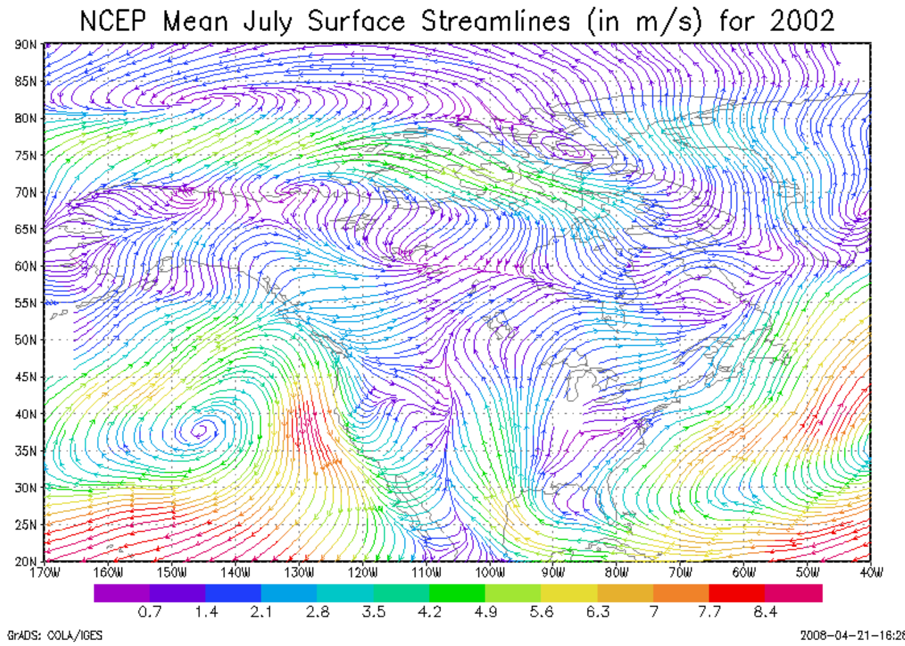

Figure A99. NCEP Mean July surface streamlines for 2002.

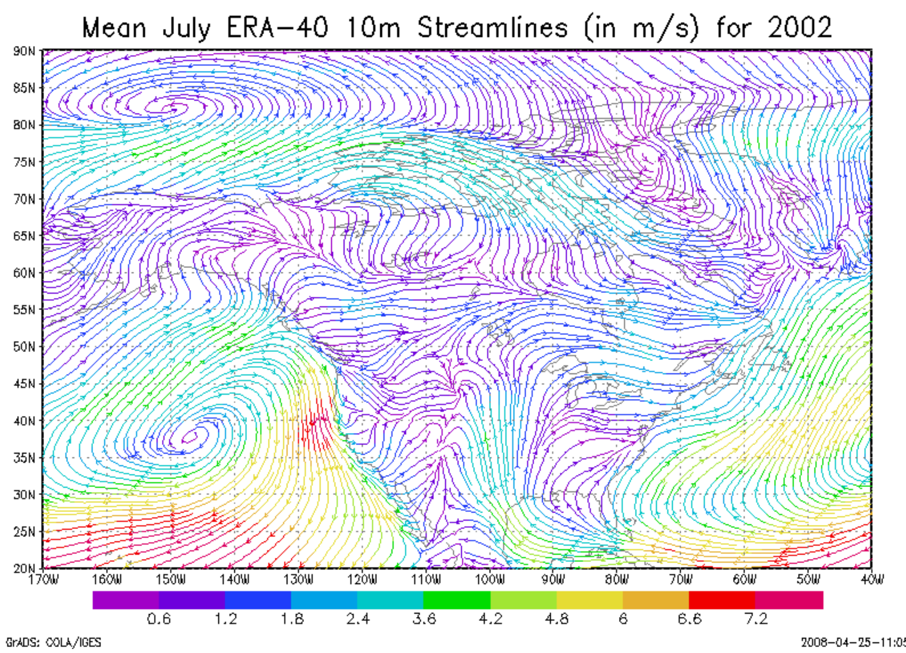

Figure A100. ERA-40 Mean July 10m streamlines for 2002.

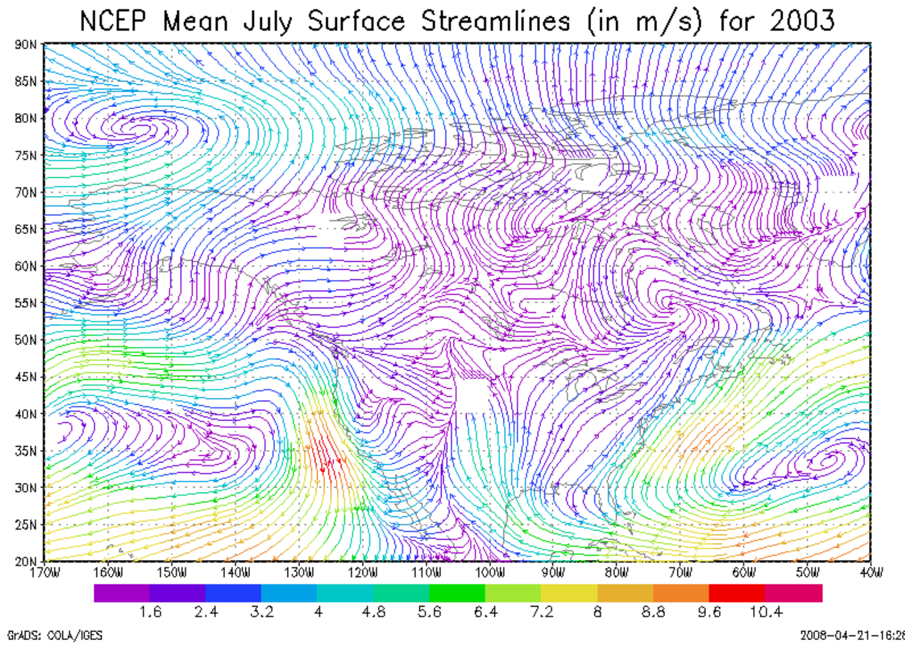

Figure A101. NCEP Mean July surface streamlines for 2003.

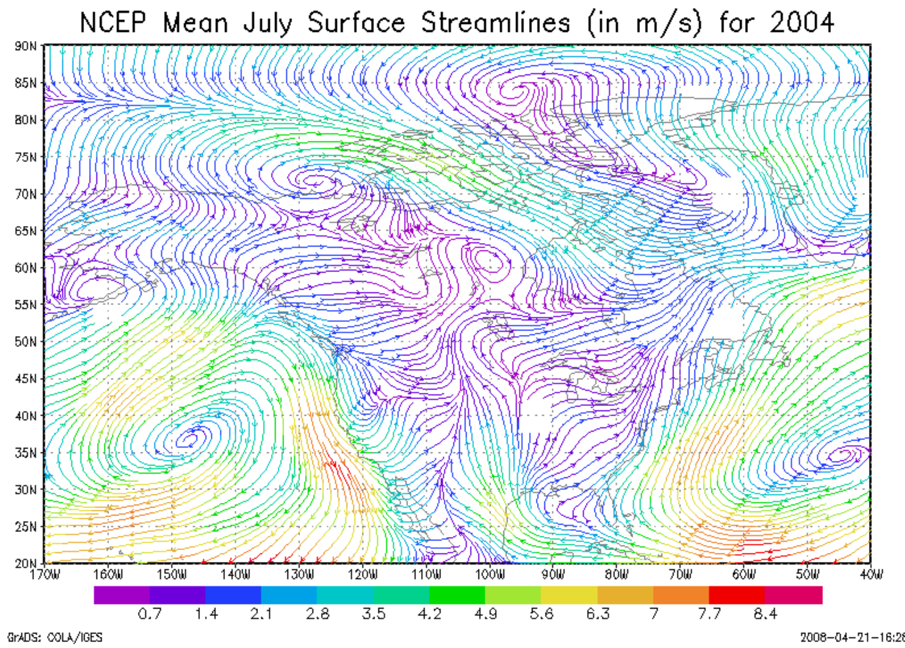

Figure A102. NCEP Mean July surface streamlines for 2004.

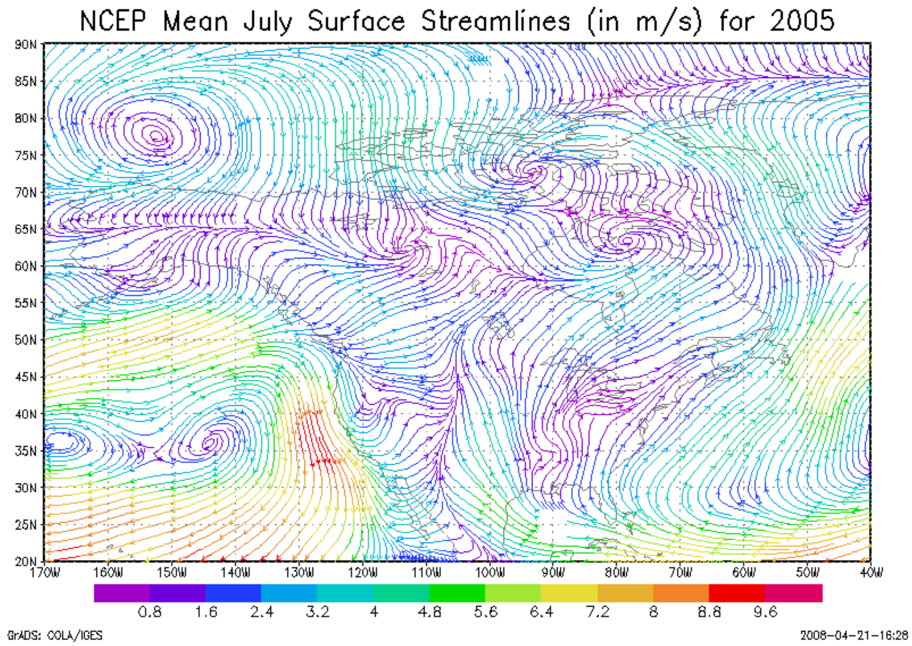

Figure A103. NCEP Mean July surface streamlines for 2005.

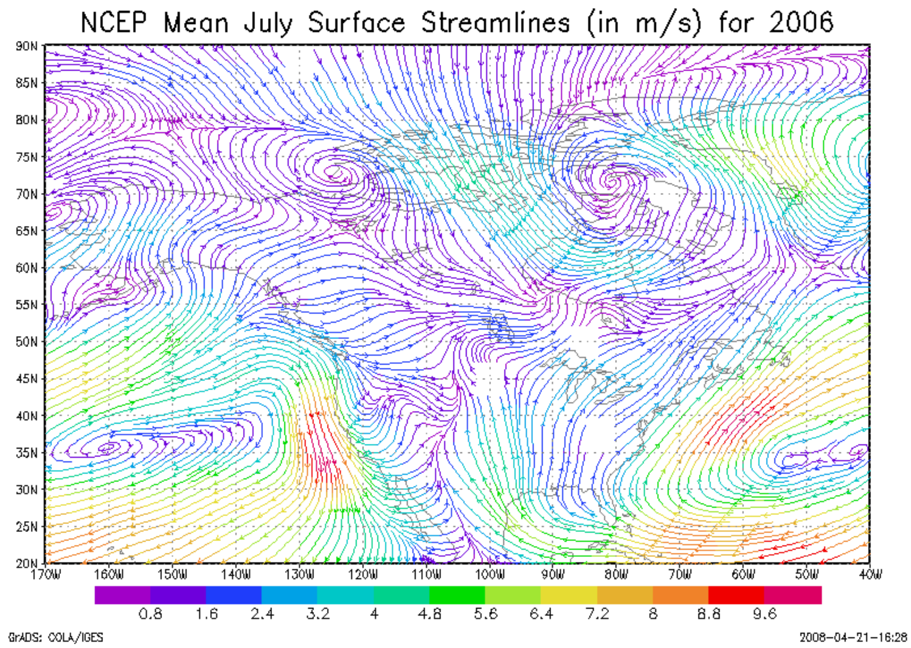

Figure A104. NCEP Mean July surface streamlines for 2006.

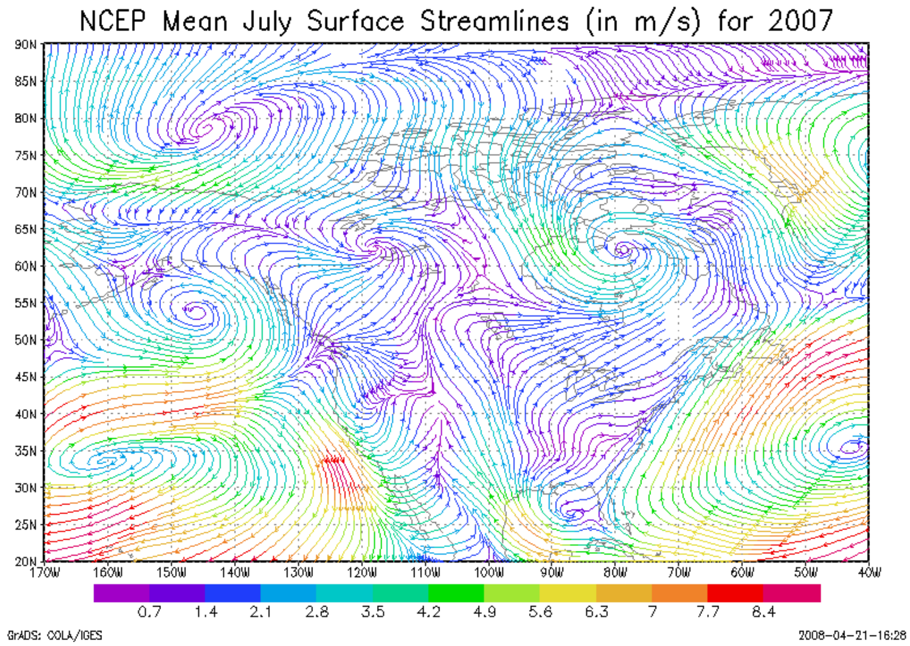

Figure A105. NCEP Mean July surface streamlines for 2007.

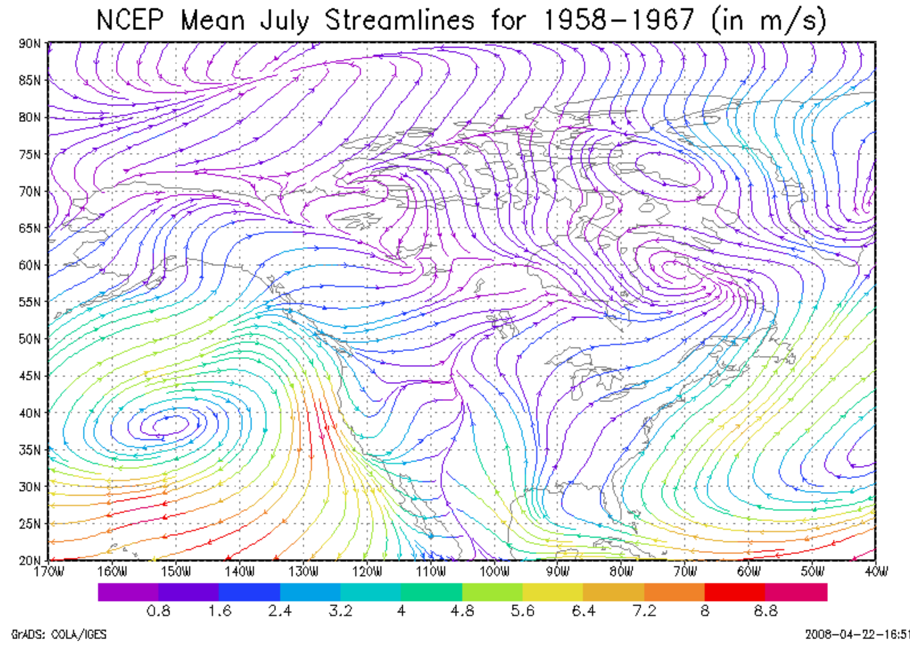

Figure A106. NCEP Mean July surface streamlines for 1958 - 1967.

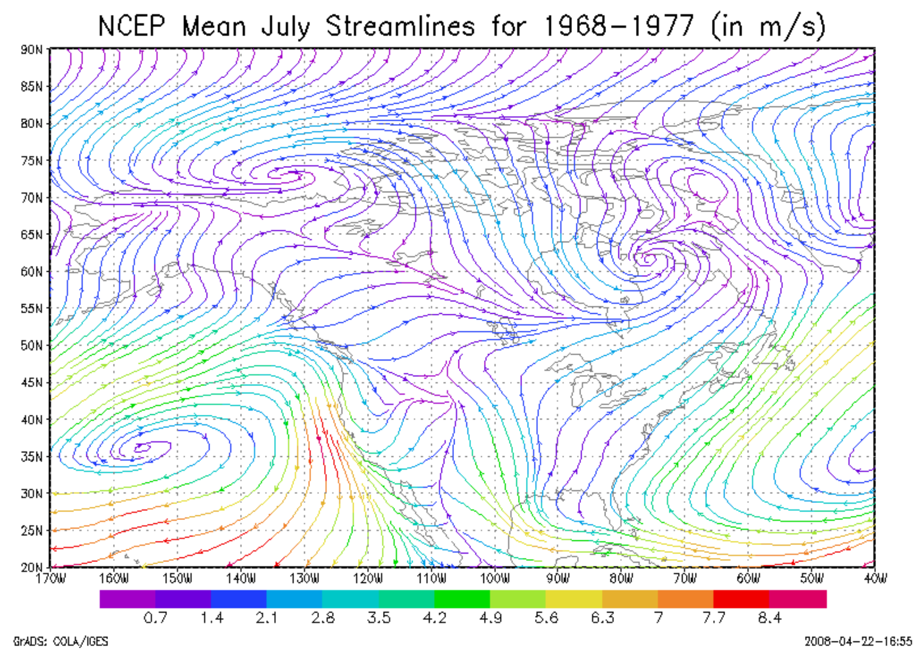

Figure A107. NCEP Mean July surface streamlines for 1968 - 1977.

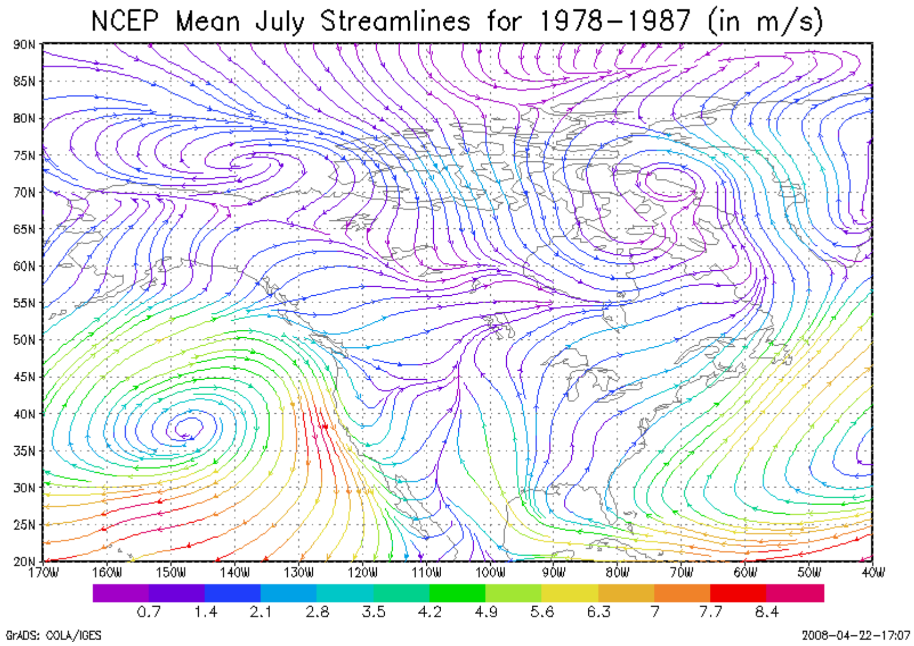

Figure A108. NCEP Mean July surface streamlines for 1978 - 1987.

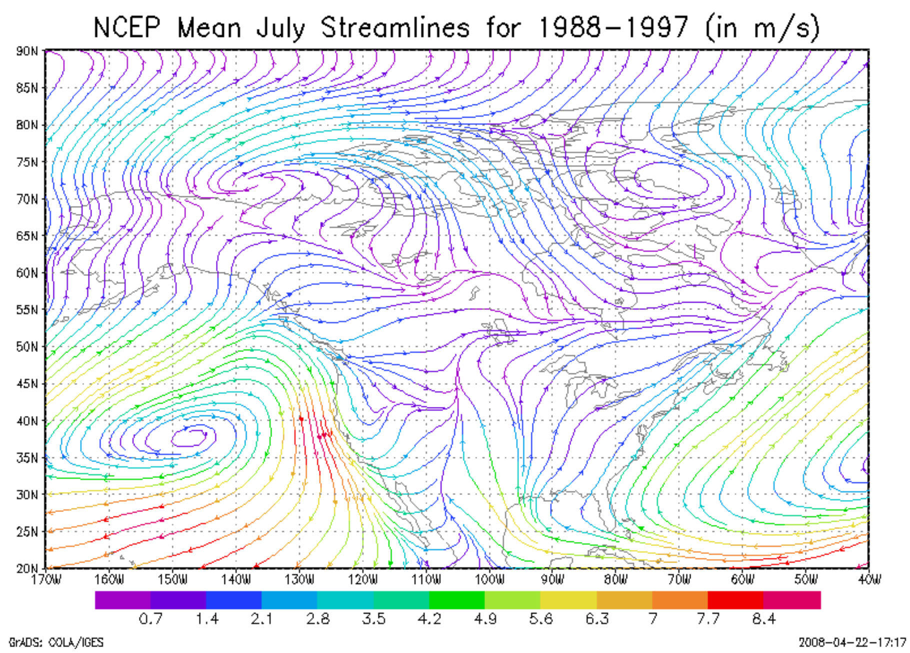

Figure A109. NCEP Mean July surface streamlines for 1988 - 1997.

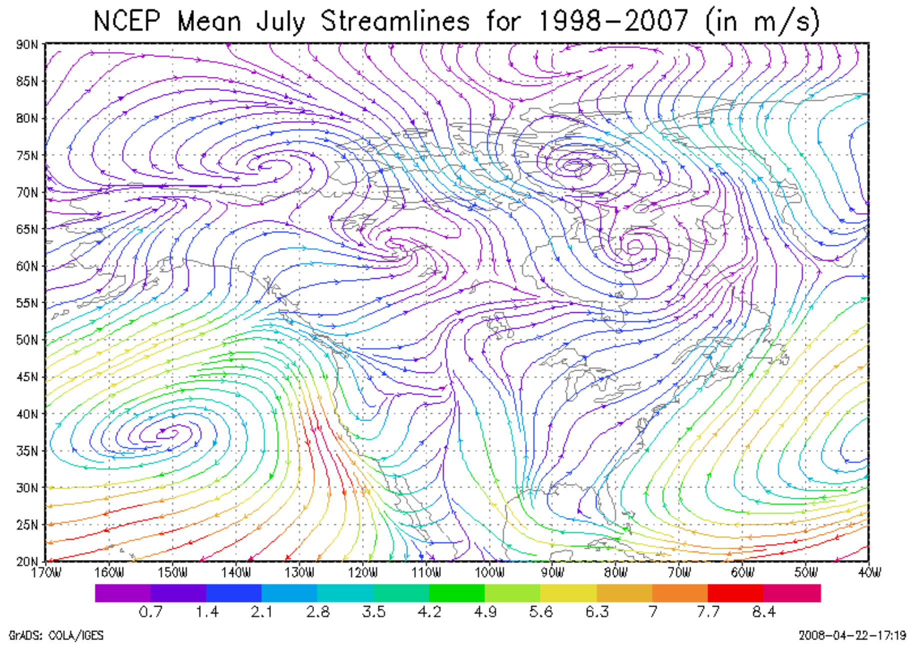

Figure A110. NCEP Mean July surface streamlines for 1998 - 2007.

Appendix B – Maps of July fronts in North America

These maps show the July front positions derived from both ERA-40 and NNR. Fronts derived from NNR (ERA-40) are coloured blue (red). Years of overlap for NNR and ERA-40 are 1958-2002. For July 2002, fronts could not be identified from NNR. A qualitative analysis of the July Arctic front and synoptic features of each year follows in section B.1. The front position data is shown in Table B1.

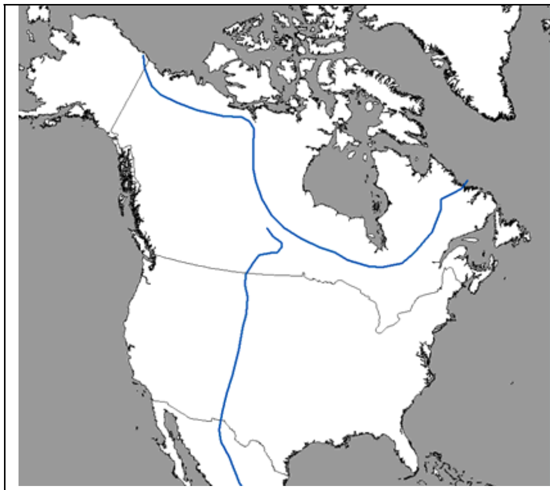

Figure B1. Fronts for July 1948.

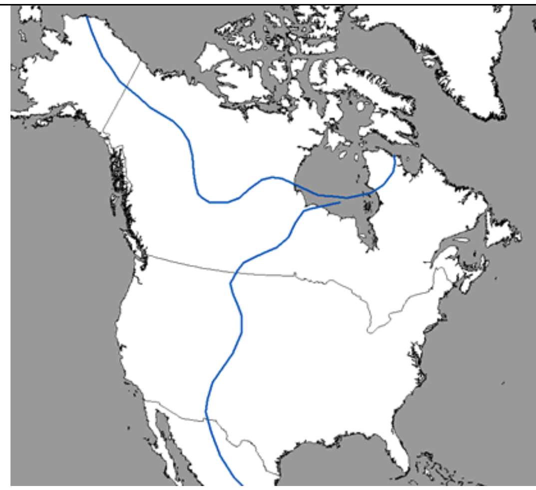

Figure B2. Fronts for July 1949.

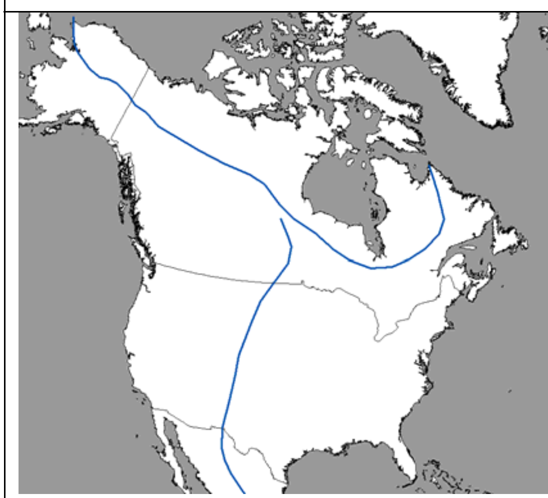

Figure B3. Fronts for July 1950.

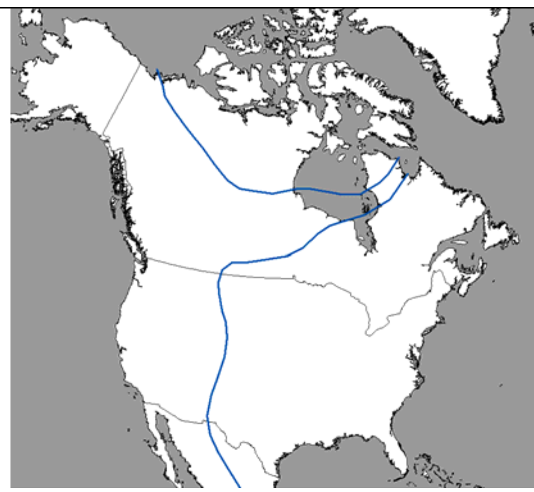

Figure B4. Fronts for July 1951.

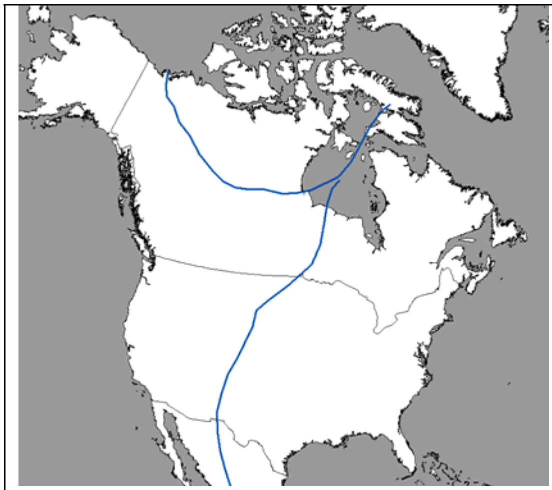 Figure B5. Fronts for July 1952.	 Figure B6. Fronts for July 1953.
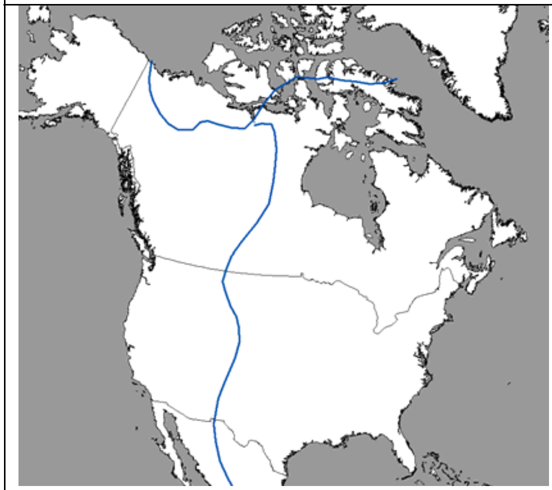 Figure B7. Fronts for July 1954.	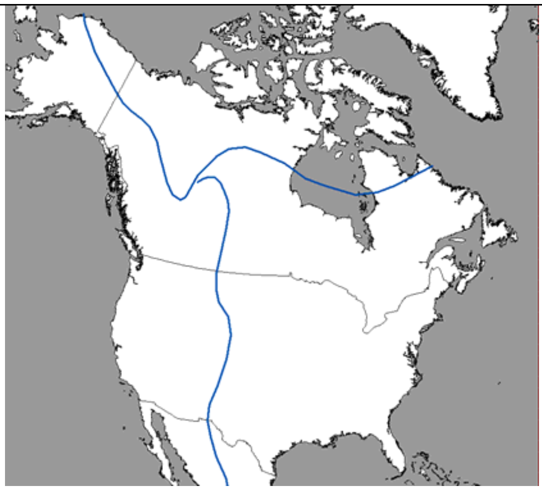 Figure B8. Fronts for July 1955.
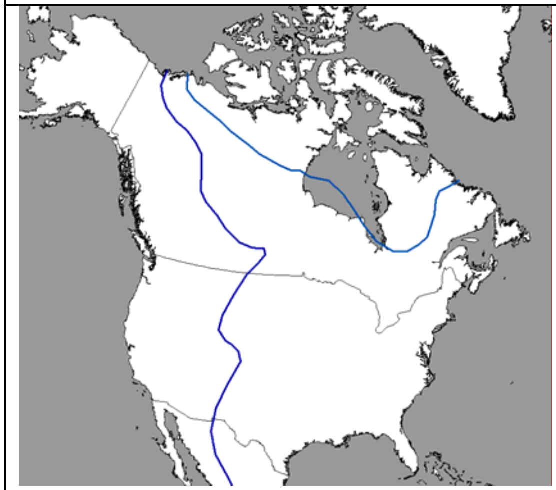 Figure B9. Fronts for July 1956.	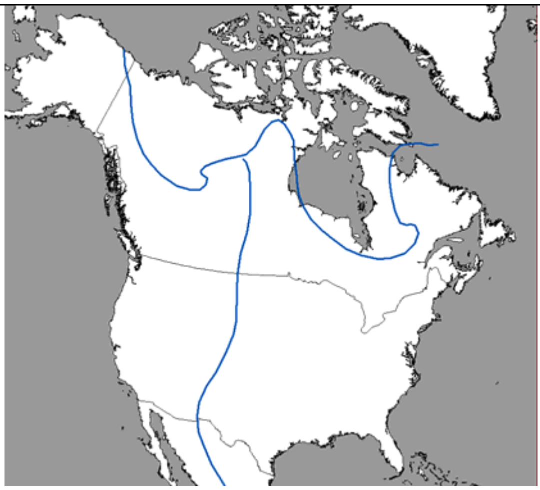 Figure B10. Fronts for July 1957.

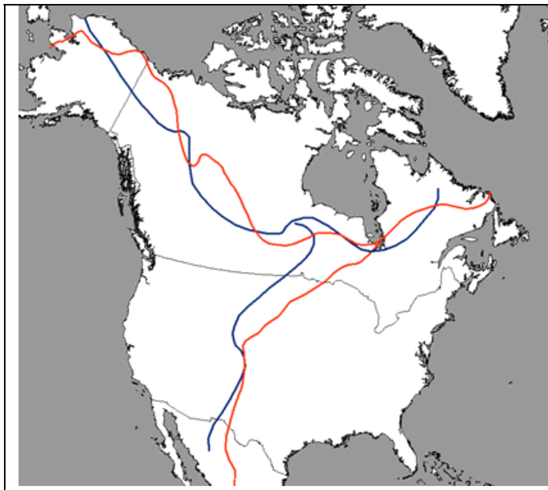

Figure B11. Fronts for July 1958.

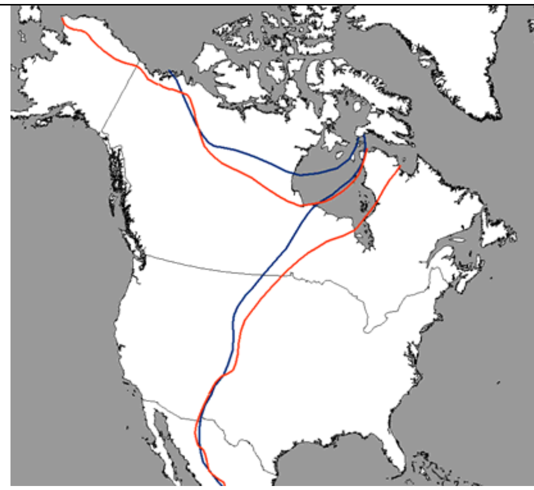

Figure B12. Fronts for July 1959.

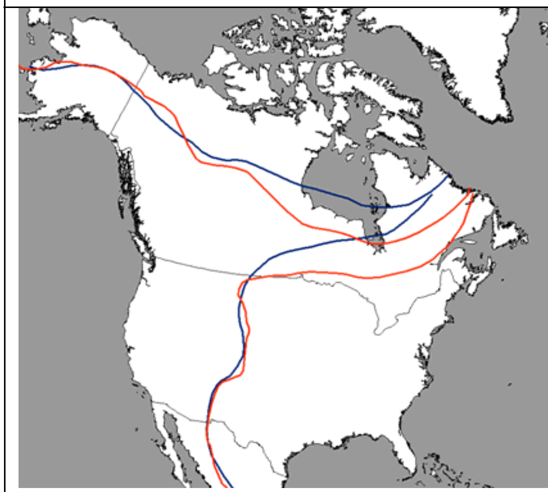

Figure B13. Fronts for July 1960.

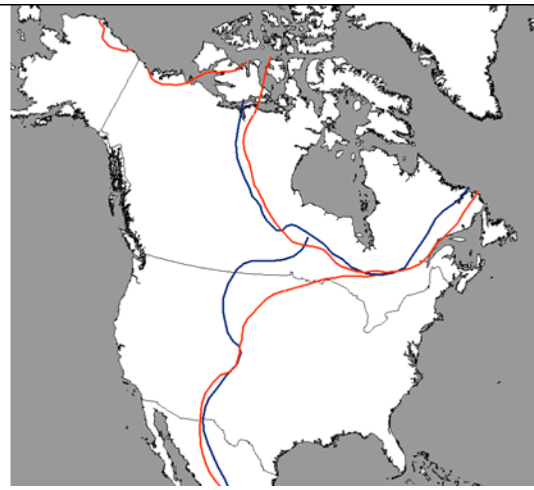

Figure B14. Fronts for July 1961.

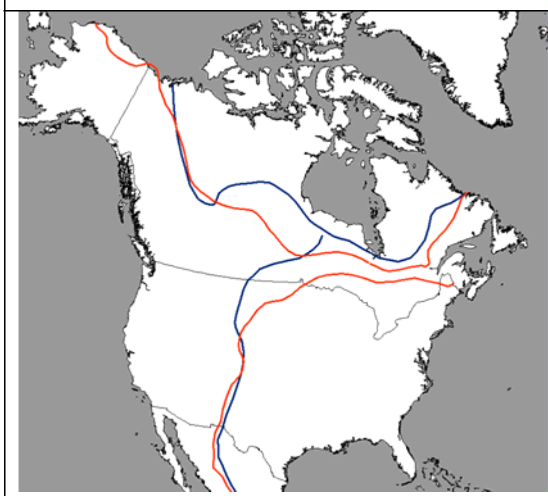

Figure B15. Fronts for July 1962.

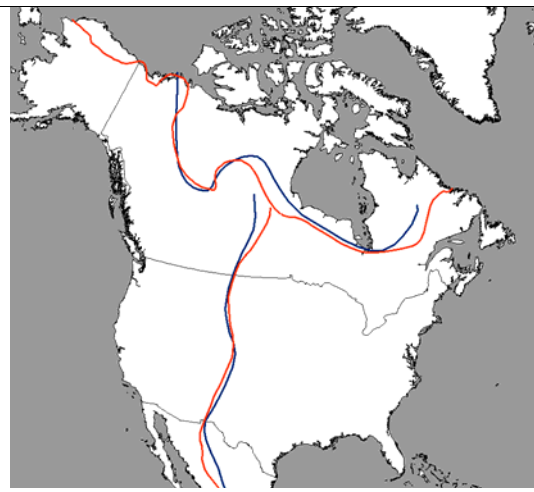

Figure B16. Fronts for July 1963.

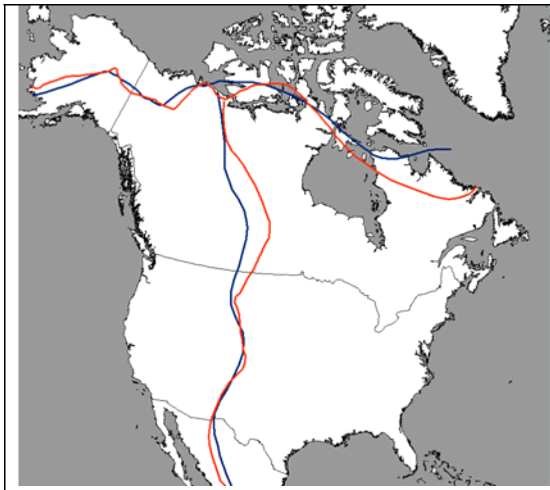

Figure B17. Fronts for July 1964.

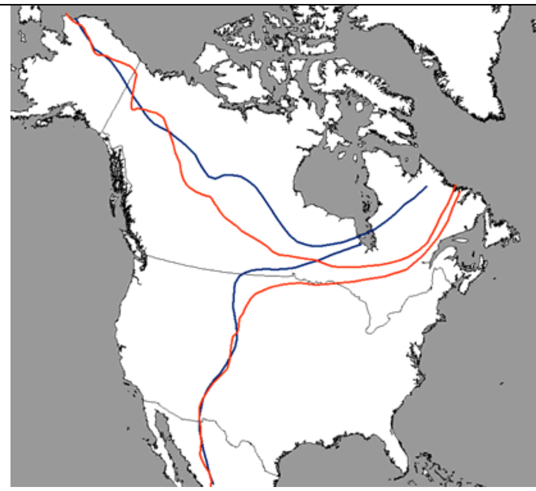

Figure B18. Fronts for July 1965.

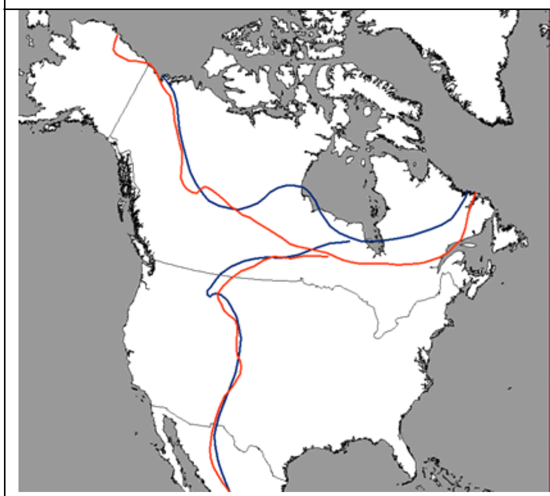

Figure B19. Fronts for July 1966.

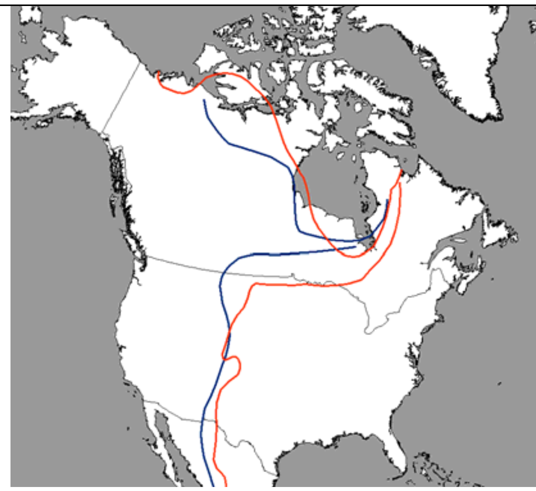

Figure B20. Fronts for July 1967.

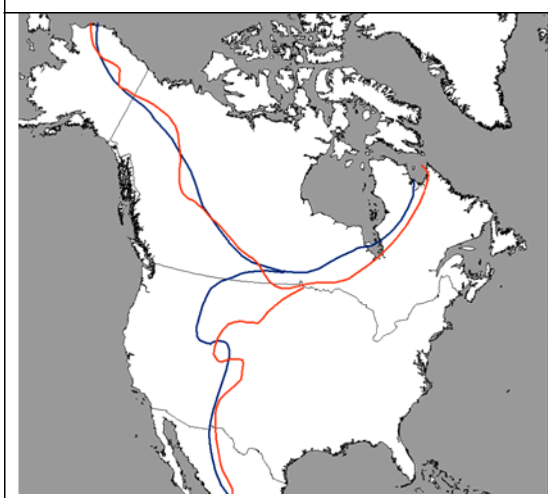

Figure B21. Fronts for July 1968.

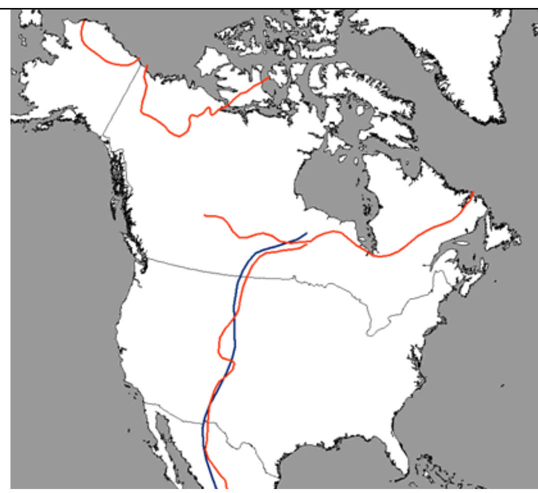

Figure B22. Fronts for July 1969.

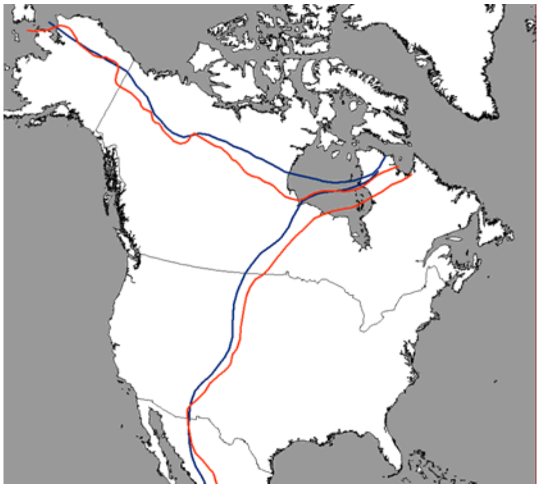

Figure B23. Fronts for July 1970

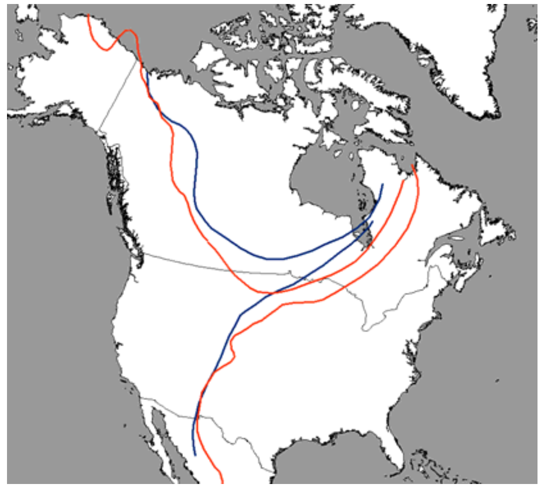

Figure B24. Fronts for July 1971.

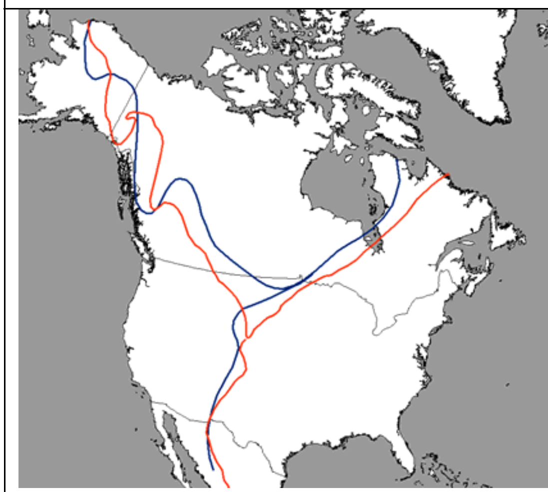

Figure B25. Fronts for July 1972.

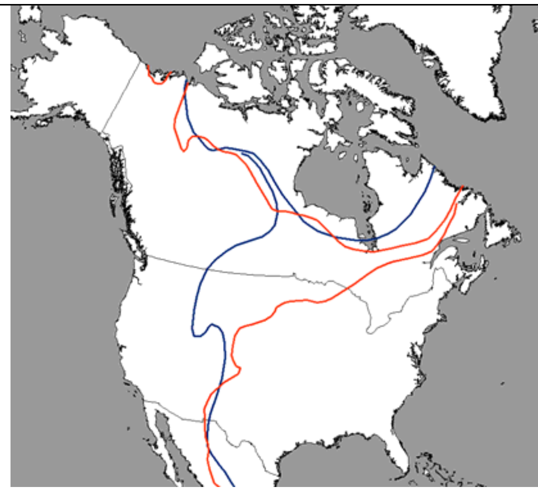

Figure B26. Fronts for July 1973.

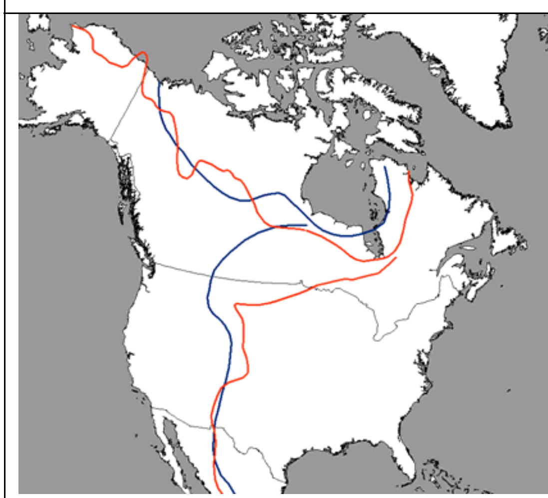

Figure B27. Fronts for July 1974.

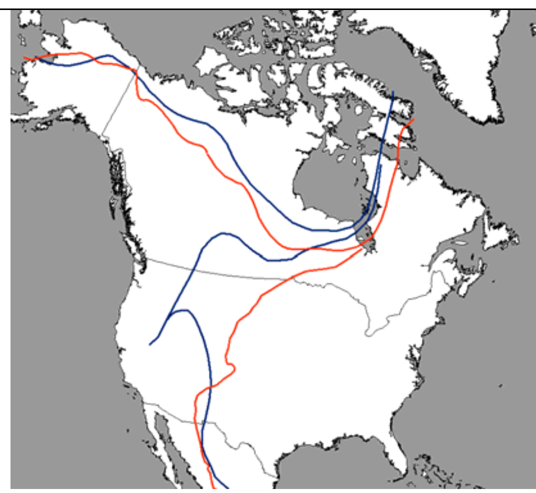

Figure B28. Fronts for July 1975.

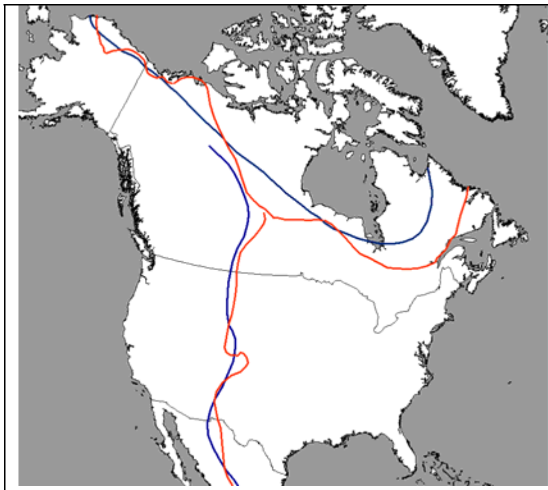

Figure B29. Fronts for July 1976.

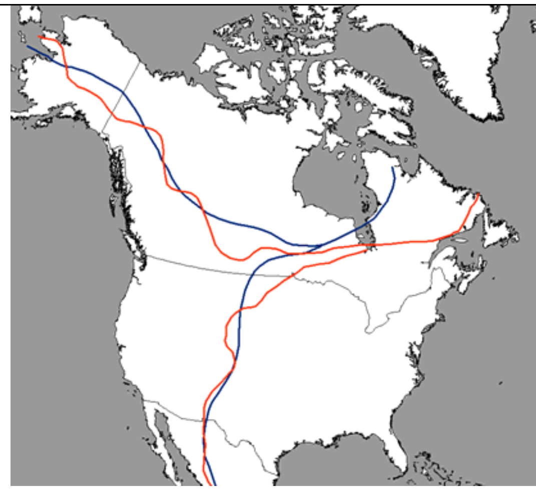

Figure B30. Fronts for July 1977.

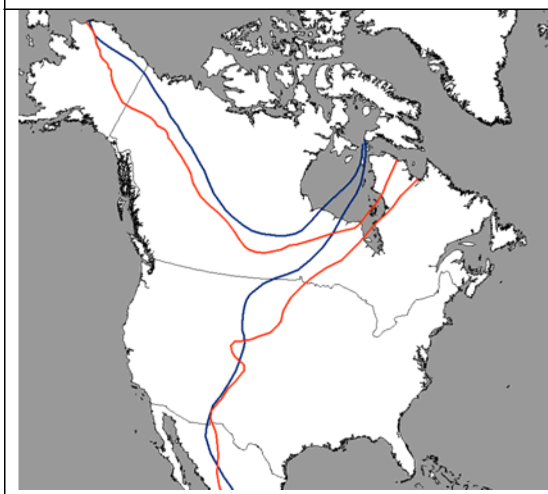

Figure B31. Fronts for July 1978.

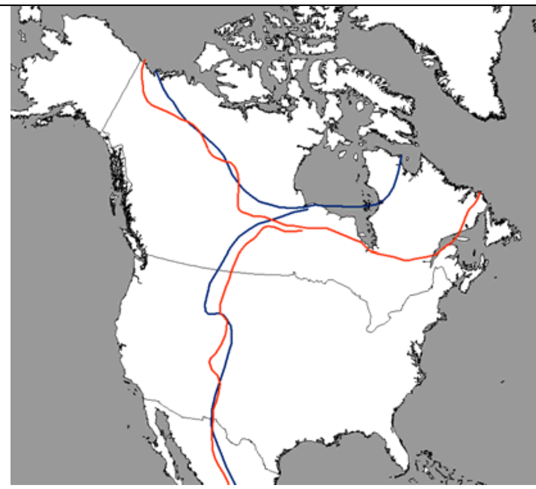

Figure B32. Fronts for July 1979.

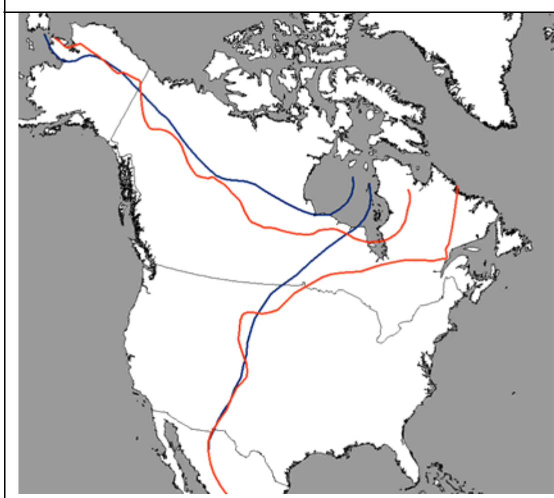

Figure B33. Fronts for July 1980.

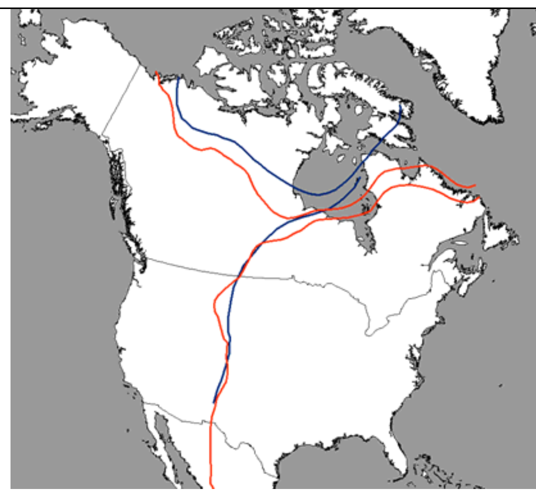

Figure B34. Fronts for July 1981.

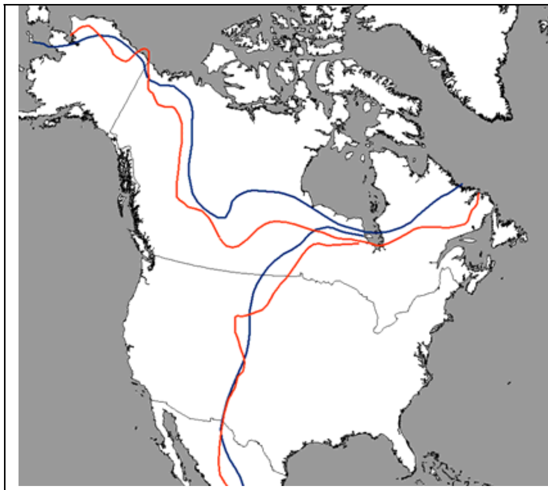

Figure B35. Fronts for July 1982.

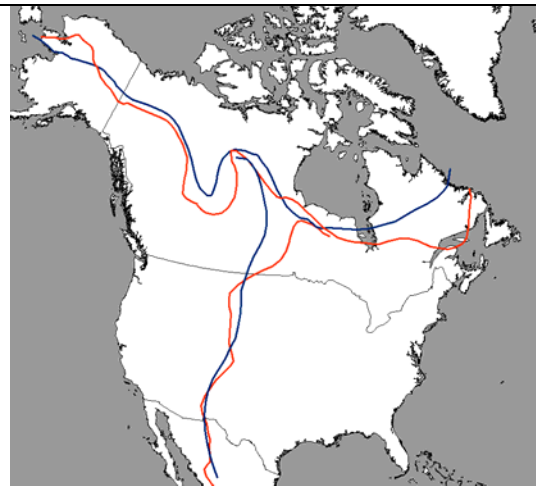

Figure B36. Fronts for July 1983

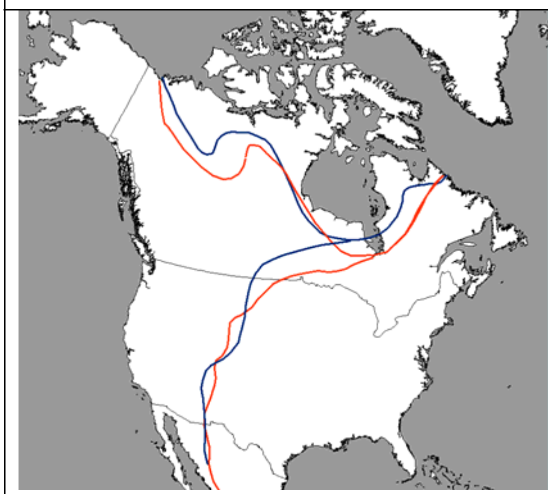

Figure B37. Fronts for July 1984.

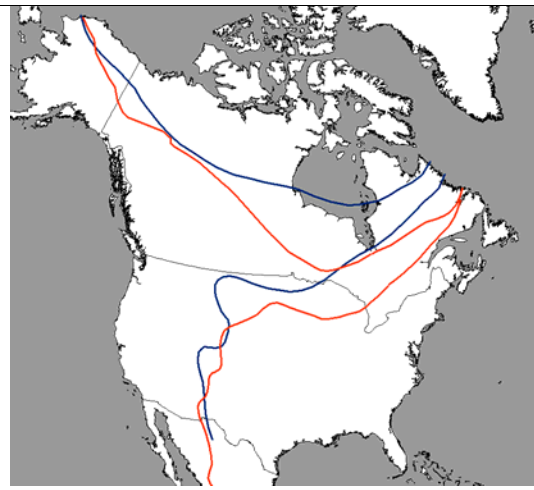

Figure B38. Fronts for July 1985.

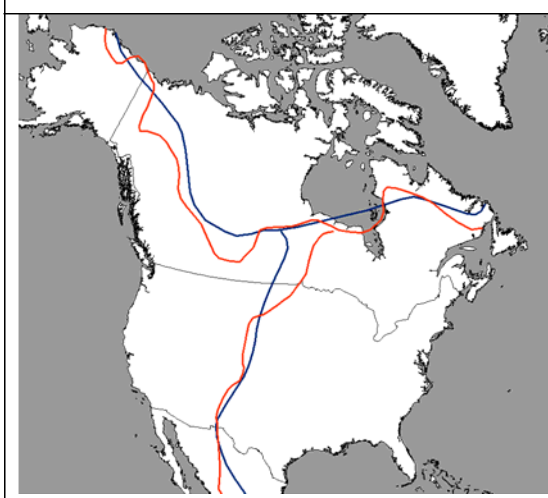

Figure B39. Fronts for July 1986.

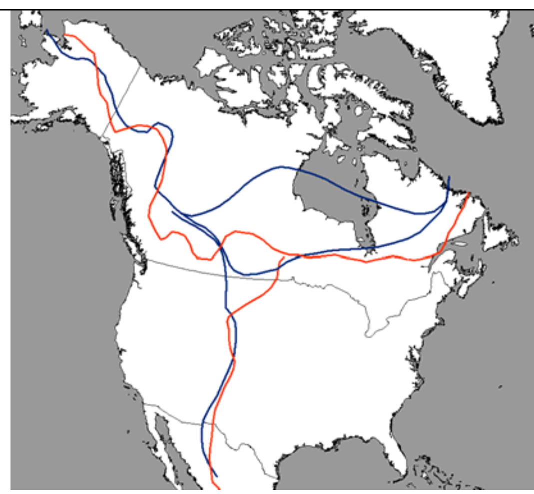

Figure B40. Fronts for July 1987.

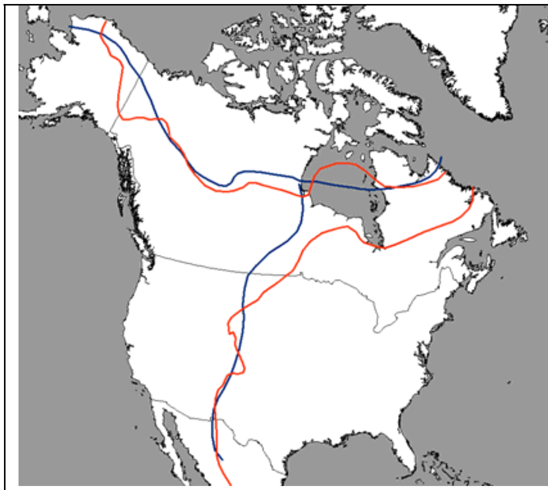

Figure B41. Fronts for July 1988.

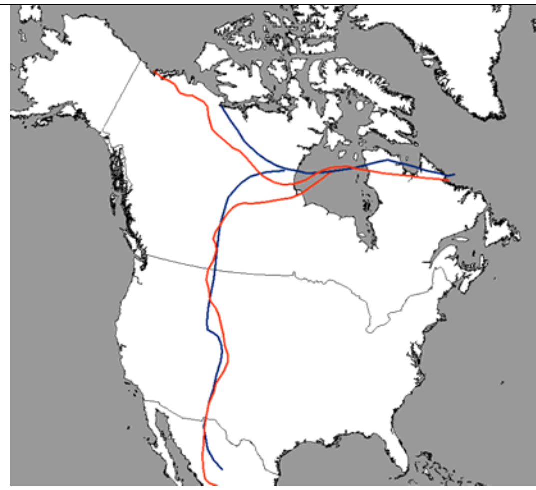

Figure B42. Fronts for July 1989.

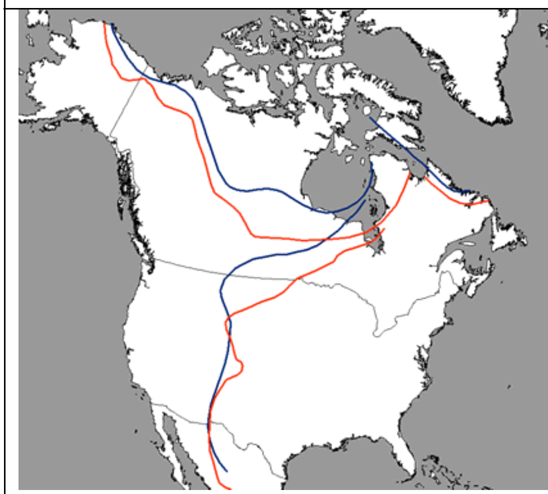

Figure B43. Fronts for July 1990.

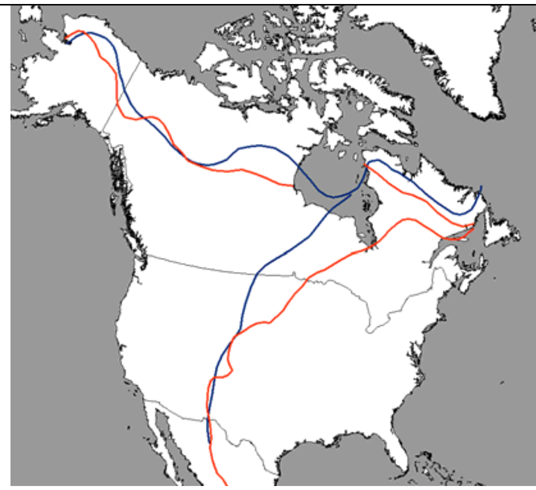

Figure B44. Fronts for July 1991.

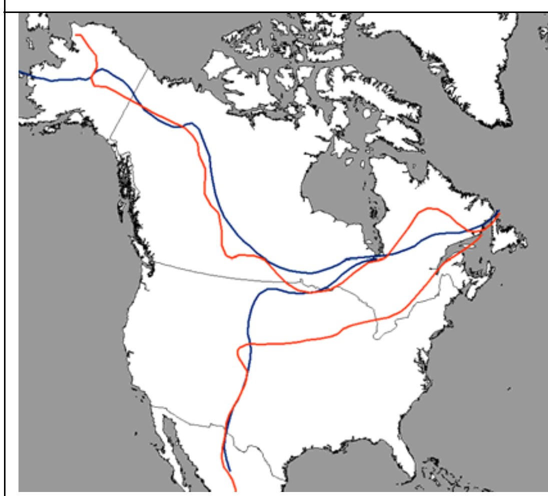

Figure B45. Fronts for July 1992.

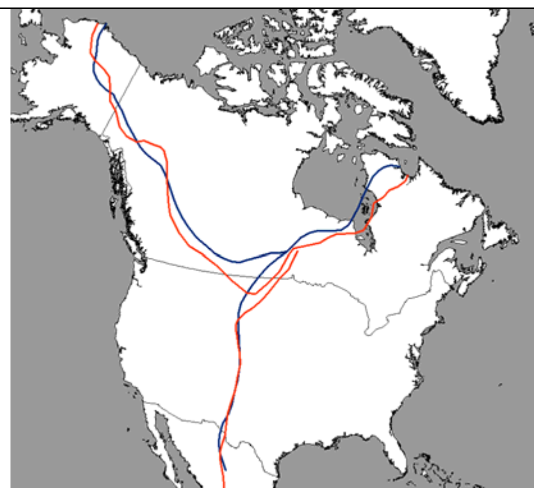

Figure B46. Fronts for July 1993.

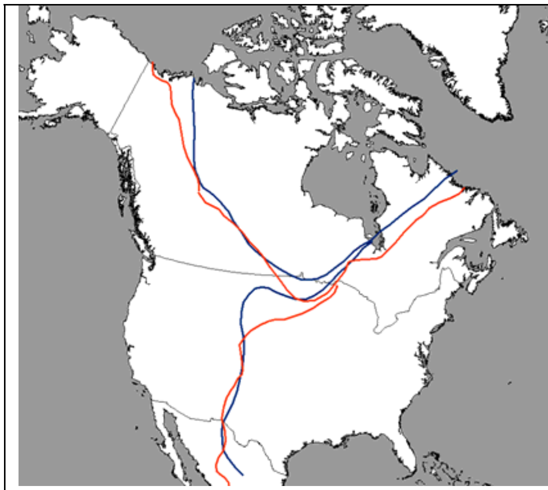

Figure B47. Fronts for July 1994.

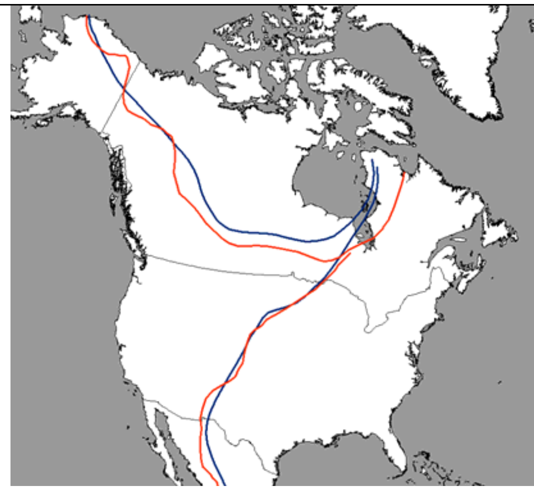

Figure B48. Fronts for July 1995.

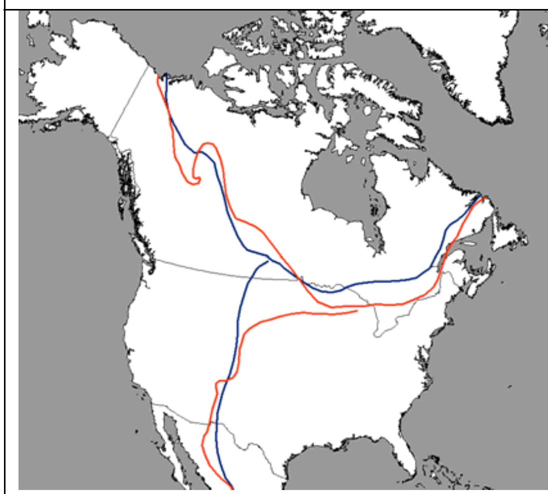

Figure B49. Fronts for July 1996.

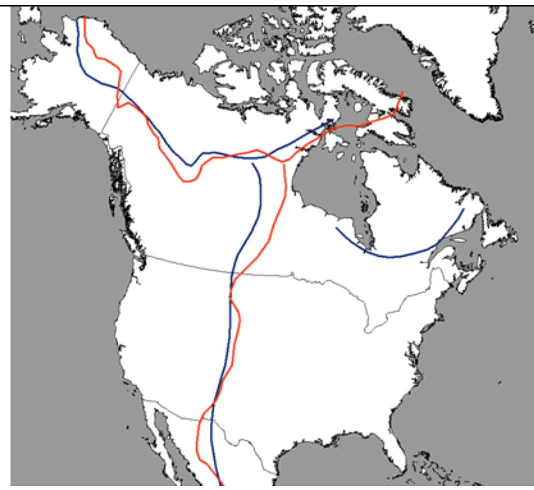

Figure B50. Fronts for July 1997.

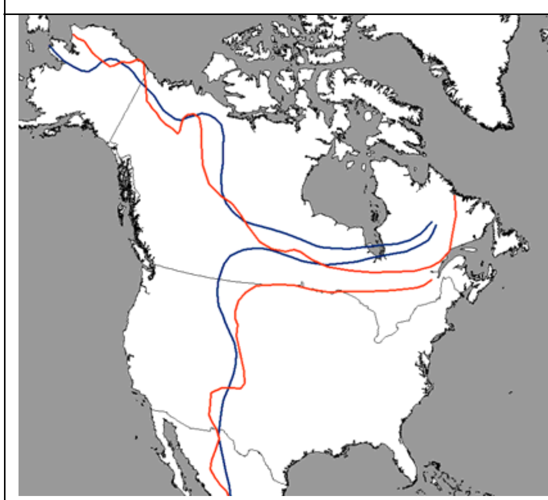

Figure B51. Fronts for July 1998.

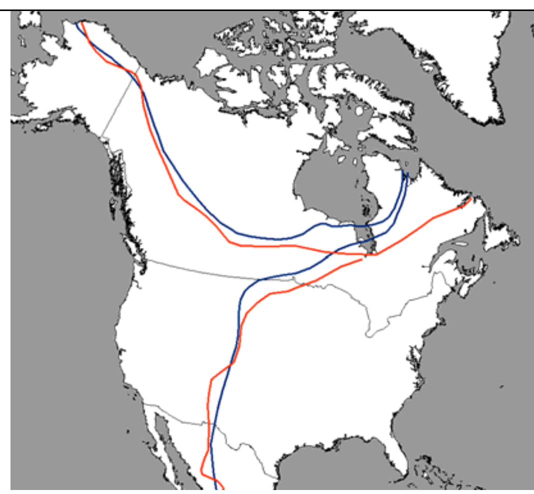

Figure B52. Fronts for July 1999.

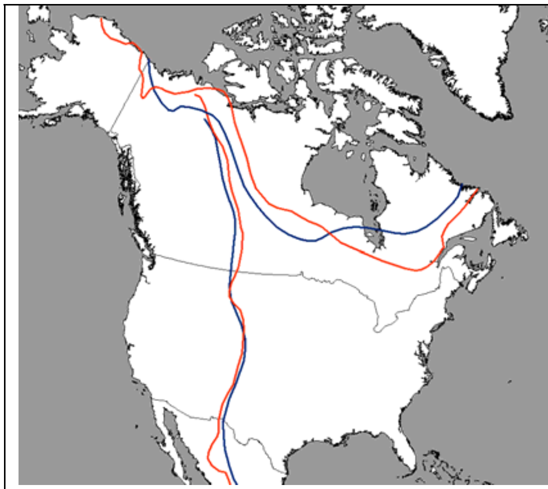

Figure B53. Fronts for July 2000.

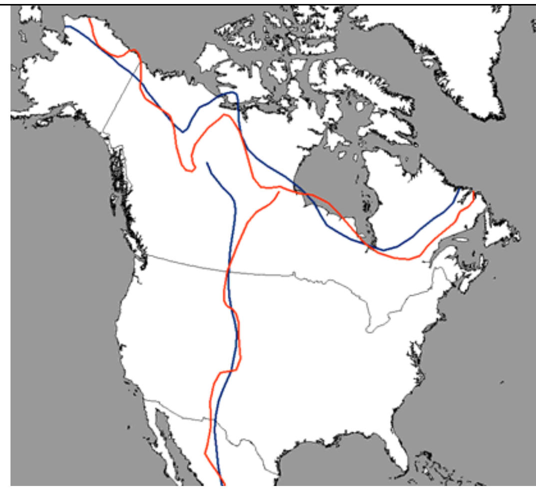

Figure B54. Fronts for July 2001.

Figure B55. Fronts for July 2002.

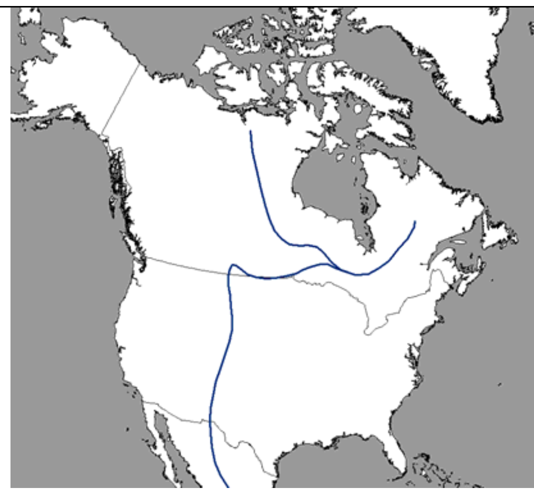

Figure B56. Fronts for July 2003.

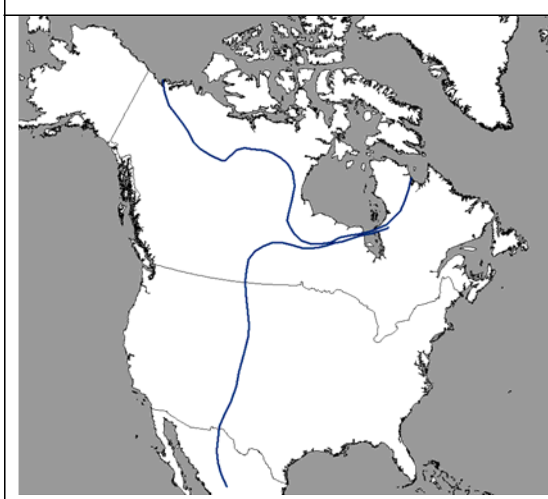

Figure B57. Fronts for July 2004.

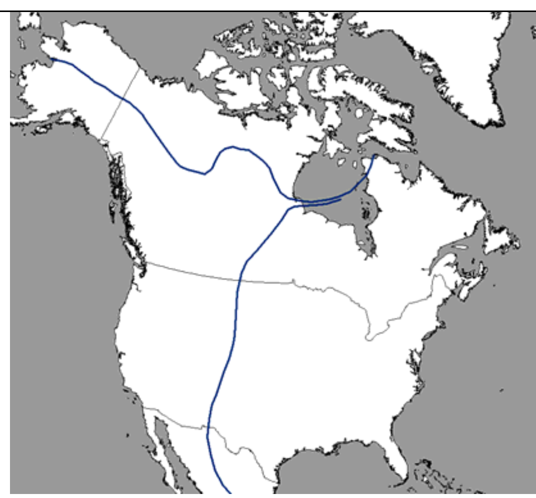

Figure B58. Fronts for July 2005.

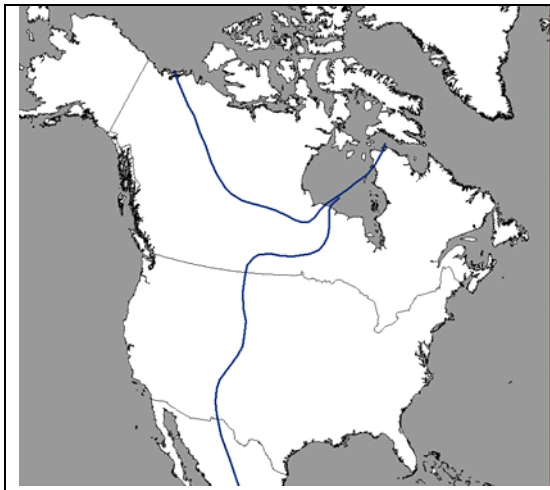

Figure B59. Fronts for July 2006.

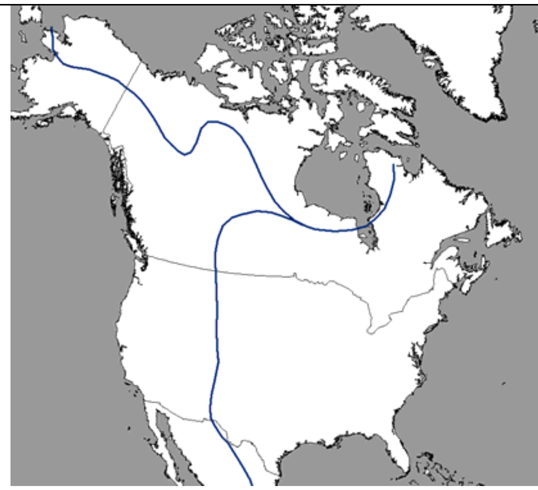

Figure B60. Fronts for July 2007.

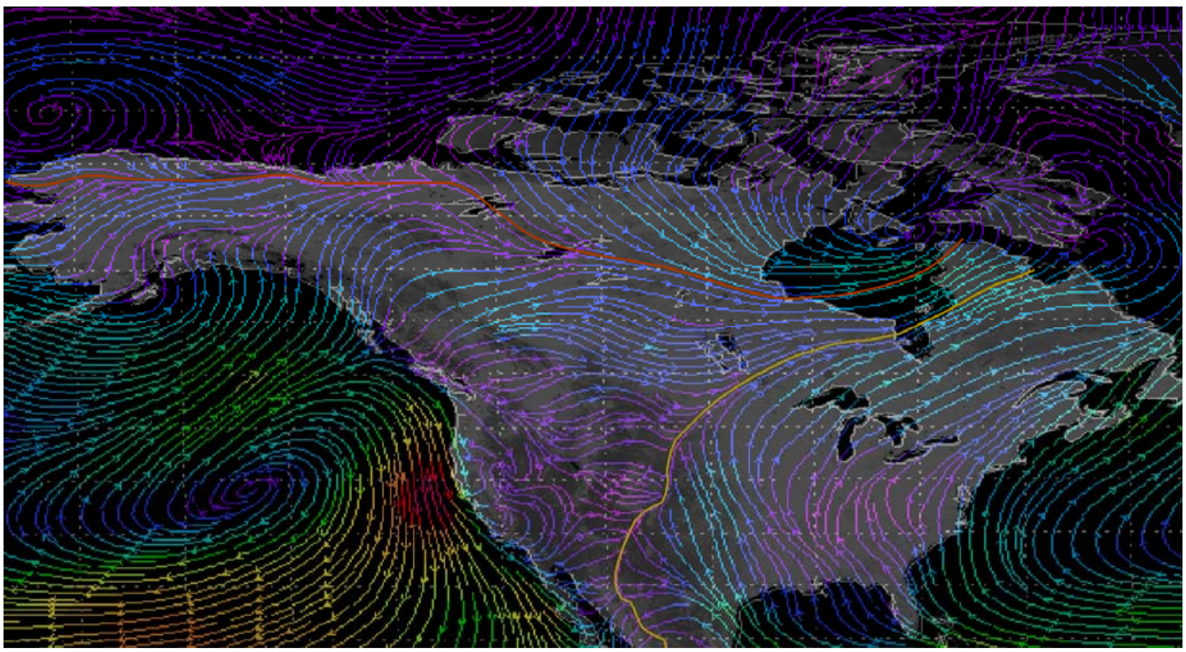

Figure B61. Mean wind streamlines for July 1959 (derived from ERA-40) with overlay of hand drawn fronts (Arctic front is red line, Pacific front is gold line).

B.1. Discussion of the July frontal maps

(NOTE: years with NCEP reanalysis only are denoted by an asterisk)

*1948 – Front is difficult to locate. It is close to the coast over Western North America. Large southward bend in the front north of Great Slave Lake, high pressure north of Hudson Bay and over Western CAA, low pressure over Northern Ellsemere Island, Western Greenland, and Northern Quebec.

*1949 – Front is close to long term mean position with a slight southward bend in the front south of Great Slave Lake. Front has SW to NE orientation over Northern Quebec. Low pressure close to the tip of Northern Quebec, further to the NW than in 1948.

*1950 – Front is difficult to locate. Front is close to long term mean position, except slightly further to the south over Ontario and Quebec. Anomalous northward bend in front over Quebec. Low pressure close to Western tip of Baffin Island and over Labrador. High pressure over Hudson Bay close to Ontario coast.

*1951 – Front is close to long term mean position except it reaches the coast much further to the East over Western North America. Strong low pressure over the southern tip of Baffin Island leads to SW-NE orientation of front over Northern Quebec. There is no high pressure center over the Beaufort Sea.

*1952 – Front position is similar to 1951 position except with a bend further northwards over Hudson Bay to reach Baffin Island. Low pressure situated over Southern Baffin Island and high pressure at the far western end of the CAA. The Beaufort high is closer to the coast.

*1953 – Front position is similar to 1952 position except slightly further to the south. Northward bend over Northern Quebec. High pressure over the Beaufort Sea and close to the coast. Low pressure near the tip of NW Quebec and two low pressure centers in Davis Strait.

*1954 – Front is anomalously far to the north except over the Yukon. Front extends to the east over Baffin Island. Southerly flow extends northward to almost 70N over parts of the CAA. Low pressure near Great Bear Lake, over Southeast Quebec, and Davis Strait. High pressure over Hudson Bay, however none present over the Beaufort Sea.

*1955 –Front has a sharp southward dip into Northeast BC then rises to the North over NWT then slight southward bend into the Keewatin region of Nunavut then extending to Ungava Bay in Quebec. Low pressure close to 120°W, 55°N and over Davis Strait.

*1956 - Front is difficult to locate. Front is further to the north over Nunavut and NWT with a sharp southward dip over Quebec before turning to the NE over Labrador. Difficult to define circulation over much of Canada with low pressure over Quebec, Northern NWT, and over South Central Canada. Possible mixtures of air masses rather than one single Arctic front. Beaufort high pressure is shifted to the West and high pressure near Victoria Island.

*1957 – Front is difficult to locate. Front is quite variable with southward dip over NWT, then rising to the north over Nunavut, then a sharp southward dip to James Bay, then bending sharply to the North over Quebec with a S shaped curve. Low pressure over Quebec, Baffin Island, and Great Slave Lake. High pressure over the far western CAA.

1958 – ERA position of front is slightly further to the north of the NCEP position. Oscillation whereby NCEP position of front is north when ERA position is south and vice-versa. Low pressure near Great Slave Lake, Ungava Bay in Quebec, over Manitoba, and near the tip of Northern Quebec. High pressure over the Beaufort Sea.

1959 – Well-defined frontal boundary. Significant difference in front position between NCEP and ERA. ERA position extends into Alaska and is further to the south over Eastern Canada. Low pressure near the Southwest tip of Baffin Island and off the coast of Northern Alaska.

1960 – Well-defined frontal boundary close to the long term mean position. Difference between NCEP and ERA front positions is greater further east in Canada. Front bends toward the SW over Alaska. High pressure near the North Pole and low pressure over Baffin Island and Labrador.

1961 – Front is difficult to locate with a discontinuous boundary along the Arctic coast (ERA) and much shorter (NCEP) front, although both positions extend far to the south in Eastern Canada. High pressure over Beaufort Sea and low pressure over Hudson Bay.

1962 - ERA position of front is close to the Alaskan coast and bends to the SE from the Yukon to Northern Ontario before a turn to the NE of Central Quebec. NCEP position is further to the N except over Western Canada. The length of the front of the front is shorter ending near the Yukon coast, however with a bend to the N over Southern Nunavut. High pressure over the CAA and over Hudson Bay. Low pressure over Gaspe and south of Great Slave Lake.

1963 – Similar to the 1962 positions, except slightly further to the North and a more pronounced S-shaped curve over Central Canada. Also, the NCEP and ERA positions are much more similar to each other. High pressure near the coast of Alaska and over Hudson Bay. Low pressure near Great Slave Lake, over Quebec, and Baffin Island.

1964 - NCEP and ERA positions of front are very close except over Quebec. East of Northwest NWT, the front is anomalously far to the north with a bend to the SE over Eastern Canada. Low pressure near the North Pole, over NW Canada, and over Central Manitoba. Strong zonal flow over much of the CAA.

1965 – NCEP position of front is close to the long term mean except slightly further to the South over Ontario. ERA position is much further to the south and more wavy over Western North America. Low pressure north of Ellesmere Island, over NW Quebec, and near Great Slave Lake. High pressure NW of Alaska and over the Western CAA.

1966 – NCEP position of front shows a large northward rise over Central Canada. ERA position of front is further to the south over much of Central and Eastern Canada. Low pressure north of Ellesmere Island, over Davis Strait and over NE Labrador.

1967 – Both NCEP and ERA positions of front are much shorter and difficult to identify with a possible second front further north. The ERA position has a large N-S range. Low pressure over the Beaufort Sea and over Central Quebec.

1968 – Front is slightly further to the south over Western North America before a significant southward dip over Central Canada, then bending to the NE over Ontario and Quebec. Well defined frontal boundary and strong circulation over the Arctic with strong high pressure over the Beaufort Sea and strong low pressure near Baffin Island.

1969 – Front could not be located using NCEP product. With the ERA the front position is problematic with significant discontinuities. Large difference in position between Eastern and Western Canada with an uncertain position over Central Canada. Southerly flow over much of the CAA.

1970 – Similar to July 1968 and 1960 positions except with weaker synoptic features, resulting in a frontal position more zonal and further to the North. Also, there is low pressure near Great Slave Lake. The NCEP and ERA positions are very similar except the ERA position is further to the south.

1971 - Similar to the July 1970 position except the low is further south over Quebec. This results in frontal position much further to the south over Central Canada. The NCEP and ERA positions are very similar except the ERA position is further to the south and the NCEP front is shorter.

1972 – Similar to the July 1971 position except the Beaufort high is shifted to the West. The ERA position is further to the south except over Western North America where it has the opposite anomaly to NCEP. The front is also unusually close to the SE Alaskan coast.

1973 – High pressure south of Victoria Island. Low pressure near Great Slave Lake and over Northern Quebec. The Quebec low is slightly further to the east resulting in a further south position of the front. The ERA position of front is slightly further south than NCEP position.

1974 – Well-defined frontal boundary close to the long term mean position except over Quebec. Similar to the July 1973 position except Quebec low is further to the west resulting in a more northward bend to the front over Quebec. The high near Victoria Island is in roughly the position as 1973 except there is another high over Labrador. The ERA position of front is slightly further south than NCEP position.

1975 –Well-defined frontal boundary close to the long term mean position except over Quebec. The ERA position of front is slightly further south than NCEP position. Low pressure north of Ellesmere Island and over Davis Strait.

1976 –Front is closer to Arctic coast than in other years. Similar to the July 1950 position. ERA position is further to the south than NCEP position and more wavy. High pressure west of the CAA. Low pressure over northern Quebec and Davis Strait.

1977 – Similar to July 1973 except further to the south. Strong high pressure North of Alaska. Low pressure over NW Quebec and over Labrador. The ERA position of front is slightly further south than NCEP position, however much further south over Quebec.

1978 – Front is further to the south over Central Canada but bends toward Baffin Island before reaching Quebec. High pressure near the western part of the CAA. Low pressure over northern Hudson Bay.

1979 – The NCEP position is almost identical to Bryson's 1948 to 1957 mean position. Low pressure over southern Baffin Island and high pressure at the western end of the CAA. Similar to July 1977, the ERA position of front is slightly further south than NCEP position, but much further south over Quebec.

1980 – Well-defined frontal boundary close to the long term mean position west of Hudson Bay. Low pressure over northern Hudson Bay in a similar position to July 1978. High pressure over Beaufort Sea rather than over the Western part of the CAA resulting in a slightly further south position of the front over Alaska than 1978. The ERA position of front is slightly further south than NCEP position.

1981 – Front is further to the north but similar to July 1979 position. Low over Baffin Island is further to the north. High pressure near Victoria Island. The ERA position of front is slightly further south than NCEP position.

1982 – Low pressure over SW Baffin Island and over the South Central prairies. High pressure near the Yukon/Alaska coast. Front is further North over Alaska and further South over Quebec. There is a significant S-shaped bend in the front over Central Canada. The ERA position of front is slightly further south than NCEP position.

1983 – Front is similar to long term mean position except for the S-shaped bend (more than in July 1982) in the front over Central Canada, the result of the low near Great Slave Lake. There is also low pressure over SE Baffin Island. The ERA position of front is slightly further south than NCEP position.

1984 – The front ends at the coast near the Yukon/NWT border. There is an S-shaped bend in the front over Central Canada followed by a southeastward dip over Northern Ontario and a northeastward rise over Quebec. The ERA position of front is slightly further south than NCEP position.

1985 – Front is very zonal with less N-S variation than other years. The NCEP position is very close to the long term mean position for 1948 to 2007. ERA position of front is much further to the south of the NCEP position especially near the Alaska/Yukon border and over Eastern Canada. The low over Baffin Island is slightly further to the East.

1986 – Front is further south over Central Canada with a slight rise towards Quebec before a southeastward bend over Labrador. Low pressure near the Manitoba-Saskatchewan border, near the Labrador coast, over Davis Strait and near the North Pole. High pressure north of the Yukon/NWT coast. ERA position of the front is further south than the NCEP position and more wavy.

1987 – Two possible fronts using the NCEP product so likely a mixture of air masses in between. More southerly NCEP position of front is closer to ERA position. Front is further to the south over Alaska-Yukon with a slight bend to the north over NWT. Front is much further to the south over much of Canada. High pressure north of Alaska and over central Manitoba. Low pressure SW of Baffin Island and NE of Labrador.

1988 – Front is close to the Alaska coast with a slight bend over southern NWT. High pressure over far Western CAA. Baffin Low is further SE resulting in a more zonal front over Quebec. There is low pressure near Great Slave Lake. Overall, over much of Canada, east of NWT the front is quite zonal.

1989 – Front is anomalously far to the north, extending from Victoria Island to Hudson bay across to far Northern Quebec. This is similar to the position in July 1981 and 1959. The more southerly ERA position is close to the NCEP position. Low pressure over Davis Strait and the Beaufort Sea. High pressure near Lake Superior, not there in most years.

1990 – Slight discontinuity in front over Northern Quebec. Unusual orientation of front over Baffin Island/Quebec/Labrador. Low pressure near the North Pole, Baffin Island, and Northern Hudson Bay. High pressure near the north coast of Alaska. The ERA position of the front is more southerly than the NCEP position. Overall, the front is close to the tree line.

1991– Front has a rise to the north over Nunavut and a sharp bend to the SE over Quebec/Labrador. Low pressure over Davis Strait, Baffin Island, and Western Alaska. High pressure over NE Hudson Bay. ERA position is further to the south than the NCEP position.

1992– West of Great Bear Lake, the front is very zonal. Front is very far to the south over Central Canada. High pressure over NW coastal Alaska and Northern Baffin Island. Low pressure near Great Bear Lake, NWT, but none over Eastern Canada. ERA position is slightly further to the south than the NCEP position.

1993–Front is very far to the south over much of North America, except over sOntario and Quebec where it is close to other years. The front is closer SE Alaskan coast than normal but not as extreme as in July 1972. Low pressure near the Saskatchewan-Manitoba border, East of James Bay and over Newfoundland. High pressure over Greenland. ERA position is slightly further to the south than the NCEP position.

1994– East of Alaska, the front is very far to the south, reaching near the Canada-USA border in Central Canada. Low pressure along NE coast of Baffin Island. Large high pressure slightly west of Great Bear Lake. This position allows for southerly/southwesterly flow over Western North America. The front reaches the coast over NWT. ERA position is slightly further to the south than the NCEP position.

1995– Both NCEP and ERA positions are further to the south except over Quebec where there is an unusual bend to the north. Baffin Low is further to the west. High pressure over the eastern Beaufort Sea and over southern Greenland. Large low pressure over northern Hudson Bay. ERA position is slightly further to the south than the NCEP position.

1996– Circulation is difficult to define over much of Central Canada. Front is very far to the South over Central and Eastern Canada. High pressure near Churchill. Low pressure SW of Great Slave Lake and over Saskatchewan-Manitoba. ERA position is slightly further to the south than the NCEP position.

1997– Front position is anomalously far to the north east of NWT, extending towards Baffin Island. The ERA position of the front is close to the NCEP position, except over Quebec. Low pressure west of Ellesmere Island, over Labrador and Northern Davis Strait, and near Great Slave Lake. High pressure near the NE coast of Alaska and over Hudson Bay.

1998– Front is further to the North in the West and further to the South in the East with a sharp bend to the south over Western NWT. High pressure to the West of the CAA. Low pressure near the NW coast of Quebec. ERA position is slightly further to the south than the NCEP position, especially over Eastern Canada.

1999– Baffin Low is further to the west. Large low pressure over NE Hudson Bay. Beaufort Sea high pressure is much further to the west almost not visible on the plot. ERA position of front is very close to NCEP position except over Ontario and Quebec where it is further south.

2000– Front position is close to the Arctic coast in the West and much further to the south in Central and Eastern Canada. Low pressure over NW Alaska and Devon Island. High pressure over the Great Lakes, near Melville Island, Baker Lake, Ungava Bay and over Greenland. E.RA position is slightly further to the south than the NCEP position

2001– Front has a northward rise toward Victoria Island and is much further to the South over Quebec. Over Baffin Island there is high pressure rather than low pressure. Low pressure near Devon Island, Great Bear Lake and NE Labrador. ERA position is slightly further to the south than the NCEP position.

2002 – Not possible to locate an Arctic front with the NCEP product. ERA position of front is further to the South over Western Canada and Quebec. No low pressure near or over Baffin Island, but over Southern Ellesmere Island instead. Also large low pressure over the Beaufort Sea.

*2003 – Front is much shorter and difficult to locate. It starts near the NWT-Nunavut border, has a southward bend into Manitoba and Ontario and ends over Central Quebec. Low pressure over Quebec and the Beaufort Sea. High pressure near Baker Lake.

*2004– Front has a rise to the north over Nunavut and an s-shaped bend over Nunavut, Manitoba, and Ontario. The position over Quebec is close to tree line. There is low pressure NW of Ellesmere Island and over the Aleutian Islands and high pressure over Southern Nunavut and over the far Western CAA.

*2005– Front position is similar to July 2004 except further north over Quebec. Low pressure over the Central CAA, between Baffin Island and Quebec, and near Great Slave Lake. High pressure over the Beaufort Sea.

*2006– Front is further south over Central Canada but much shorter than in other years. Strong low pressure over northern Baffin Island and high pressure near Melville Island. Strong northerly flow over the CAA due to the position of the Baffin Island low pressure.

*2007– Front has a significant s-shaped bend to the north over NWT followed by a southward bend across Nunavut and Manitoba into northern Ontario and a sharp northward rise over Quebec. Main synoptic features are high pressure over the Beaufort Sea, low pressure near Great Slave Lake and over Quebec.

Table B1. July Arctic front position 1948 to 2007 by longitude, derived from NNR.

	140W	130W	120W	110W	100W	90W	80W	70W
1948-1957 (Bryson)			64.6	61.6	58.3	56.5	55.9	
July1948	68.4	66.4	66.6	66.6	55.7	52.2	49.3	51.4
July1949	66	65	62.7	56.8	60.6	58.5	57.7	61.2
July1950	65	63.8	62.9	61.6	58.7	54.1	50.1	51.1
July1951		67.3	67.4	64.9	64.6	65.6	59.2	60.1
July1952		65.2	66.3	62.4	58.8	58.8	59.3	63
July1953		63.5	61.4	58.2	58.3	56.2	57.2	
July1954	70	64.2	65.6	65.7	71.3	71.9	71.4	
July1955	65	63.2	57	63.1	63.2	60.3	58	57.9
July1956			66.9	64.3	62.1	60.2	52.5	51.7
July1957	67.5	61	58.2	61.8	66.4	55.9	50.8	50.6
July1958	65.3	63.2	59.5	54.7	54.1	55	51.1	53.1
July1959			65.6	63	62.2	60.7	62	
July1960	65.8	64	62.7	62.1	61.2	59.1	56.6	55.8
July1961				57.3	59.8	49.4	49.4	51.2
July1962		67.1	59	59.6	60.3	55	51.4	51.9
July1963			59.6	61.3	62.1	55.6	51.5	52.8
July1964	65.7	66.7	70.1	70.7	70.4	68.2	63.8	60.9
July1965	66.1	63.5	62.6	60	57.5	52.5	53.2	55.6
July1966		67.7	59.8	56.8	59.9	56.9	52.9	52.5
July1967			63.2	65	59.9	53.7		
July1968	65.8	64	60.2	53.7	50.9	51.1	52.9	56.9
July1969								
July1970	67.8	65.09	63.6	63.8	62.4	60.4	59.4	61.3
July1971			62.3	64.7	51.5	44.8	50.8	54.5
July1972	65.8	55.2	58.7	74.3	48	50.8	54.1	61.4
July1973			64.5	63.1	61.2	54.3	52.5	54.5
July1974		64.4	61.1	58.3	59.8	55.3	54.5	
July1975	68.2	66.4	66.2	63.4	58.3	54.6	55.4	64.5
July1976	68.6	67.6	65.6	62.7	59.8	55.4	52	52.4
July1977	65.09	62	57.7	54.9	54.3	52.4	54.1	60.2
July1978	68.3	65.6	61.9	56	54.5	57	61.7	
July1979		67.3	64.8	61.2	57.3	57	56.4	59.5
July1980	66.5	65	62.5	60.5	59.1	57		
July1981			65.1	64.4	61.7	58.8	60.5	64.2
July1982	68.4	68	59.2	55.6	58.9	56	53.3	54.1
July1983	65.2	65.2	62.1	62.8	61	54.7	53.7	54.3
July1984		66.9	63	65.6	63.6	54.3	53.2	58
July1985	66.6	64.2	61.9	60.5	60.1	58.2	56.6	57.3
July1986	66.1	62.4	53.8	57.3	62.4	57.9	56.7	50.9
July1987	63.3	64.1	55.8	53.2	50.1	52	51.8	52.1
July1988	67.3	63.3	60.1	59.4	60.8	59.8	58.5	57.8
July1989				66	62.2	60.8	60.8	60.3
July1990	68.2	68.6	65.8	58.9	59.6	56.8	58.4	63.6
July1991	65.3	63.3	61.1	62.1	64.1	59.9	58.4	59.1
July1992	65.7	64.4	64.8	55.4	51.5	50.5	51.3	51.9
July1993	64	60.4	56.3	51.3	52	54.5	56.6	60.3

July1994			61.4	55.9	50.6	49.2	52.7	55.4
July1995	65.6	63.8	61.3	54.6	54	52.9	55.7	
July1996		65.8	62.3	55.8	51.4	47.5	48.2	48.8
July1997	65.4	63.4	60.7	62.4	63.3	65.5	51.3	49.8
July1998	67.6	65.8	67.5	57.3	55.6	53.3	52.9	53.2
July1999	67.7	64	59.2	55	53.9	55.2	54.6	58
July2000	69.3	65.2	66.5	61.5	55	53.3	53.5	52.3
July2001	67.6	65.4	67.2	69	61.8	57.4	51.7	51.9
July2002								
July2003					57.1	52.6	48.7	52.5
July2004		66.5	63.6	64.2	64.1	53.7	54.6	58.4
July2005	65.6	63.5	60.8	64.1	62.3	58.5	59.6	
July2006		68.6	64.1	57.7	56.7	56.9	59.8	
July2007	66.1	63.9	62	65.5	59	54.3	54.1	
mean	66.6	64.7	62.4	60.8	58.9	56.1	55.2	56.0
median	66.1	64.4	62.3	61.4	59.8	55.6	54.1	55.5
mode	65.8	65.2	65.6	57.3	59.8	54.3	56.6	51.9
min	63.3	55.2	53.8	51.3	48.0	44.8	48.2	48.8
max	70.0	68.6	70.1	74.3	71.3	71.9	71.4	64.5
range	6.7	13.4	16.3	23.0	23.3	27.1	23.2	15.7
std dev	1.6	2.8	3.6	5.1	5.3	5.2	4.8	4.3

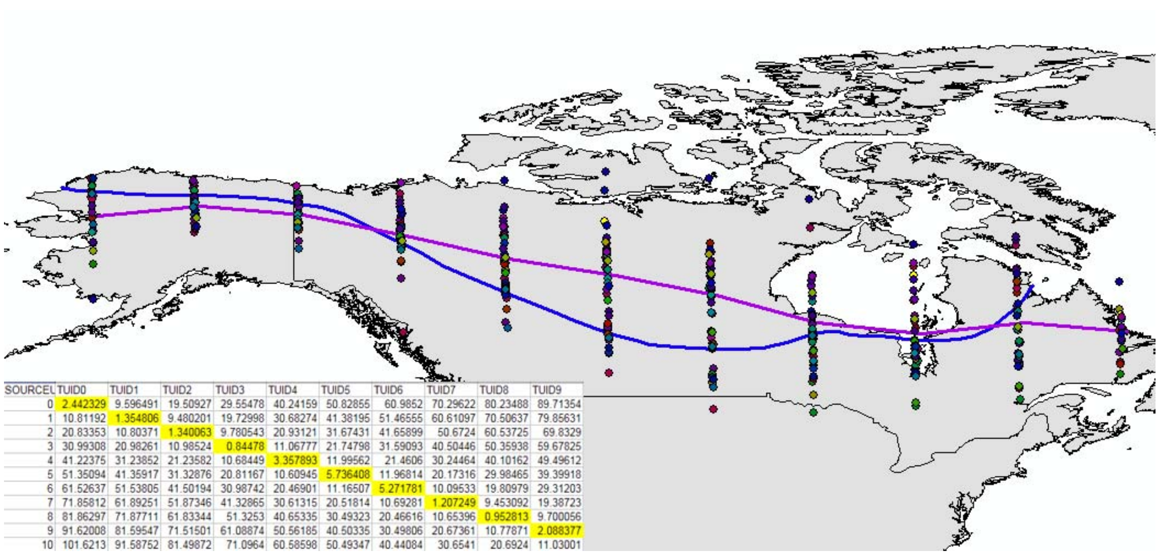

SOURCEL	TUID0	TUID1	TUID2	TUID3	TUID4	TUID5	TUID6	TUID7	TUID8	TUID9
0	2.442329	9.596491	19.50927	29.55478	40.24159	50.82855	60.9852	70.29622	80.23488	89.71354
1	10.81192	1.354806	9.480201	19.72998	30.68274	41.38195	51.46555	60.61097	70.50637	79.85631
2	20.83353	10.80371	1.340063	9.780543	20.93121	31.67431	41.65899	50.6724	60.53725	69.8329
3	30.99308	20.98261	10.98524	0.84478	11.06777	21.74798	31.59093	40.50446	50.35938	59.67825
4	41.22375	31.23852	21.23582	10.68449	3.357893	11.99562	21.4606	30.24464	40.10162	49.49612
5	51.35094	41.35917	31.32876	20.81167	10.60945	5.736408	11.96814	20.17316	29.98465	39.39918
6	61.52637	51.53805	41.50194	30.98742	20.46901	11.16507	5.271781	10.09533	19.80979	29.31203
7	71.85812	61.89251	51.87346	41.32865	30.61315	20.51814	10.69281	1.207249	9.453092	19.38723
8	81.86297	71.87711	61.83344	51.3253	40.65335	30.49323	20.46616	10.65396	0.952813	9.700056
9	91.62008	81.59547	71.51501	61.08874	50.56185	40.50335	30.49806	20.67361	10.77871	2.088377
10	101.6213	91.58752	81.49872	71.0964	60.58598	50.49347	40.44084	30.6541	20.6924	11.03001

Figure B62. July 1999 versus 1958 to 2002 mean position (derived from NNR) of Arctic front. Table of values produced using Hawths tools (distance between points tool).

Appendix C – Additional maps derived from ERA-40

This section contains additional maps created with variables from the ERA-40 product. Once familiar with the ERA-40 it was possible to apply the same techniques to analyze variables in the NNR product.

Maps of specific ERA-40 variables (Table C1) were produced for the summer months (June, July, and August) in order to examine the atmospheric boundary layer conditions along where the summer Arctic front should be located. This was accomplished by bringing the gridded data into Excel (Table C2) and developing a macro that would process the data and reformat it to be mapped in ArcGIS. Maps of the mean monthly surface wind streamlines were produced in order to compare with those of Bryson (1966).

The following variables are available from the ECMWF ERA-40 data server website (ECMWF, 2008) at the 1000, 925, 850, 775, 600, 500, 400, 300, 250, 200, 150, 100, 70, 50, 30, 20, 10, 7, 5, 3, 2, and 1 mb levels:

Ozone mass mixing ratio
Potential vorticity
Relative humidity
Specific humidity
Temperature
U velocity
V velocity
Vertical velocity
Vorticity (relative)

The following variables are available at the surface level:

10 metre U wind component	10 metre V wind component
2 metre dewpoint temperature	2 metre temperature
Boundary layer height	Convective precipitation
East-West surface stress	Evaporation
High cloud cover	Ice surface temperature layer 1
Ice surface temperature layer 2	Ice surface temperature layer 3
Ice surface temperature layer 4	Latitudinal component of gravity wave stress
Low cloud cover	Mean sea level pressure
Mean wave direction	Mean wave period
Medium cloud cover	Meridional component of gravity wave stress
North-South surface stress	Runoff
Sea-ice cover	Significant wave height

Snow depth | Snow evaporation
Snowfall | Snowmelt
Soil temperature level 1 | Soil temperature level 2
Soil temperature level 3 | Soil temperature level 4
Stratiform precipitation (Large-scale precipitation) | Surface latent heat flux
Surface net solar radiation, clear sky | Surface net thermal radiation, clear sky
Surface sensible heat flux | Surface solar radiation
Surface solar radiation downwards | Surface thermal radiation
Surface thermal radiation downwards | Temperature of snow layer
Top net solar radiation, clear sky | Top net thermal radiation, clear sky
Top solar radiation | Top thermal radiation
Total cloud cover | Total column ozone
Total column water | Total column water vapour
Total precipitation | Volumetric soil water layer 1
Volumetric soil water layer 2 | Volumetric soil water layer 3
Volumetric soil water layer 4

Table C1. Variables selected for mapping from the ECMWF ERA-40 reanalysis.

Variable	**Justification for inclusion**
2m air temperature	There should be a greater change in temperature along the frontal boundary at the surface.
2m wet bulb temperature	There should be a strong wet bulb temperature difference north and south of the front at the surface.
Surface relative humidity	There should be lower humidity in the air mass north of the front and higher humidity south of the front.
Total cloud cover	There should be should be a difference in total cloud cover across the frontal boundary.
Boundary Layer Height	There should be a change in the boundary layer height across the frontal boundary with a thicker boundary layer south of the front.
Latent Heat Flux	There should be some difference in latent heat flux across the frontal boundary, with higher values to the south of the front.
Vertical Velocity (1000mb)	There should be positive vertical motion along the frontal boundary.
Divergence (1000mb)	There should be a higher probability of negative divergence (convergence) at the surface where the front is located which leads to the rising motion along the frontal zone.

Table C2. ERA-40 2m temperature data for June 2002 mean (values in °K). Source is ECMWF ERA-40 data server.

	0	2.5	5	7.5	10	12.5
90.000:	2.73E+02	2.73E+02	2.73E+02	2.73E+02	2.73E+02	2.73E+02
87.500:	2.74E+02	2.73E+02	2.73E+02	2.73E+02	2.73E+02	2.73E+02
85.000:	2.74E+02	2.74E+02	2.74E+02	2.74E+02	2.74E+02	2.74E+02
82.500:	2.75E+02	2.75E+02	2.75E+02	2.75E+02	2.75E+02	2.75E+02
80.000:	2.75E+02	2.75E+02	2.74E+02	2.74E+02	2.74E+02	2.74E+02
77.500:	2.74E+02	2.75E+02	2.76E+02	2.76E+02	2.76E+02	2.76E+02
75.000:	2.75E+02	2.76E+02	2.77E+02	2.78E+02	2.78E+02	2.78E+02
72.500:	2.78E+02	2.79E+02	2.79E+02	2.79E+02	2.80E+02	2.80E+02

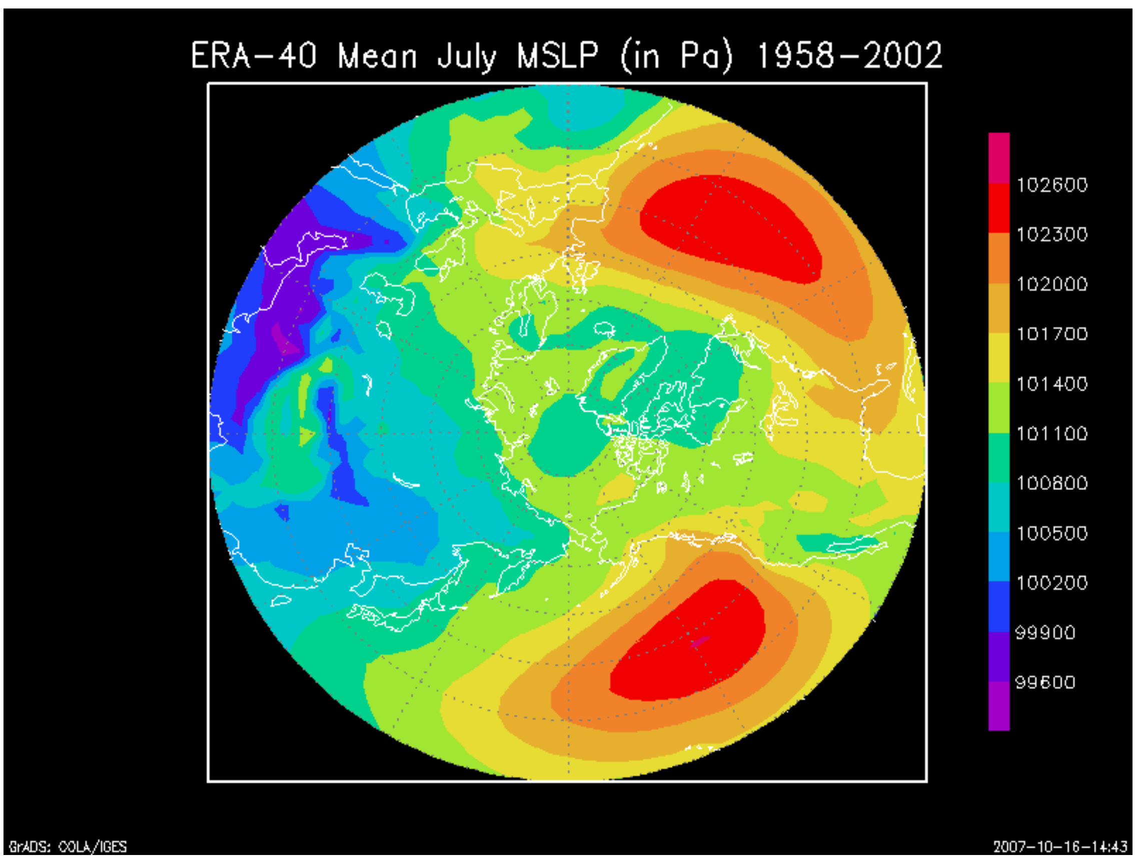

Figure C1. ERA-40 Mean July MSLP for 1958-2002 for the northern hemisphere.

C.1. Mean monthly wind streamlines and analysis of July frontal parameters using ERA-40

Mean 10m wind streamline maps have been produced for all months and compared with those of Bryson (1966). Each streamline map shows the major air mass boundaries and serves as a starting point for the location of the Arctic summer frontal boundary. However, it is necessary to examine long term mean maps of several gridded variables to determine the likely areas in which the boundary resides. The analysis is for the summer months of June, July and August. For these months the following maps are shown:

2m temperature, wet bulb temperature, relative humidity (surface), latent heat flux, boundary layer height, total cloud cover, negative divergence at 1000 mb, positive vertical velocity at 1000 mb

C.1.1. Mean surface streamlines for January

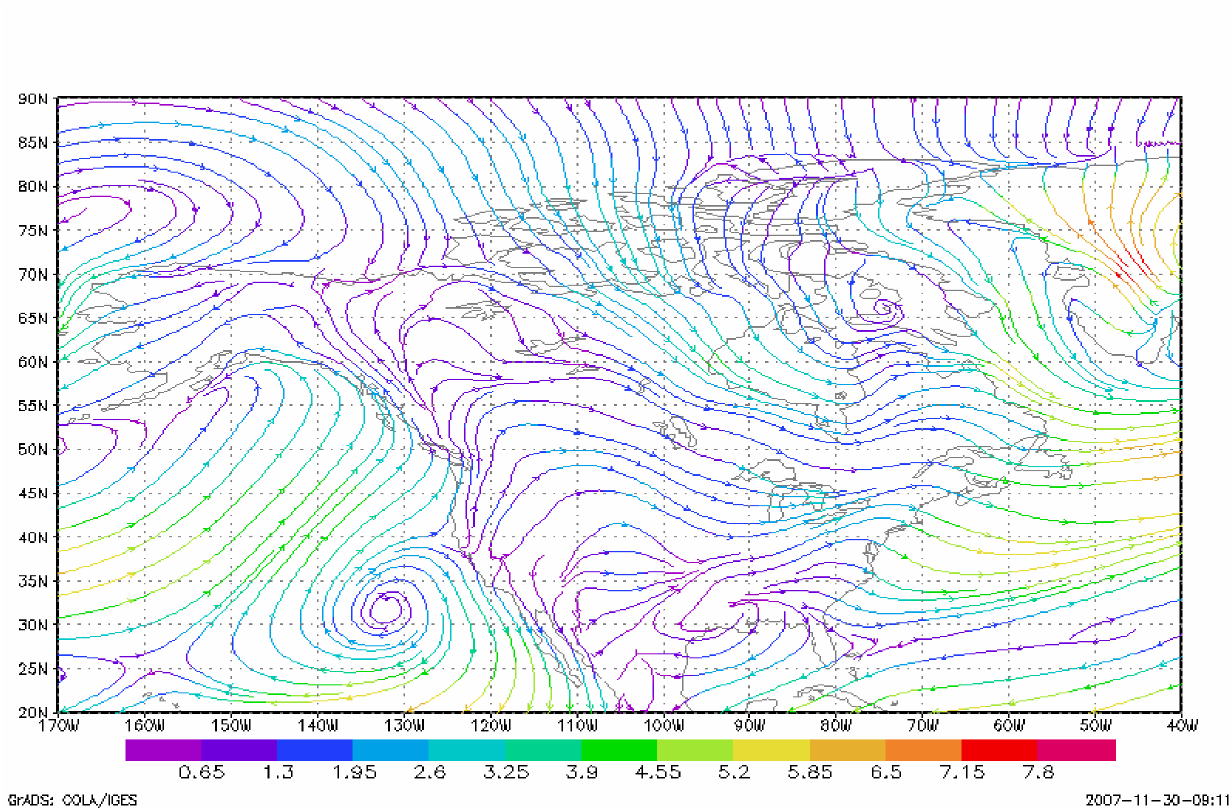

Figure C2. Mean January 10m Streamlines (in m/s) for 1958-2002 from the ERA-40 reanalysis.

C.1.2. Mean surface streamlines for February

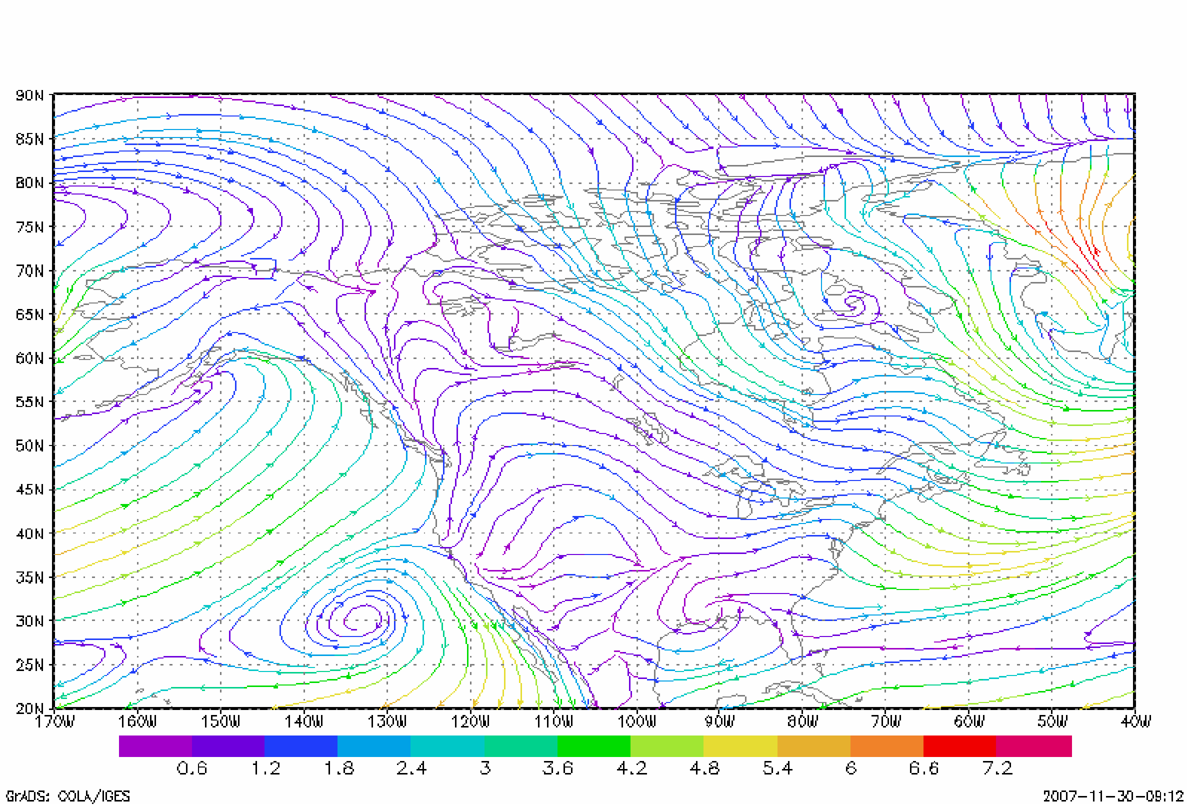

Figure C3. Mean February 10m Streamlines (in m/s) for 1958-2002 from the ERA-40 reanalysis.

C.1.3. Mean surface streamlines for March

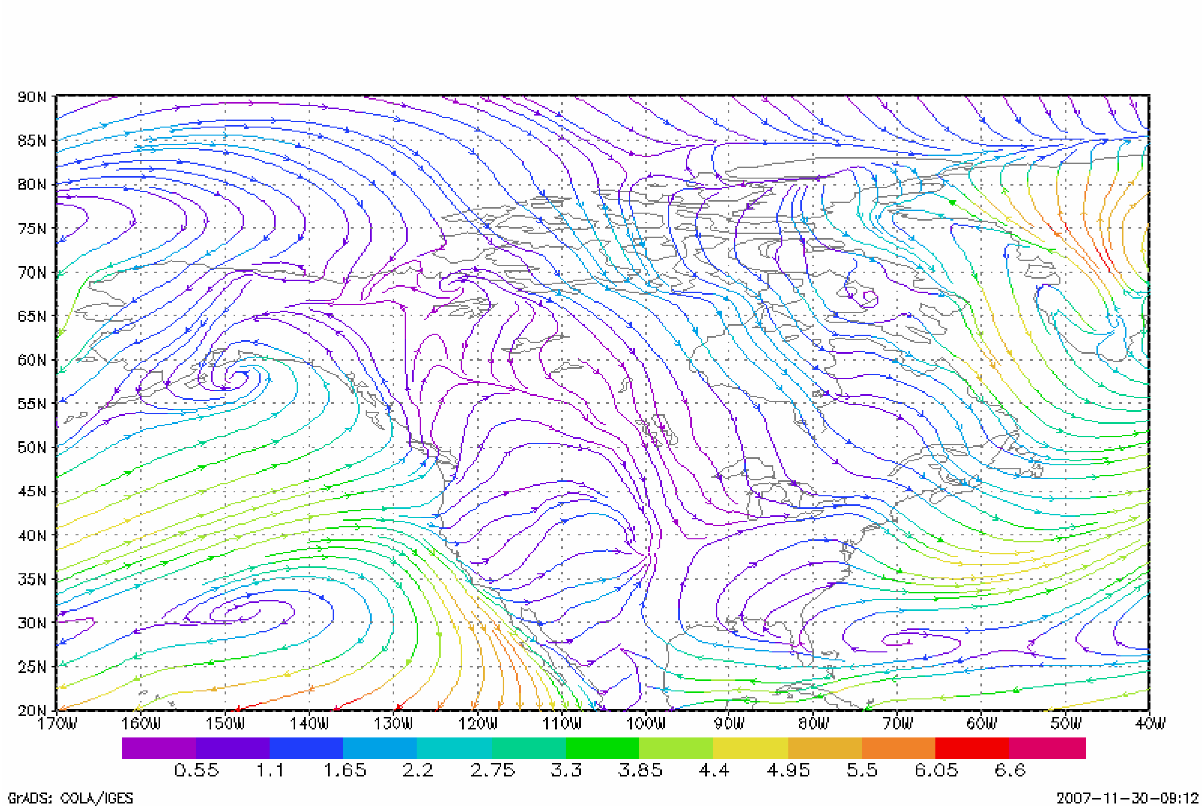

Figure C4. Mean March 10m Streamlines (in m/s) for 1958-2002 from the ERA-40 reanalysis.

C.1.4. Mean surface streamlines for April

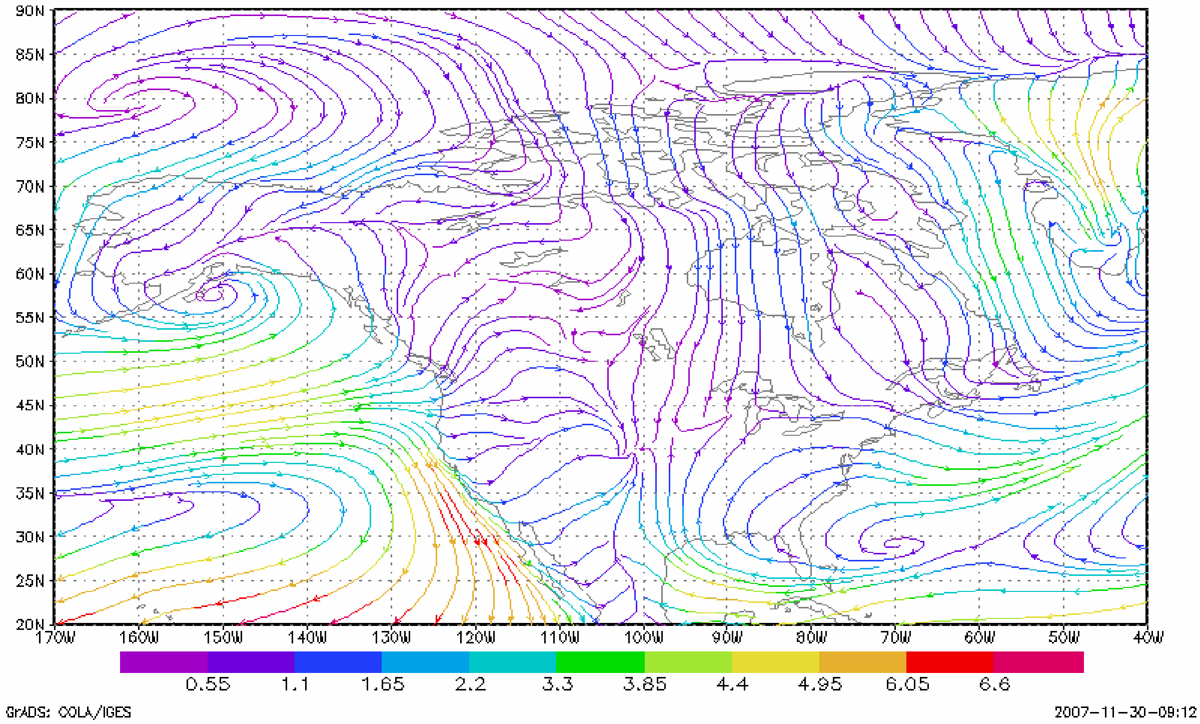

Figure C5. Mean April 10m Streamlines (in m/s) for 1958-2002 from the ERA-40 reanalysis.

C.1.5. Mean surface streamlines for May

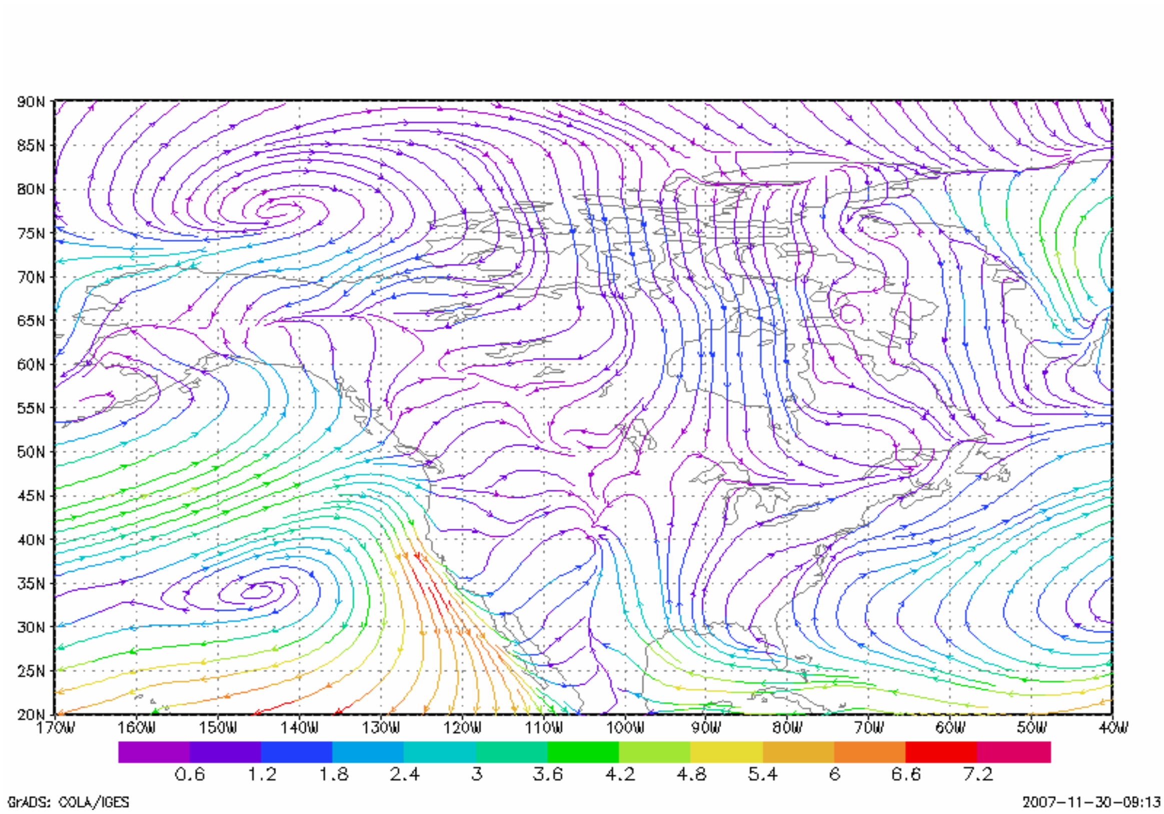

Figure C6. Mean May 10m Streamlines (in m/s) for 1958-2002 from the ERA-40 reanalysis.

C.1.6. Mean surface streamlines for June

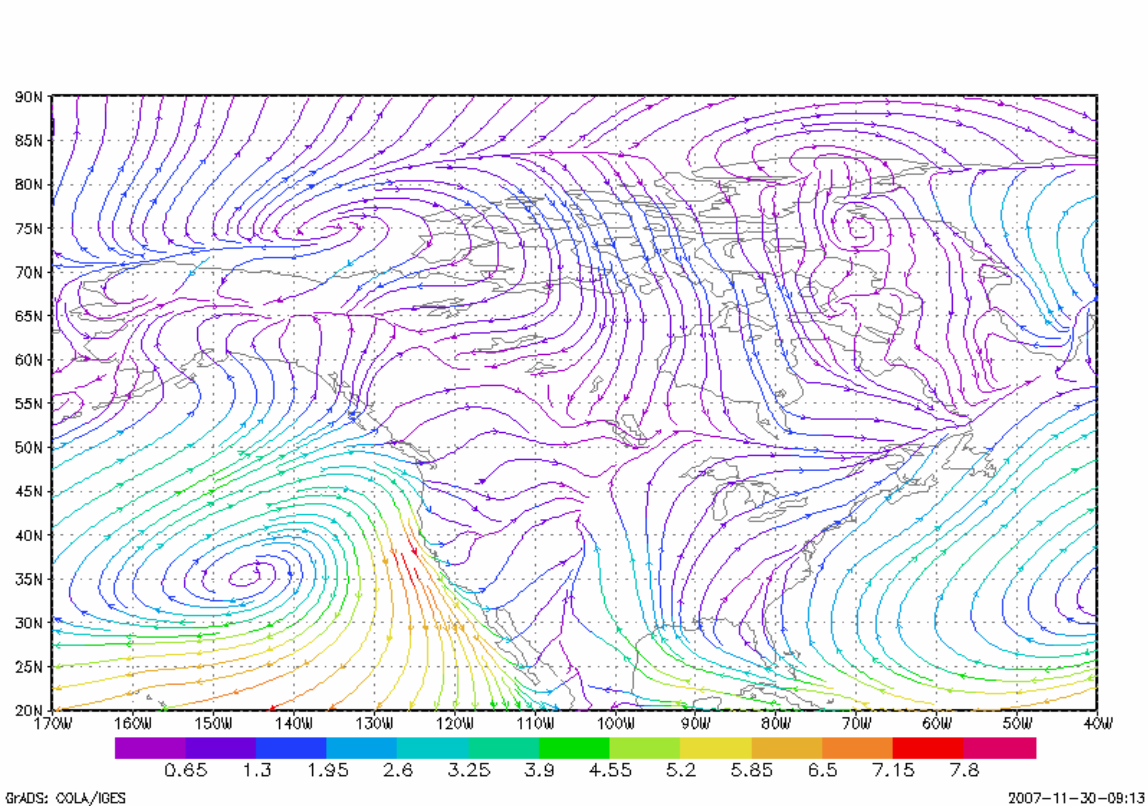

Figure C7. Mean June 10m Streamlines (in m/s) for 1958-2002 from the ERA-40 reanalysis.

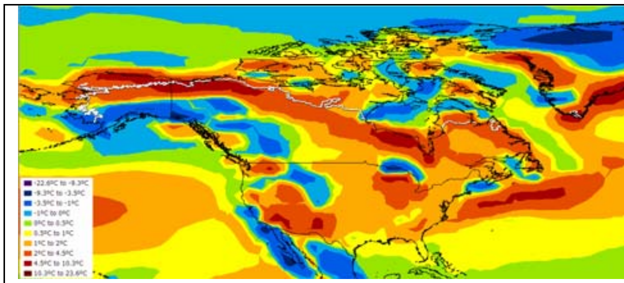

Figure C8. Mean June surface (2m) temperature change per -2.5º latitude for 1958 to 2002

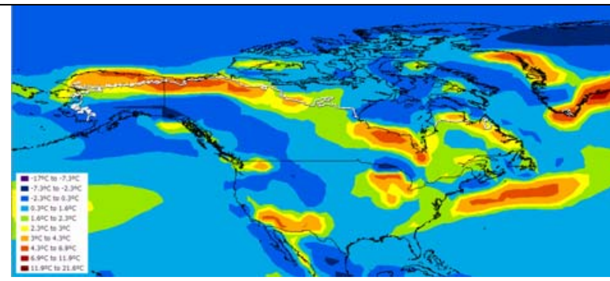

Figure C9. Mean June wet bulb temperature change per -2.5º latitude for 1958 to 2002.

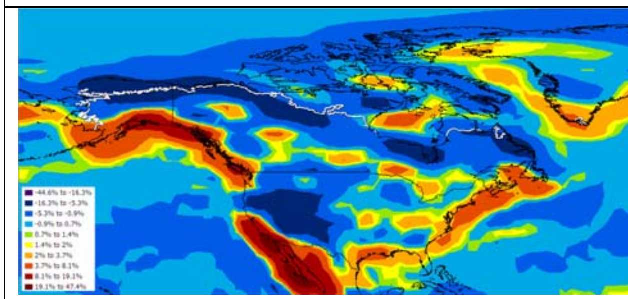

Figure C10. Mean June relative humidity change per -2.5º latitude for 1958 to 2002.

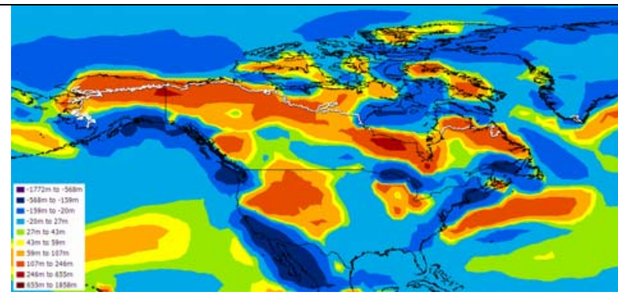

Figure C11. Mean June boundary layer height change per -2.5º latitude for 1958 to 2002.

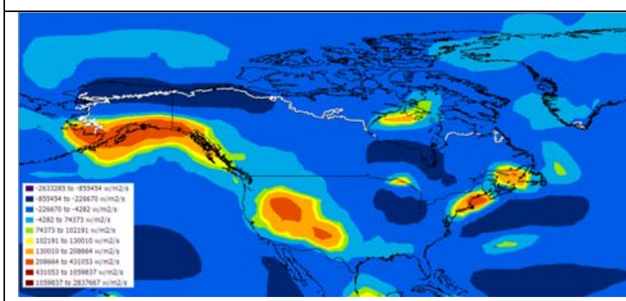

Figure C12. Mean June latent heat flux change per -2.5º latitude for 1958 to 2002.

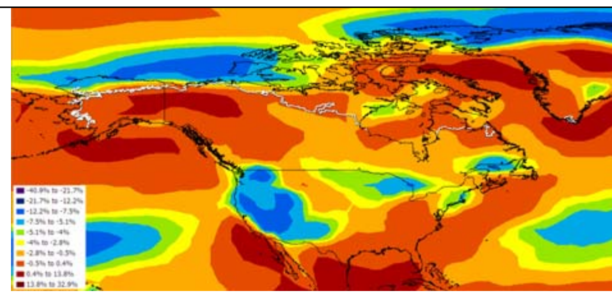

Figure C13. Mean June total cloud cover change per -2.5º latitude

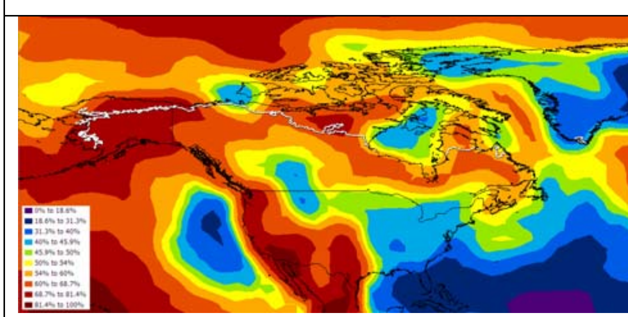

Figure C14. Probability of positive Mean June vertical velocity at 1000mb for 1958 to 2002.

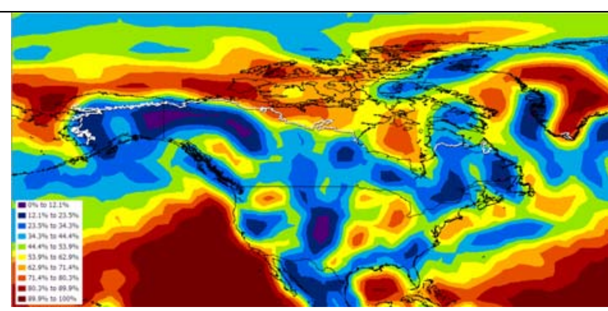

Figure C15. Probability of negative Mean June divergence at 1000mb for 1958 to 2002.

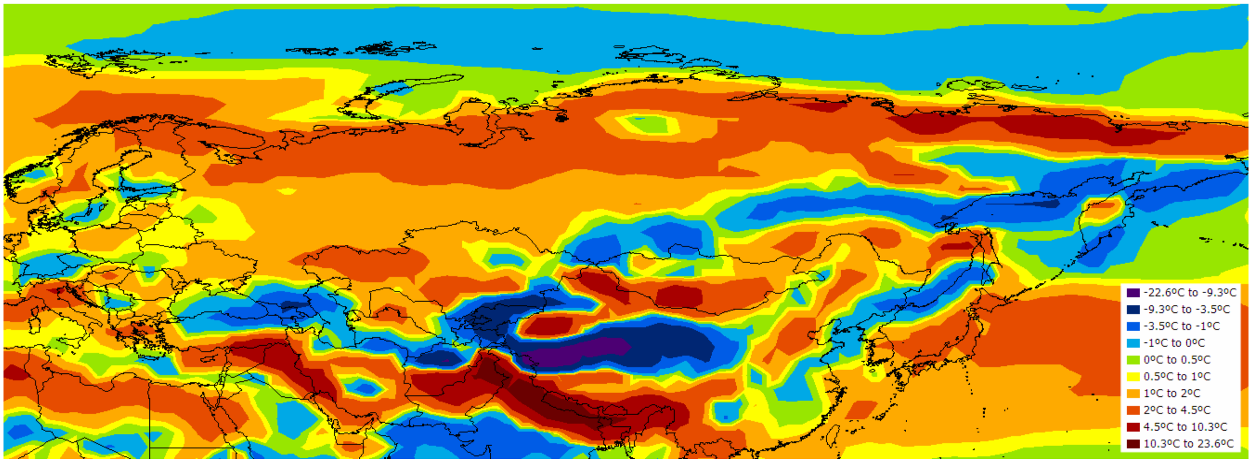

Figure C16. Mean June surface (2m) temperature change per -2.5º latitude for 1958 to 2002.

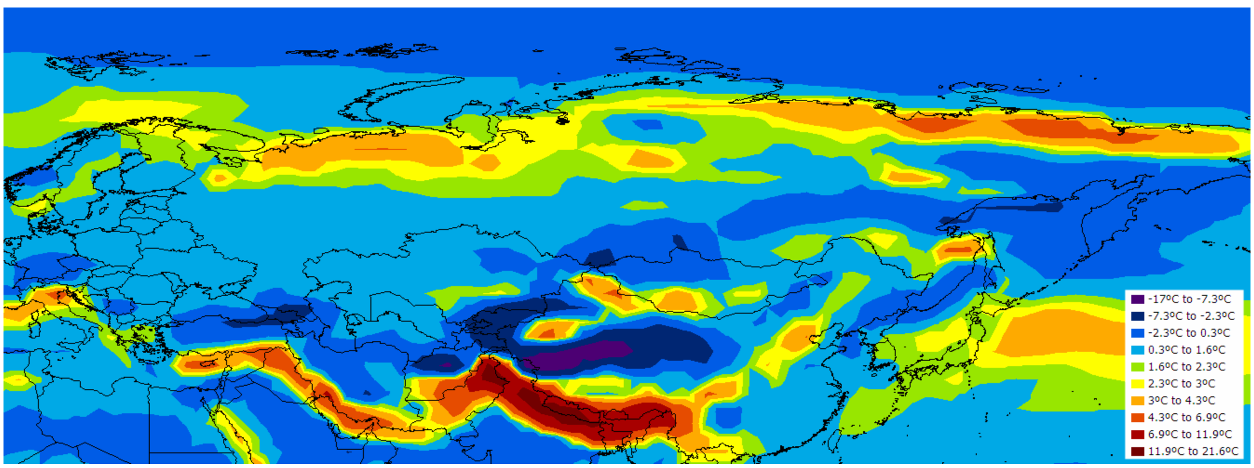

Figure C17. Mean June wet bulb temperature change per -2.5º latitude for 1958 to 2002.

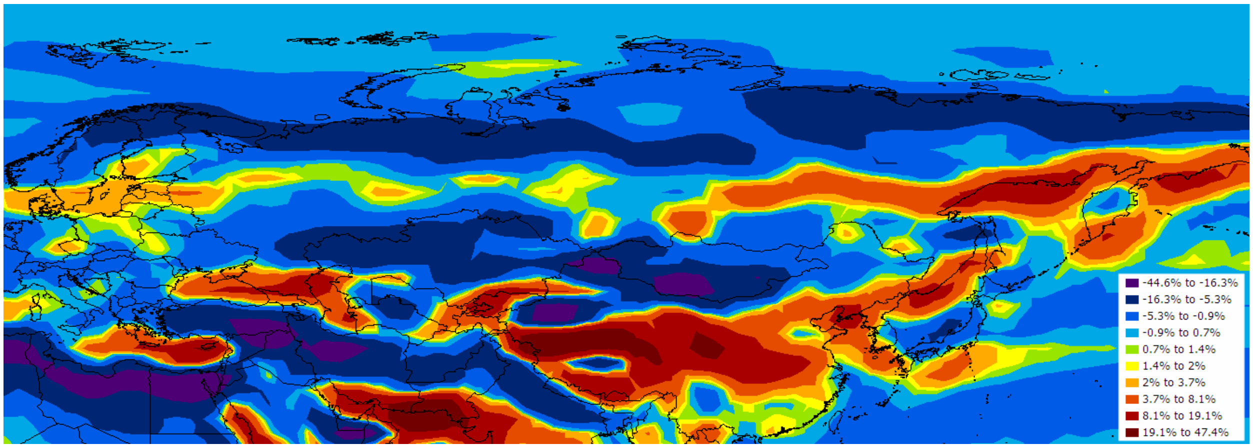

Figure C18. Mean June relative humidity change per -2.5º latitude for 1958 to 2002.

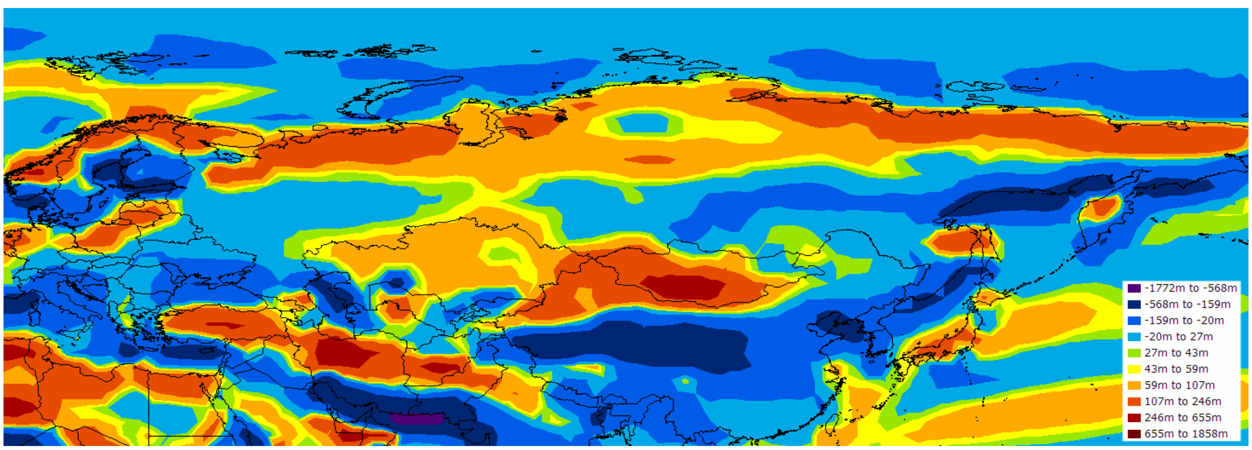

Figure C19. Mean June boundary layer height change per -2.5º latitude for 1958 to 2002.

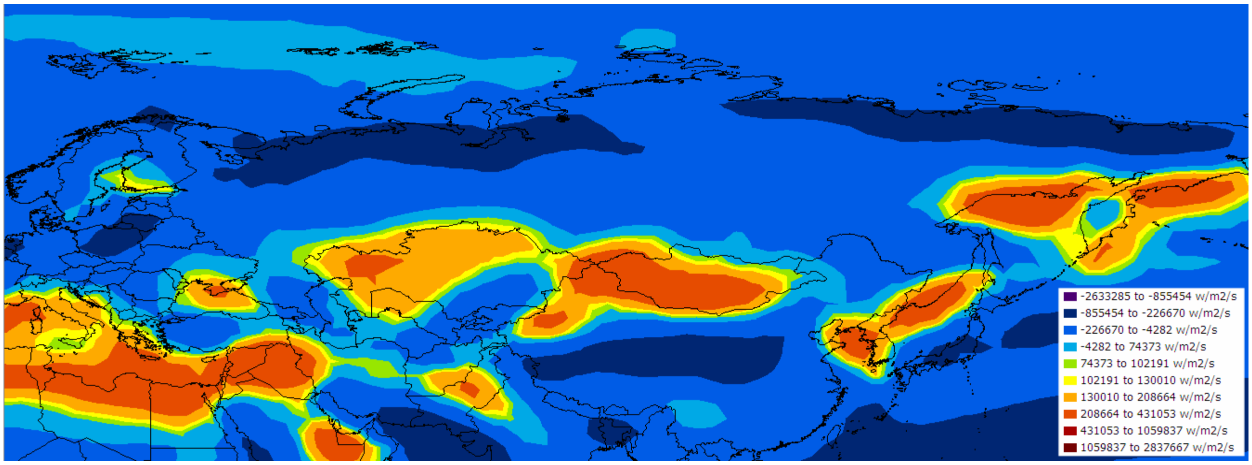

Figure C20. Mean June latent heat flux change per -2.5º latitude for 1958 to 2002.

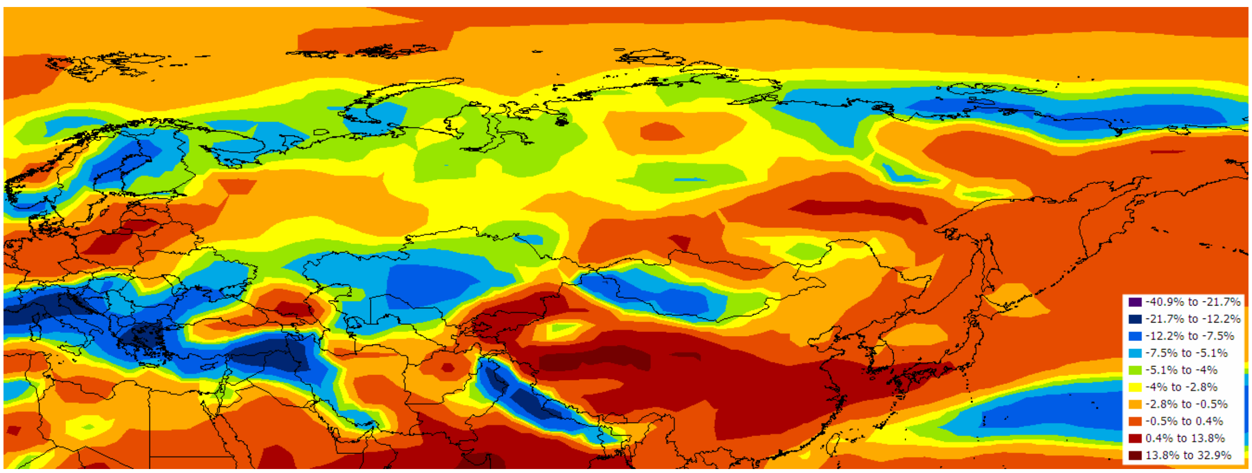

Figure C21. Mean June total cloud cover change per -2.5º latitude for 1958 to 2002.

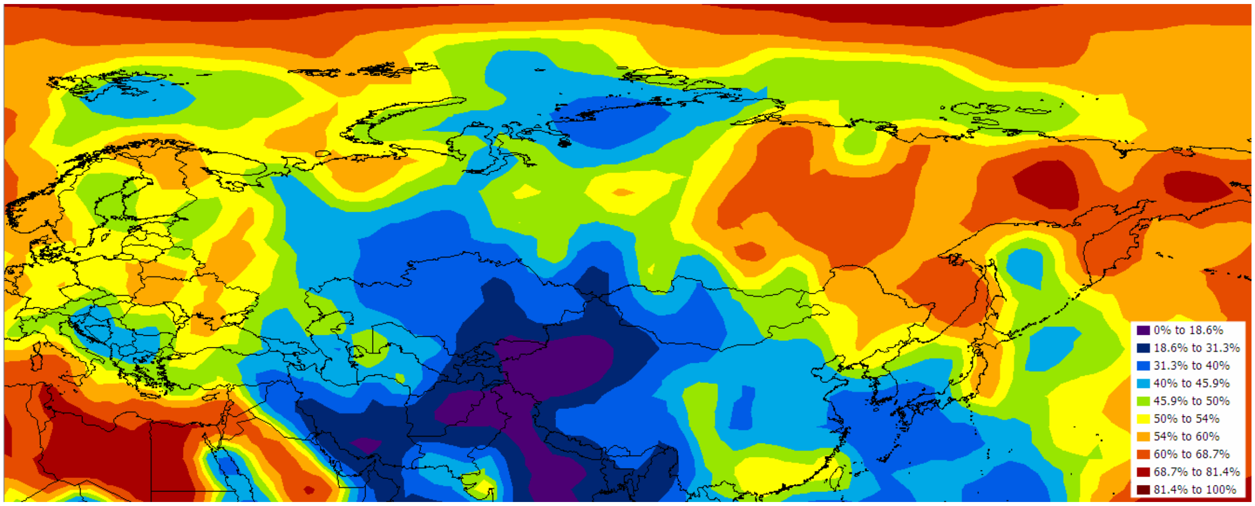

Figure C22. Probability of positive Mean June vertical velocity at 1000mb for 1958 to 2002.

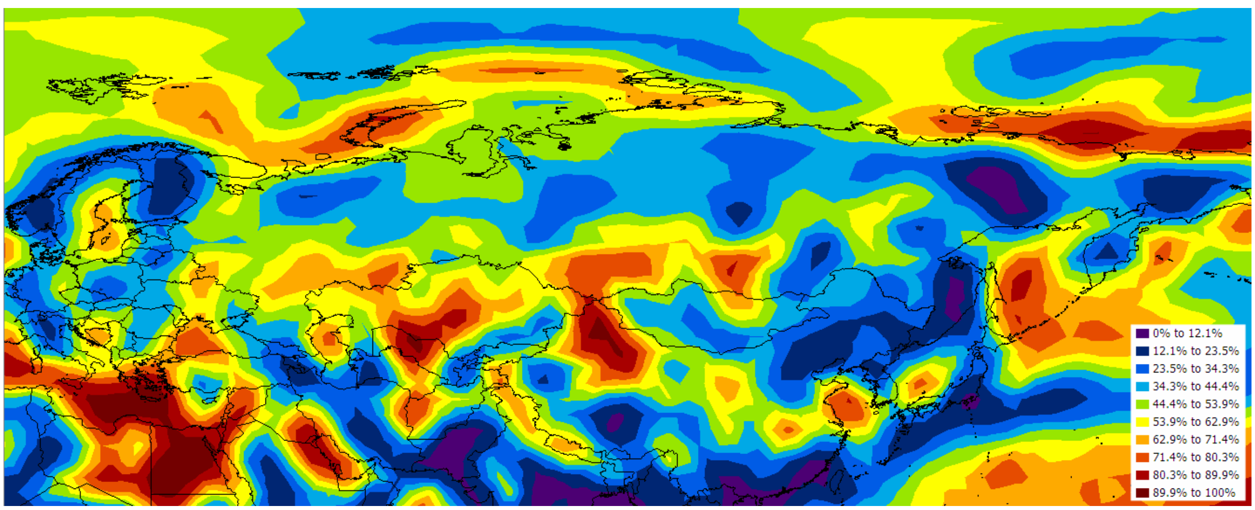

Figure C23. Probability of negative Mean June divergence at 1000mb for 1958 to 2002.

C.1.7. Mean surface streamlines for July

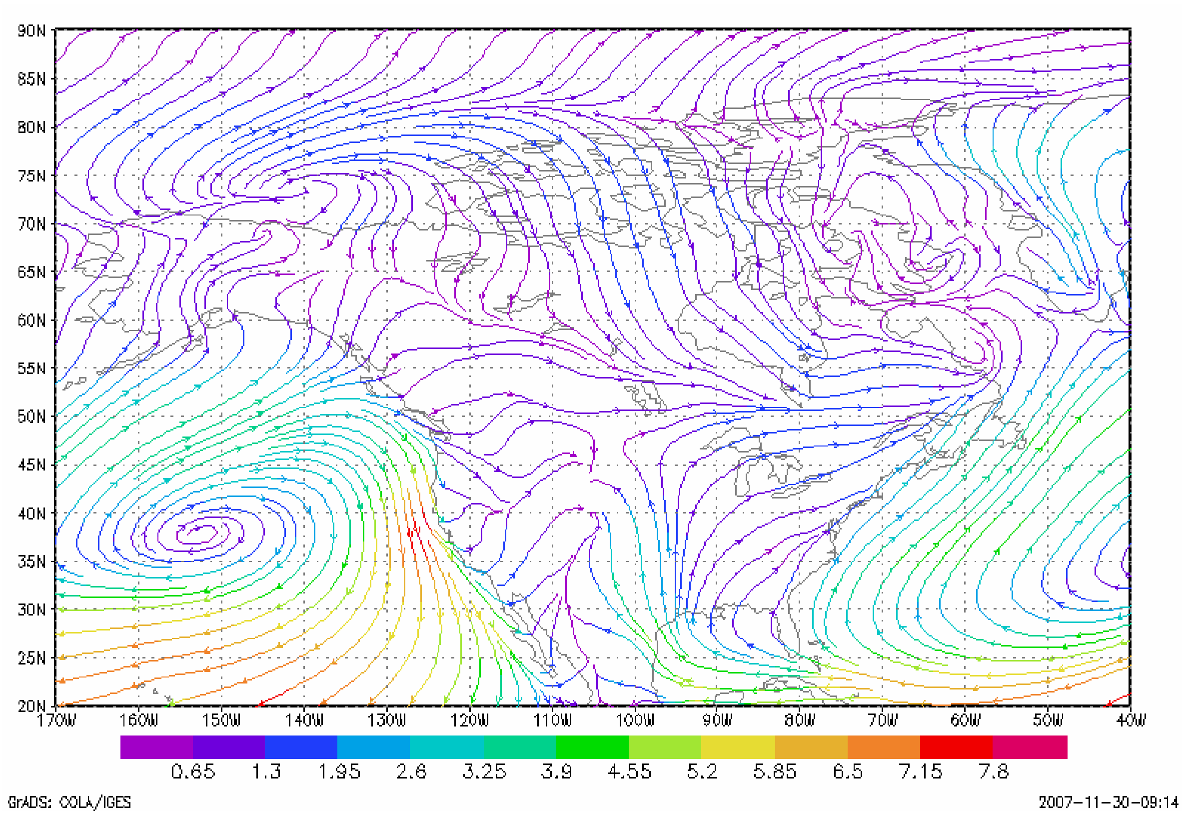

Figure C24. Mean July 10m Streamlines (in m/s) for 1958-2002 from the ERA-40 reanalysis.

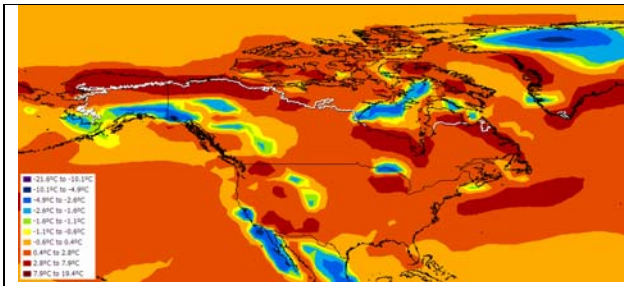

Figure C25. Mean July surface (2m) temperature change per -2.5º latitude for 1958 to 2002.

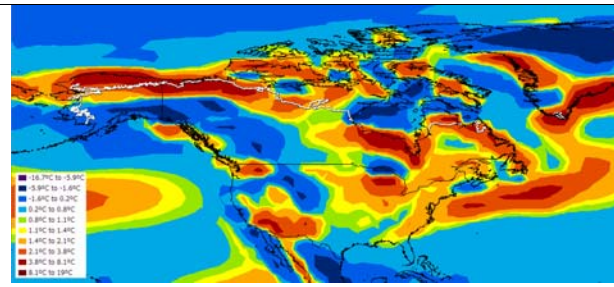

Figure C26. Mean July wet bulb temperature change per -2.5º latitude

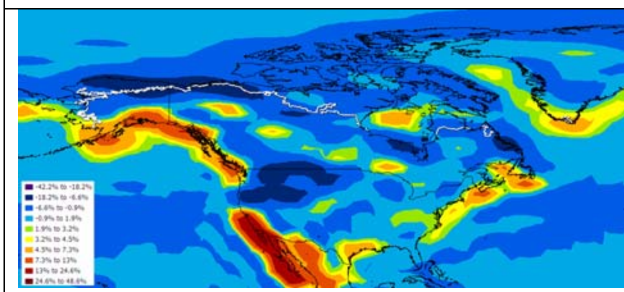

Figure C27. Mean July relative humidity change per -2.5º latitude for 1958 to 2002.

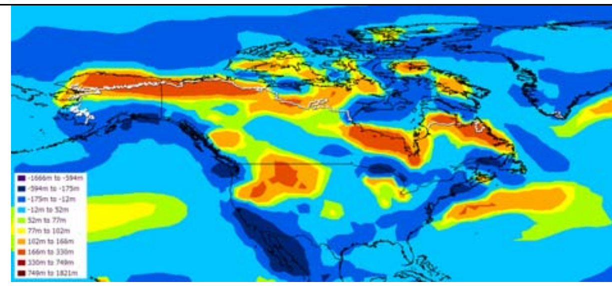

Figure C28. Mean July boundary layer height change per -2.5º latitude

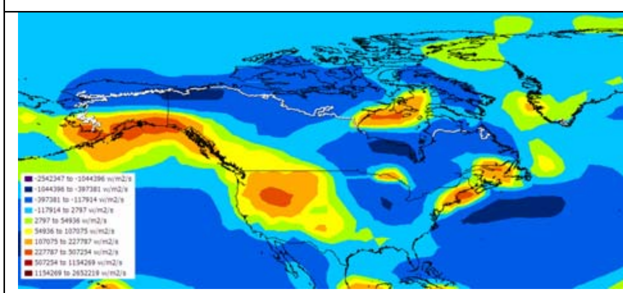

Figure C29. Mean July latent heat flux change per -2.5º latitude

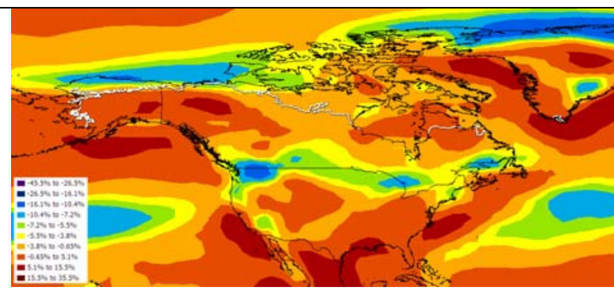

Figure C30. Mean July total cloud cover change per -2.5º latitude

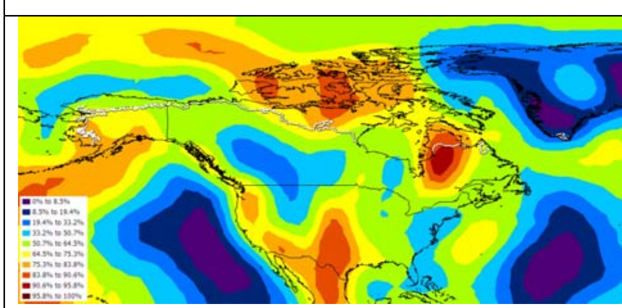

Figure C31. Probability of positive Mean July vertical velocity at 1000mb for 1958 to 2002.

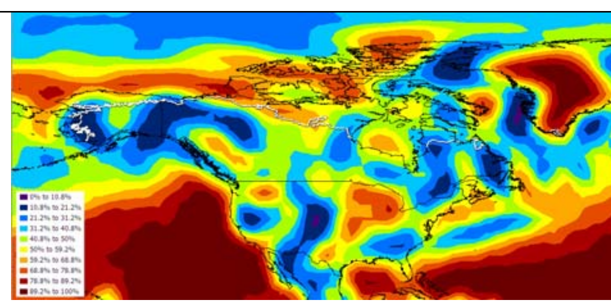

Figure C32. Probability of negative Mean July divergence at 1000mb

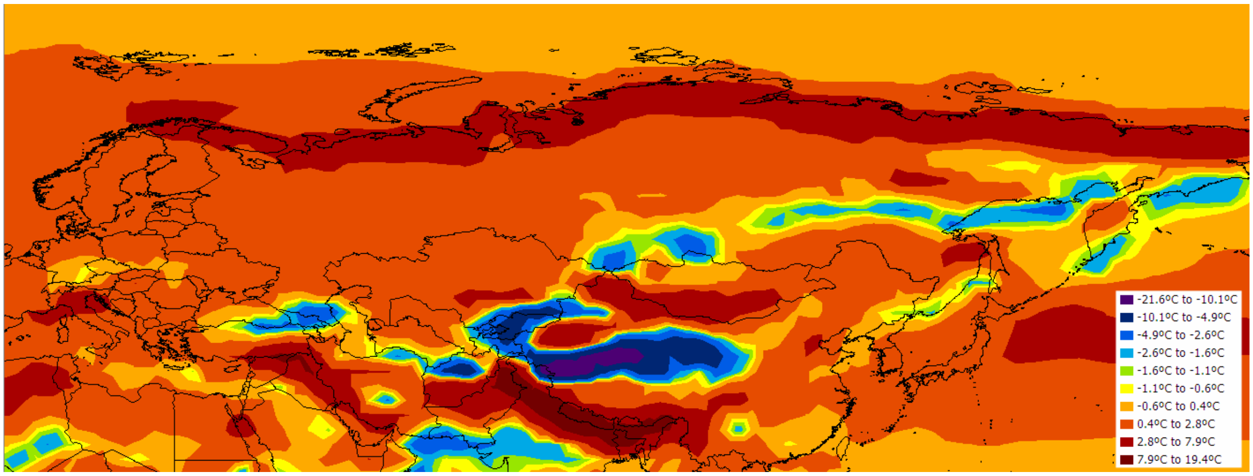

Figure C33. Mean July surface (2m) temperature change per -2.5º latitude for 1958 to 2002.

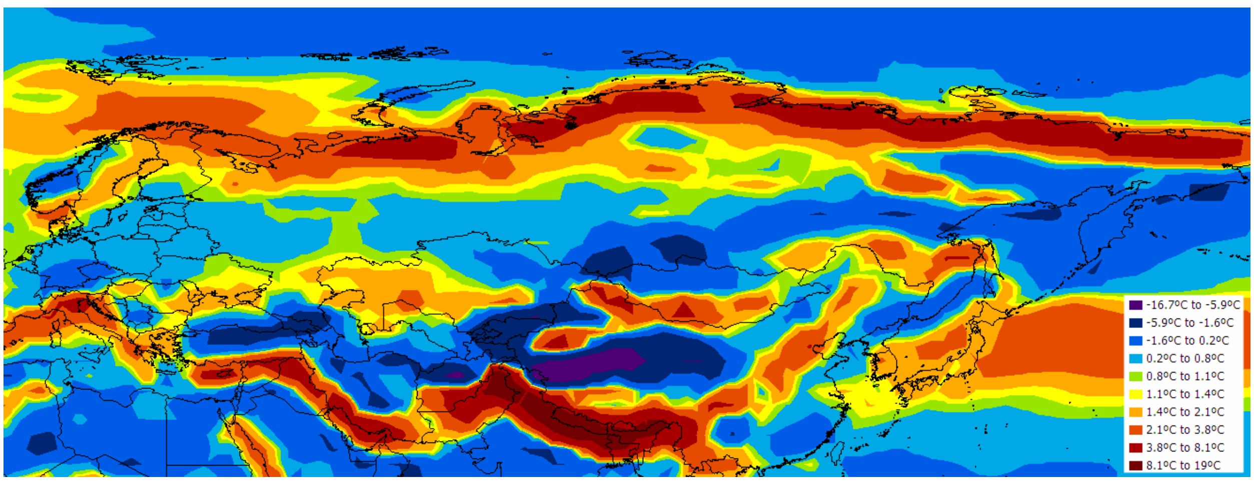

Figure C34. Mean July wet bulb temperature change per -2.5º latitude for 1958 to 2002.

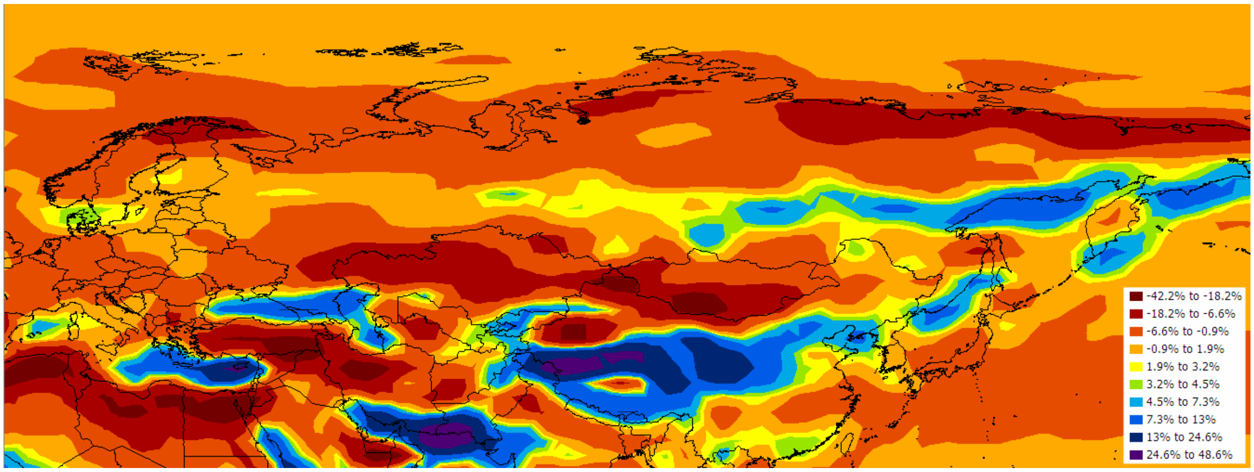

Figure C35. Mean July relative humidity change per -2.5º latitude for 1958 to 2002.

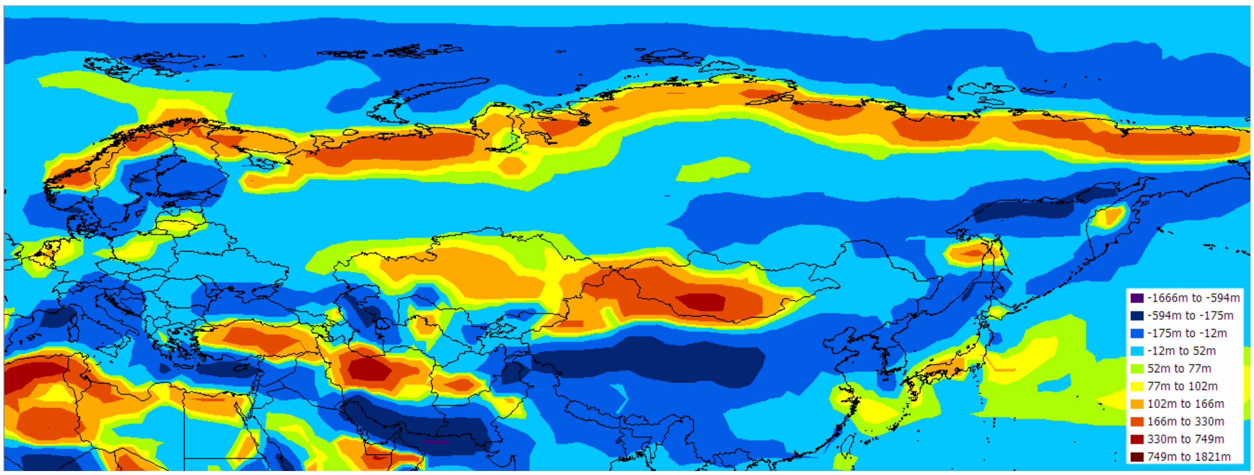

Figure C36. Mean July boundary layer height change per -2.5º latitude for 1958 to 2002.

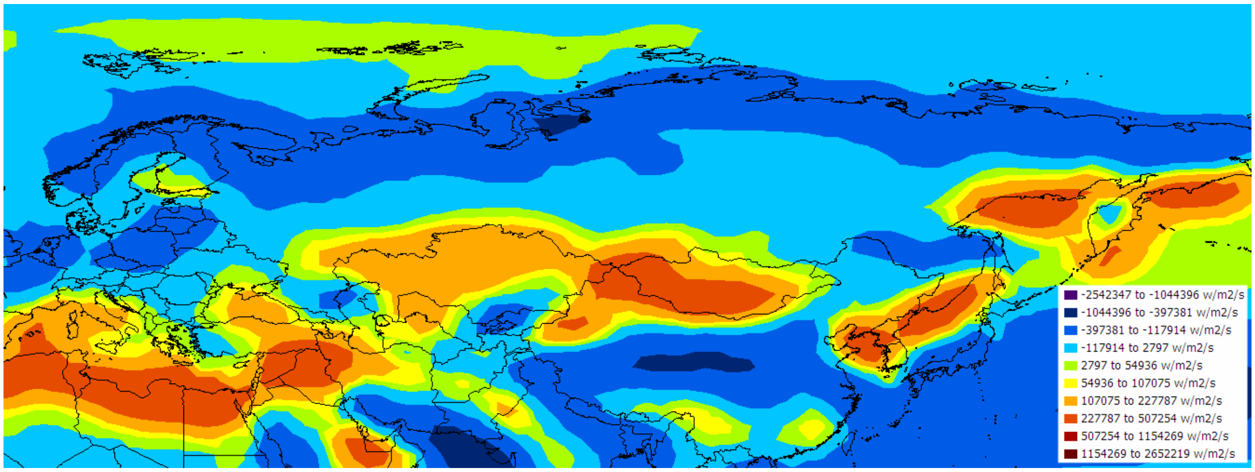

Figure C37. Mean July latent heat flux change per -2.5º latitude for 1958 to 2002.

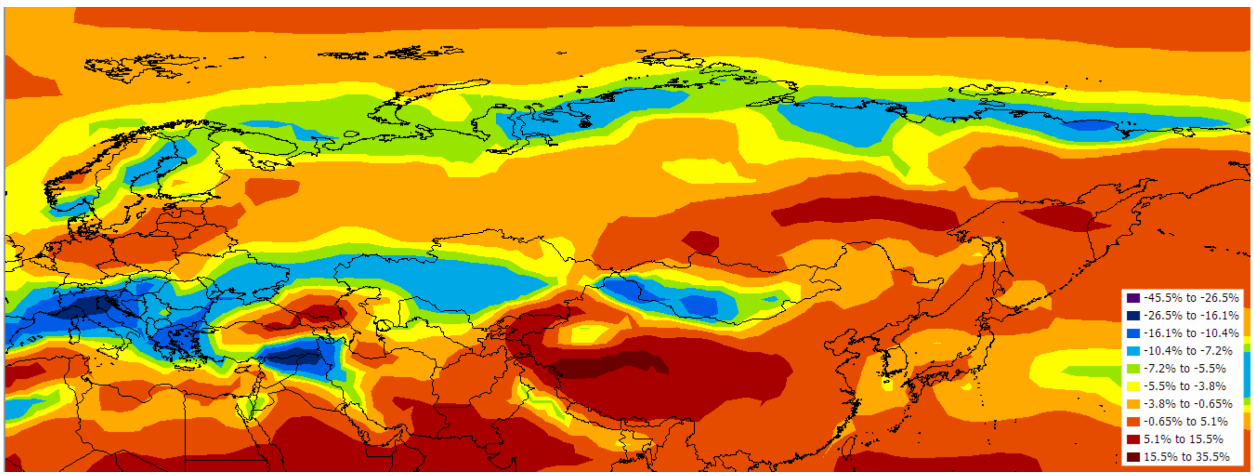

Figure C38. Mean July total cloud cover change per -2.5º latitude for 1958 to 2002.

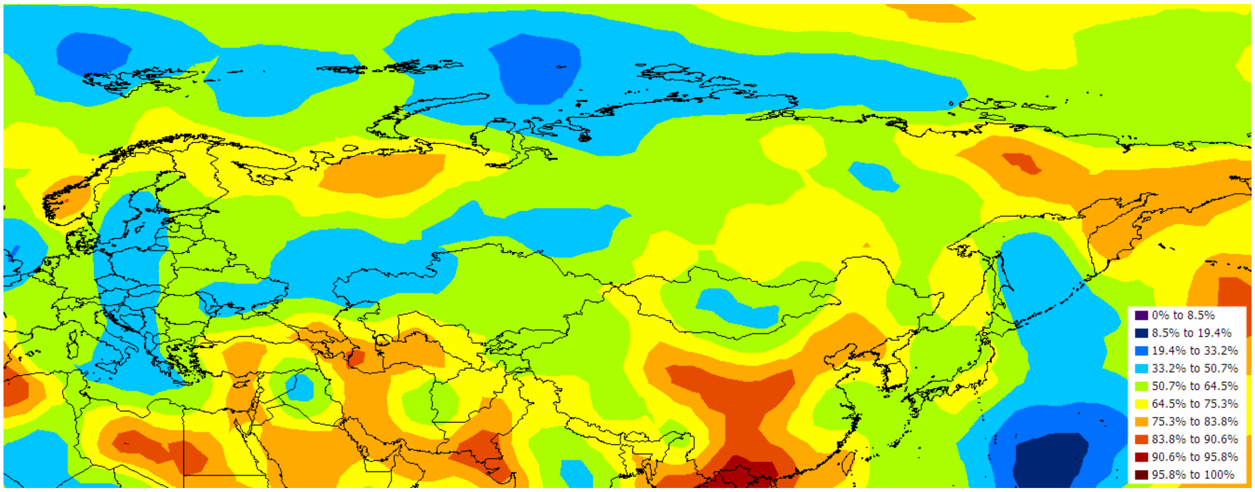

Figure C39. Probability of positive Mean July vertical velocity at 1000mb for 1958 to 2002.

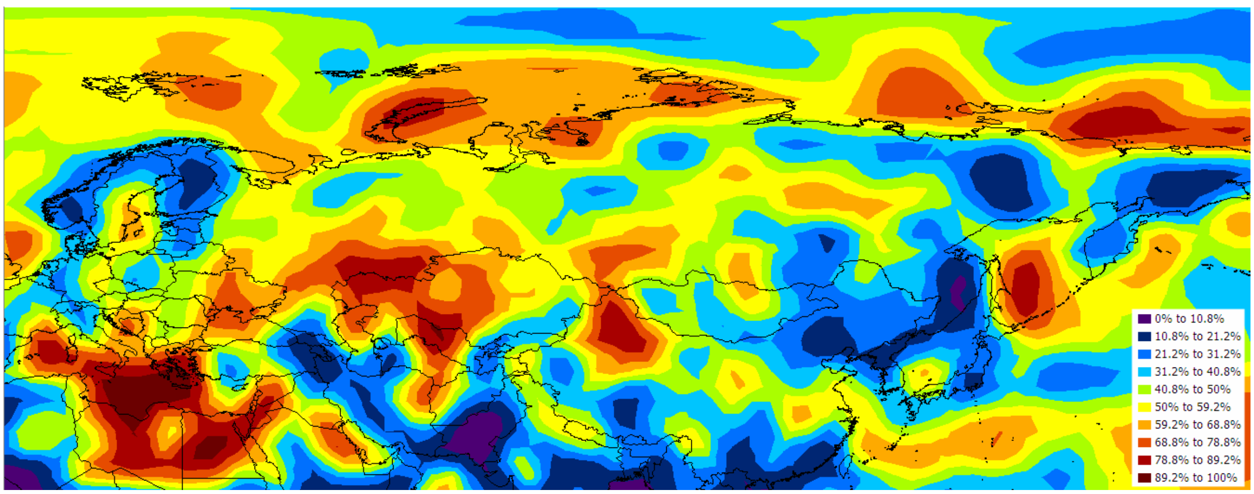

Figure C40. Probability of negative Mean July divergence at 1000mb for 1958 to 2002.

C.1.8. Mean surface streamlines for August

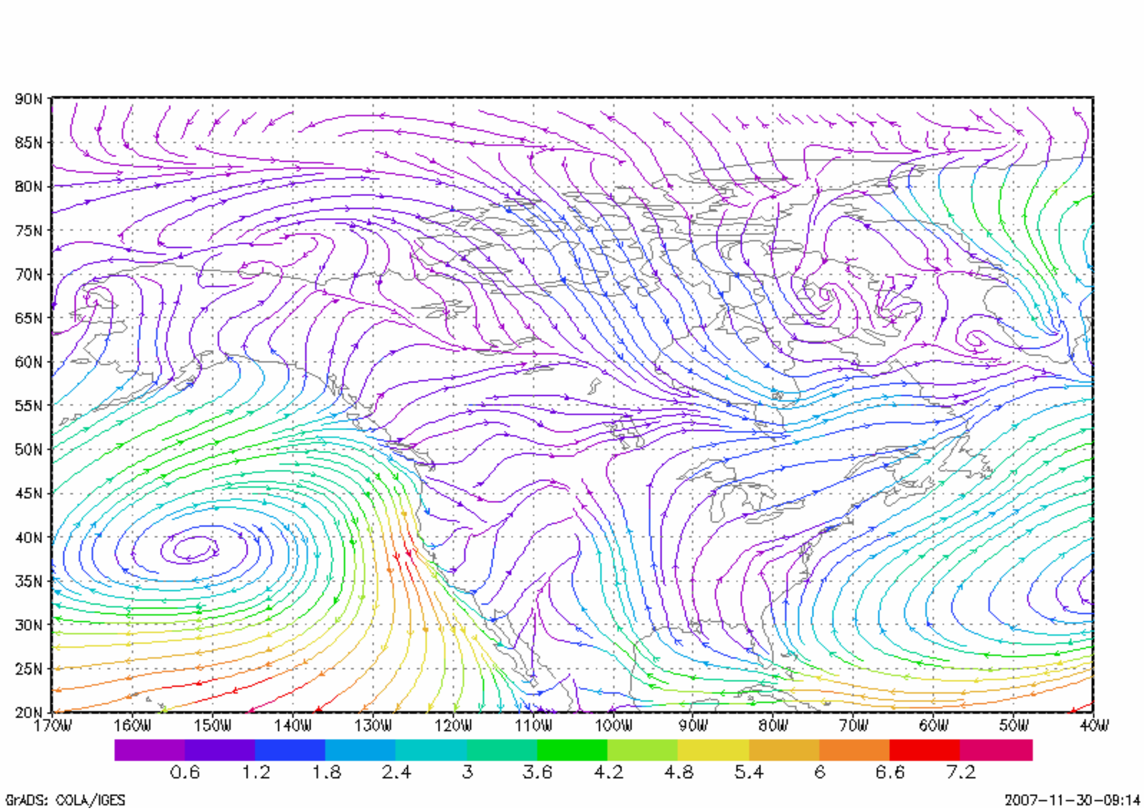

Figure C41. Mean August 10m Streamlines (in m/s) for 1958-2002 from the ERA-40 reanalysis.

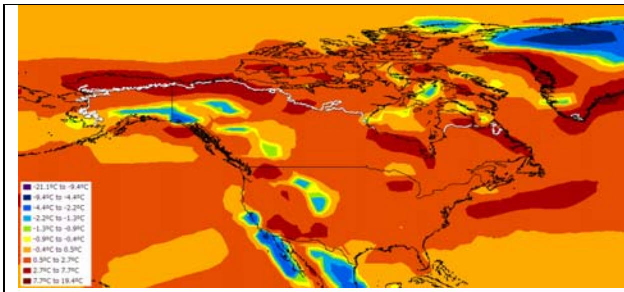

Figure C42. Mean August surface (2m) temperature change per -2.5º latitude for 1958 to 2002.

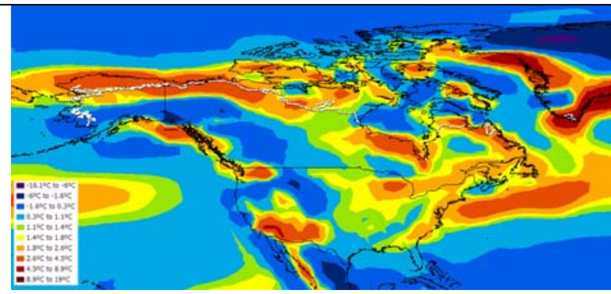

Figure C43. Mean August wet bulb temperature change per -2.5º latitude

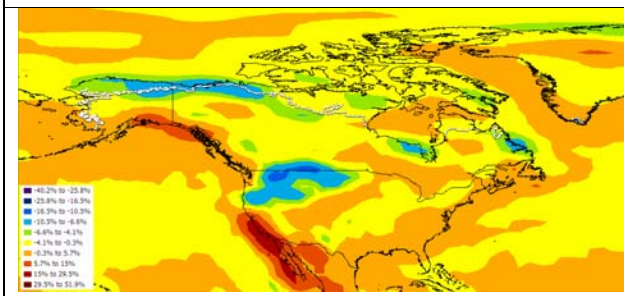

Figure C44. Mean August relative humidity change per -2.5º latitude for 1958 to 2002.

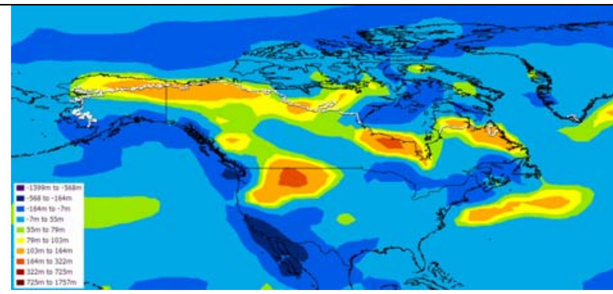

Figure C45. Mean August boundary layer height change per -2.5º latitude for 1958 to 2002.

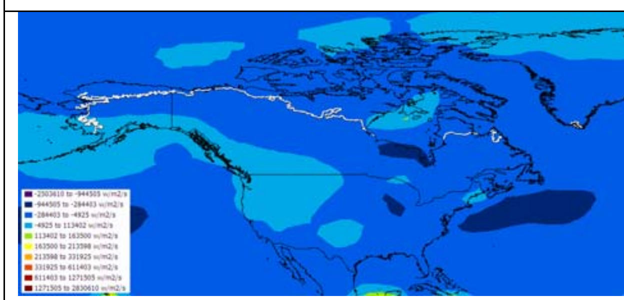

Figure C46. Mean August latent heat flux change per -2.5º latitude

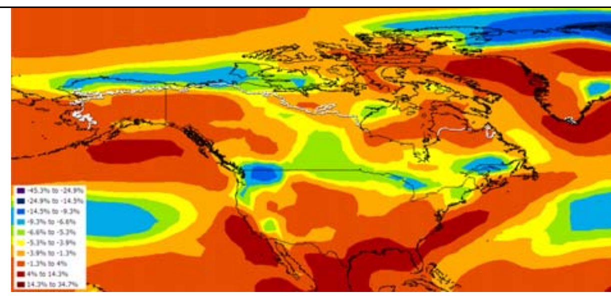

Figure C47. Mean August total cloud cover change per -2.5º latitude

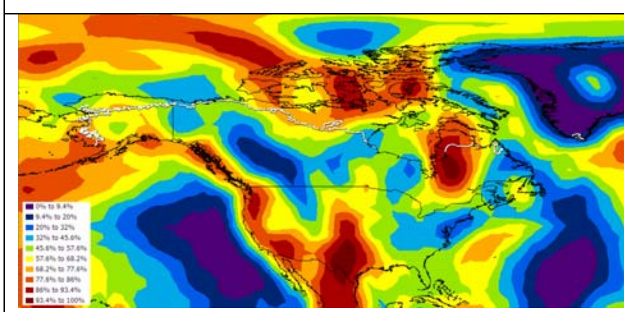

Figure C48. Probability of positive Mean August vertical velocity at 1000mb for 1958 to 2002.

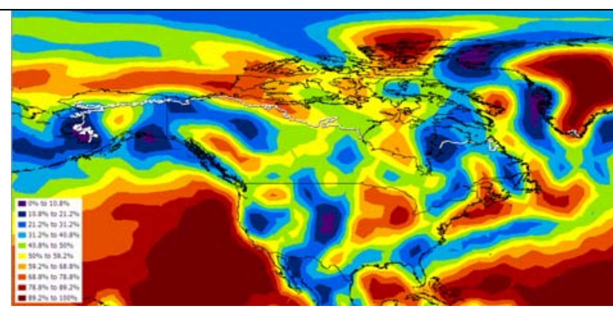

Figure C49. Probability of negative Mean August divergence at 1000mb

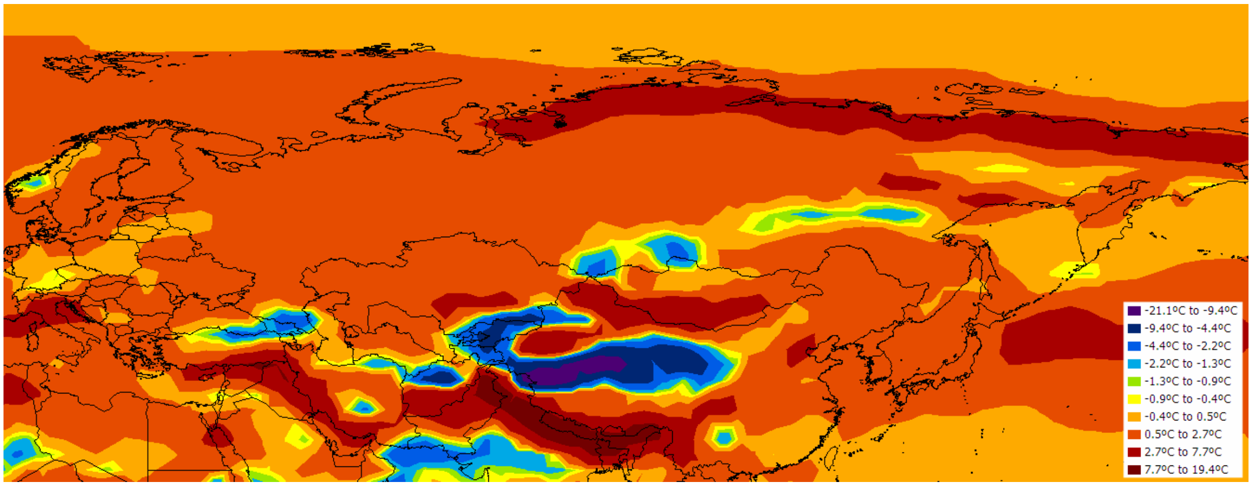

Figure C50. Mean August surface (2m) temperature change per -2.5º latitude for 1958 to 2002.

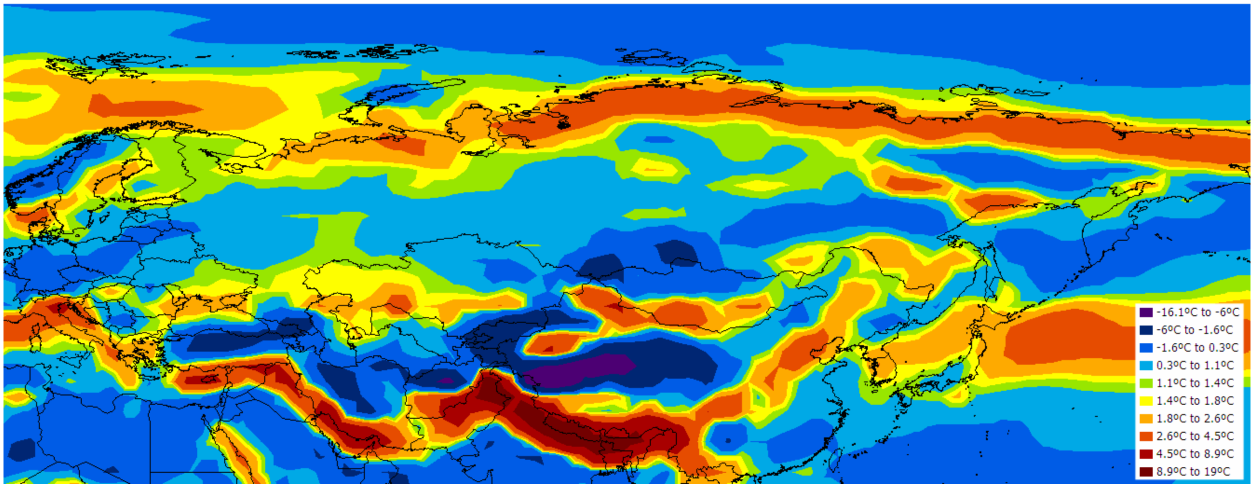

Figure C51. Mean August wet bulb temperature change per -2.5º latitude for 1958 to 2002.

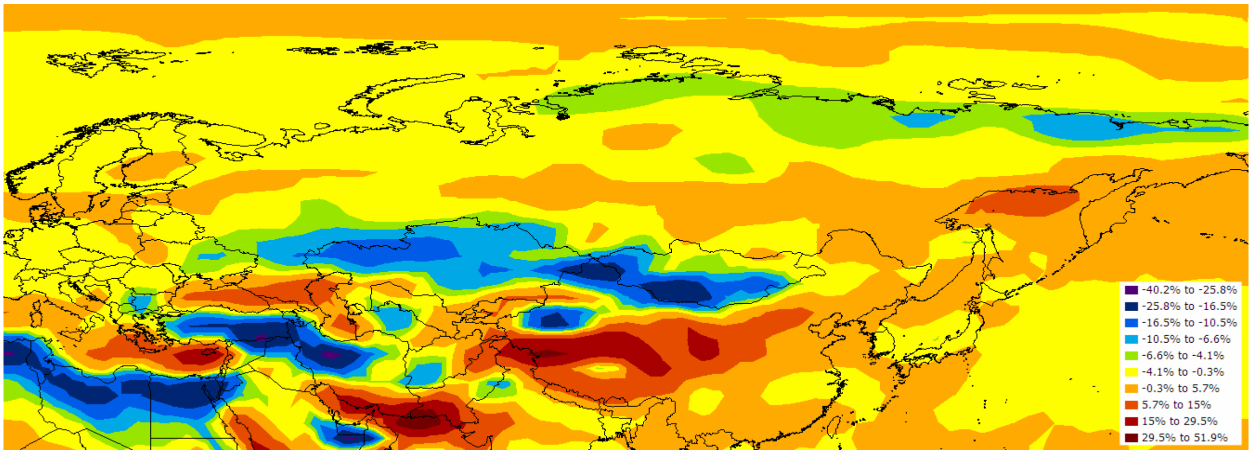

Figure C52. Mean August relative humidity change per -2.5º latitude for 1958 to 2002.

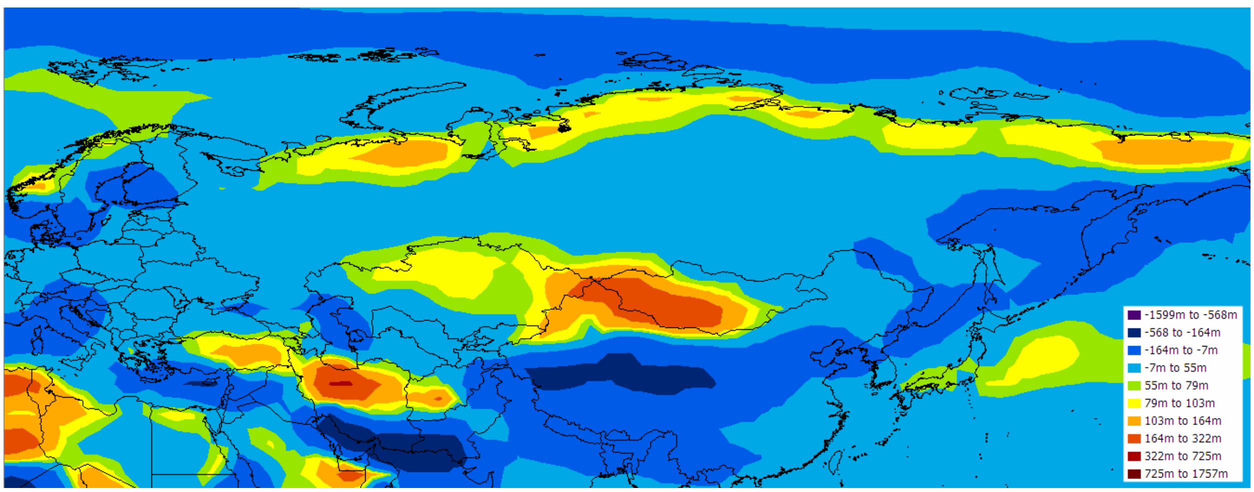

Figure C53. Mean August boundary layer height change per -2.5º latitude for 1958 to 2002.

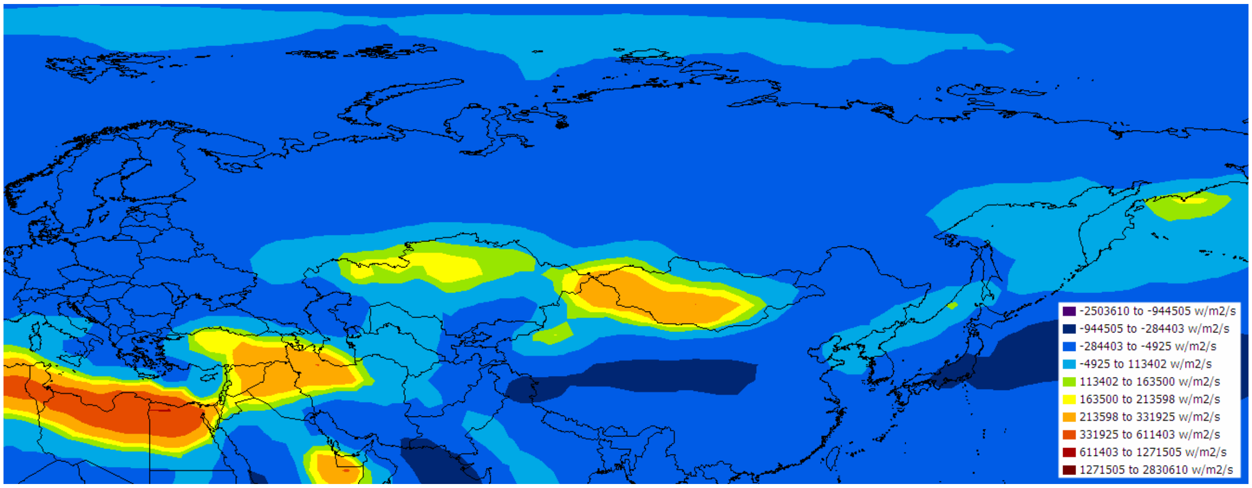

Figure C54. Mean August latent heat flux change per -2.5º latitude for 1958 to 2002.

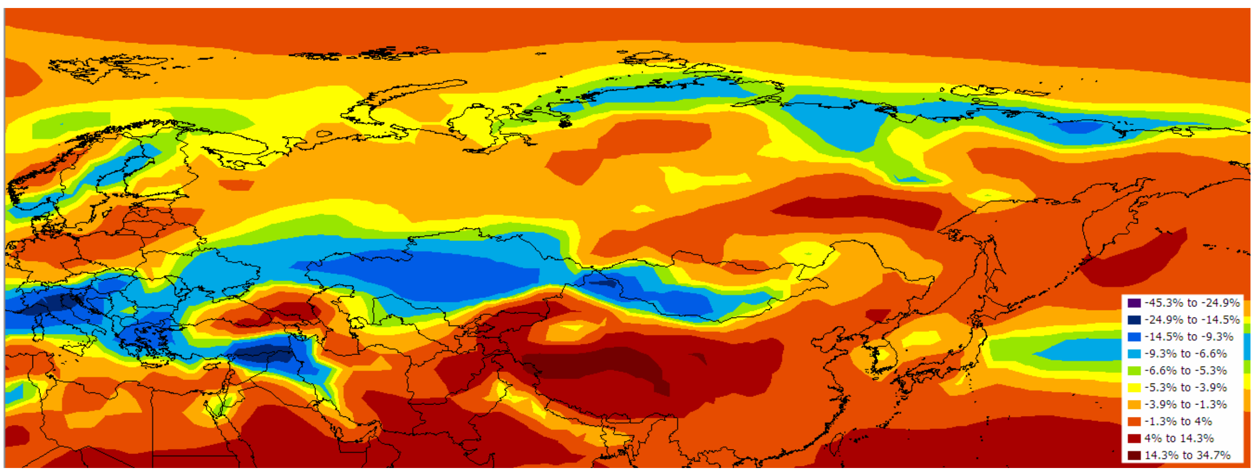

Figure C55. Mean August total cloud cover change per -2.5º latitude for 1958 to 2002.

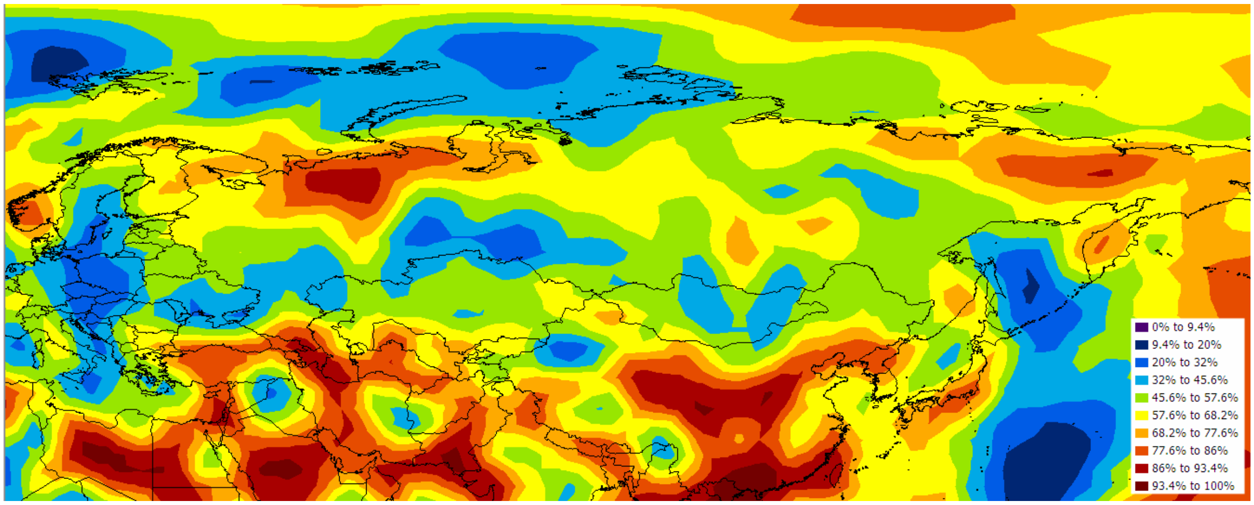

Figure C56. Probability of positive Mean August vertical velocity at 1000mb for 1958 to 2002.

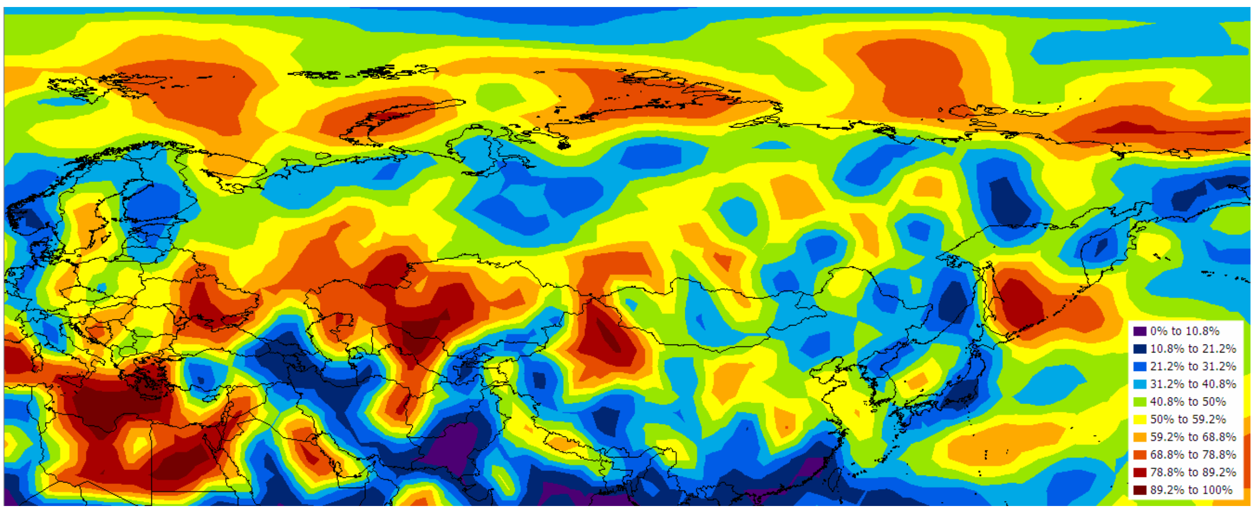

Figure C57. Probability of negative Mean August divergence at 1000mb for 1958 to 2002.

C.1.9. Mean surface streamlines for September

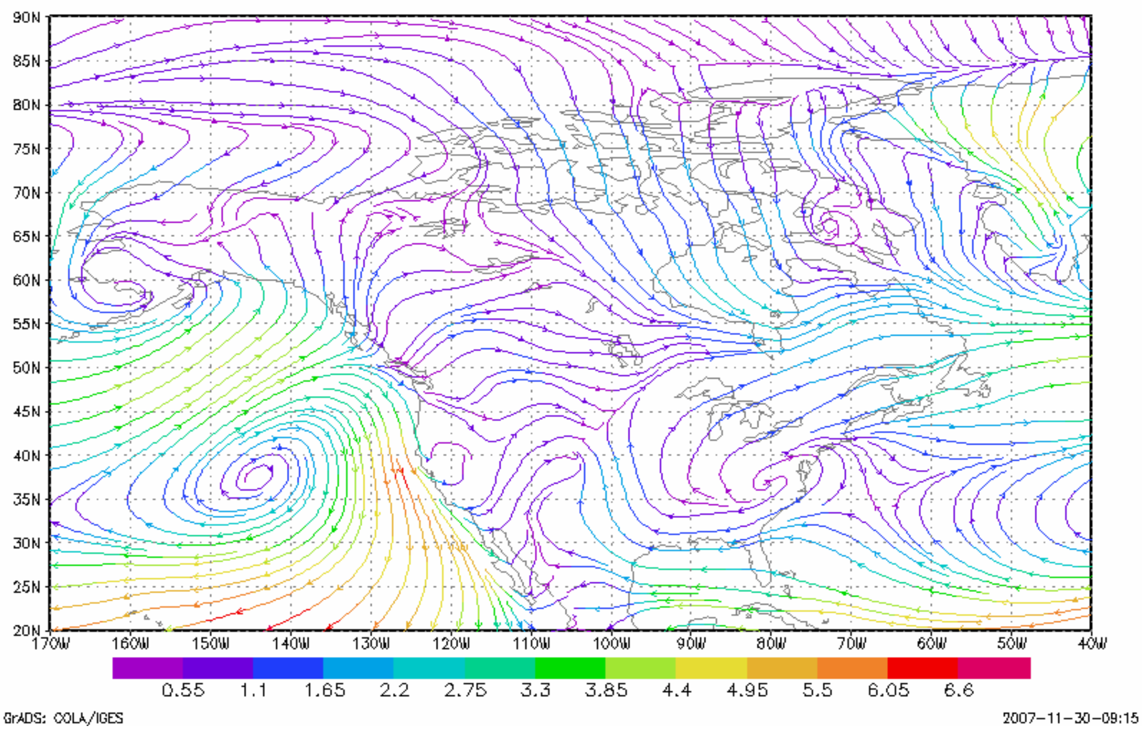

Figure C58. Mean September 10m Streamlines (in m/s) for 1958-2002 from the ERA-40 reanalysis.

C.1.10. Mean surface streamlines for October

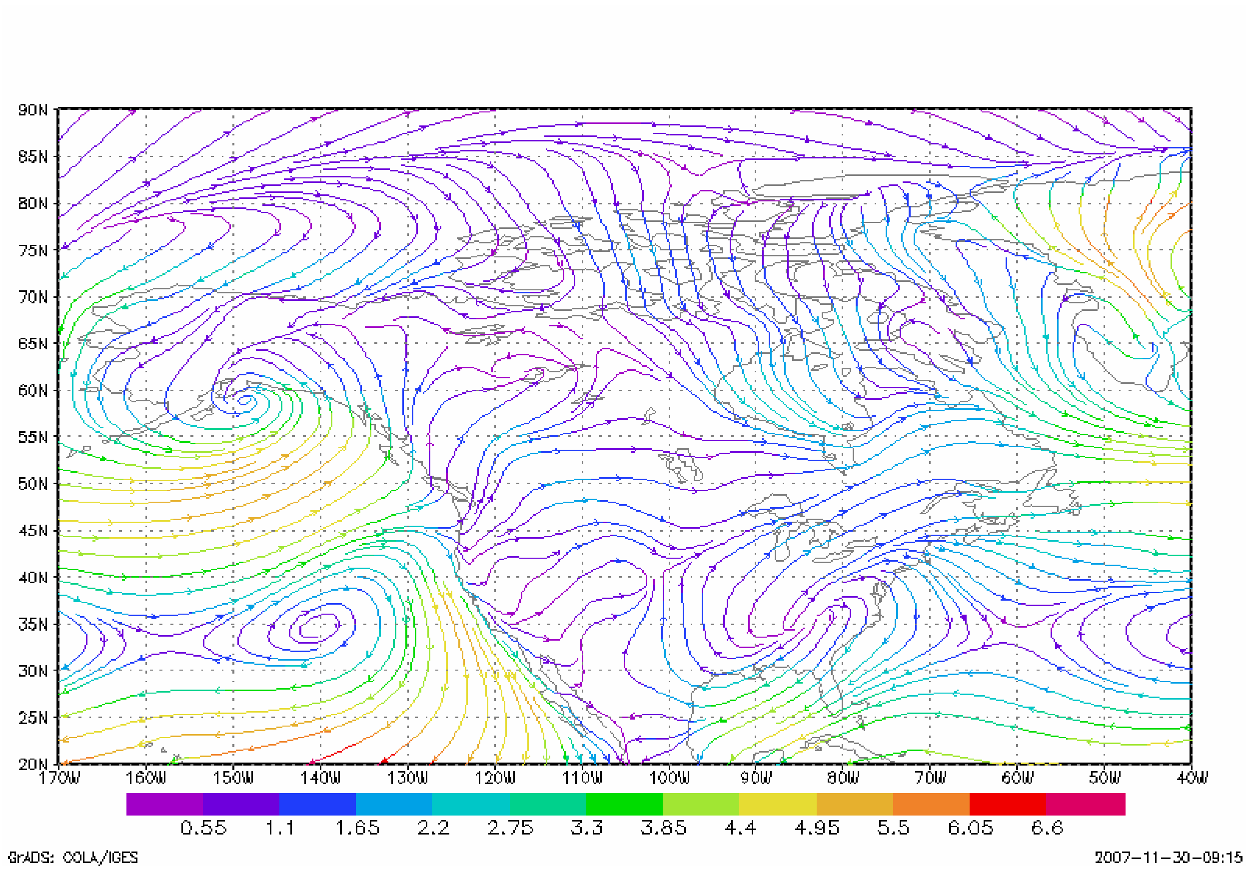

Figure C59. Mean October 10m Streamlines (in m/s) for 1958-2002 from the ERA-40 reanalysis.

C.11.1. Mean surface streamlines for November

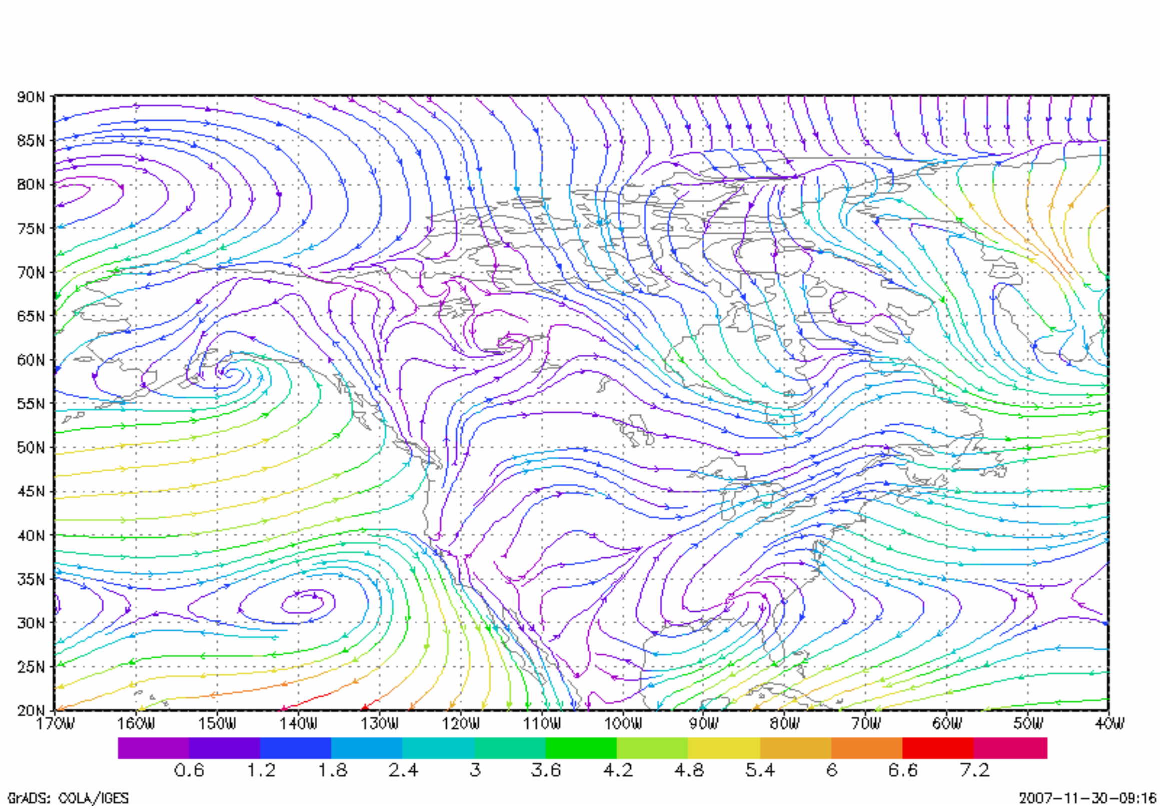

Figure C60. Mean November 10m Streamlines (in m/s) for 1958-2002 from the ERA-40 reanalysis.

C.1.12. Mean surface streamlines for December

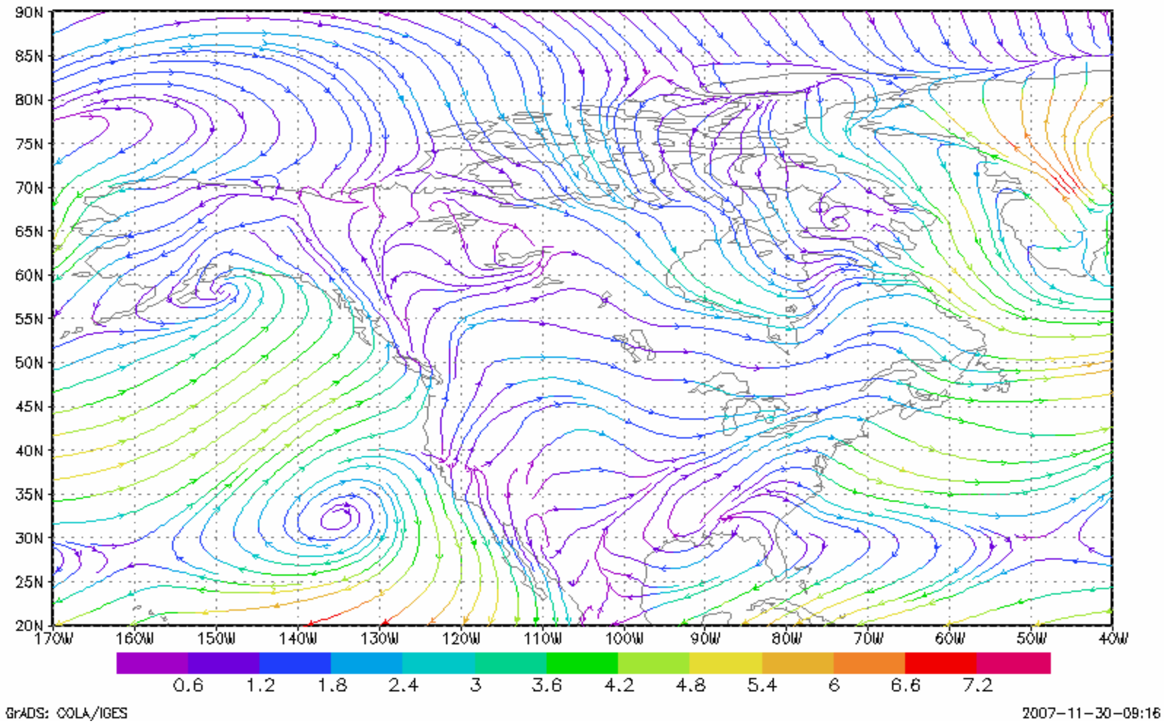

Figure C61. Mean December 10m Streamlines (in m/s) for 1958-2002 from the ERA-40 reanalysis.

Appendix D – Additional NDVI results

The following tables are the complete results for the analysis of vegetation productivity in relation to the July Arctic front position. There are results based on the front positions derived from ERA-40 (Table D1) and NNR (Table D2). The polygons are the area of interest and are drawn north (south) of the front if the front is south (north) of the mean frontal position. The polygons will only extend as far north or south as the long term mean position of the front. If a polygon is (south) north of the mean frontal position we would expect a higher frequency (greater than 50%) of (negative) positive Normalized Difference Vegetation Index (NDVI) anomalies representing (less) more productive vegetation.

Table D1. NDVI anomaly frequency distribution table (July Arctic front position derived from ERA-40).

July	Polygon (W to E)	N or S of mean	Negative	Positive	Freq Neg	Freq Pos	Result > 50%
1981	1	North	22871	29954	43.3%	56.7%	Yes
1982	1	South	234	1929	10.8%	89.2%	No
	2	North	12	46	20.7%	79.3%	Yes
	3	South	453	407	52.7%	47.3%	Yes
	4	South	110	300	26.8%	73.2%	No
	5	North	921	215	81.1%	18.9%	No
	6	South	10970	7172	60.5%	39.5%	Yes
	7	North	2398	1107	68.4%	31.6%	No
	8	South	279	476	37.0%	63.0%	No
	9	North	0	64	0.0%	100.0%	Yes
	Totals	South	12046	10284	53.9%	46.1%	Yes
		North	3331	1432	69.9%	30.1%	No
1983	1	South	8569	10156	45.8%	54.2%	No
	2	North	429	139	75.5%	24.5%	No
	3	South	3476	3543	49.5%	50.5%	No
	4	North	8472	8538	49.8%	50.2%	Yes
	5	South	228	3940	5.5%	94.5%	No
	6	North	29	104	21.8%	78.2%	Yes
	Totals	South	12273	17639	41.0%	59.0%	No
		North	8930	8781	50.4%	49.6%	No
1984	1	North	1162	723	61.6%	38.4%	No
	2	South	934	319	74.5%	25.5%	Yes
	3	North	13928	6416	68.5%	31.5%	No
	4	South	67	306	18.0%	82.0%	No
	5	North	5400	6312	46.1%	53.9%	Yes

	Totals		South	1001	625	61.6%	38.4%	Yes
			North	20490	13451	60.4%	39.6%	No
1985		1	South	5252	10809	32.7%	67.3%	No
		2	North	292	1382	17.4%	82.6%	Yes
		3	South	3933	5314	42.5%	57.5%	No
		4	North	929	964	49.1%	50.9%	Yes
	Totals		South	9185	16123	36.3%	63.7%	No
			North	1221	2346	34.2%	65.8%	Yes
1986		1	North	194	8	96.0%	4.0%	No
		2	North	250	3	98.8%	1.2%	No
		3	South	145	11	92.9%	7.1%	Yes
		4	North	383	18	95.5%	4.5%	No
		5	South	15580	9924	61.1%	38.9%	Yes
		6	North	14440	8627	62.6%	37.4%	No
		7	South	492	1307	27.3%	72.7%	No
	Totals		South	16217	11242	59.1%	40.9%	Yes
			North	15267	8656	63.8%	36.2%	No
1987		1	South	24572	40143	38.0%	62.0%	No
		2	North	99	438	18.4%	81.6%	Yes
1988		1	North	78	60	56.5%	43.5%	No
		2	South	191	362	34.5%	65.5%	No
		3	South	9617	8604	52.8%	47.2%	Yes
		4	North	9911	27952	26.2%	73.8%	Yes
	Totals		South	9808	8966	52.2%	47.8%	Yes
			North	9989	28012	26.3%	73.7%	Yes
1989		1	North	15423	54765	22.0%	78.0%	Yes
1990		1	North	6	177	3.3%	96.7%	Yes
		2	North	37	161	18.7%	81.3%	Yes
		3	South	2964	2313	56.2%	43.8%	Yes
		4	North	1585	5039	23.9%	76.1%	Yes
		5	South	1019	5178	16.4%	83.6%	No
		6	North	11009	8404	56.7%	43.3%	No
		7	South	11	153	6.7%	93.3%	No
	Totals		South	3994	7644	34.3%	65.7%	No
			North	12637	13781	47.8%	52.2%	Yes
1991		1	South	74	3674	2.0%	98.0%	No
		2	South	5611	7964	41.3%	58.7%	No
		3	North	6706	28125	19.3%	80.7%	Yes

		4	South	1988	235	89.4%	10.6%	Yes
	Totals		South	7673	11873	39.3%	60.7%	No
			North	6706	28125	19.3%	80.7%	Yes
1992		1	South	3835	12558	23.4%	76.6%	No
		2	North	322	2682	10.7%	89.3%	Yes
		3	South	20117	10024	66.7%	33.3%	Yes
		4	North	5068	160	96.9%	3.1%	No
		5	South	2441	23	99.1%	0.9%	Yes
	Totals		South	26393	22605	53.9%	46.1%	Yes
			North	5390	2842	65.5%	34.5%	No
1993		1	South	41313	15425	72.8%	27.2%	Yes
		2	North	7947	13647	36.8%	63.2%	Yes
1994		1	North	3190	776	80.4%	19.6%	No
		2	South	21489	11172	65.8%	34.2%	Yes
		3	North	5463	1811	75.1%	24.9%	No
	Totals		South	21489	11172	65.8%	34.2%	Yes
			North	8653	2587	77.0%	23.0%	No
1995		1	South	874	553	61.2%	38.8%	Yes
		2	South	22624	12292	64.8%	35.2%	Yes
		3	North	7344	10877	40.3%	59.7%	Yes
	Totals		South	23498	12845	64.7%	35.3%	Yes
			North	7344	10877	40.3%	59.7%	Yes
1996		1	North	1455	1406	50.9%	49.1%	No
		2	South	1855	1756	51.4%	48.6%	Yes
		3	North	2194	1341	62.1%	37.9%	No
		4	South	11270	30050	27.3%	72.7%	No
		5	North	145	166	46.6%	53.4%	Yes
	Totals		South	13125	31806	29.2%	70.8%	No
			North	3794	2913	56.6%	43.4%	No
1997		1	South	7952	10816	42.4%	57.6%	No
		2	North	15998	47063	25.4%	74.6%	Yes
		3	North	1806	4007	31.1%	68.9%	Yes
	Totals		South	7952	10816	42.4%	57.6%	No
			North	17804	51070	25.9%	74.1%	Yes
1998		1	South	2554	4826	34.6%	65.4%	No
		2	South	101	169	37.4%	62.6%	No
		3	North	4326	1133	79.2%	20.8%	No

		4	South	9869	7603	56.5%	43.5%	Yes
		5	North	1227	1493	45.1%	54.9%	Yes
	Totals		South	12524	12598	49.9%	50.1%	No
			North	5553	2626	67.9%	32.1%	No
1999		1	South	92	1939	4.5%	95.5%	No
		2	South	1055	3030	25.8%	74.2%	No
		3	South	15094	9552	61.2%	38.8%	Yes
		4	South	159	64	71.3%	28.7%	Yes
		5	North	1233	1626	43.1%	56.9%	Yes
	Totals		South	16400	14585	52.9%	47.1%	Yes
			North	1233	1626	43.1%	56.9%	Yes
2000		1	South	29	263	9.9%	90.1%	No
		2	North	91	1474	5.8%	94.2%	Yes
		3	South	751	1499	33.4%	66.6%	No
		4	North	16205	19019	46.0%	54.0%	Yes
		5	South	5120	2785	64.8%	35.2%	Yes
		6	North	131	720	15.4%	84.6%	Yes
	Totals		South	5900	4547	56.5%	43.5%	Yes
			North	16427	21213	43.6%	56.4%	Yes
2001		1	South	112	963	10.4%	89.6%	No
		2	North	35	73	32.4%	67.6%	Yes
		3	South	363	1193	23.3%	76.7%	No
		4	North	355	275	56.3%	43.7%	No
		5	South	665	17	97.5%	2.5%	Yes
		6	North	16837	18936	47.1%	52.9%	Yes
		7	South	3754	1114	77.1%	22.9%	Yes
	Totals		South	4894	3287	59.8%	40.2%	Yes
			North	17227	19284	47.2%	52.8%	Yes
2002		1	South	45	434	9.4%	90.6%	No
		2	North	21	1577	1.3%	98.7%	Yes
		3	South	9	215	4.0%	96.0%	No
		4	North	751	1498	33.4%	66.6%	Yes
		5	South	3444	2424	58.7%	41.3%	Yes
		6	North	9603	12301	43.8%	56.2%	Yes
	Totals		South	3498	3073	53.2%	46.8%	Yes
			North	10375	15376	40.3%	59.7%	Yes
All years	Grand Totals		South	249183	227155	52.3%	47.7%	Yes
			North	218612	333364	39.6%	60.4%	Yes

Table D2. NDVI anomaly frequency distribution table (July Arctic front position derived from NNR).

July	Polygon (W to E)	N or S of mean	Negative	Positive	Freq Neg	Freq Pos	Result > 50%
1981	1	N	26220	27239	49.0%	51.0%	Y
	2	N	4744	7815	37.8%	62.2%	Y
	3	N	729	1467	33.2%	66.8%	Y
	4	N	424	308	57.9%	42.1%	N
	Totals	N	32117	36829	46.6%	53.4%	Y
1982	1	N	7064	9604	42.4%	57.6%	Y
	2	S	9558	4849	66.3%	33.7%	Y
	3	S	4046	3148	56.2%	43.8%	Y
	Totals	S	13604	7997	63.0%	37.0%	Y
1983	1	S	2864	3098	48.0%	52.0%	N
	2	N	675	594	53.2%	46.8%	N
	3	S	2913	1203	70.8%	29.2%	Y
	4	N	4855	655	88.1%	11.9%	N
	5	S	2811	6243	31.0%	69.0%	N
	6	N	50	162	23.6%	76.4%	Y
	Totals	N	5580	1411	79.8%	20.2%	N
		S	8588	10544	44.9%	55.1%	N
1984	1	N	4542	1947	70.0%	30.0%	N
	2	N	11166	5179	68.3%	31.7%	N
	3	S	2398	3499	40.7%	59.3%	N
	4	N	1510	2613	36.6%	63.4%	Y
	Totals	N	17218	9739	63.9%	36.1%	N
1985	1	N	2964	1685	63.8%	36.2%	N
	2	S	463	991	31.8%	68.2%	N
	3	N	2294	914	71.5%	28.5%	N
	4	N	2484	2481	50.0%	50.0%	N
	Totals	N	7742	5080	60.4%	39.6%	N
1986	1	N	12667	2057	86.0%	14.0%	N
	2	S	13066	12376	51.4%	48.6%	Y
	3	N	1678	548	75.4%	24.6%	N
	4	S	559	1733	24.4%	75.6%	N

	Totals		N	14345	2605	84.6%	15.4%	N
			S	13625	14109	49.1%	50.9%	N
1987		1	S	2009	8183	19.7%	80.3%	N
		2	S	23667	29975	44.1%	55.9%	N
		3	S	4484	5959	42.9%	57.1%	N
	Totals		S	30160	44117	40.6%	59.4%	N
1988		1	N	2751	4397	38.5%	61.5%	Y
		2	S	2932	6601	30.8%	69.2%	N
		3	N	1571	3501	31.0%	69.0%	Y
		4	N	2528	3942	39.1%	60.9%	Y
	Totals		N	6850	11840	36.7%	63.3%	Y
1989		1	N	10036	20747	32.6%	67.4%	Y
		2	N	3865	6618	36.9%	63.1%	Y
	Totals		N	13901	27365	33.7%	66.3%	Y
1990		1	N	8758	17647	33.2%	66.8%	Y
		2	S	580	1831	24.1%	75.9%	N
		3	N	1039	435	70.5%	29.5%	N
	Totals		N	9797	18082	35.1%	64.9%	Y
1991		1	N	713	4348	14.1%	85.9%	Y
		2	S	1720	5378	24.2%	75.8%	N
		3	N	1534	11842	11.5%	88.5%	Y
		4	N	3347	3598	48.2%	51.8%	Y
		5	S	2941	925	76.1%	23.9%	Y
	Totals		N	5594	19788	22.0%	78.0%	Y
			S	4661	6303	42.5%	57.5%	N
1992		1	S	2982	8028	27.1%	72.9%	N
		2	N	223	2734	7.5%	92.5%	Y
		3	S	24231	13739	63.8%	36.2%	Y
		4	S	16740	770	95.6%	4.4%	Y
	Totals		S	43953	22537	66.1%	33.9%	Y
1993		1	N	704	552	56.1%	43.9%	N
		2	S	50577	11798	81.1%	18.9%	Y
		3	N	3762	2339	61.7%	38.3%	N
	Totals		N	4466	2891	60.7%	39.3%	N
1994		1	N	2411	582	80.6%	19.4%	N

		2	S	32230	13226	70.9%	29.1%	Y
		3	N	1719	385	81.7%	18.3%	N
		4	S	468	759	38.1%	61.9%	N
	Totals		N	4130	967	81.0%	19.0%	N
			S	32698	13985	70.0%	30.0%	Y
1995		1	N	3665	2511	59.3%	40.7%	N
		2	S	23957	8553	73.7%	26.3%	Y
		3	N	326	504	39.3%	60.7%	Y
	Totals		N	3991	3015	57.0%	43.0%	N
1996		1	N	1076	990	52.1%	47.9%	N
		2	S	343	208	62.3%	37.7%	Y
		3	S	12324	55318	18.2%	81.8%	N
	Totals		S	12667	55526	18.6%	81.4%	N
1997		1	N	1021	982	51.0%	49.0%	N
		2	S	4147	7226	36.5%	63.5%	N
		3	N	5089	11554	30.6%	69.4%	Y
		4	S	7958	13458	37.2%	62.8%	N
	Totals		N	6110	12536	32.8%	67.2%	Y
			S	12105	20684	36.9%	63.1%	N
1998		1	S	1400	1577	47.0%	53.0%	N
		2	N	10230	4489	69.5%	30.5%	N
		3	S	11366	14037	44.7%	55.3%	N
	Totals		S	12766	15614	45.0%	55.0%	N
1999		1	N	1776	5696	23.8%	76.2%	Y
		2	S	22354	10202	68.7%	31.3%	Y
		3	N	566	510	52.6%	47.4%	N
	Totals		N	2342	6206	27.4%	72.6%	Y
2000		1	N	8358	8609	49.3%	50.7%	Y
		2	S	11225	13317	45.7%	54.3%	N
2001		1	N	15209	16545	47.9%	52.1%	Y
		2	S	2077	409	83.5%	16.5%	Y
		3	S	8725	3078	73.9%	26.1%	Y
	Totals		S	10802	3487	75.6%	24.4%	Y
2002	N/A		N/A	N/A	N/A	N/A	N/A	N/A

2003	1	N	814	1096	42.6%	57.4%	Y
	2	S	18450	8172	69.3%	30.7%	Y

July	Polygon (W to E)	N or S of mean	Negative	Positive	Freq Neg	Freq Pos	Result > 50%
All years	Grand Totals	North	177157	202421	46.7%	53.3%	Y
		South	328565	279867	54.0%	46.0%	Y

D1. NDVI Anomaly maps with July Arctic front 1981-2001 (derived from NNR) and long term mean July Arctic front. No front was identified for July 2002.

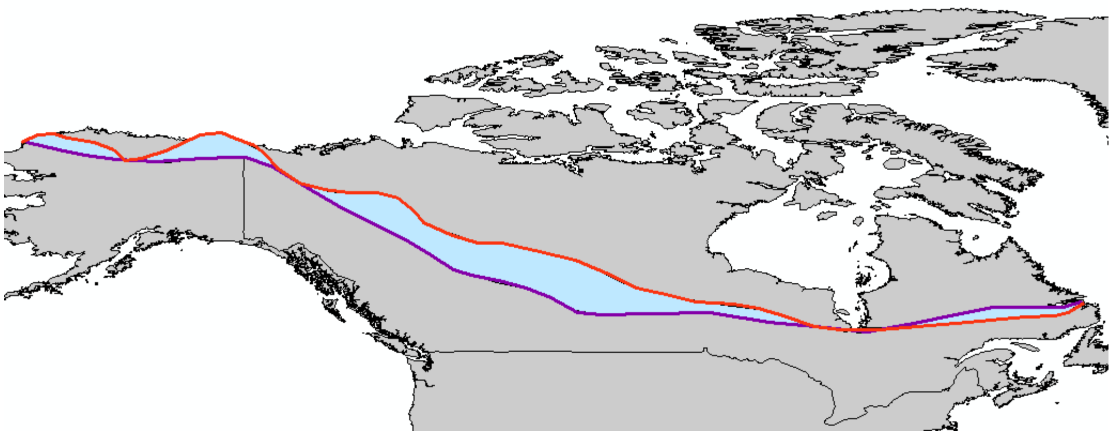

Figure D1. Polygons representing the areas of analysis for vegetation productivity anomalies for July 1999. Mean July Arctic front for 1958 to 2002 (derived from ERA-40) is in red and July Arctic front for 1999 is in purple.

Figure D2. NDVI vegetation anomaly map for July 1981 with front position (purple line) and long term mean position (red line). Anomalies are dark green representing the largest positive anomalies (most productive) to brown representing the largest negative anomalies (least productive). White areas represent an anomaly of zero.

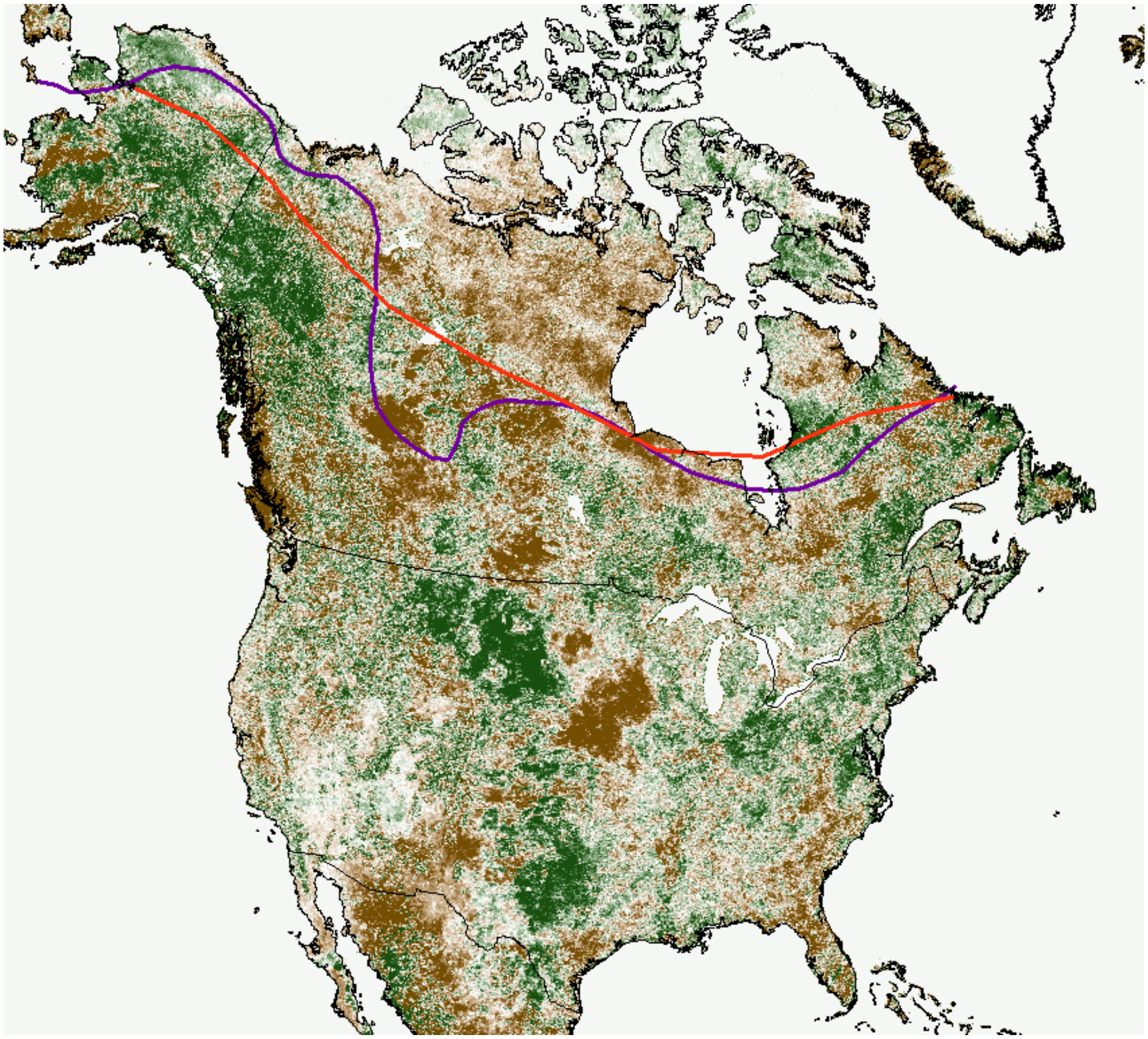

Figure D3. NDVI vegetation anomaly map for July 1982 with front position (purple line) and long term mean position (red line). Anomalies are dark green representing the largest positive anomalies (most productive) to brown representing the largest negative anomalies (least productive). White areas represent an anomaly of zero.

Figure D4. NDVI vegetation anomaly map for July 1983 with front position (purple line) and long term mean position (red line). Anomalies are dark green representing the largest positive anomalies (most productive) to brown representing the largest negative anomalies (least productive). White areas represent an anomaly of zero.

Figure D5. NDVI vegetation anomaly map for July 1984 with front position (purple line) and long term mean position (red line). Anomalies are dark green representing the largest positive anomalies (most productive) to brown representing the largest negative anomalies (least productive). White areas represent an anomaly of zero.

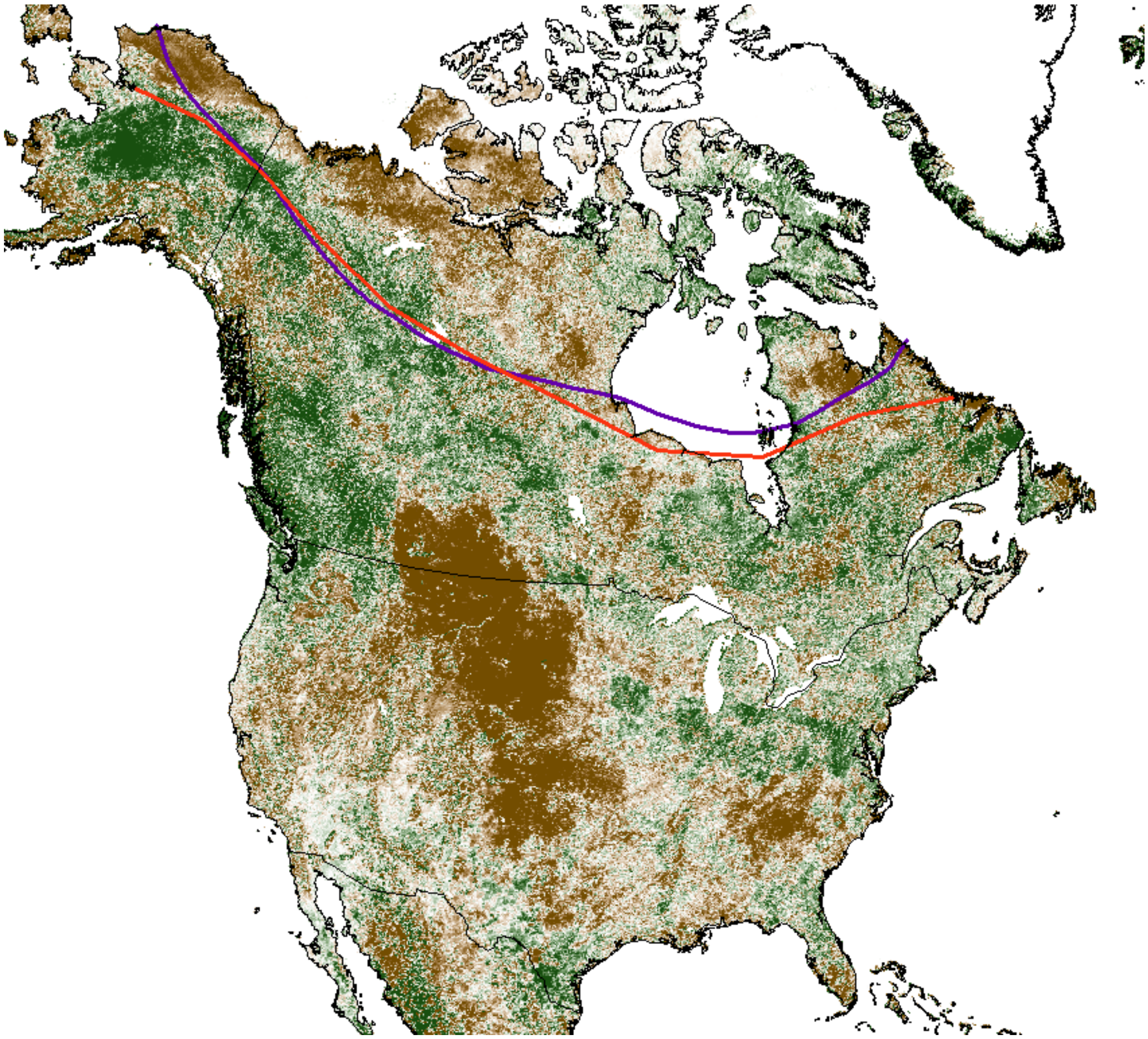

Figure D6. NDVI vegetation anomaly map for July 1985 with front position (purple line) and long term mean position (red line). Anomalies are dark green representing the largest positive anomalies (most productive) to brown representing the largest negative anomalies (least productive). White areas represent an anomaly of zero.

Figure D7. NDVI vegetation anomaly map for July 1986 with front position (purple line) and long term mean position (red line). Anomalies are dark green representing the largest positive anomalies (most productive) to brown representing the largest negative anomalies (least productive). White areas represent an anomaly of zero.

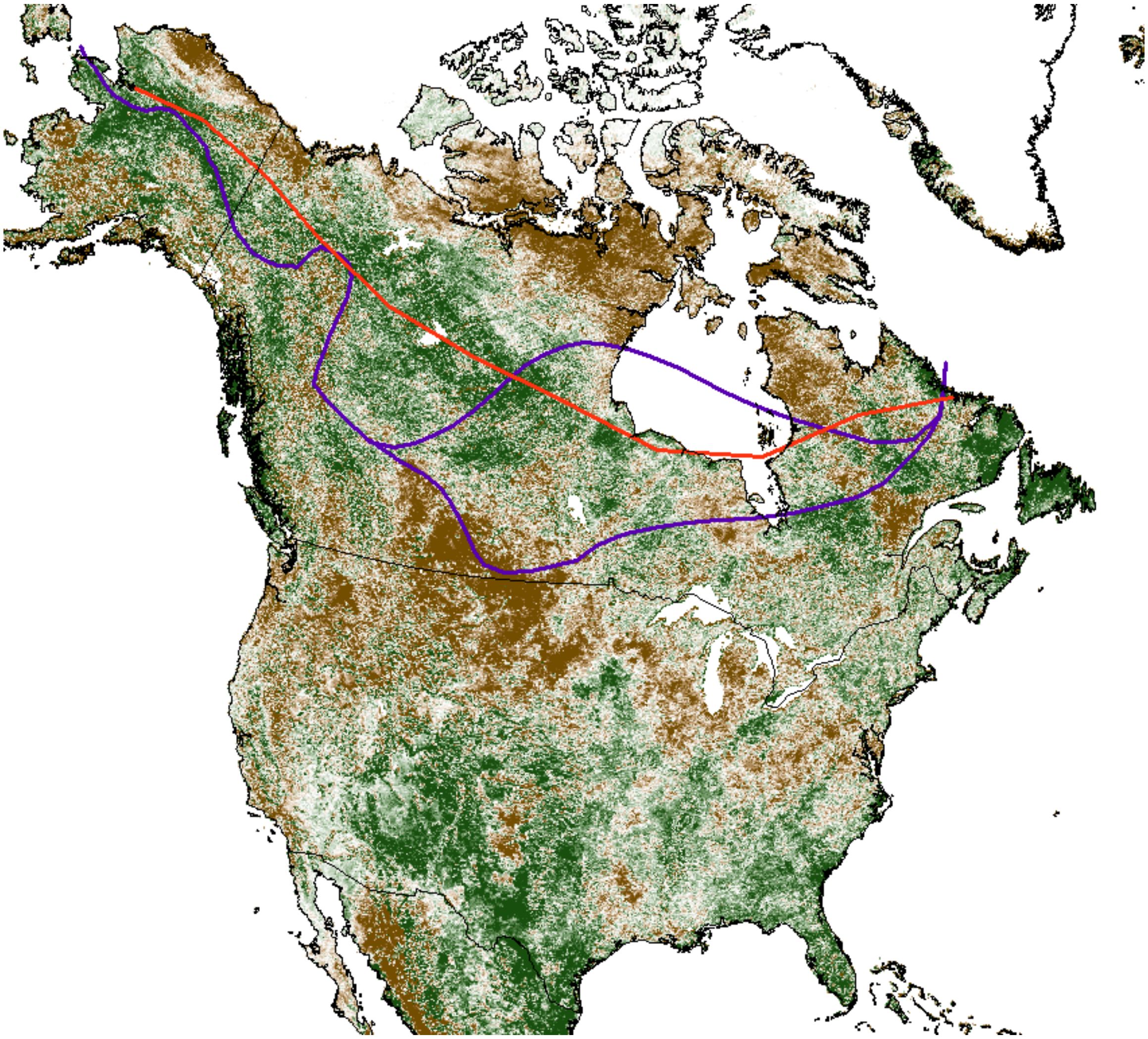

Figure D8. NDVI vegetation anomaly map for July 1987 with front position (purple line) and long term mean position (red line). Anomalies are dark green representing the largest positive anomalies (most productive) to brown representing the largest negative anomalies (least productive). White areas represent an anomaly of zero.

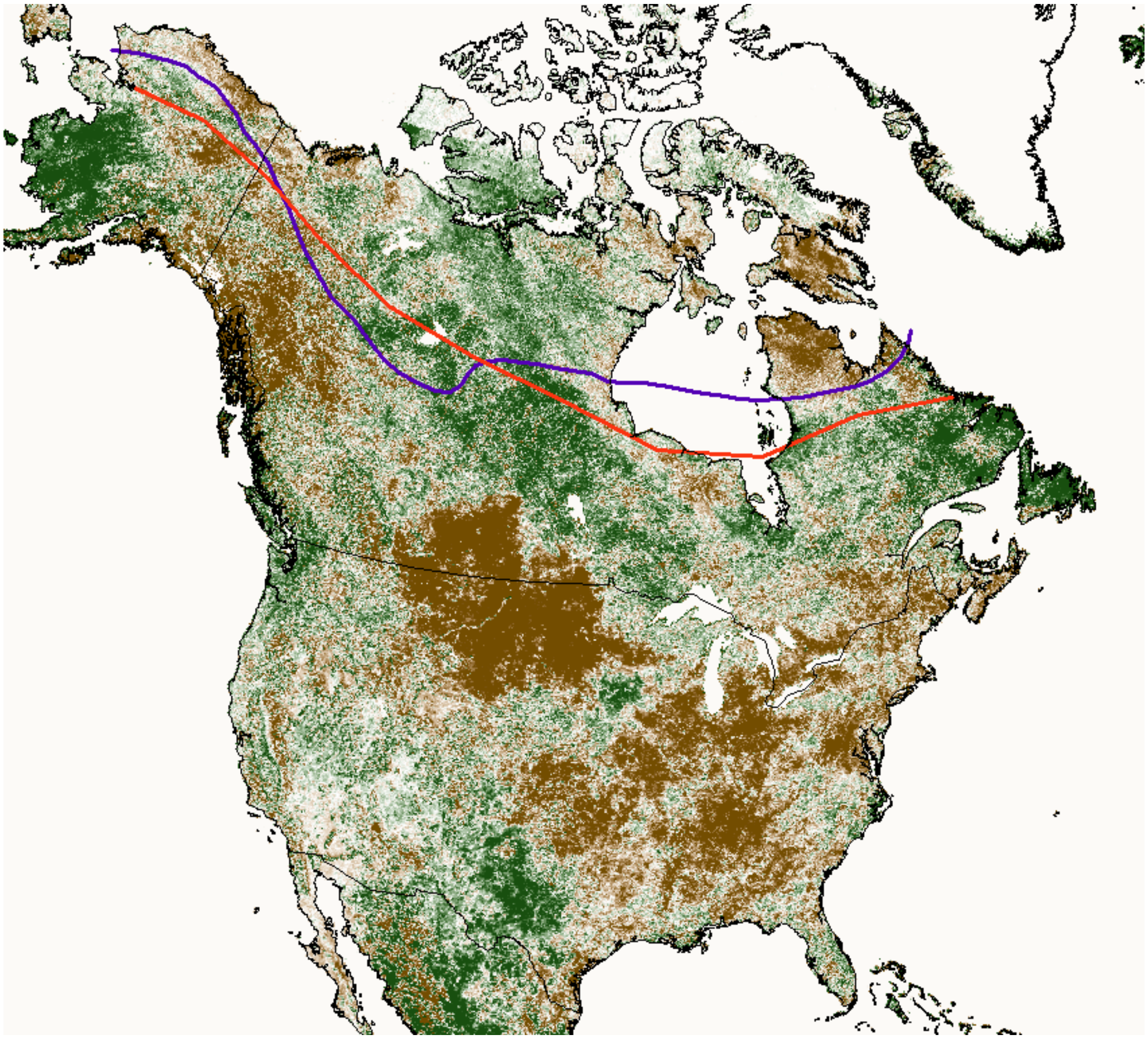

Figure D9. NDVI vegetation anomaly map for July 1988 with front position (purple line) and long term mean position (red line). Anomalies are dark green representing the largest positive anomalies (most productive) to brown representing the largest negative anomalies (least productive). White areas represent an anomaly of zero.

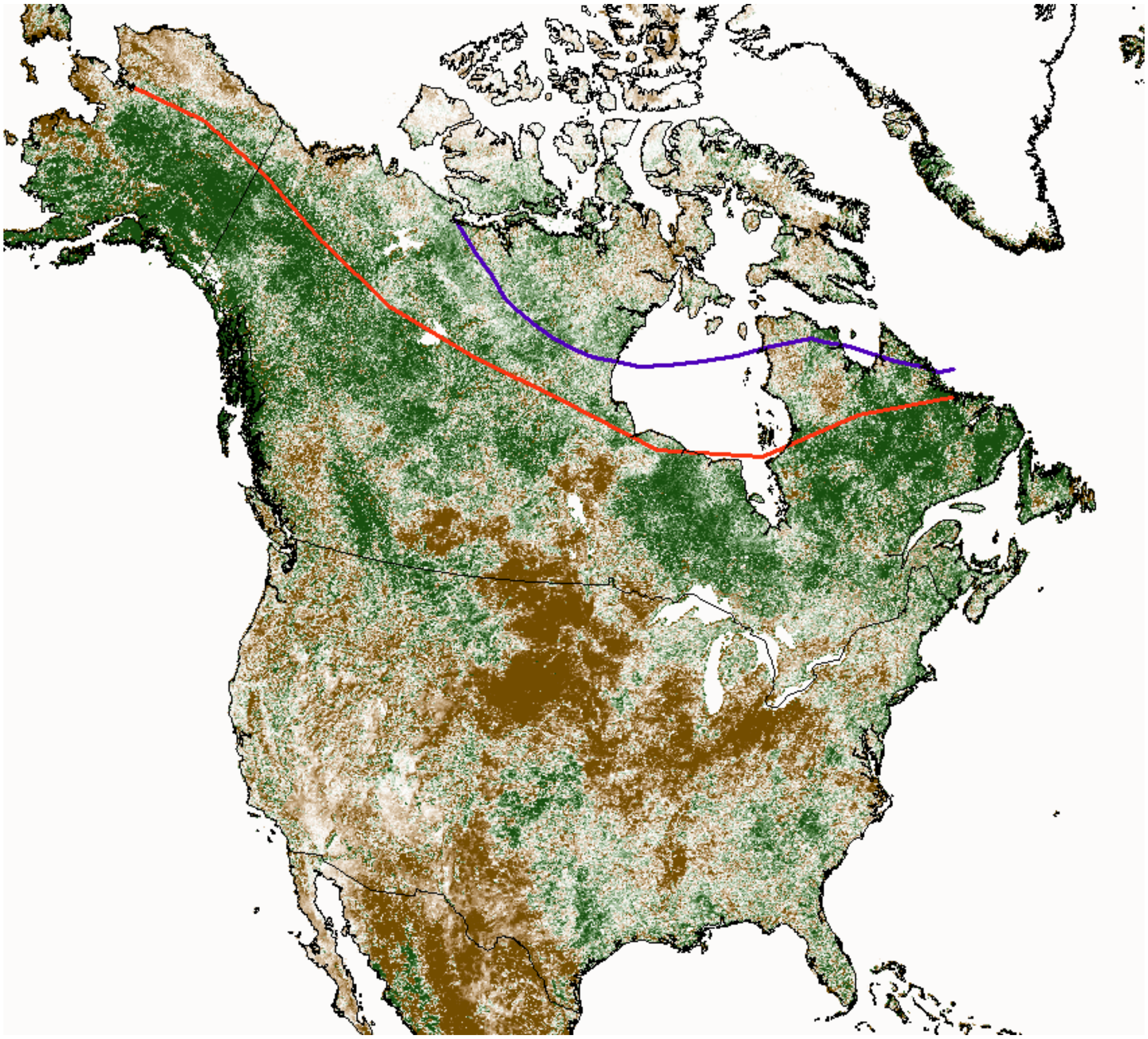

Figure D10. NDVI vegetation anomaly map for July 1989 with front position (purple line) and long term mean position (red line). Anomalies are dark green representing the largest positive anomalies (most productive) to brown representing the largest negative anomalies (least productive). White areas represent an anomaly of zero.

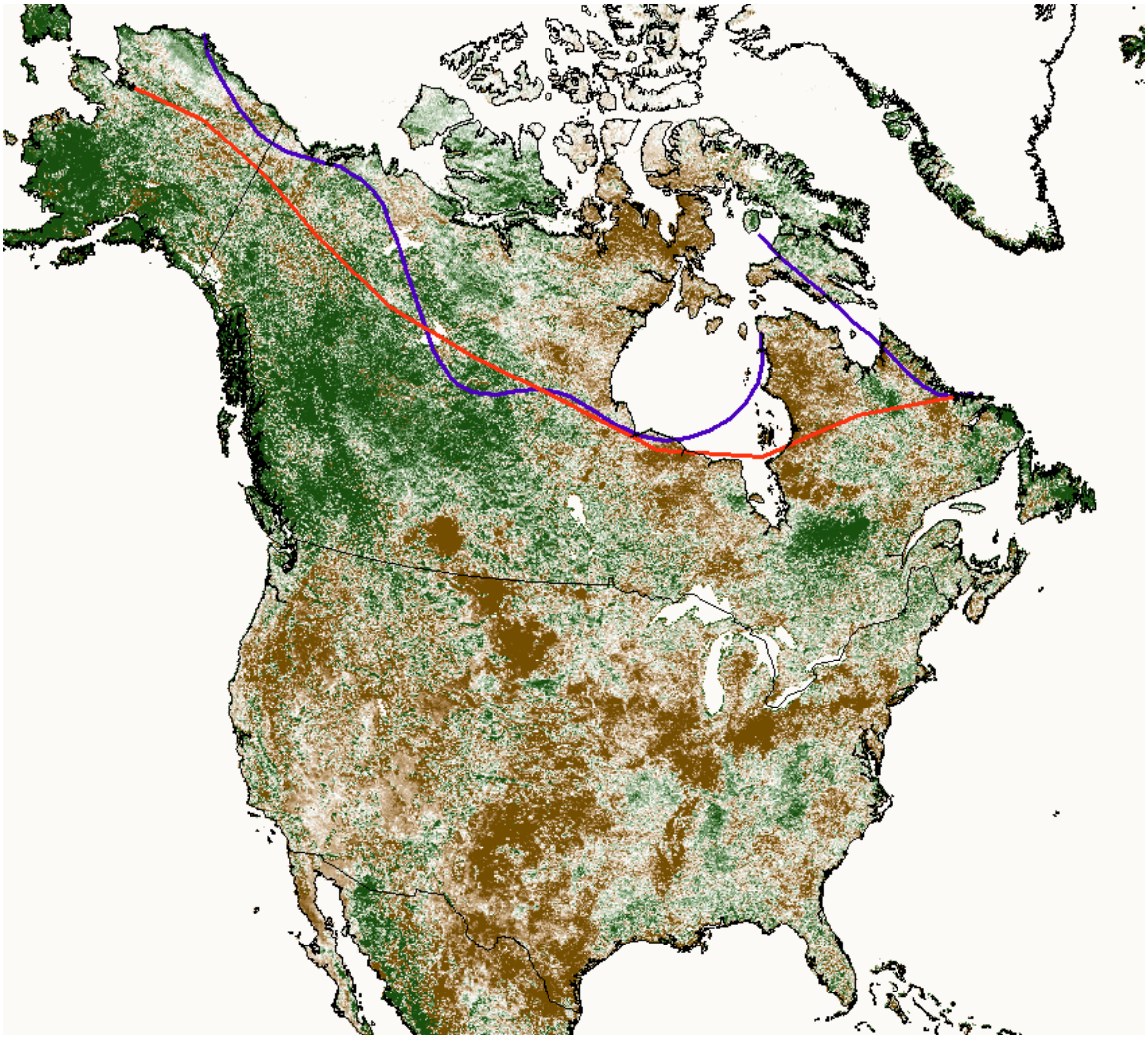

Figure D11. NDVI vegetation anomaly map for July 1990 with front position (purple line) and long term mean position (red line). Anomalies are dark green representing the largest positive anomalies (most productive) to brown representing the largest negative anomalies (least productive). White areas represent an anomaly of zero.

Figure D12. NDVI vegetation anomaly map for July 1991 with front position (blue line) and long term mean position (red line). Anomalies are dark green representing the largest positive anomalies (most productive) to brown representing the largest negative anomalies (least productive). White areas represent an anomaly of zero.

Figure D13. NDVI vegetation anomaly map for July 1992 with front position (blue line) and long term mean position (red line). Anomalies are dark green representing the largest positive anomalies (most productive) to brown representing the largest negative anomalies (least productive). White areas represent an anomaly of zero.

Figure D14. NDVI vegetation anomaly map for July 1993 with front position (blue line) and long term mean position (red line). Anomalies are dark green representing the largest positive anomalies (most productive) to brown representing the largest negative anomalies (least productive). White areas represent an anomaly of zero.

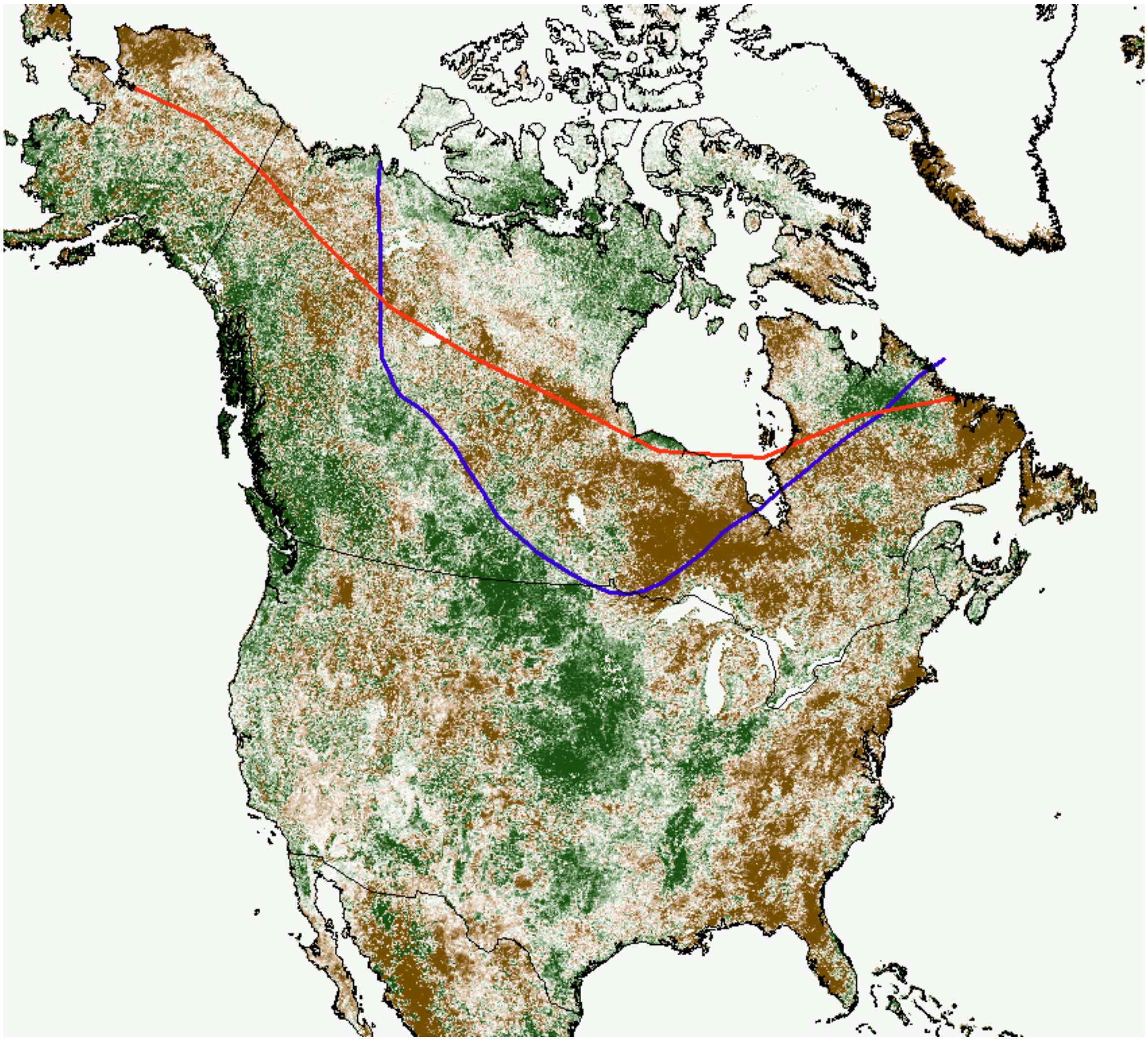

Figure D15. NDVI vegetation anomaly map for July 1994 with front position (blue line) and long term mean position (red line). Anomalies are dark green representing the largest positive anomalies (most productive) to brown representing the largest negative anomalies (least productive). White areas represent an anomaly of zero.

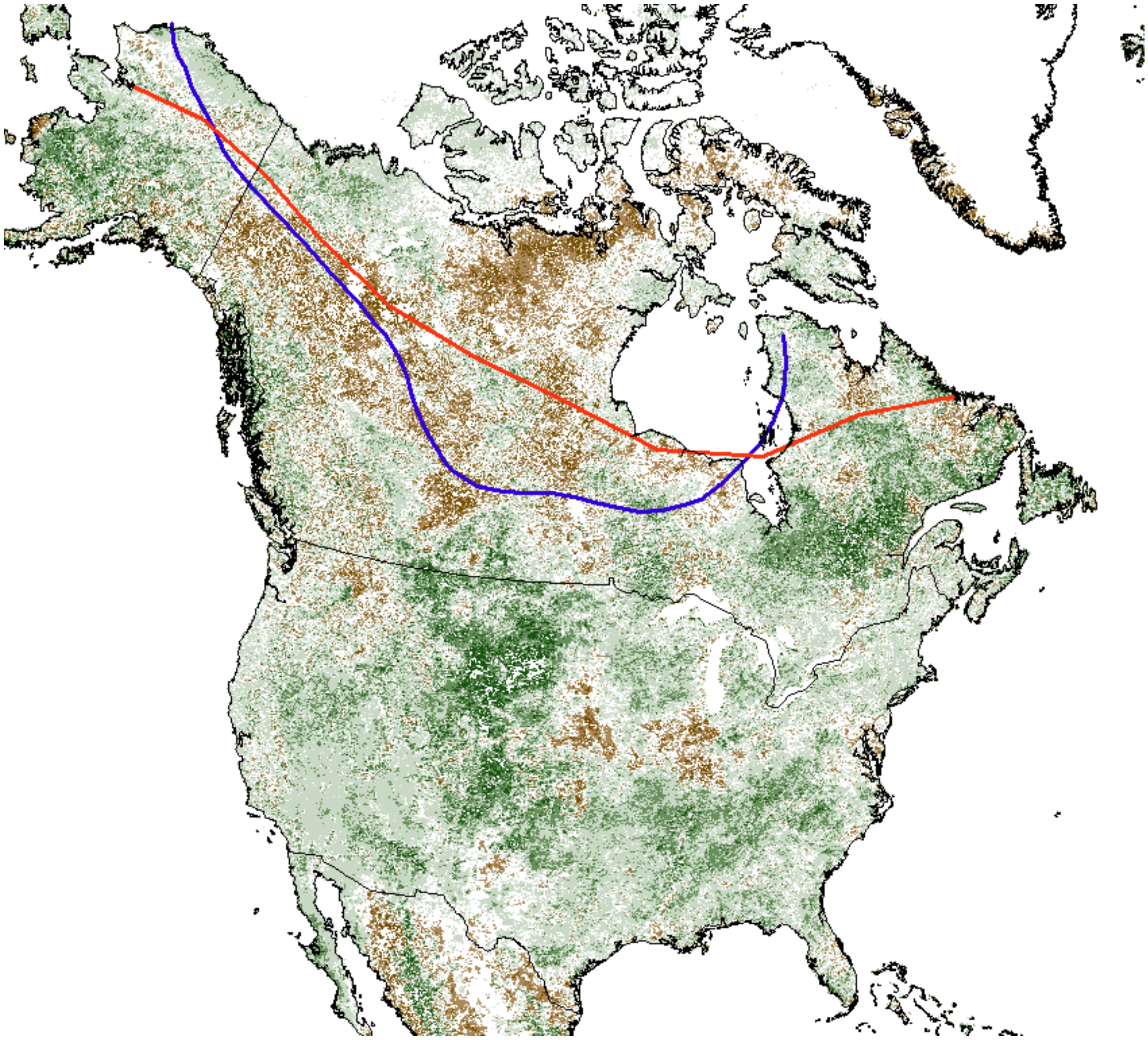

Figure D16. NDVI vegetation anomaly map for July 1995 with front position (blue line) and long term mean position (red line). Anomalies are dark green representing the largest positive anomalies (most productive) to brown representing the largest negative anomalies (least productive). White areas represent an anomaly of zero.

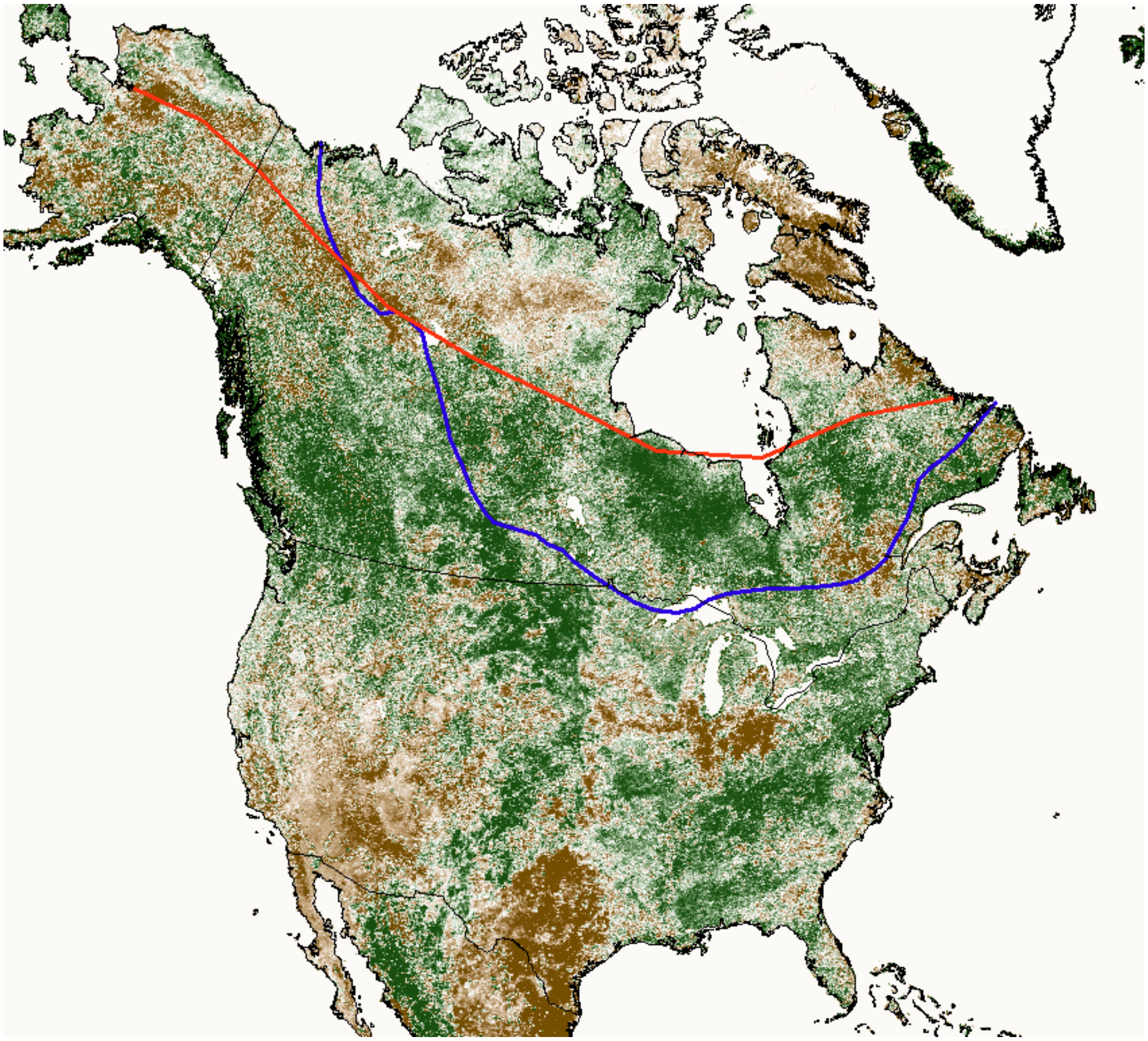

Figure D17. NDVI vegetation anomaly map for July 1996 with front position (blue line) and long term mean position (red line). Anomalies are dark green representing the largest positive anomalies (most productive) to brown representing the largest negative anomalies (least productive). White areas represent an anomaly of zero.

Figure D18. NDVI vegetation anomaly map for July 1997 with front position (blue line) and long term mean position (red line). Anomalies are dark green representing the largest positive anomalies (most productive) to brown representing the largest negative anomalies (least productive). White areas represent an anomaly of zero.

Figure D19. NDVI vegetation anomaly map for July 1998 with front position (blue line) and long term mean position (red line). Anomalies are dark green representing the largest positive anomalies (most productive) to brown representing the largest negative anomalies (least productive). White areas represent an anomaly of zero.

Figure D20. NDVI vegetation anomaly map for July 1999 with front position (blue line) and long term mean position (red line). Anomalies are dark green representing the largest positive anomalies (most productive) to brown representing the largest negative anomalies (least productive). White areas represent an anomaly of zero.

Figure D21. NDVI vegetation anomaly map for July 2000 with front position (blue line) and long term mean position (red line). Anomalies are dark green representing the largest positive anomalies (most productive) to brown representing the largest negative anomalies (least productive). White areas represent an anomaly of zero.

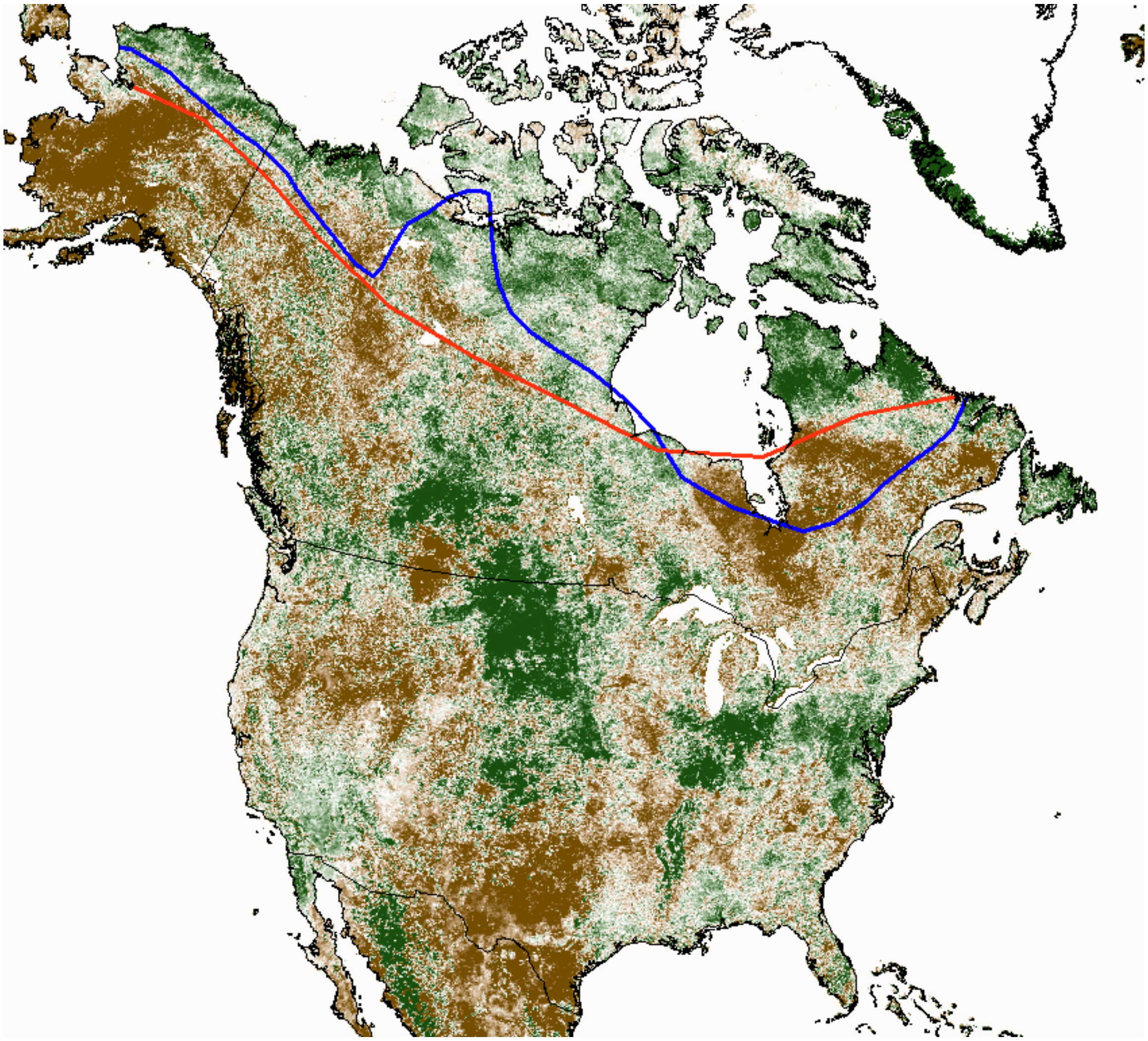

Figure D22. NDVI vegetation anomaly map for July 2001 with front position (blue line) and long term mean position (red line). Anomalies are dark green representing the largest positive anomalies (most productive) to brown representing the largest negative anomalies (least productive). White areas represent an anomaly of zero.

Appendix E – Environment Canada meteorological station data

The data was downloaded from the Canadian climate data online site at http://www.climate.weatheroffice.ec.gc.ca/climateData/canada_e.html. The format is zipped CSV files of daily, monthly, and in some cases hourly data. Some of the stations have records going back to the 1930s, however most are shorter with several stations having incomplete records for the time range. A Visual Basic for Applications (VBA) script was developed in Microsoft Excel to extract only the July data for a given station.

E.1. Frequency distribution of mean July temperatures for selected Canadian meteorological stations

The purpose of creating histograms of July maximum temperature for selected Canadian stations is to aid in the analysis of air masses and better understand the July climate. Bryson (1966) proposed that stations located near the Arctic front should have a multi-modal distribution of July maximum temperature, because of the mixtures of air masses present. Stations north (south) of the front appear to have a negatively (positively) skewed July maximum temperature distribution although there are a few exceptions. Generally, stations further to the south are closer to a normal distribution of July maximum temperature.

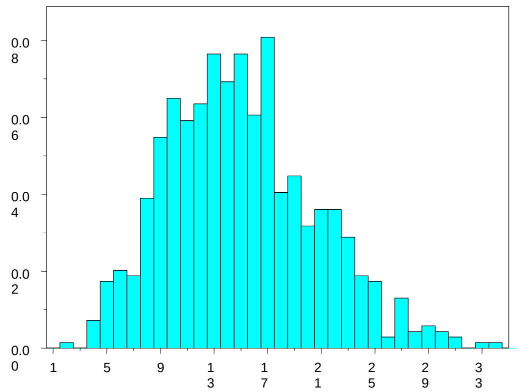

Figure E1. Frequency distribution of July maximum temperature for Arviat, NT.

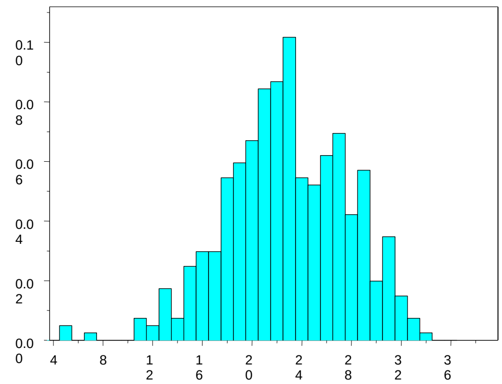

Figure E2. Frequency distribution of July maximum temperature for Banff, AB.

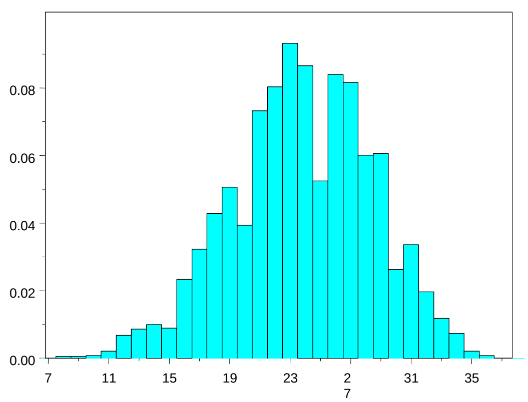

Figure E3. Frequency distribution of July maximum temperature for Calgary, AB.

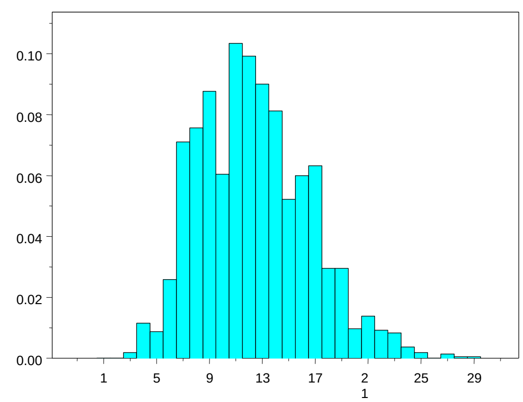

Figure E4. Frequency distribution of July maximum temperature for Cambridge Bay, NU.

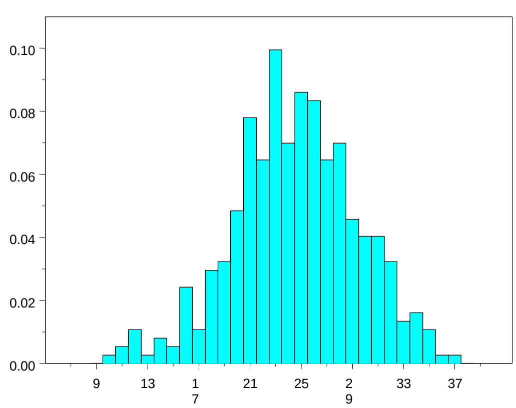

Figure E5. Frequency distribution of July maximum temperature for Coronation, AB.

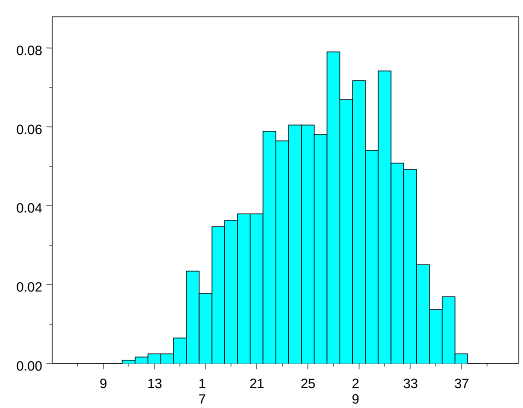

Figure E6. Frequency distribution of July maximum temperature for Cranbrook, BC.

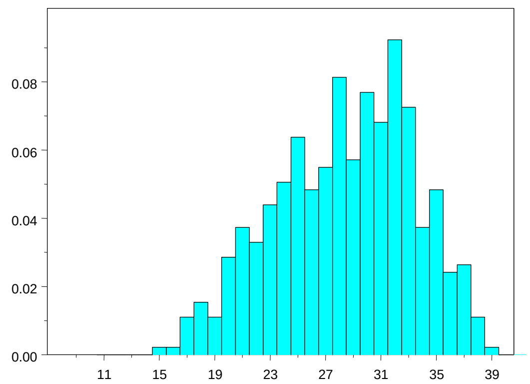

Figure E7. Frequency distribution of July maximum temperature for Creston, BC.

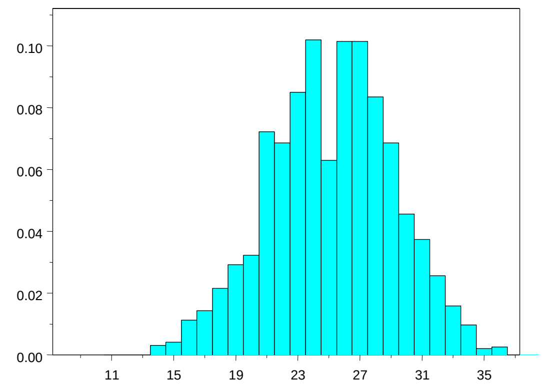

Figure E8. Frequency distribution of July maximum temperature for Dauphin, MB.

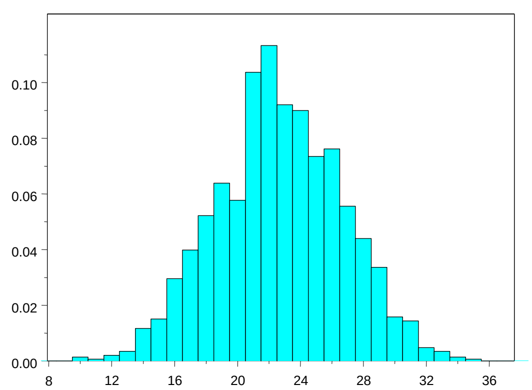

Figure E9. Frequency distribution of July maximum temperature for Edmonton, AB.

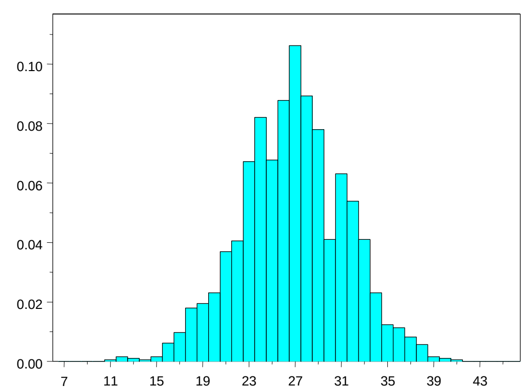

Figure E10. Frequency distribution of July maximum temperature for Estevan, SK.

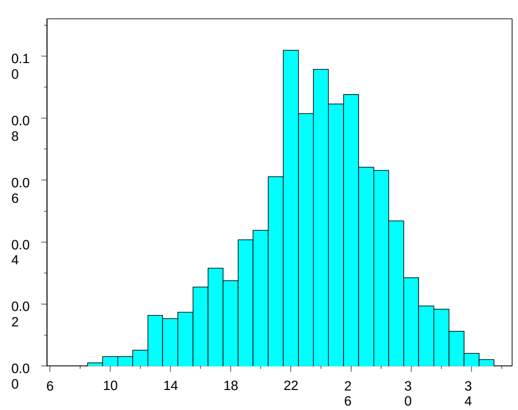

Figure E11. Frequency distribution of July maximum temperature for Fort Liard, NT.

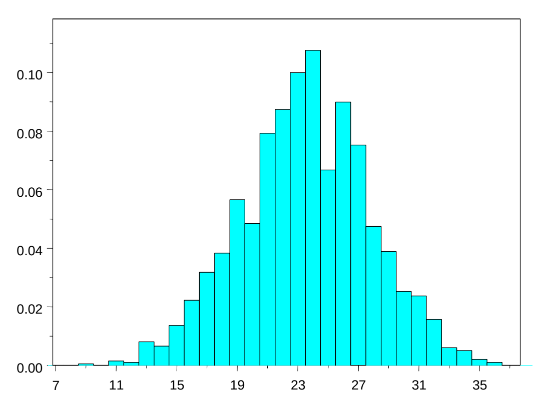

Figure E12. Frequency distribution of July maximum temperature for Fort McMurray, AB.

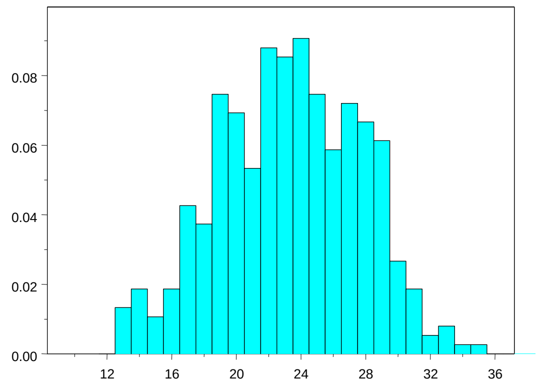

Figure E13. Frequency distribution of July maximum temperature for Fort Providence, NT.

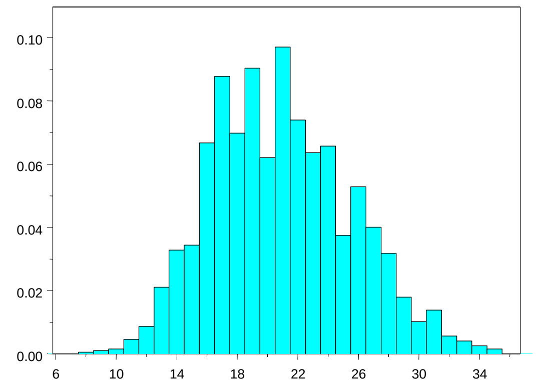

Figure E14. Frequency distribution of July maximum temperature for Hay River, NT.

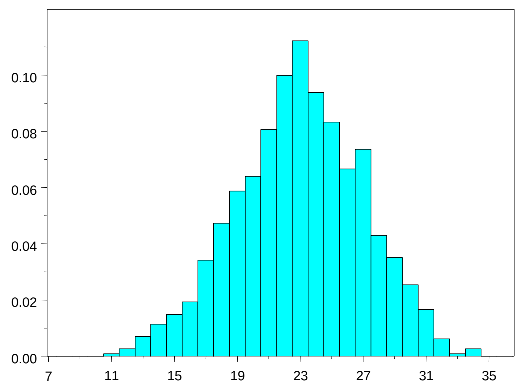

Figure E15. Frequency distribution of July maximum temperature for High Level, AB.

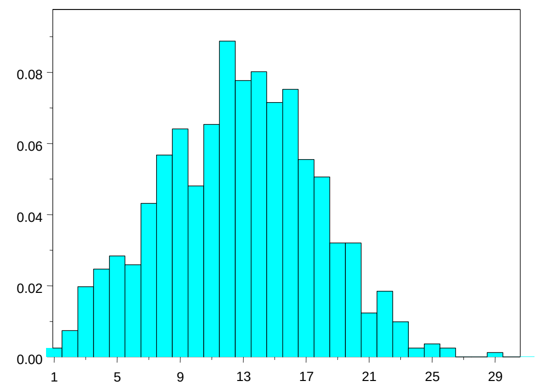

Figure E16. Frequency distribution of July maximum temperature for Holman, NT.

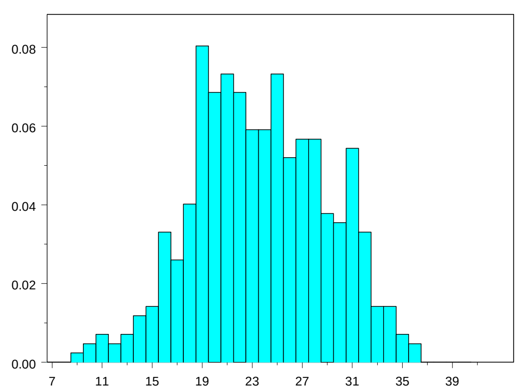

Figure E17. Frequency distribution of July maximum temperature for Jasper, AB.

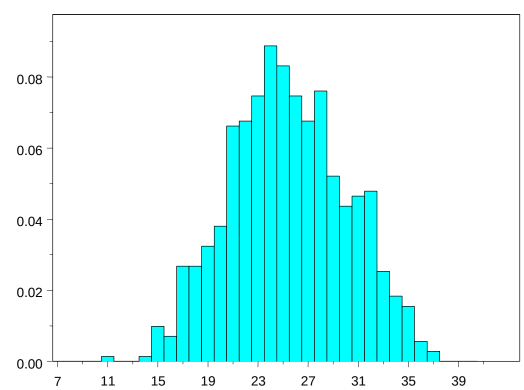

Figure E18. Frequency distribution of July maximum temperature for Kindersley, SK.

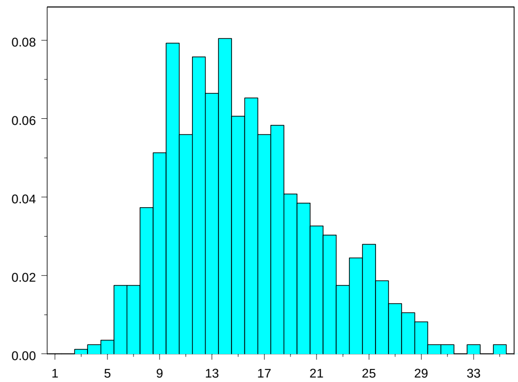

Figure E19. Frequency distribution of July maximum temperature for Kugluktuk, NU.

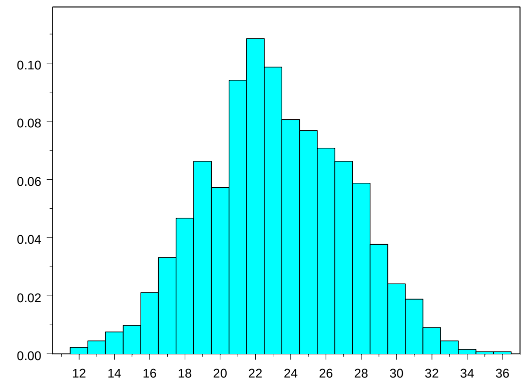

Figure E20. Frequency distribution of July maximum temperature for La Ronge, SK.

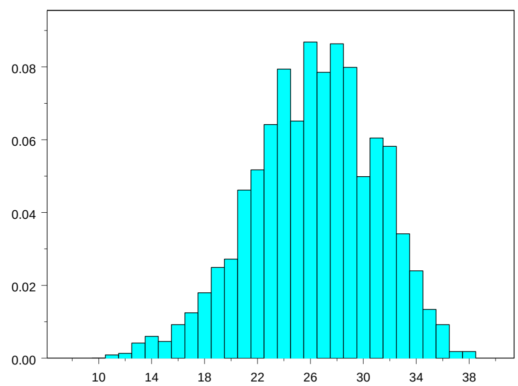

Figure E21. Frequency distribution of July maximum temperature for Lethbridge, AB.

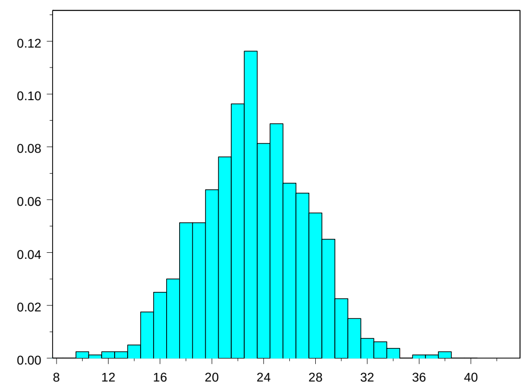

Figure E22. Frequency distribution of July maximum temperature for Lloydminster, AB.

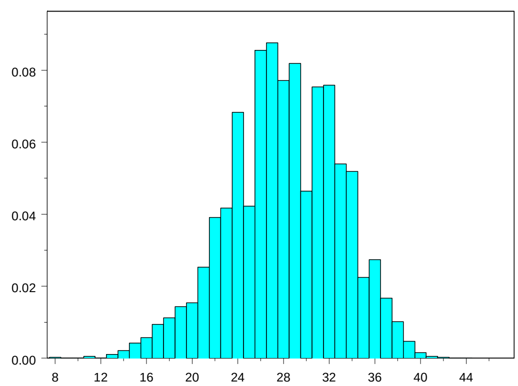

Figure E23. Frequency distribution of July maximum temperature for Medicine Hat, AB.

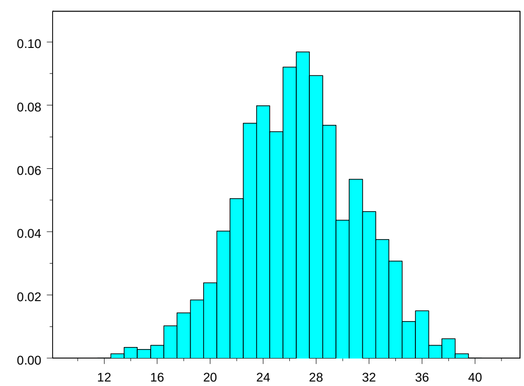

Figure E24. Frequency distribution of July maximum temperature for Moose Jaw, SK.

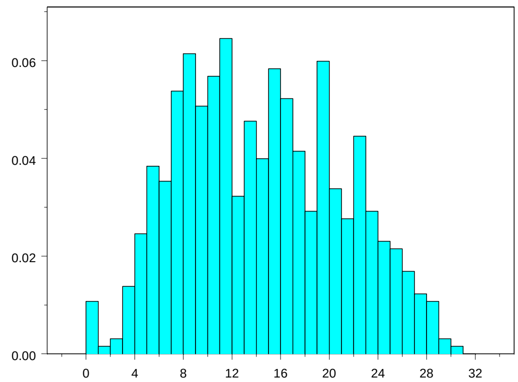

Figure E25. Frequency distribution of July maximum temperature for Paulatuk, NT.

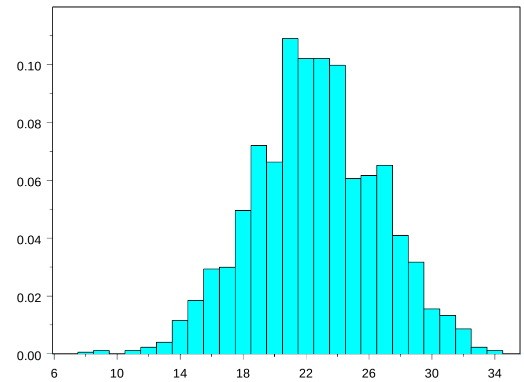

Figure E26. Frequency distribution of July maximum temperature for Peace River, AB.

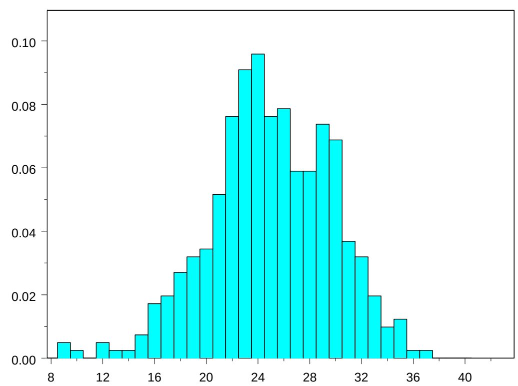

Figure E27. Frequency distribution of July maximum temperature for Pincher Creek, AB.

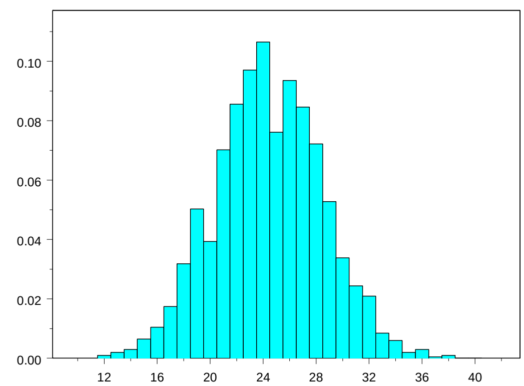

Figure E28. Frequency distribution of July maximum temperature for Prince Albert, SK.

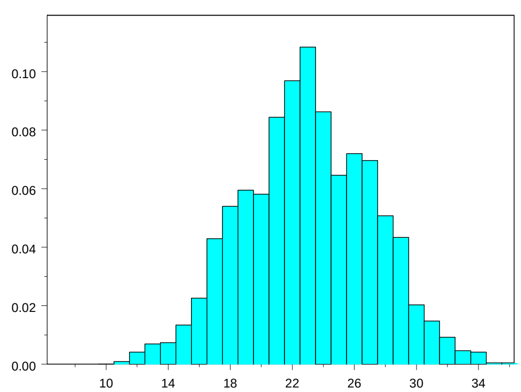

Figure E29. Frequency distribution of July maximum temperature for Red Deer, AB.

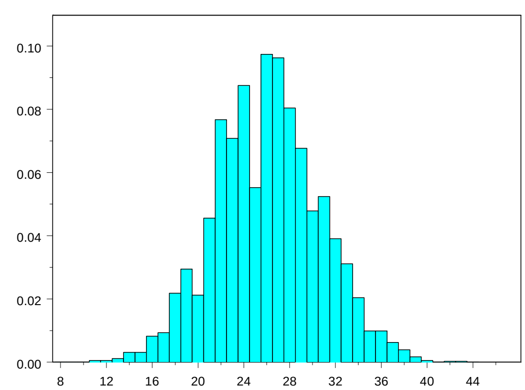

Figure E30. Frequency distribution of July maximum temperature for Regina, SK.

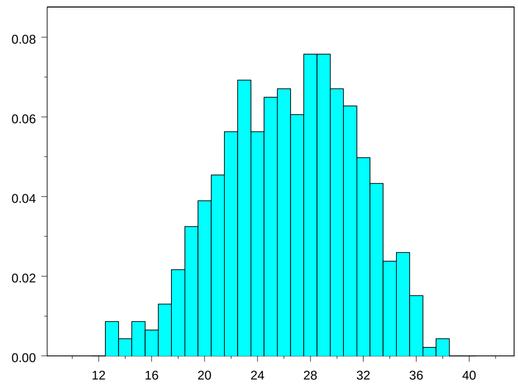

Figure E31. Frequency distribution of July maximum temperature for Revelstoke, BC.

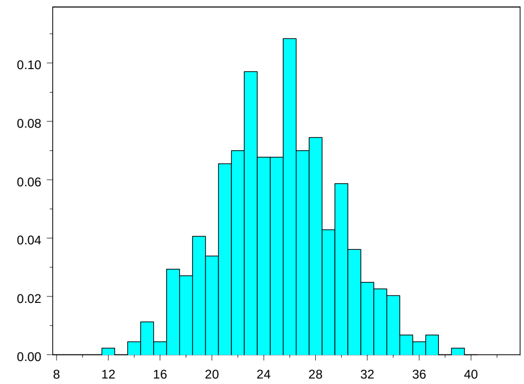

Figure E32. Frequency distribution of July maximum temperature for Rosetown, SK.

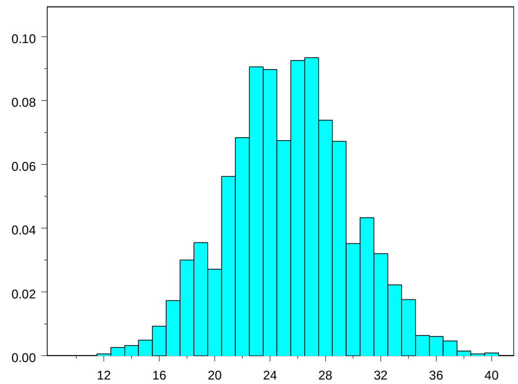

Figure E33. Frequency distribution of July maximum temperature for Saskatoon, SK.

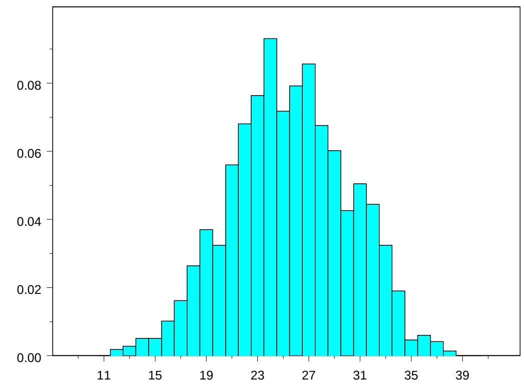

Figure E34. Frequency distribution of July maximum temperature for Swift Current, SK.

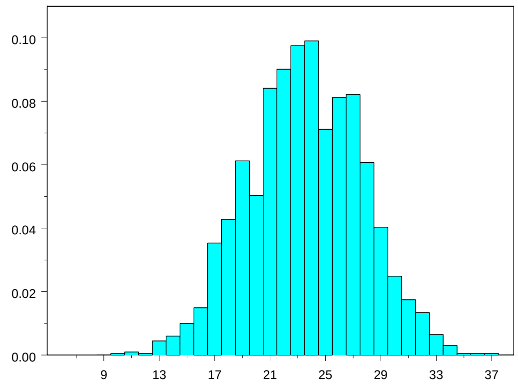

Figure E35. Frequency distribution of July maximum temperature for The Pas, MB.

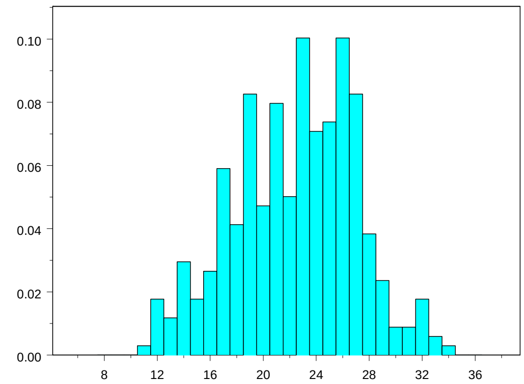

Figure E36. Frequency distribution of July maximum temperature for Wha Ti, NT.

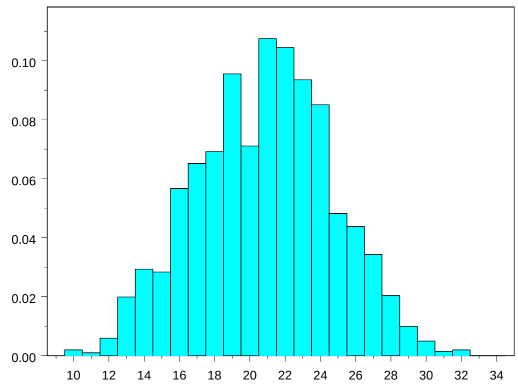

Figure E37. Frequency distribution of July maximum temperature for Yellowknife, NT.

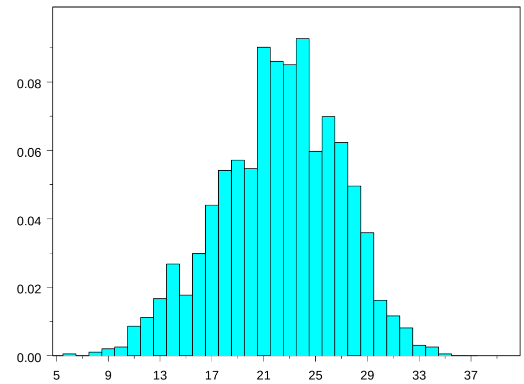

Figure E38. Frequency distribution of July maximum temperature for Norman, NT.

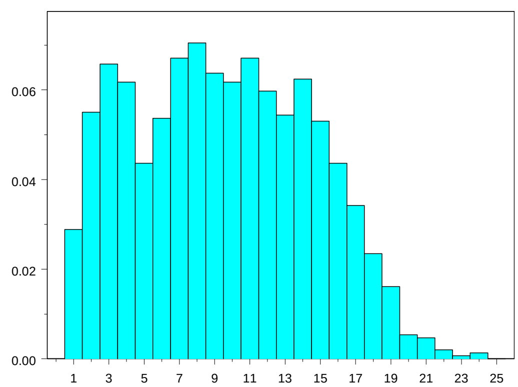

Figure E39. Frequency distribution of July maximum temperature for Sachs Harbour, NT.

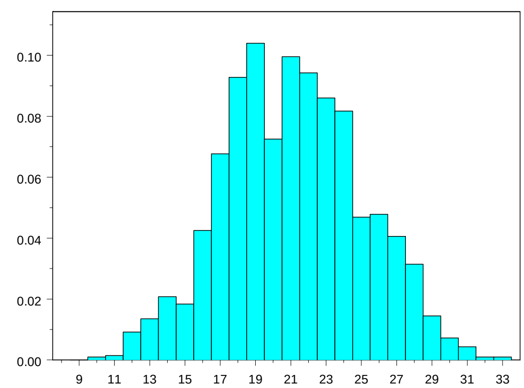

Figure E40. Frequency distribution of July maximum temperature for Watson Lake, YT.

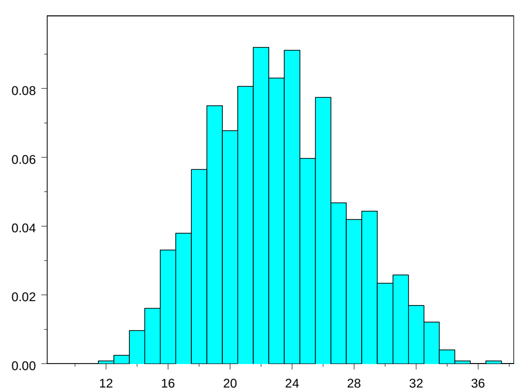

Figure E41. Frequency distribution of July maximum temperature for Campbell, BC.

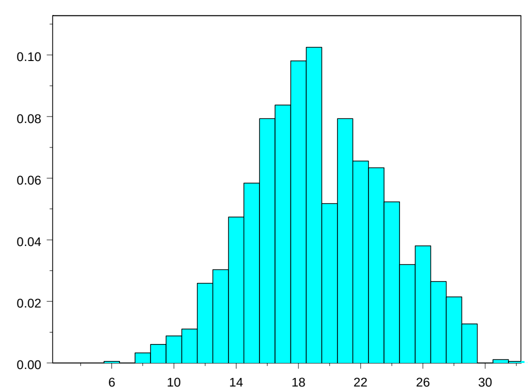

Figure E42. Frequency distribution of July maximum temperature for Dease Lake, BC.

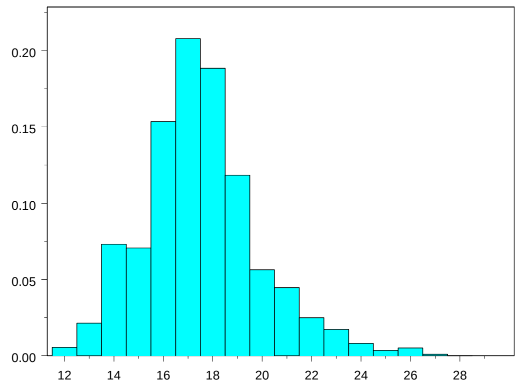

Figure E43. Frequency distribution of July maximum temperature for Port Hardy, BC.

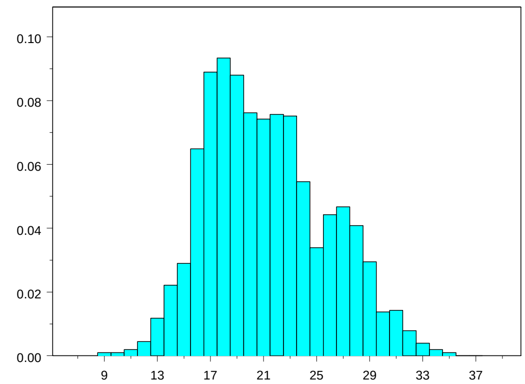

Figure E44. Frequency distribution of July maximum temperature for Smithers, BC.

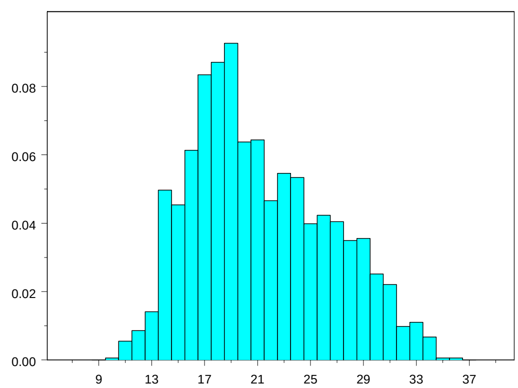

Figure E45. Frequency distribution of July maximum temperature for Terrace, BC.

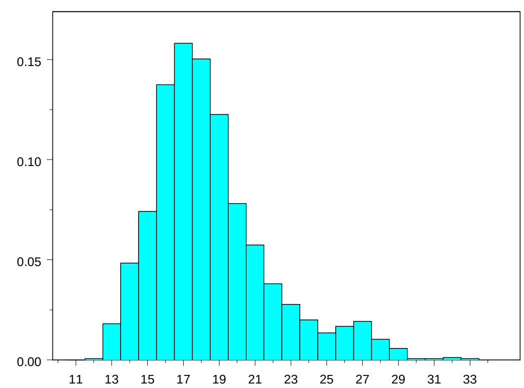

Figure E46. Frequency distribution of July maximum temperature for Tofino, BC.

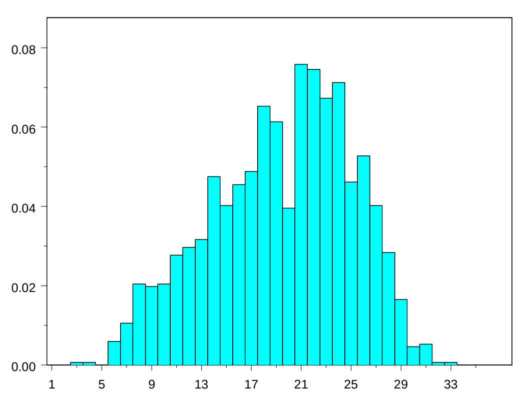

Figure E47. Frequency distribution of July maximum temperature for Inuvik, NT.

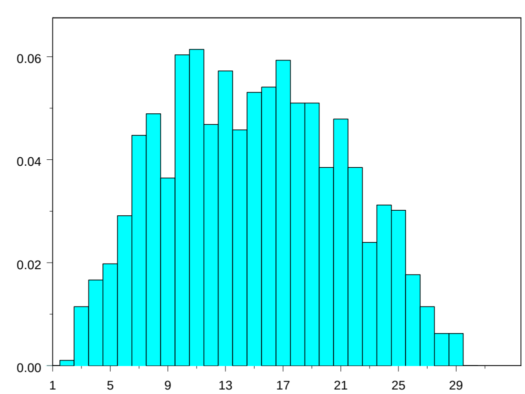

Figure E48. Frequency distribution of July maximum temperature for Tuktoyaktuk, NT.

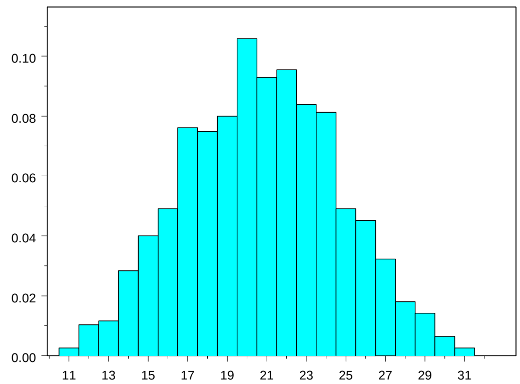

Figure E49. Frequency distribution of July maximum temperature for Faro, YT.

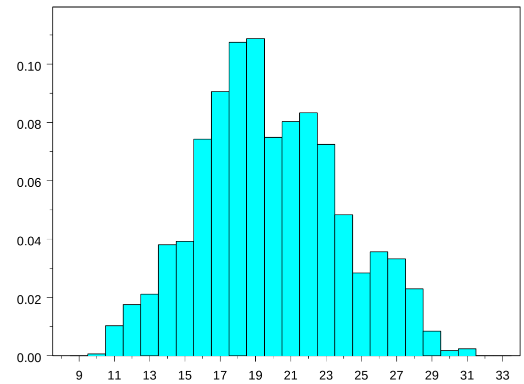

Figure E50. Frequency distribution of July maximum temperature for Teslin, YT.

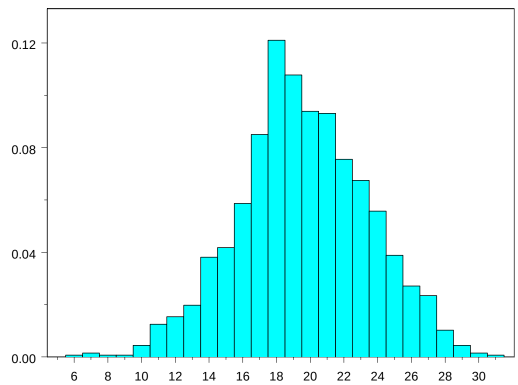

Figure E51. Frequency distribution of July maximum temperature for Burwash, YT.

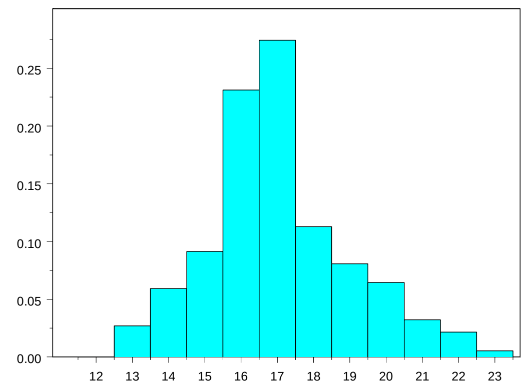

Figure E52. Frequency distribution of July maximum temperature for Sandspit, BC.

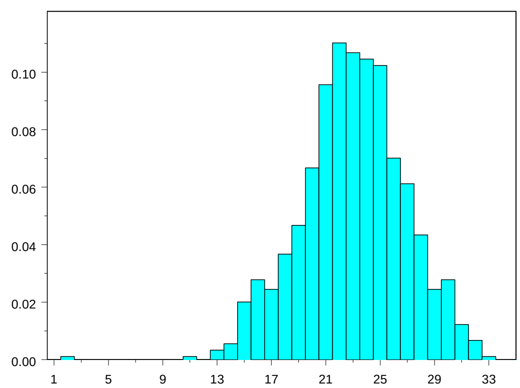

Figure E53. Frequency distribution of July maximum temperature for Dawson, YT.

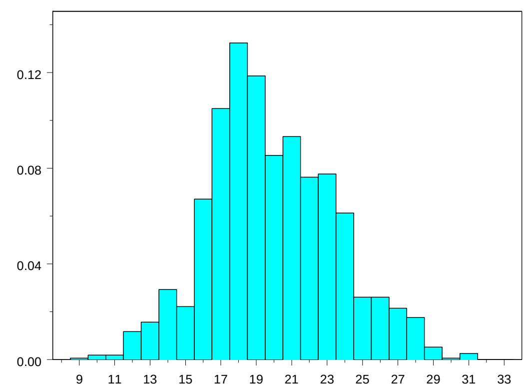

Figure E54. Frequency distribution of July maximum temperature for Haines Junction, YT.

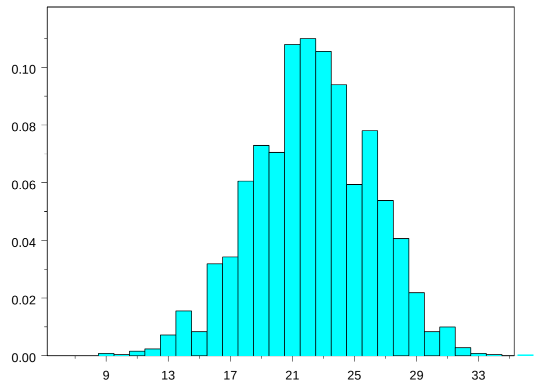

Figure E55. Frequency distribution of July maximum temperature for Mayo, YT.

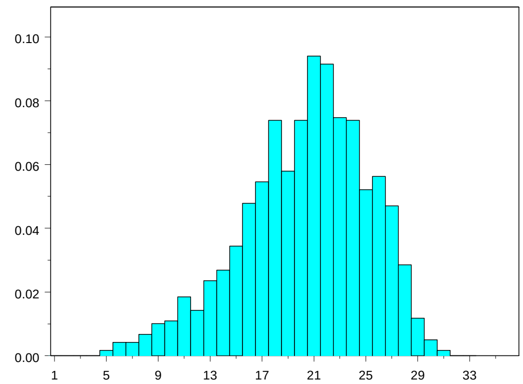

Figure E56. Frequency distribution of July maximum temperature for Old Crow, YT.

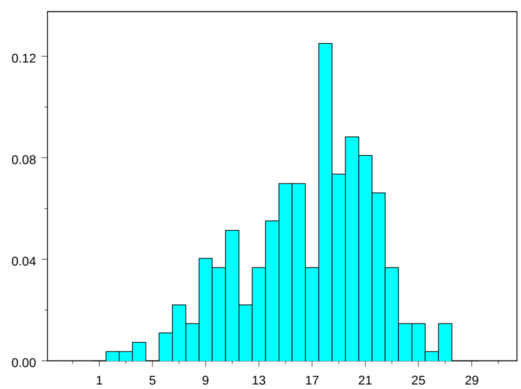

Figure E57. Frequency distribution of July maximum temperature for Rock River, YT.

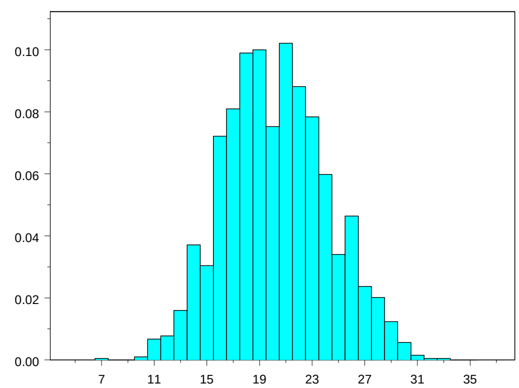

Figure E58. Frequency distribution of July maximum temperature for Whitehorse, YT.

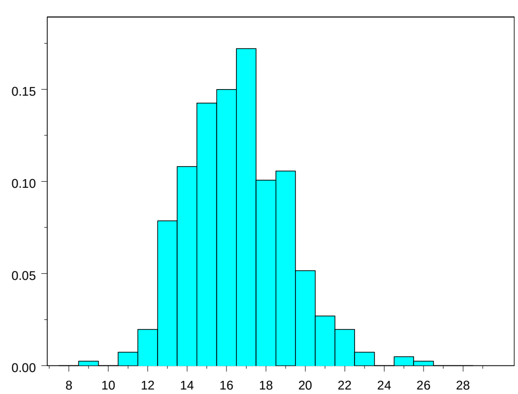

Figure E59. Frequency distribution of July maximum temperature for Argentia, NF.

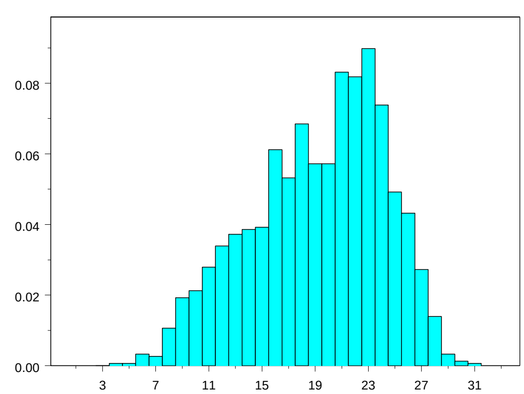

Figure E60. Frequency distribution of July maximum temperature for Bonavista, NF.

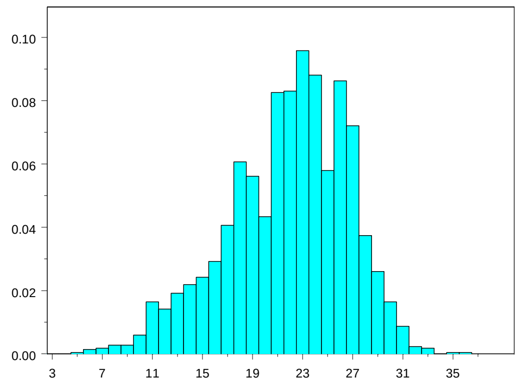

Figure E61. Frequency distribution of July maximum temperature for Gander, NF.

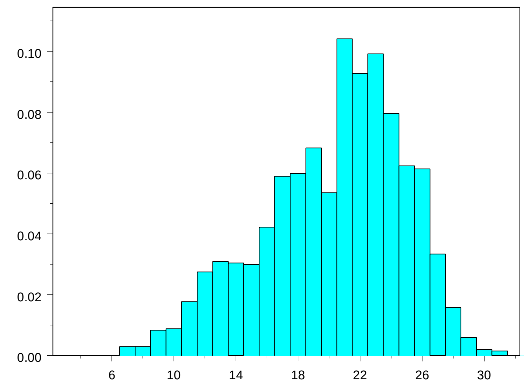

Figure E62. Frequency distribution of July maximum temperature for St. Johns, NF.

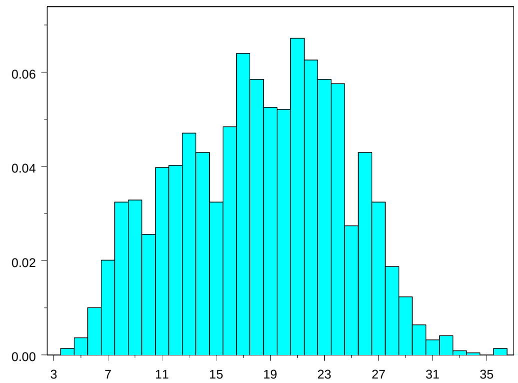

Figure E63. Frequency distribution of July maximum temperature for Cartwright, NF.

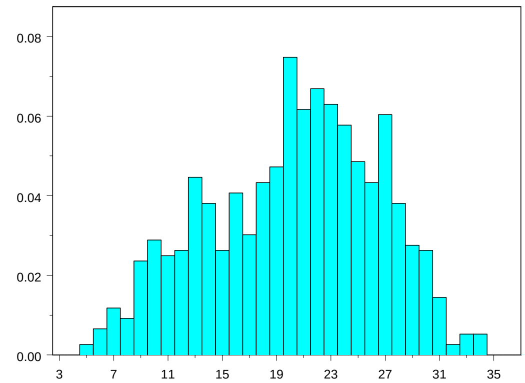

Figure E64. Frequency distribution of July maximum temperature for Mary's Harbour, NF.

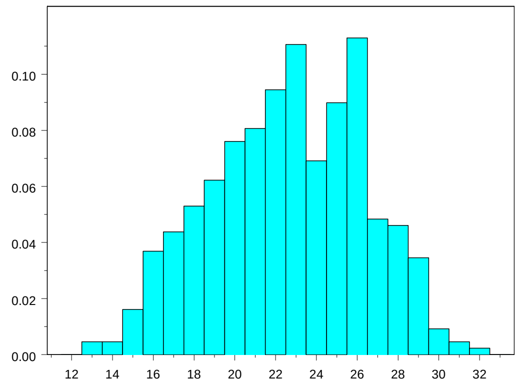

Figure E65. Frequency distribution of July maximum temperature for Corner Brook, NF.

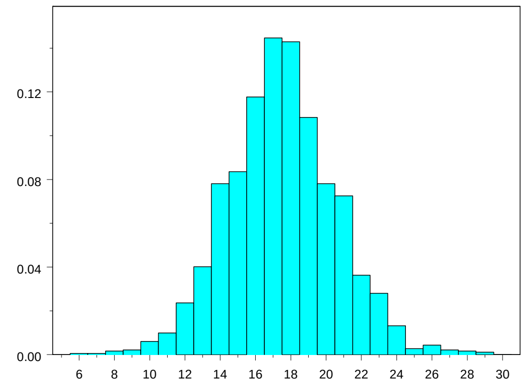

Figure E66. Frequency distribution of July maximum temperature for Daniels, NF.

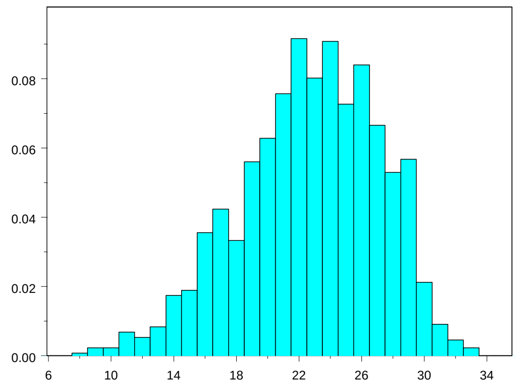

Figure E67. Frequency distribution of July maximum temperature for Deer Lake, NF.

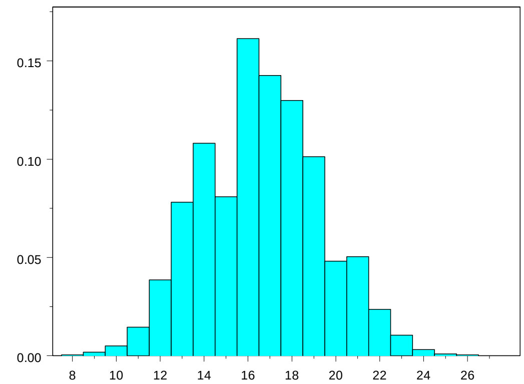

Figure E68. Frequency distribution of July maximum temperature for Port Aux Basques, NF.

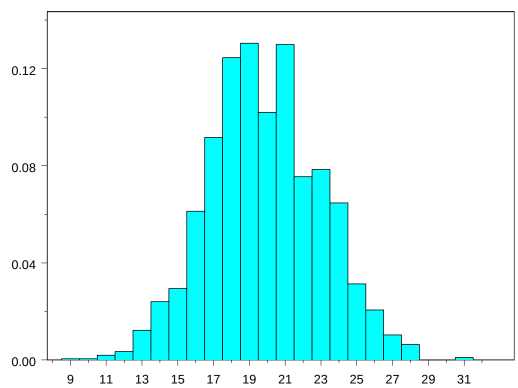

Figure E69. Frequency distribution of July maximum temperature for Stephenville, NF.

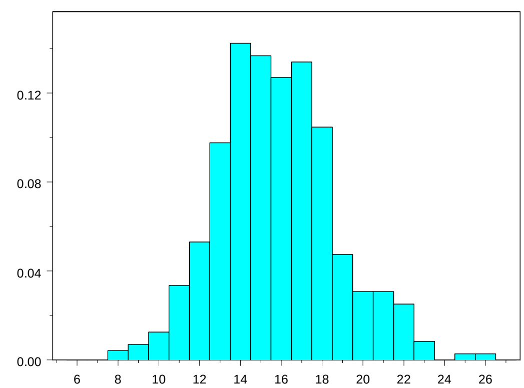

Figure E70. Frequency distribution of July maximum temperature for Blanc Sablon, QC.

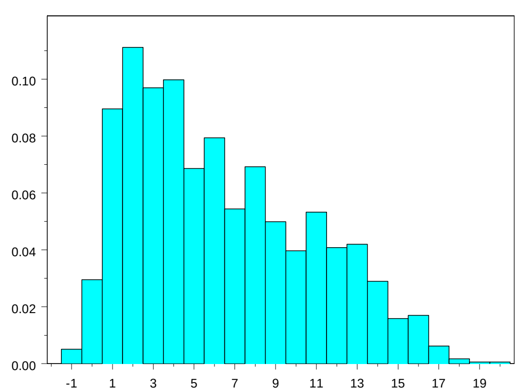

Figure E71. Frequency distribution of July maximum temperature for Alert, NU.

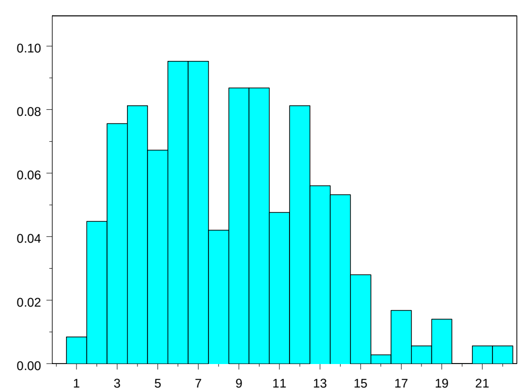

Figure E72. Frequency distribution of July maximum temperature for Qikiqtarq, NU.

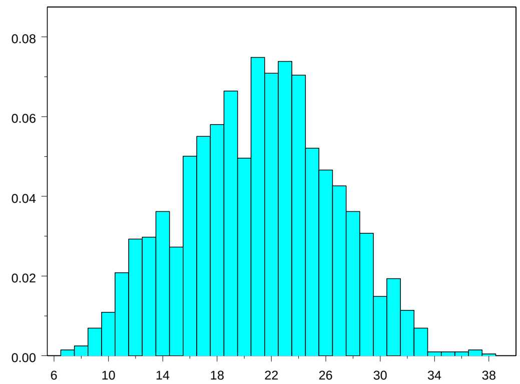

Figure E73. Frequency distribution of July maximum temperature for Goose Bay, NF.

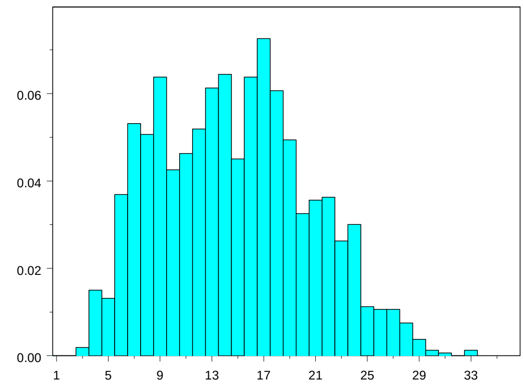

Figure E74. Frequency distribution of July maximum temperature for Hopedale, NF.

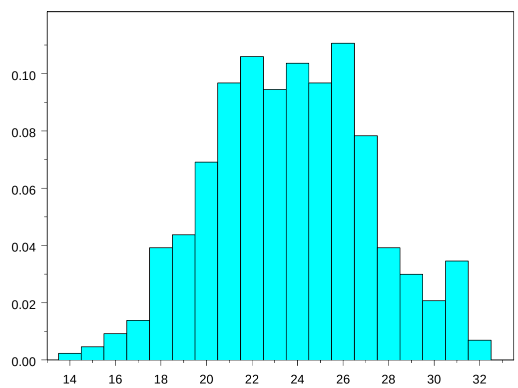

Figure E75. Frequency distribution of July maximum temperature for Bas Caraquet, NB.

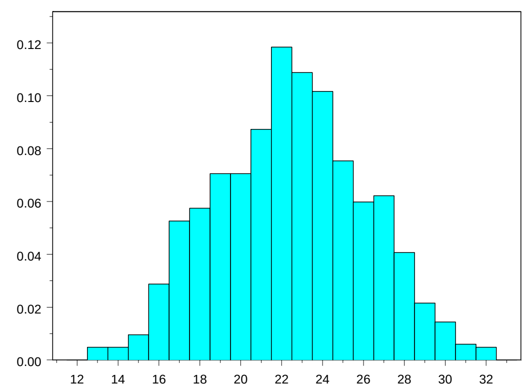

Figure E76. Frequency distribution of July maximum temperature for Miscou Island, NB.

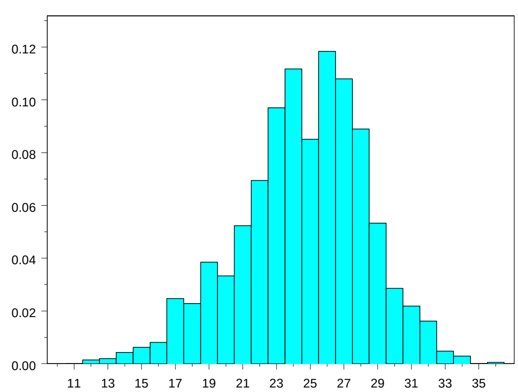

Figure E77. Frequency distribution of July maximum temperature for Moncton, NB.

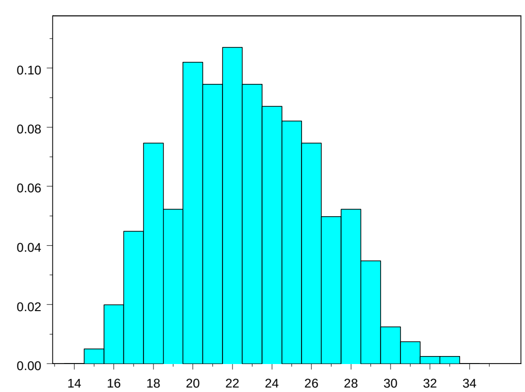

Figure E78. Frequency distribution of July maximum temperature for Caribou, NS.

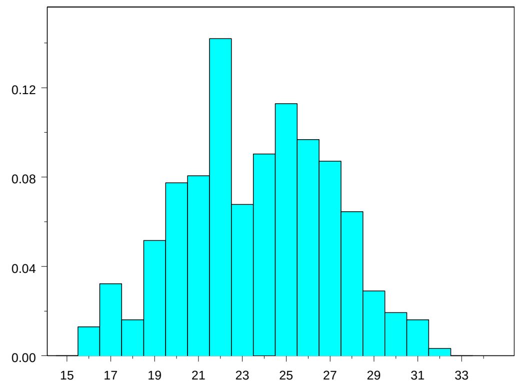

Figure E79. Frequency distribution of July maximum temperature for Cheticamp, NS.

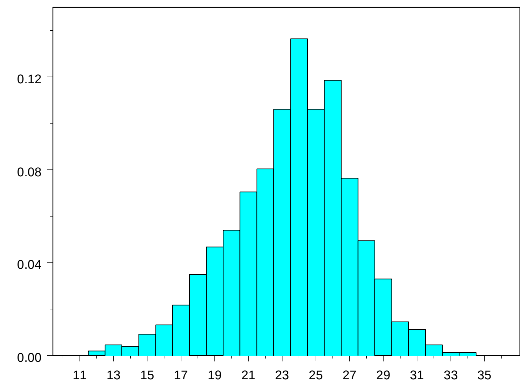

Figure E80. Frequency distribution of July maximum temperature for Halifax, NS.

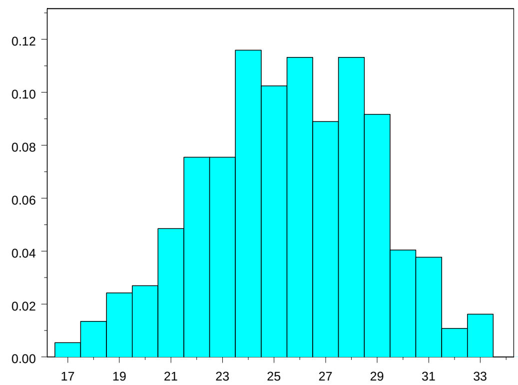

Figure E81. Frequency distribution of July maximum temperature for Kentville, NS.

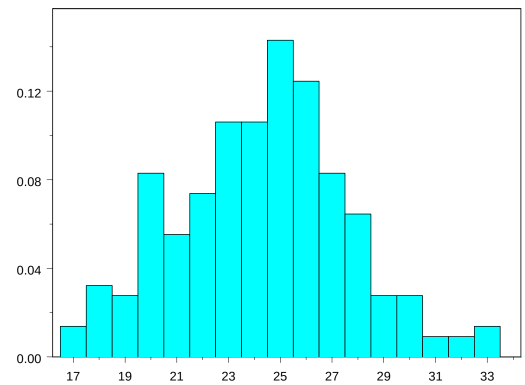

Figure E82. Frequency distribution of July maximum temperature for Malay Falls, NS.

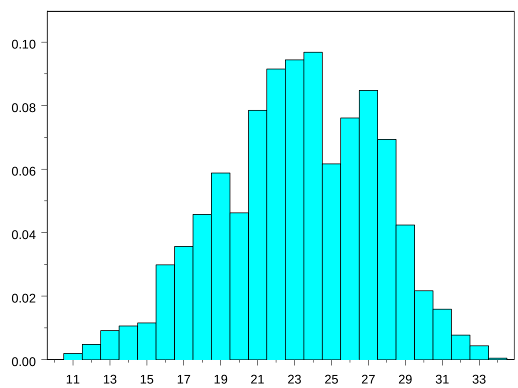

Figure E83. Frequency distribution of July maximum temperature for Sydney, NS.

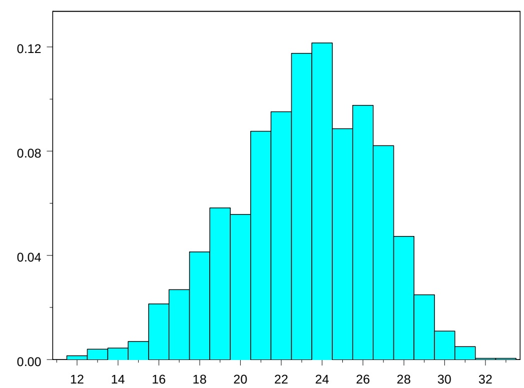

Figure E84. Frequency distribution of July maximum temperature for Charlottetown, PE.

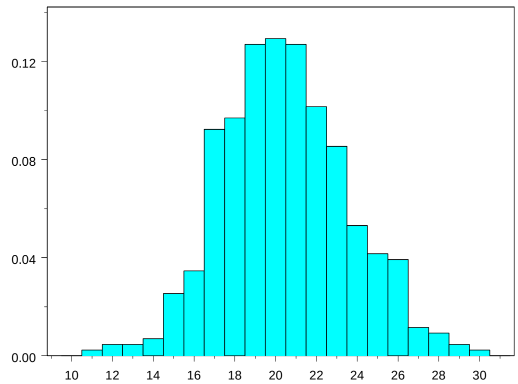

Figure E85. Frequency distribution of July maximum temperature for East Point, PE.

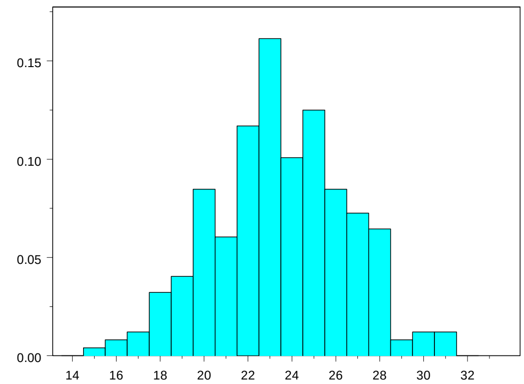

Figure E86. Frequency distribution of July maximum temperature for Summerside, PE.

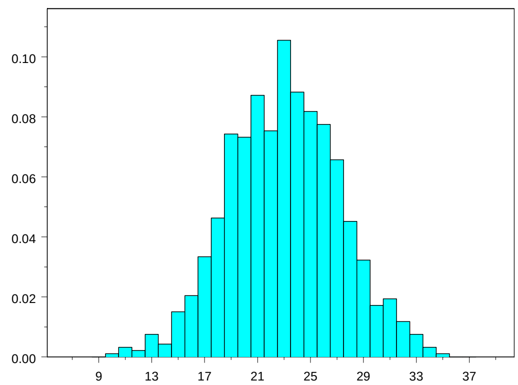

Figure E87. Frequency distribution of July maximum temperature for Gaspe, QC.

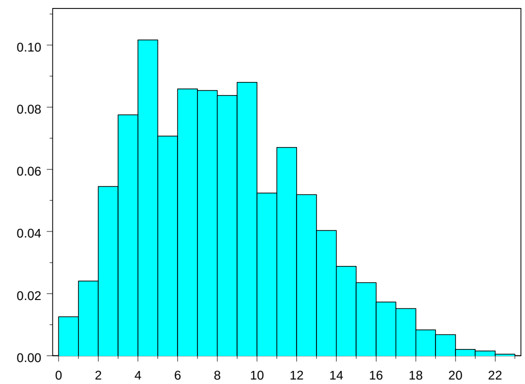

Figure E88. Frequency distribution of July maximum temperature for Clyde River, NU.

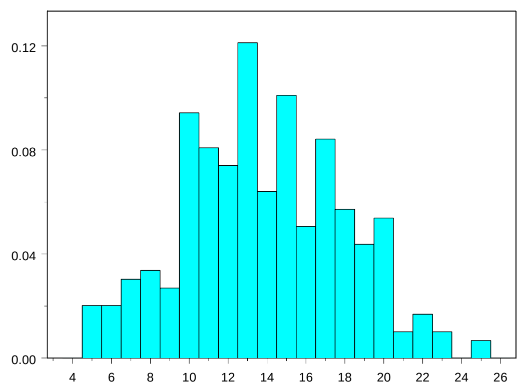

Figure E89. Frequency distribution of July maximum temperature for Kimmirut, NU.

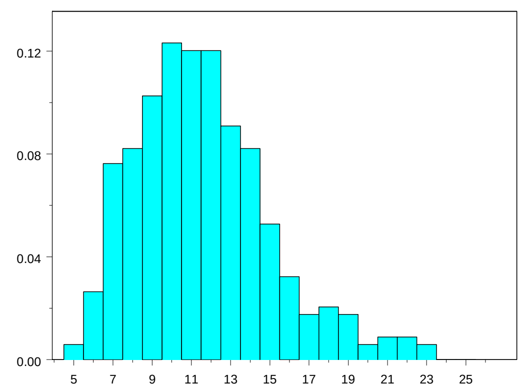

Figure E90. Frequency distribution of July maximum temperature for Pangnirtung, NU.

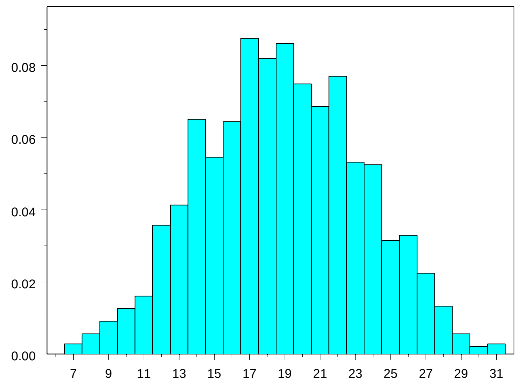

Figure E91. Frequency distribution of July maximum temperature for Wabush, NF.

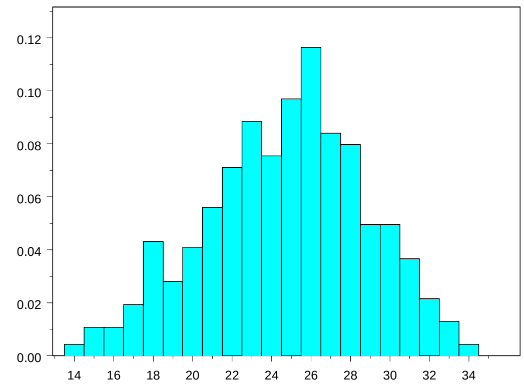

Figure E92. Frequency distribution of July maximum temperature for Bathurst, NB.

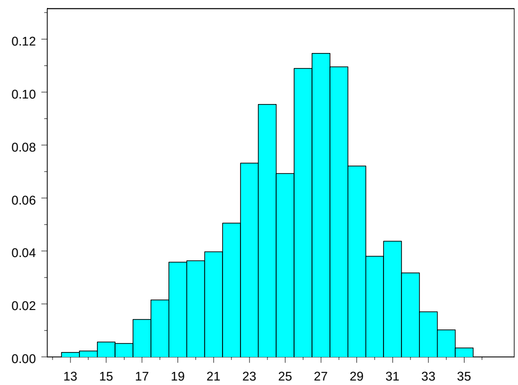

Figure E93. Frequency distribution of July maximum temperature for Fredericton, NB.

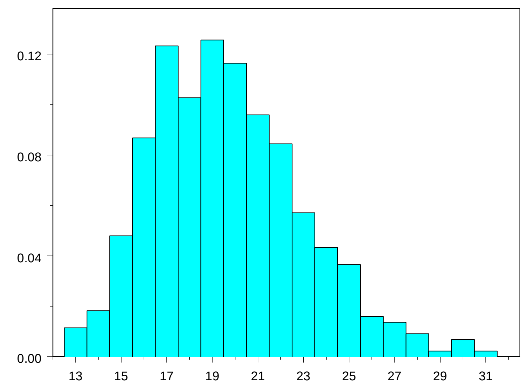

Figure E94. Frequency distribution of July maximum temperature for Point Lepreau, NB.

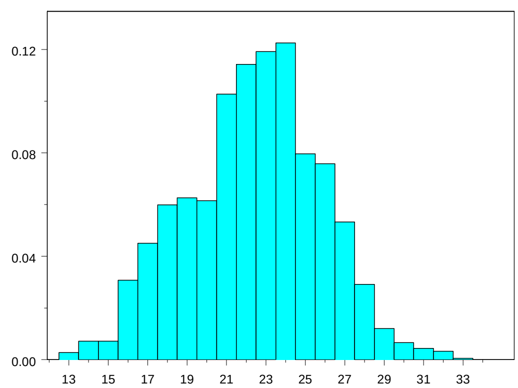

Figure E95. Frequency distribution of July maximum temperature for St. John, NB.

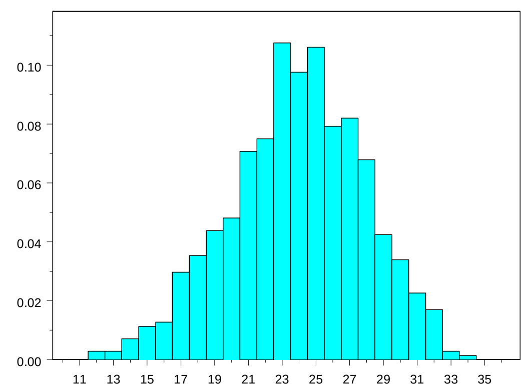

Figure E96. Frequency distribution of July maximum temperature for St. Leonard, NB.

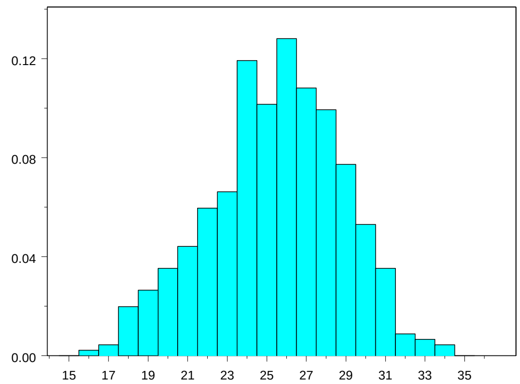

Figure E97. Frequency distribution of July maximum temperature for Kejimkujik, NS.

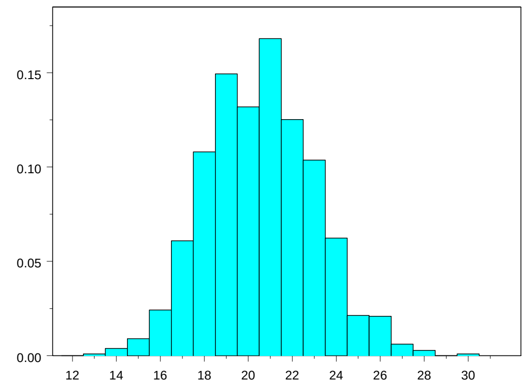

Figure E98. Frequency distribution of July maximum temperature for Yarmouth, NS.

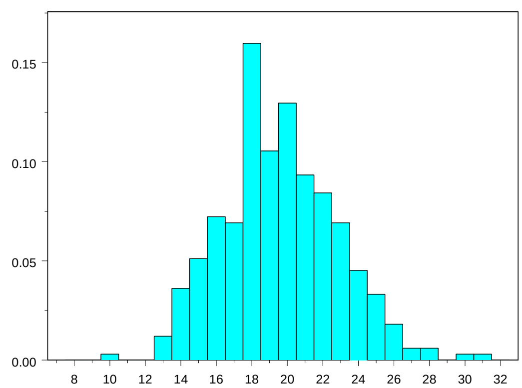

Figure E99. Frequency distribution of July maximum temperature for Cap Chat, QC.

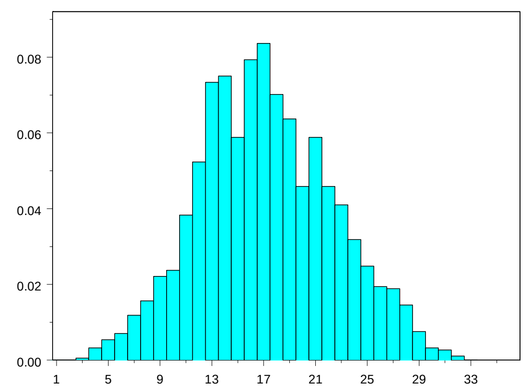

Figure E100. Frequency distribution of July maximum temperature for Kuujjuaq, QC.

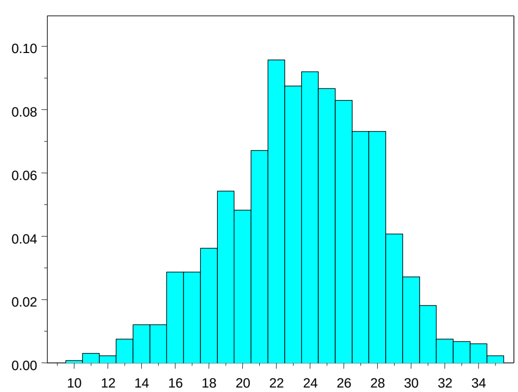

Figure E101. Frequency distribution of July maximum temperature for Fort Simpson, NT.

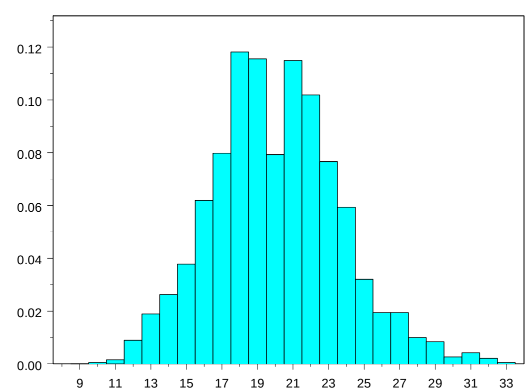

Figure E102. Frequency distribution of July maximum temperature for Sept-Iles, QC.

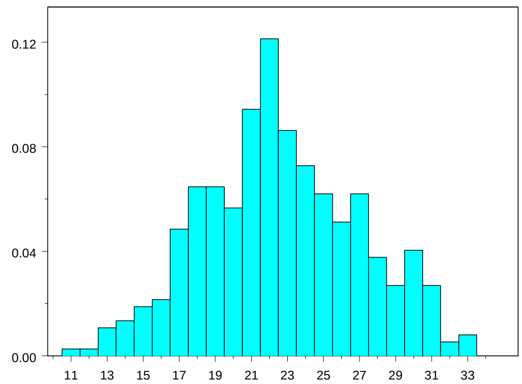

Figure E103. Frequency distribution of July maximum temperature for Chibougamou, QC.

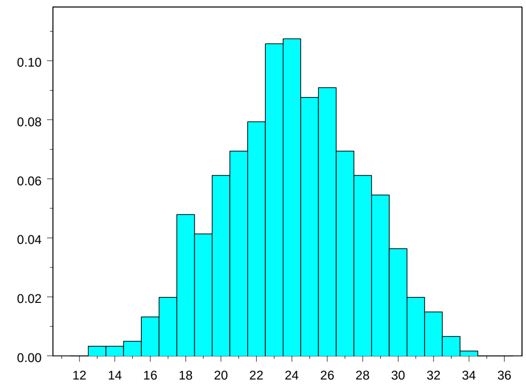

Figure E104. Frequency distribution of July maximum temperature for Jonquiere, QC.

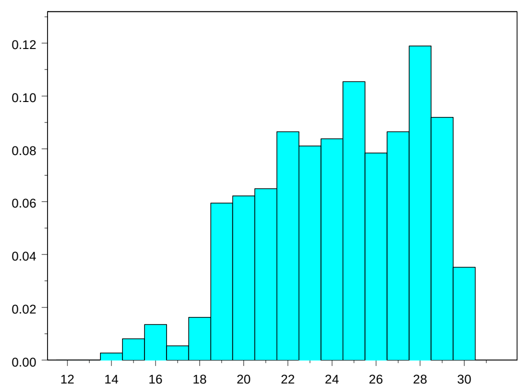

Figure E105. Frequency distribution of July maximum temperature for La Tuque, QC.

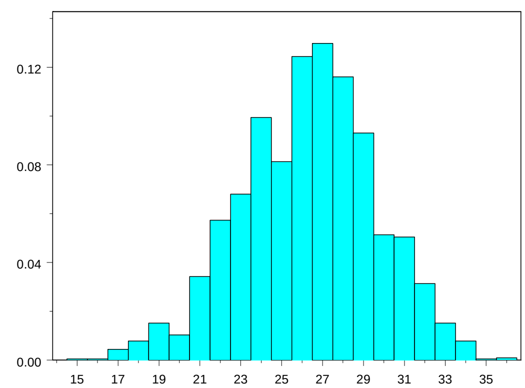

Figure E106. Frequency distribution of July maximum temperature for Montreal, QC.

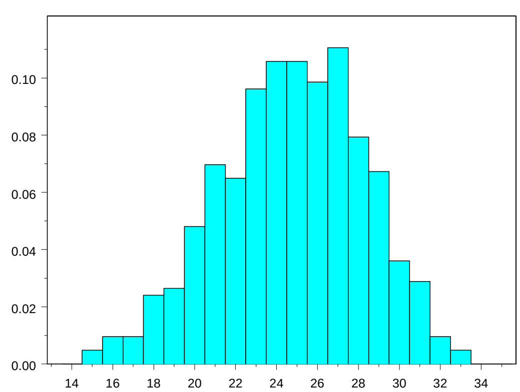

Figure E107. Frequency distribution of July maximum temperature for Quebec City, QC.

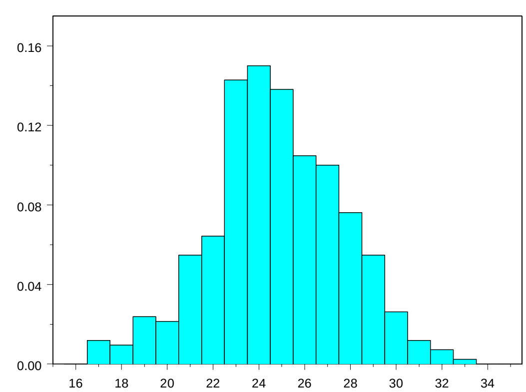

Figure E108. Frequency distribution of July maximum temperature for Trois Rivieres, QC.

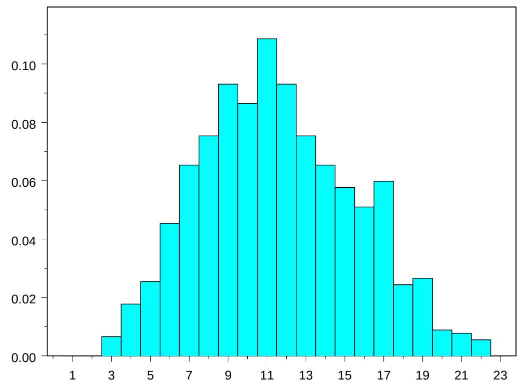

Figure E109. Frequency distribution of July maximum temperature for Cape Dorset, NU.

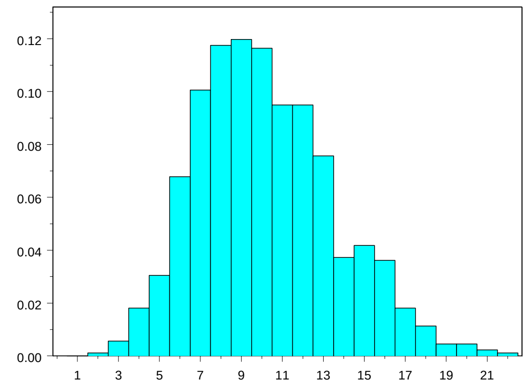

Figure E110. Frequency distribution of July maximum temperature for Pond Inlet, NU.

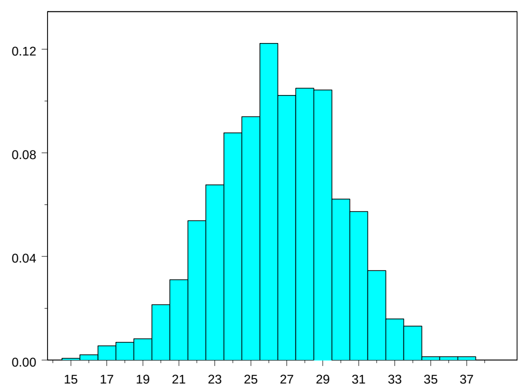

Figure E111. Frequency distribution of July maximum temperature for Hamilton, ON.

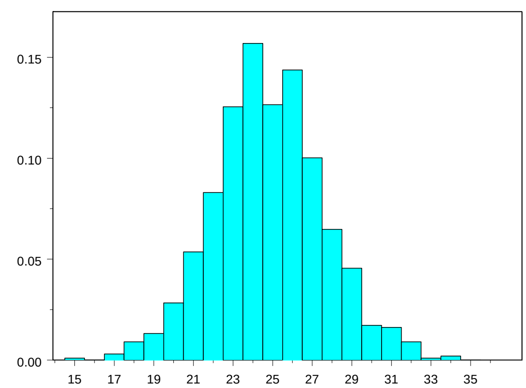

Figure E112. Frequency distribution of July maximum temperature for Kingston, ON.

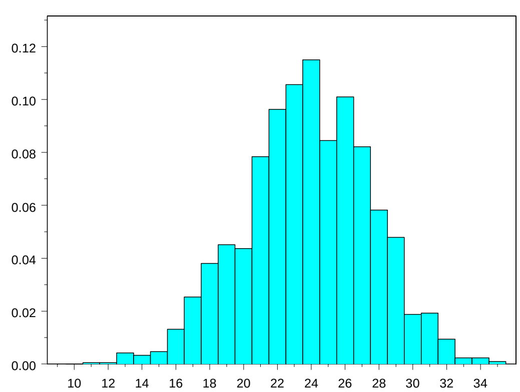

Figure E113. Frequency distribution of July maximum temperature for North Bay, ON.

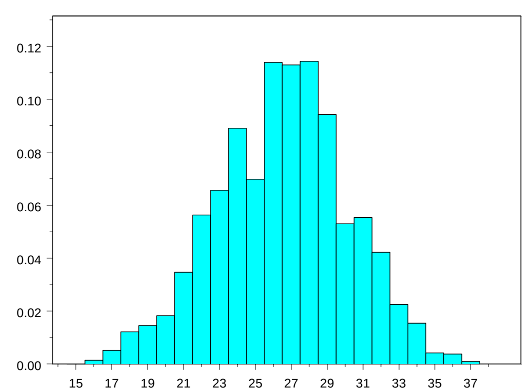

Figure E114. Frequency distribution of July maximum temperature for Ottawa, ON.

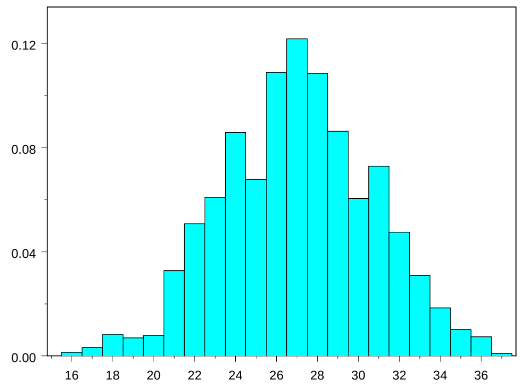

Figure E115. Frequency distribution of July maximum temperature for Toronto, ON.

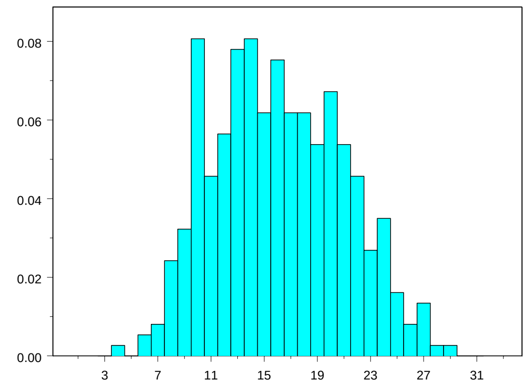

Figure E116. Frequency distribution of July maximum temperature for Inukjuak, QC.

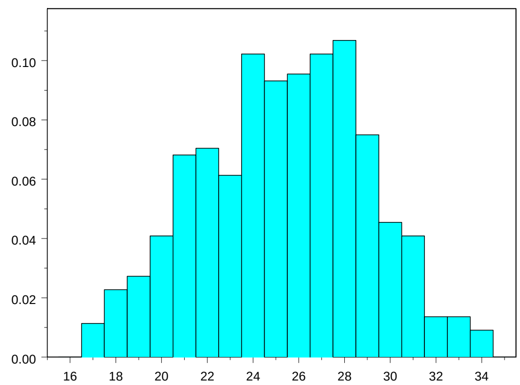

Figure E117. Frequency distribution of July maximum temperature for Maniwaki, QC.

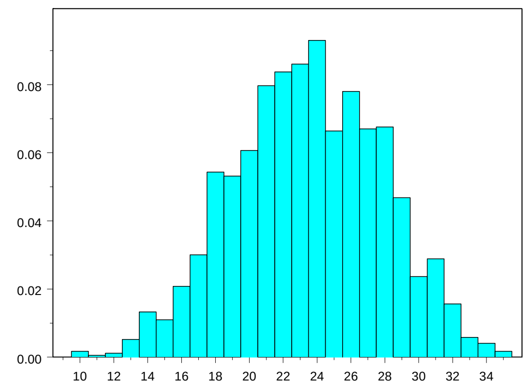

Figure E118. Frequency distribution of July maximum temperature for Val d'Or, QC.

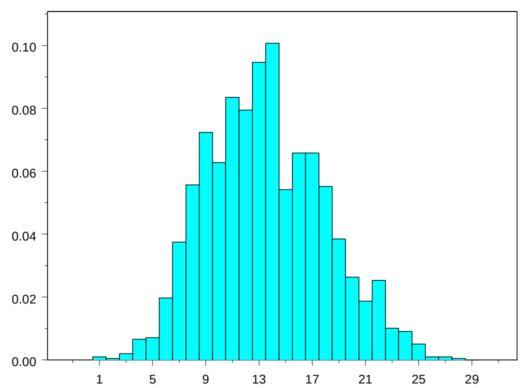

Figure E119. Frequency distribution of July maximum temperature for Coral Harbour, NU.

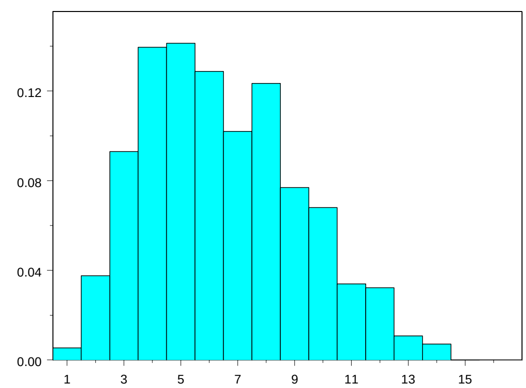

Figure E120. Frequency distribution of July maximum temperature for Grise Fiord, NU.

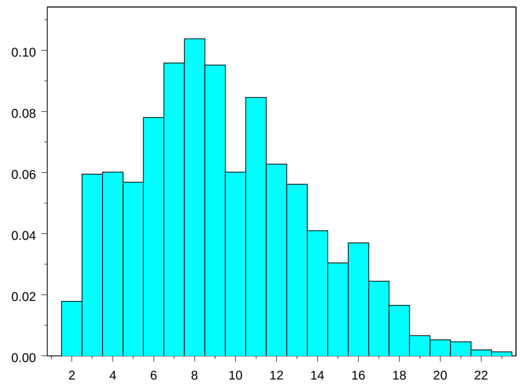

Figure E121. Frequency distribution of July maximum temperature for Hall Beach, NU.

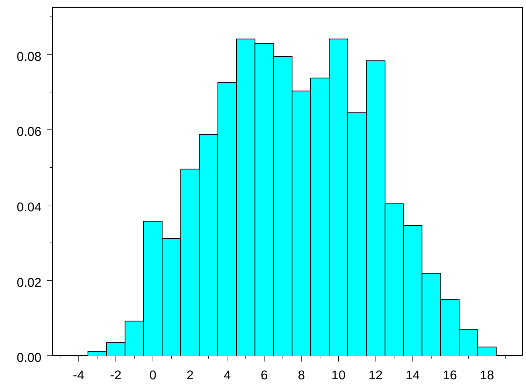

Figure E122. Frequency distribution of July maximum temperature for Nanisivik, NU.

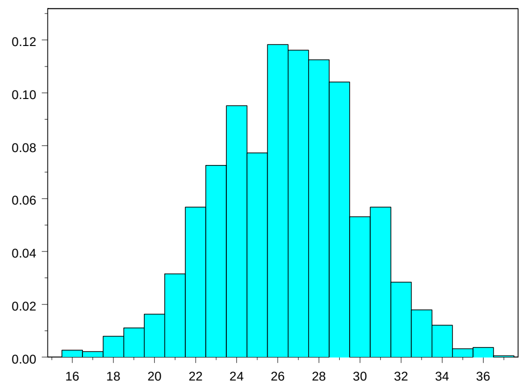

Figure E123. Frequency distribution of July maximum temperature for London, ON.

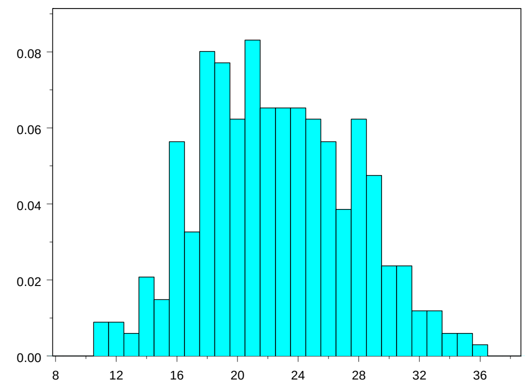

Figure E124. Frequency distribution of July maximum temperature for Moosonee, ON.

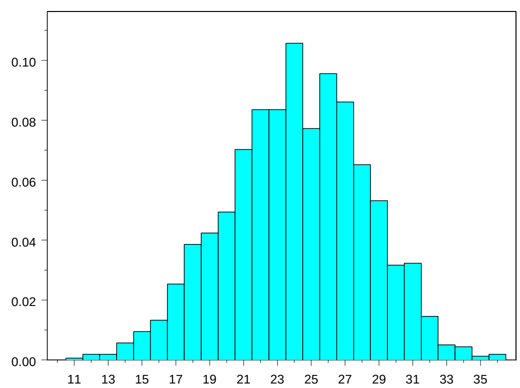

Figure E125. Frequency distribution of July maximum temperature for Sault Ste Marie, ON.

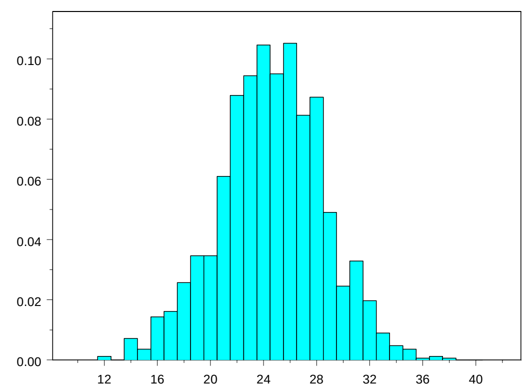

Figure E126. Frequency distribution of July maximum temperature for Sudbury, ON.

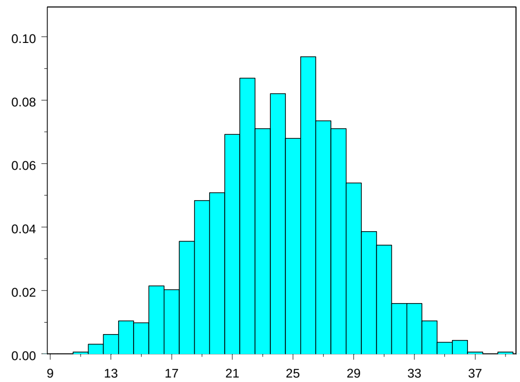

Figure E127. Frequency distribution of July maximum temperature for Timmins, ON.

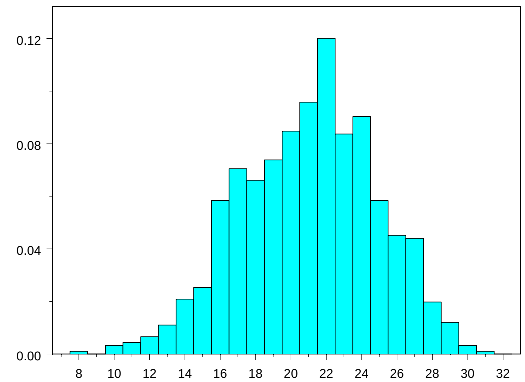

Figure E128. Frequency distribution of July maximum temperature for Wawa, ON.

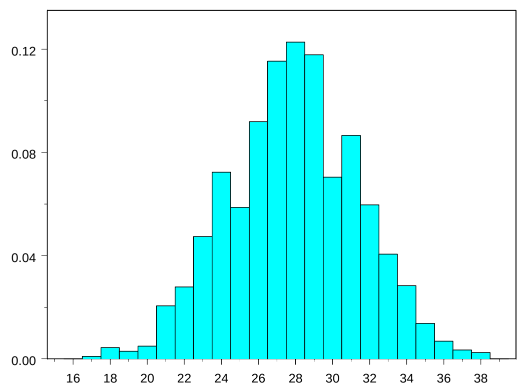

Figure E129. Frequency distribution of July maximum temperature for Windsor, ON.

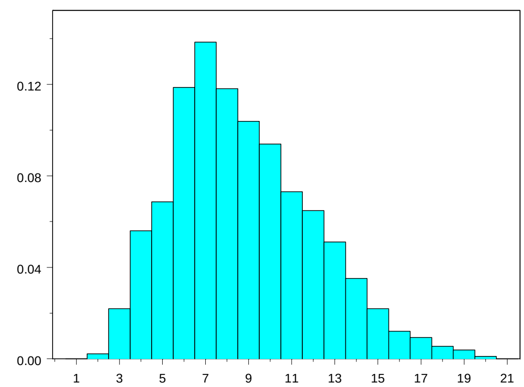

Figure E130. Frequency distribution of July maximum temperature for Eureka, NU.

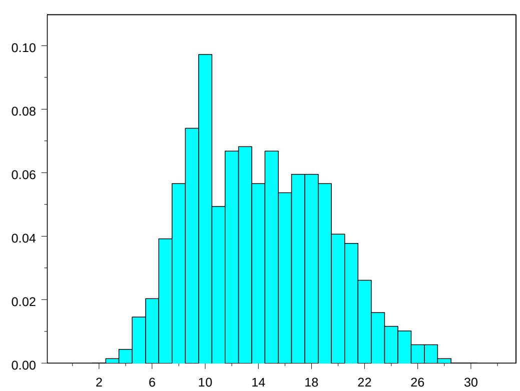

Figure E131. Frequency distribution of July maximum temperature for Kuugaruk, NU.

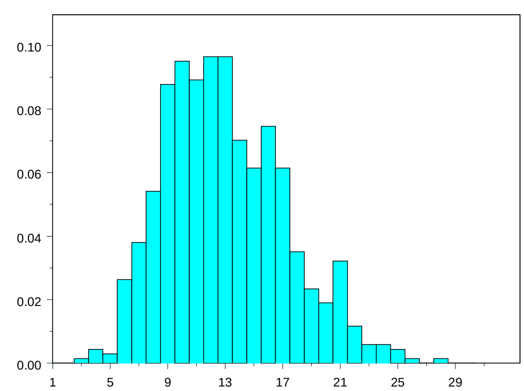

Figure E132. Frequency distribution of July maximum temperature for Repulse Bay, NU.

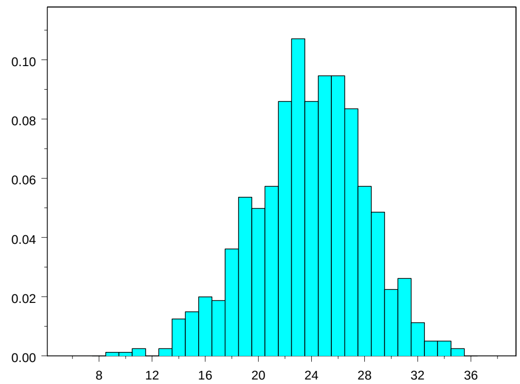

Figure E133. Frequency distribution of July maximum temperature for Geraldton, ON.

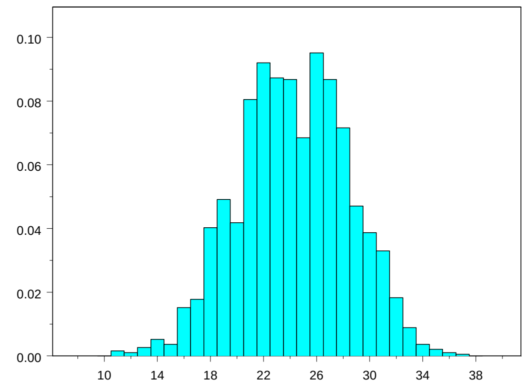

Figure E134. Frequency distribution of July maximum temperature for Thunder Bay, ON.

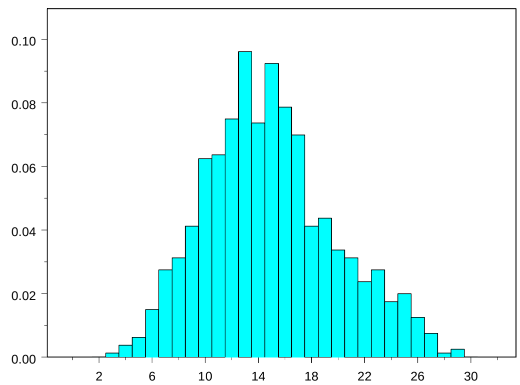

Figure E135. Frequency distribution of July maximum temperature for Rankin Inlet, NU.

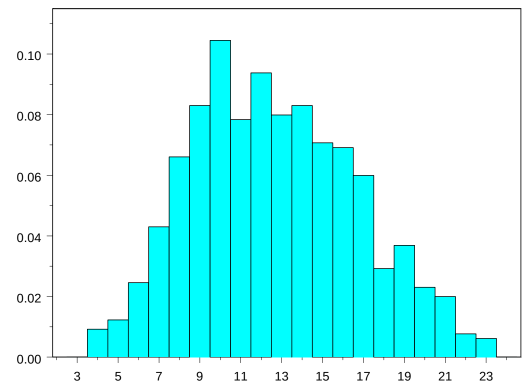

Figure E136. Frequency distribution of July maximum temperature for Taloyoak, NU.

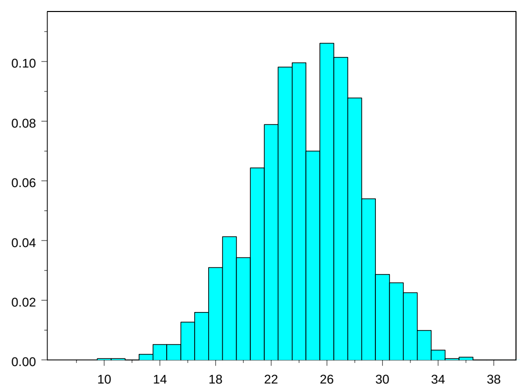

Figure E137. Frequency distribution of July maximum temperature for Kenora, ON.

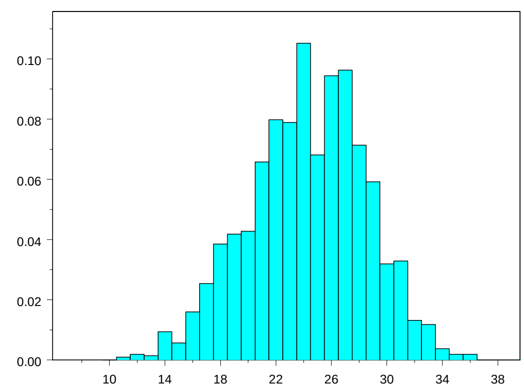

Figure E138. Frequency distribution of July maximum temperature for Sioux Lookout, ON.

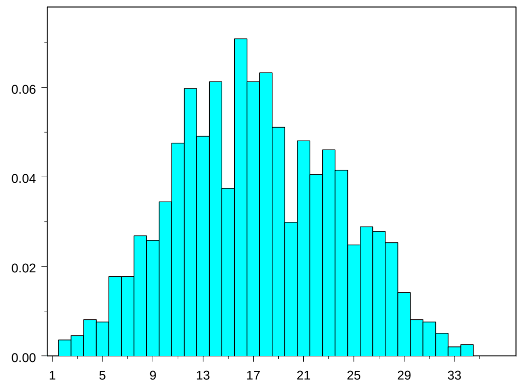

Figure E139. Frequency distribution of July maximum temperature for Churchill, MB.

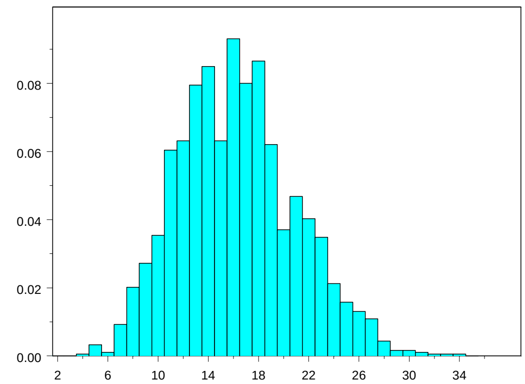

Figure E140. Frequency distribution of July maximum temperature for Baker Lake, NU.

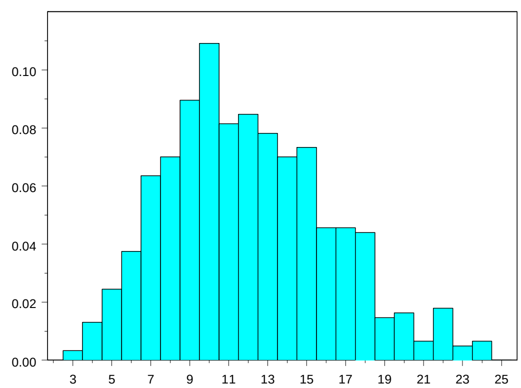

Figure E141. Frequency distribution of July maximum temperature for Gjoa Haven, NU

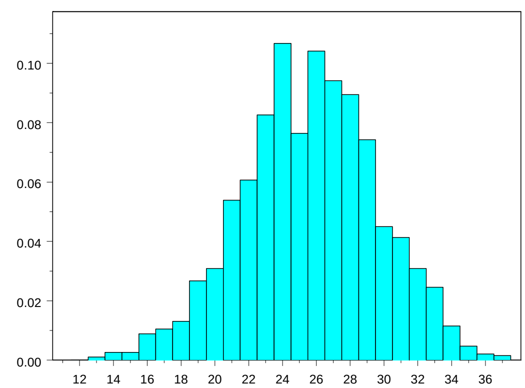

Figure E142. Frequency distribution of July maximum temperature for Brandon, MB.

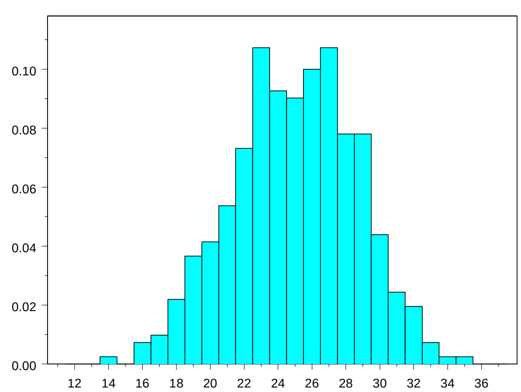

Figure E143. Frequency distribution of July maximum temperature for Gimli, MB.

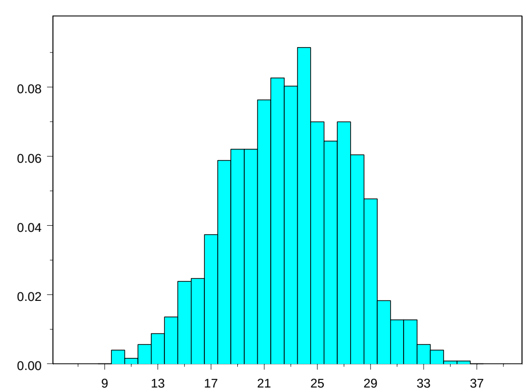

Figure E144. Frequency distribution of July maximum temperature for Thompson, MB.

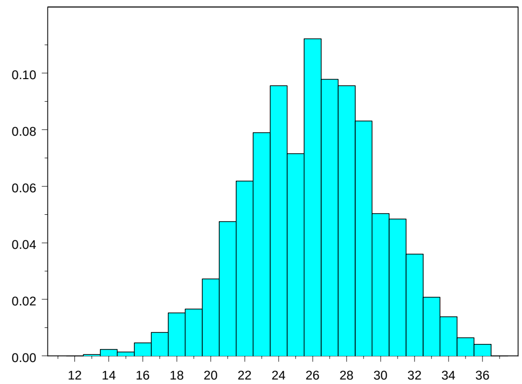

Figure E145. Frequency distribution of July maximum temperature for Winnipeg, MB.

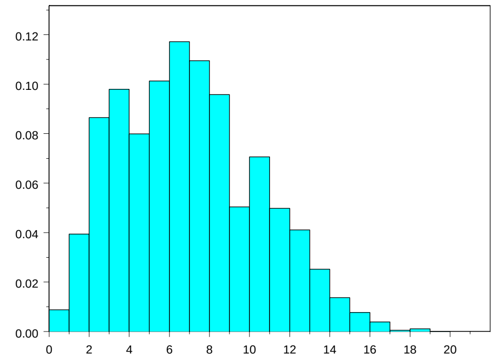

Figure E146. Frequency distribution of July maximum temperature for Resolute, NU

Appendix F – Other climate datasets

The following are additional climate data sets that are useful for analysis. These were used in order to learn more about climate data analysis.

F.1. North American Regional Reanalysis (NARR)

The dataset covers the period from 1979 to present. The data can easily be acquired from the NOAA operational model and distribution system (Nomads) server at http://nomads.ncdc.noaa.gov/data/narr/ using a shell script that was modified (Appendix H). For detailed information about the NARR see Mesinger (2006). NARR data can be easily mapped in GRADS or ArcGIS.

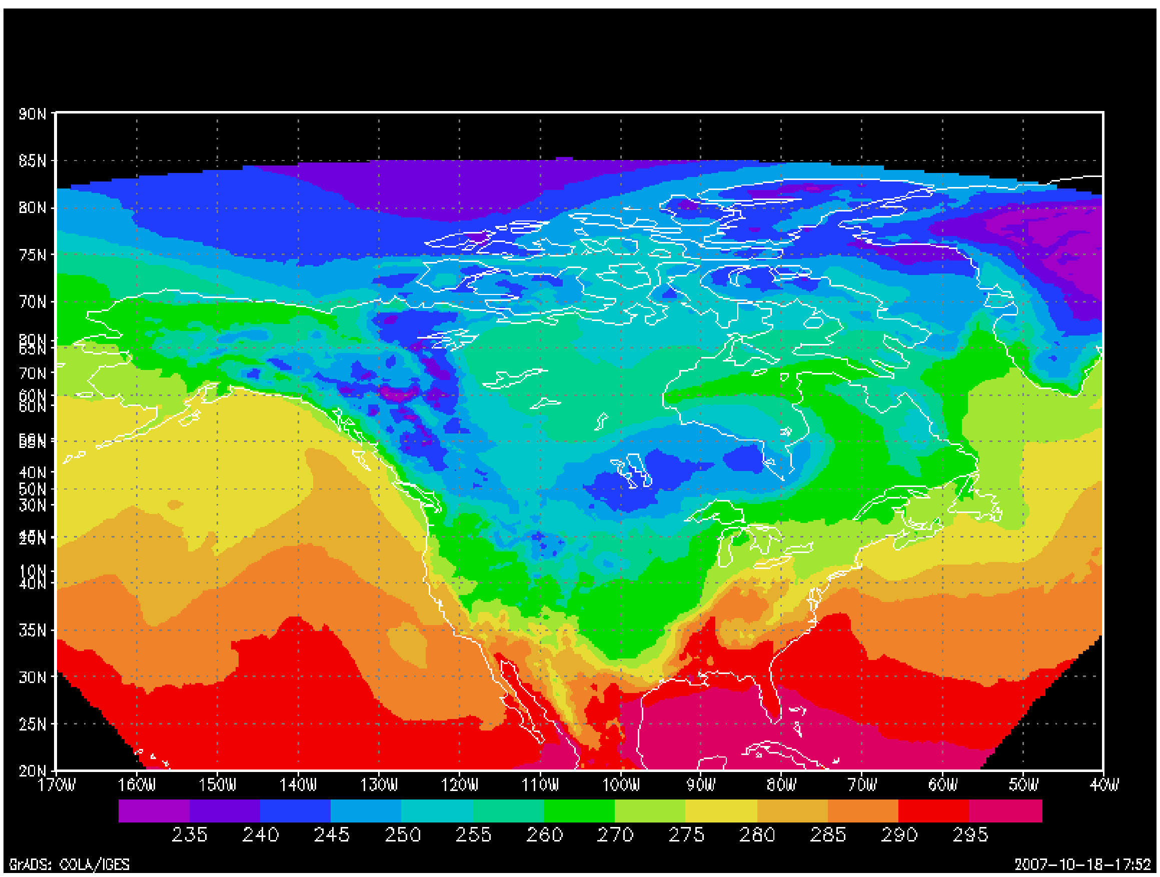

Figure F1. NARR 2m (surface) temperature data (values in K) plotted in GRADS.

F.2. NCEP DOE-II (R-2)

The NCEP Department of Energy (DOE) -II Reanalysis is the second reanalysis (R-2) with improvements and updates on the original NCEP/NCAR reanalysis, which was prone to human processing errors (Kanamitsu *et al*., 2002). This reanalysis covers the period from January 1979 to 2007. NCEP DOE-II data is provided by the NOAA/OAR/ESRL PSD, Boulder, Colorado, USA, from their web site at http://nomad3.ncep.noaa.gov/ncep_data/index.html. A sample control file created by a NOAA script (grib2ctl) shown below allows the grib file to be displayed using GRADS software.

F.2.1. Sample control file for a NCEP DOE-II grib file

```
dset ^../data/pgb.anl.200609.avrg.grib
index ^../data/pgb.anl.200609.avrg.idx
undef 9.999E+20
title ../data/pgb.anl.200609.avrg.grib
*  produced by grib2ctl v0.9.12.5p39a
dtype grib 2
options yrev
ydef 73 linear -90.000000 2.5
xdef 144 linear 0.000000 2.500000
tdef 1 linear 00Z01sep2006 1mo
*  z has 17 levels, for prs
zdef 17 levels
1000 925 850 700 600 500 400 300 250 200 150 100 70 50 30 20 10
vars 12
ABSVprs 17 41,100,0 ** (profile) Absolute vorticity [/s]
HGTsfc  0 7,1,0  ** surface Geopotential height [gpm]
HGTprs 17 7,100,0 ** (profile) Geopotential height [gpm]
PRATEsfc  0 59,1,0  ** surface Precipitation rate [kg/m^2/s]
PRESsfc  0 1,1,0  ** surface Pressure [Pa]
PRESmsl  0 1,102,0  ** unknown level Pressure [Pa]
PWATclm  0 54,200,0 ** atmos column Precipitable water [kg/m^2]
RHprs 17 52,100,0 ** (profile) Relative humidity [%]
TMPprs 17 11,100,0 ** (profile) Temp. [K]
UGRDprs 17 33,100,0 ** (profile) u wind [m/s]
VGRDprs 17 34,100,0 ** (profile) v wind [m/s]
VVELprs 17 39,100,0 ** (profile) Pressure vertical velocity [Pa/s]
ENDVARS
```

F.3. National Climatic Data Centre (NCDC)

The global summary of the day is a summary for data from additional stations that are not available through Environment Canada. The format of the data is CSV and stations can be located easily using the web mapping application available at http://lwf.ncdc.noaa.gov/oa/climate/climatedata.html. Again, a VBA script was used to extract the July data.

F.4. Tree-ring data

Tree ring chronologies enable researchers to determine the spatial changes in climate on annual to millennial timescales. Tree-ring data are provided by the International Tree Ring Data Base (ITRDB) stored at the World Data Center (WDC-A) for Paleoclimatology in Boulder, Colorado from their web site at http://hurricane.ncdc.noaa.gov/pls/paleo/fm_createpages.treering. The tree-ring data contain information on the annual growth increment of sampled trees, which is linked to climate variables such as monthly temperature and total precipitation, which are related to atmospheric circulation (Fritts, 1991). A tree-ring series can consist of as many as 40 separate cores taken from different trees at a site that have been subsequently checked for gross errors, combined, and cross-validated to create a single, composite series for that site (Fritts 1976). Scripts to read and format the tree-ring data were developed in SAS (Appendix H). These scripts facilitate statistical analysis of the data and the creation of an MS Access database. Although there are programs/scripts with this functionality, it was felt that writing these scripts would allow for a better understanding of the of the data structure.

F.5. July teleconnection data

The mean July values were used to compare the July atmospheric circulation with the position of the July Arctic front. The source of the SOI data is the Climate Research Unit at the University of East Anglia (Norwich, UK). The source of the AO data is the Joint Institute for the Study of the Atmosphere and Ocean (JISAO), between the University of Washington and the National Oceanic and Atmospheric Administration (NOAA).

Table F1. July AO and SOI values compared to the July Arctic front position anomaly.

	Anomaly (deg N)	July AO	July SOI
July_1954			0.4
July_1967	6.9	0.271	0
July_1989	5.9	0.97	1.4
July_1964	4.6	0.893	0.7
July_1981	4.1	0.607	1.2
July_1997	3.9	-0.208	-1.7
July_1959	2.5	0.198	-0.8
July_1970	2.3	0.219	-1
July_1961	2.2	-0.045	0.2
July_1984	1.8	0.052	0.1
July_1988	1.8	-0.095	1.7
July_1973	1.7	0.418	0.9
July_1952	1.5	0.58	0.7
July_2000	1.4	-0.569	-0.7
July_2001	1.2	0.069	-0.7
July_1963	1.1	-0.239	-0.5
July_1976	1.1	-0.055	-1.9
July_2002	1	NoData	-1.1
July_1990	0.9	-0.167	0.8
July_1979	0.6	0.137	2.2
July_1951	0.5	0.21	-2.3
July_1975	0.5	0.557	3.4

July_1974	0.5	0.439	1.9
July_1969	-0.1	0.458	-1.2
July_1960	-0.1	-0.512	0.6
July_1991	-0.1	-0.063	-0.2
July_1958	-0.1	-0.553	0.4
July_1986	-0.3	0.006	0.2
July_1962	-0.4	-0.903	-0.2
July_1980	-0.5	-0.506	-0.4
July_1956	-0.5	-0.16	1.7
July_1949	-0.5	0.08	NoData
July_1955	-0.7	0.63	2.7
July_1966	-0.8	0.099	-0.2
July_1983	-0.9	0.301	-1.3
July_1982	-1	0.192	-3.2
July_1985	-1.1	-0.298	-0.4
July_1998	-1.1	-0.245	2
July_1978	-1.3	-0.478	0.7
July_1965	-1.4	-0.473	-3.6
July_1999	-1.4	-0.003	0.8
July_1995	-1.5	-0.099	0.6
July_1971	-1.8	-0.409	0.1
July_1994	-1.8	0.508	-2.9
July_1948	-2	-0.06	NoData
July_1992	-2.4	0.284	-1.3
July_1953	-2.4	0.53	-0.2
July_1957	-2.6	-0.49	0.1
July_1968	-2.7	-0.594	1
July_1993	-2.8	-0.497	-1.8
July_1996	-3	0.759	1
July_1950	-3.2	-0.52	NoData
July_1977	-3.3	-0.432	-2.5
July_1987	-3.4	-0.297	-2.8
July_1972	-4.2	-0.453	-3.1

Appendix G – Additional maps, figures and discussion

G.1. An adaptation of Bryson’s original July streamline map

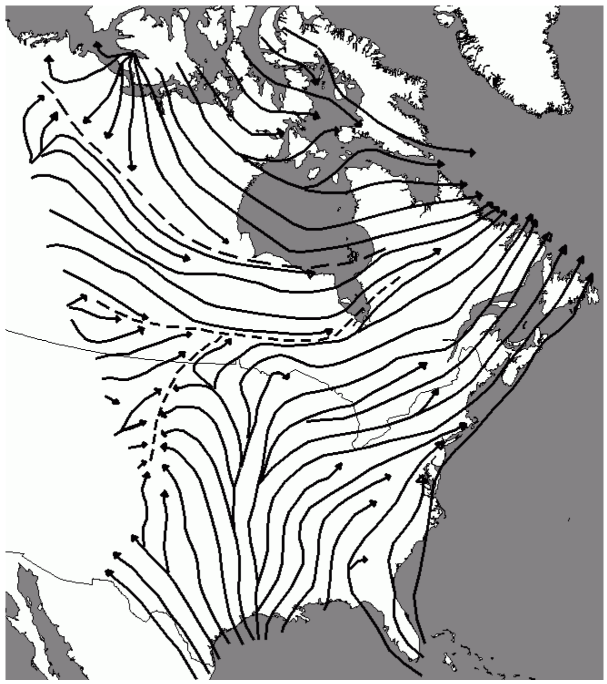

Figure G1. Bryson’s July streamline plot for 1948-1957 created using ArcGIS (adapted from Bryson, 1966)

In order to reproduce Bryson’s plot it was necessary to scan in the plot from the printed version of the publication. The scan was saved as an image and then added to an ArcGIS map document with a shape file of the world loaded in the same projection as Bryson’s plot (Lambert Conformal Conic). The next step was to georeference the North American boundaries in the image to the world shape file (zoomed in on North America). Then the transparency of the image was set to 30%. A new line shape file was created and edited by tracing Bryson’s streamlines as accurately as possible. The result is a close reproduction of Bryson’s original plot.

G.2. Wind direction maps from NNR

Mean wind direction anomaly maps for July 1948 to 2007 (derived from NNR) using the method in Appendix H. Only the map for July 2007 is shown (Figure G2) along with the long term mean wind direction (Figure G3). South (north) of the front the mean July wind direction should have southerly (northerly) component.

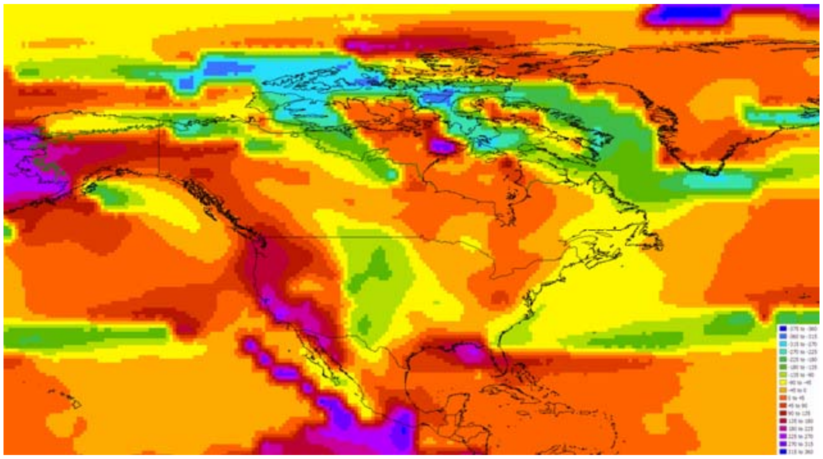

Figure G2. Wind direction anomaly map (derived from NNR) for July 2007.

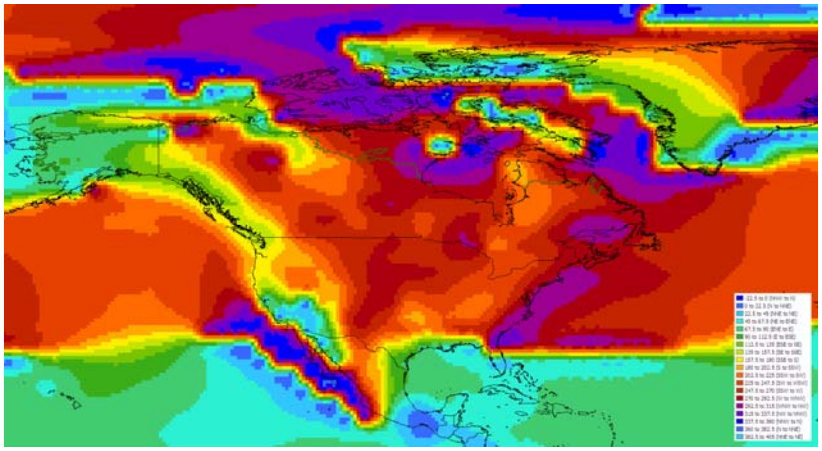

Figure G3. July long term mean wind direction (derived from NNR) for 1948-2007.

Appendix H - Scripts and programs

H.1. Scripts developed by this thesis

H.1.1. Unix scripts

GRADS and VCDAT were not able to read the control files (.ctl) associated with the grib (.grb) files on the NCEP/NCAR reanalysis CD-ROMs. Thus new control files were created using the following series of scripts: list_grb.sh, process_all.awk and awkoutput.sh.

(1) script: list_grb.sh

This script basically lists all of the grib files in specified directories and writes the list to a text file called gribfiles.txt

```
ls /home/lpc/Desktop/cd_feb2001/clim79-98/*.GRB
/home/lpc/Desktop/cd_feb2001/monthly/*.GRB /home/lpc/Desktop/cd_feb2001/data/*.GRB
/home/lpc/Desktop/cd_feb2001/obs/*.GRB /home/lpc/Desktop/cd_feb2001/obs/cdiv/*.GRB
/home/lpc/Desktop/cd_mar1996/climate/*.GRB /home/lpc/Desktop/cd_mar1996/fixed/*.GRB
/home/lpc/Desktop/cd_mar1996/daily/*.GRB /home/lpc/Desktop/cd_mar1996/monthly/*.GRB
/home/lpc/Desktop/cd_mar1996/observed/*.GRB >
/home/lpc/Desktop/ML/scripts/shell/gribfiles.txt
```

(2) script: process_all.awk

This script will build a list of commands for each file to create a .ctl file for each grib file using grib2ctl.pl then run gribmap (part of GRADS) to create an index file when a control file is associated with a grib file. This script is run at the command line to redirect the output to a shell script:

```
awk -f process_all.awk gribfiles.txt > awkoutput.sh

# start of script
{
print  "/home/lpc/Desktop/GRADS/grib2ctl.pl " $1 " > " $1 ".ctl"
print  "/home/lpc/Desktop/GRADS/bin/gribmap -v -i " $1 ".ctl"
}
```

(3) script: awkoutput.sh

This script will create a .ctl file for each grib file using grib2ctl then run gribmap to create an index file when a control file is associated with a grib file. Only a subset of the file is shown below.

```
/home/lpc/Desktop/GRADS/grib2ctl.pl /home/lpc/Desktop/cd_feb2001/clim79-98/HGT.GRB >
/home/lpc/Desktop/cd_feb2001/clim79-98/HGT.GRB.ctl
/home/lpc/Desktop/GRADS/bin/gribmap -v -i /home/lpc/Desktop/cd_feb2001/clim79-
98/HGT.GRB.ctl
/home/lpc/Desktop/GRADS/grib2ctl.pl /home/lpc/Desktop/cd_feb2001/clim79-98/LHTFL.GRB >
/home/lpc/Desktop/cd_feb2001/clim79-98/LHTFL.GRB.ctl
/home/lpc/Desktop/GRADS/bin/gribmap -v -i /home/lpc/Desktop/cd_feb2001/clim79-
98/LHTFL.GRB.ctl
```

(4) script: selyears_era40.awk

```
################################################################
#selyears_era40.awk
{
print  "./cdo selyear," $1 " /mnt/removable/CLIMATE_DATA/REANALYSIS_DATA/ERA-
40/grib/vert_velocity_850gph/july_vert_velocity_850gph_1958-2002.grib
/home/lpc/Desktop/Working/output/monthly/vv850/july_vert_velocity_850gph_" $1 ".grib"
# repeat statement for additional months
}
```

(5) script: ymonmean_era40.awk

```
################################################################
# ymonmean_era40.awk
{
print  "./cdo ymonmean /home/lpc/Desktop/output/monthly/500hgt/july_500hgt_" $1 ".grib
/home/lpc/Desktop/output/monthly/500hgt/july_mean_500hgt_" $1 ".grib"
# repeat statement for additional months
}
```

(6) script: process_all.awk (revised version)

```
################################################################
# process_all.awk (revised version)
# start of script
# to get gribfiles.txt run the following unix command:
# ls /home/lpc/Desktop/Working/output/monthly/div850/july/*.grib > gribfiles.txt
# this file will contain the full paths to the grib files to be processed
```

```
# usage: awk -f process_all.awk gribfiles.txt > awkoutput.sh
{
print  "./grib2ctl " $1 " > " $1 ".ctl"
print  "./gribmap -v -i " $1 ".ctl"
}
```

(7) script: ncep_mean_july_streamlines.gs

```
*Filename: ncep_mean_july_streamlines.gs

*Author: Matthew Ladd, Laboratory for Paleoclimatology and Climatology

*Date modified: April 21, 2008

*Requirements:
*All NCEP monthly (July) mean 10m wind component files in NetCDF (.nc) format.

*Description:
*This is a script to loop through the NCEP Mean July 10m wind component files (1948-2007)
*and for each file make a nice plot for July of each year of the mean streamlines.


******************Variables to be modified*********************

*dataset name
datname = "NCEP"

*zonal wind component is uwnd
*meridional wind component is vwnd

*do not worry about time steps since files are already monthly means

*For ERA-40 dataset the starting year for Jan to Aug data is 1958
*NOTE: If month of interest is Sep, Oct, Nov, or Dec change starting year to 1957
yr = 1958


* Setup the months for the plot titles
t.1="January"
t.2="February"
t.3="March"
t.4="April"
t.5="May"
t.6="June"
t.7="July"
t.8="August"
t.9="September"
t.10="October"
t.11="November"
t.12="December"

* Setup the months for the file names
n.1="jan"
n.2="feb"
n.3="mar"
n.4="apr"
n.5="may"
n.6="jun"
n.7="jul"
n.8="aug"
n.9="sep"
n.10="oct"
n.11="nov"
n.12="dec"
```

```
* the directory where all of the monthly mean files are located
indir = "/home/lpc/Desktop/ml/wind_monthly_means/july/"

* image files will start with this name
outplot = "/home/lpc/Desktop/ncep/ncep_streamlines_"


* starting values for month of interest (change m to month of interest)
m = 7
t = 1

***********************************************************************

* change this if newer data is required
while (yr <= 2007)

* file name example is wndcmp.jul.1952.mon.mean.nc
infile = indir % "wndcmp." % n.m % "." % yr % ".mon.mean.nc"

* NetCDF file so use proper command
'sdfopen 'infile''

* set the area of the plot here
'set lat 20 90'
'set lon -170 -40'

* change projection here (options are latlon, nps, ...)
'set mproj latlon'

* use stream for streamlines, or vector for wind vectors
'set gxout stream'

* default value is 5
'set strmden 6'

* ensure the map background is set
'set mpdraw on'
'set map auto'
'set poli on'

* magnitude function will colorize the wind vectors
'd uwnd;vwnd;mag(uwnd,vwnd)'

* this ensures the plot has a legend
'run /home/lpc/Desktop/ml/scripts/grads/cbar.gs'

* this is the title of the plot
'Draw Title 'datname' Mean 't.m' Surface Streamlines (in m/s) for 'yr''

* x is plot width, y is plot height
'printim 'outplot''t.m''yr'.gif x800 y600 black'
'printim 'outplot''t.m''yr'_v2.gif x800 y600 white'
*'disable printim'
'clear'

'close 1'

yr = yr + 1


endwhile

************************END OF SCRIPT**************************************
```

(8) script : windcomp_era40_ltmean.gs (GRADS script)

```
***********************************************************************
*Filename: windcomp_era40_ltmean.gs (GRADS script)

*Author: Matthew Ladd, Laboratory for Paleoclimatology and Climatology
```

```
*Date modified: November 29, 2007

*Requirements:
*All ERA-40 monthly 10m wind component files in a single directory (converted to Grads
format).
*e.g. jan_windcomp10m_1958-2002.dat, jan_windcomp10m_1958-2002.ctl
*This can be done by opening the grib file in XConv and converting the file

*Description:
*This is a script to loop through the ERA-40 monthly 10m wind component files
*and for each file make 2 plots of the mean wind component vectors or streamlines for all
ERA-40 years.


*********************Variables to be modified*************************

*dataset name
datname = "ERA-40"

*zonal wind component
uwnd = "u10"

*meridional wind component
vwnd = "v10"

*starting time step for monthly avg is always 1
tstart = 1

*ending time step for monthly avg depends on number of timesteps in a month x 45 years
*e.g. - July has 4x daily x 31 days = 124 timesteps x 45 yrs = 5580 timesteps
*this will be set later on in the script
tend = 5580


* Setup the months for the plot titles
t.1="January"
t.2="February"
t.3="March"
t.4="April"
t.5="May"
t.6="June"
t.7="July"
t.8="August"
t.9="September"
t.10="October"
t.11="November"
t.12="December"

* Setup the months for the file names
n.1="jan"
n.2="feb"
n.3="mar"
n.4="apr"
n.5="may"
n.6="june"
n.7="july"
n.8="aug"
n.9="sep"
n.10="oct"
n.11="nov"
n.12="dec"


* the directory where all of the control files are located
indir = "/mnt/removable-2/CLIMATE_DATA/REANALYSIS_DATA/ERA-40/grib/OUTPUT/windcomp/"

* image files will start with this name
outplot = "/home/lpc/Desktop/era40windcomp/era40windcomp"

* starting values for month of interest
```

```
m = 1

**********************************************************************

* Loop through all the monthly long term mean files
while (m <= 12)

* need to set ending timestep based on current month
if (m = 4 | m = 6 | m = 9 | m = 11)
   tend = 5400
endif

if (m = 2)
   tend = 5084
endif

if (m < 9)
   infile = indir % n.m % "_windcomp10m_1958-2002"
else
   infile = indir % n.m % "_windcomp10m_1957-2001"
endif

'open 'infile''

* set the area of the plot here
* for a global plot comment the following two lines
'set lat 20 90'
'set lon -170 -40'

* change projection here (options are latlon, nps, ...)
'set mproj latlon'

* use stream for streamlines, or vector for wind vectors
'set gxout stream'

* default value is 5
'set strmden 5'

* ensure the map background is set
'set mpdraw on'
'set map auto'
'set poli on'

* calculate monthly avg for each month of wind comp data.
'define u10ave=mean(u10,t='tstart',t='tend')'
'define v10ave=mean(v10,t='tstart',t='tend')'

* magnitude function will colorize the wind vectors
'd u10ave;v10ave;mag(u10ave,v10ave)'

* this ensures the plot has a legend
'run /home/lpc/Desktop/Working/programs/scripts/grads/cbar.gs'

* modify this to change the title of the plot
if (m < 9)
   'Draw Title Mean 't.m' 'datname' 10m Streamlines (in m/s) 1958-2002'
else
   'Draw Title Mean 't.m' 'datname' 10m Streamlines (in m/s) 1957-2001'
endif

* x is plot width, y is plot height, background is black or white
'printim 'outplot''t.m'.gif x800 y600 black'
'printim 'outplot''t.m'_v2.gif x800 y600 white'
*'disable printim'
'clear'

'close 1'

m = m + 1
```

```
endwhile

********************END OF SCRIPT******************************
```

(9) script: output_getNARRdata_script.awk

```
################################################################
# Name: output_getNARRdata_script.awk
#
# Author: Matthew Ladd, Laboratory for Paleoclimatology and Climatology
#
# Modified: July 27, 2007
#
# Description: This script will output the code (shell script) neccessary to download a
specific
# variable from the North American Regional Renanalysis (NARR) dataset
#
# Usage: awk -f output_getNARRdata_script.awk narr_years.txt > getNARRdata.sh
################################################################

# format of variables in output must be as follows:
# yymm=197901
# date=19790101
# hr=00

# start of script
BEGIN {
# header information and comments for script
print "#!/bin/sh"
print "# Download selected variable (GFLUX) from NARR merged-a dataset at NCDC"
print "\n"
}

{

yymm = ""
date = ""
hr = ""

m = 0
d = 0
h = 0

# WARNING: specifying all years from 1979 to 2007 will create a text file over 300 MB!
# It is better to use a subset of the period  (e.g. 1985 to 1990) defined in
narr_years.txt

for (yr=$1; yr<=1979; yr++)
{
```

```
  for (m=1; m<=12; m++)
  {
     # ensure leading zero is added
     if (m < 10)
     {
       mm = "0" m
     }
     else
     {
       mm = m
     }
     # check for month to set the number of days (n)
     if (m == 4 || m == 6 || m == 9 || m == 11 )
     {
        n = 30
     }
     else if (m == 2)
     {
        # deal with leap years here
        if (yr == 1980 || yr == 1984 || yr == 1988 || yr == 1992 || yr == 1996 || yr ==
2000 || yr == 2004)
       {
           n = 29
        }
        else  # not a leap year
        {
           n = 28
        }
     }
     else
     {
        n = 31
     }

     for (d=1; d<=n; d++)
     {
        # ensure leading zero is added
        if (d < 10)
       {
          dy = "0" d
        }
       else
        {
          dy = d
        }

        # timesteps for NARR are every 3 hrs
       for (h=0; h<24; h=h+3)
```

```
        {
           # ensure leading zero is added
           if (h < 10)
          {
             hr = "0" h
           }
          else
           {
             hr = h
           }

          # ensure these are formatted properly
           date = yr mm dy
           yymm = yr mm

           # output the values
           print "yymm=" yymm
           print "date=" date
           print "hr=" hr
           print "\n"

          # NOTE: variable of interest is GFLUX (ground heat flux)
          # When changing the variable, check the NARR documentation to get the correct
abbrieviation for the variable
           # Also, it is wise to run one command in the terminal file to check to make
sure the code is correct

           print "a=\"http://nomads.ncdc.noaa.gov/data/narr/" yymm "/" date "/narr-
a_221_" date "_" hr "00_000\""
           print "/home/lpc/Desktop/Working/programs/scripts/get_inv.pl $a.inv | egrep
\":(GFLUX)\" | /home/lpc/Desktop/Working/programs/scripts/get_grib.pl $a.grb
/home/lpc/Desktop/temp/NARR_GFLUX_" date "_" hr "00.grb"
           print "echo \"Finished downloading NARR GFLUX data [year:" yr " month:" mm "
hour:" hr "z]\""
          print "\n"
        }
     }
  }
}

}

END {
}
```

H.1.2. VBA scripts used in Excel

Script 1: This script formats data into a continuous series. For example, the input worksheet has rows for each year and columns for each month with the data values in each intersecting cell. The output worksheet will have two columns with each row having (year + fraction of year) in the cell of the first column and the corresponding data value in each cell of the second column.

```
Sub format_data()

    ' Developed by Matthew Ladd (LPC) fall of 2007.



    Dim basebook, newbook As Workbook
    Dim curCol, lastCol, curRow, lastRow, curYear, yrCount As Long
    Dim curMon, curYearVal As Single
    Dim cellVal, cRef As String

    curRow = 2
    yrCount = 0
    lastCol = 13

    lastRow = GetLastUsedCell(1)

    Set basebook = ThisWorkbook

    MsgBox "Ensure sheet to be processed is the first worksheet of the workbook " &
vbCrLf & "and that sheet2 is empty"

    Do While curRow <= lastRow

        cRef = "A" & curRow
        curYear = basebook.Worksheets(1).Range(cRef).Value

        curCol = 2

        Do While curCol <= lastCol

        If curCol = 2 Then
            curMon = 0.5 / 12
        ElseIf curCol = 3 Then
            curMon = 1.5 / 12
        ElseIf curCol = 4 Then
            curMon = 2.5 / 12
        ElseIf curCol = 5 Then
            curMon = 3.5 / 12
        ElseIf curCol = 6 Then
            curMon = 4.5 / 12
        ElseIf curCol = 7 Then
            curMon = 5.5 / 12
        ElseIf curCol = 8 Then
            curMon = 6.5 / 12
        ElseIf curCol = 9 Then
            curMon = 7.5 / 12
        ElseIf curCol = 10 Then
            curMon = 8.5 / 12
        ElseIf curCol = 11 Then
            curMon = 9.5 / 12
        ElseIf curCol = 12 Then
            curMon = 10.5 / 12
        ElseIf curCol = 13 Then
```

```
            curMon = 11.5 / 12
        End If

        curYearVal = curYear + curMon

        basebook.Worksheets(2).Range("A" & yrCount + 1).Value = curYearVal

        cellVal = basebook.Worksheets(1).Cells(curRow, curCol).Value
        basebook.Worksheets(2).Range("B" & yrCount + 1).Value = cellVal

        curCol = curCol + 1
        yrCount = yrCount + 1

        Loop

    curYear = curYear + 1
    curRow = curRow + 1

    Loop

    MsgBox "Done! Formatted data is in the second worksheet"

End Sub
```

Script 2: The script formats gridded climate data opened with XConv into a format which can be x-y mapped in ArcMap.

```
Sub output_values()


    'Created by Matthew Ladd (LPC), modified on November 30, 2007
    'Notes: each year should be on a separate worksheet with data imported from XConv
output
    'Lat values are in column A and EQ and Lon values are in row 1 and should range from
0 to 180 then -177.5 to 0

    Dim basebook, newbook As Workbook
    Dim curCol, lastCol, curRow, lastRow As Long
    Dim curWS, lastWS, wsLast, wsCount, dCount, rowPos, colPos As Long
    Dim cellVal, c0, c1, c2, ctot, tempVal, tempVal2, tempDiff, tempDiffPerKm, latVal,
lonVal As Single
    Dim cellRef As String


    Set basebook = ThisWorkbook

    wsCount = basebook.Sheets.Count ' number of years

    lastWS = wsCount
    wsLast = wsCount - 1

    ' this is the worksheet with the long term mean values (over 45 years)
    curWS = 45

    curRow = 35  ' difference values start at this row
    lastCol = 145  ' last column of data values - col 147 has latitude values

    rowPos = 65  ' start output of formatted data in this row

    lastRow = GetLastUsedCell(1)

    MsgBox "Ensure the last sheet avg has the avg values starting at row 3, difference
values starting at row 35, lat values in row 1, and lon values in column A and EQ."

    Do While curRow <= lastRow

        curCol = 2  ' data values start in this column

        Do While curCol <= lastCol
```

```
            curWS = 45  'this needs to be set each time through the loop

            ' prevent runaway script
            ' Note: the 4097 rows assume that you're using an area 20N to 90N
            Do While curWS <= lastWS And rowPos < 4097

                cellVal = basebook.Worksheets(curWS).Cells(curRow, curCol).Value
                'convert temp values from K to C
                'basebook.Worksheets(curWS).Cells(curRow, curCol).Value = cellVal -
273.15
                latVal = basebook.Worksheets(curWS).Cells(curRow, 147).Value
                lonVal = basebook.Worksheets(curWS).Cells(1, curCol).Value

               ' this is where we write the lat & lon values
                basebook.Worksheets(curWS).Cells(rowPos, 1).Value = latVal
                basebook.Worksheets(curWS).Cells(rowPos, 2).Value = lonVal

                'basebook.Worksheets(wsLast).Cells(rowPos, 6).Value = lastWS

                colPos = 3  'write difference values starting in this column

                    'If curRow = 3 Then
                    '   basebook.Worksheets(wsLast).Cells(rowPos, colPos).Value = 0
                    'Else

                       'tempVal = basebook.Worksheets(curWS).Cells(rowPos, colPos).Value
                       'tempVal2 = basebook.Worksheets(curWS).Cells(rowPos - 1,
colPos).Value
                       'tempDiff = tempVal - tempVal2
                       'tempDiffPerKm = tempDiff / 111
               ' here is where we output the difference value
                basebook.Worksheets(curWS).Cells(rowPos, colPos).Value = cellVal

                    'End If

                'If cellVal = 0 Then

                '    colPos = 3
                '    tempVal = basebook.Worksheets(wsLast).Cells(rowPos, colPos).Value
                '    basebook.Worksheets(wsLast).Cells(rowPos, colPos).Value = 1 +
tempVal

                'ElseIf cellVal > 0 Then

                '    colPos = 4
                '    tempVal = basebook.Worksheets(wsLast).Cells(rowPos, colPos).Value
                '    basebook.Worksheets(wsLast).Cells(rowPos, colPos).Value = 1 +
tempVal

                'Else 'cellVal < 0

                '    colPos = 5
                '    tempVal = basebook.Worksheets(wsLast).Cells(rowPos, colPos).Value
                '    basebook.Worksheets(wsLast).Cells(rowPos, colPos).Value = 1 +
tempVal
                '
                'End If

                'c0 = basebook.Worksheets(wsLast).Cells(rowPos, 3).Value
                'c1 = basebook.Worksheets(wsLast).Cells(rowPos, 4).Value
                'c2 = basebook.Worksheets(wsLast).Cells(rowPos, 5).Value

                'ctot = basebook.Worksheets(wsLast).Cells(rowPos, 6).Value

                'basebook.Worksheets(wsLast).Cells(rowPos, 8).Value = c0 / ctot
                'basebook.Worksheets(wsLast).Cells(rowPos, 9).Value = c1 / ctot
                'basebook.Worksheets(wsLast).Cells(rowPos, 10).Value = c2 / ctot

                curWS = curWS + 1

            Loop
```

```
        rowPos = rowPos + 1
        curCol = curCol + 1

        Loop

    curRow = curRow + 1

    Loop

    'MsgBox "Done! Probability table is in the last worksheet"
    MsgBox "Task completed!  Be sure to save output to a separate workbook and save as a
CSV with headers lat, lon, val for ArcMap."

End Sub
```

Script 3: This script extracts July data from merged ENV CAN climate data files in csv format.

```
Sub extractJulyData()

Dim wb As Workbook
Dim basebook As Workbook
Dim mybook As Workbook
Dim sourceRange As Range
Dim destrange As Range
Dim num As Long
Dim cCount As Long
Dim i, a As Long
Dim cValue As String
Dim strMonth, strMid

Const BottomRowNum = 65536

rCount = GetLastUsedCell(4)
'MsgBox "last used cell is " & rCount

Set basebook = ThisWorkbook

rnum = 1
cCount = 1

' copy header first
Set sourceRange = basebook.Worksheets(1).Rows(cCount & ":" & 10)
With sourceRange
    Set destrange = basebook.Worksheets(2).Cells(rnum, 1).Resize(.Rows.Count,
.Columns.Count)
End With
destrange.Value = sourceRange.Value

' data values start in row 11
rnum = 11
cCount = 11

' get the values for field Month (col C) and determine if MM = 7
' if so copy entire row to new workbook

Do While cCount <= rCount
    'strDate = Range("C" & cCount).Value
    cValue = "C" & cCount
    strMid = Worksheets(1).Range(cValue).Value
    'MsgBox "strMid is " & strMid
    If cCount < 10 Then
```

```
        strMonth = Mid(strMid, 1, 1)
    Else
        strMonth = Mid(strMid, 1, 2)
    End If
    'MsgBox "month is " & strMonth
    If strMonth = 7 Then
        ' copy row values here
        Set sourceRange = basebook.Worksheets(1).Rows(cCount & ":" & cCount)
        With sourceRange
            Set destrange = basebook.Worksheets(2).Cells(rnum, 1).Resize(.Rows.Count,
.Columns.Count)
        End With
        destrange.Value = sourceRange.Value
        rnum = rnum + 1
    End If
    cCount = cCount + 1
Loop

' create a new workbook with only July data
Set wb = NewWorkbook(1)

' now copy worksheet 2 to new workbook
basebook.Worksheets(2).Copy

Set wb = ActiveWorkbook

' paste the data into the second worksheet
wb.Worksheets(1).Paste

MsgBox "Extraction of July data is complete. Ensure new workbook is saved as a CSV file"

End Sub
```

Script 4: This script extracts July data from merged ENV CAN climate data files in csv format.

```
Sub format_wcompdata()

Dim wb As Workbook
Dim basebook As Workbook
Dim strLat, cValue As String
Dim lat, lon, wcomp As Single
Dim rCount, cCount, wkCount, wkCurr, idCount, rlon, clon As Long

Set basebook = ThisWorkbook

' first lat value is in row 3
cCount = 3

' last lat value is in row 31
rCount = 31

' first lon value is in col 2
clon = 2

' last lon value is in col 145
rlon = 145

' ERA-40 years are 1958 - 2002
' for years 1960 - 1969, wkCurr should be 3, wkCount should be 12

' current worksheet
wkCurr = 1

' number of worksheets
wkCount = 45

' loop for worksheets
```

```
Do While wkCurr <= wkCount

    ' create a new workbook with formatted data
    Set wb = NewWorkbook(1)

    idCount = 1

    ' add header info to new workbook
    wb.Worksheets(1).Range("A" & idCount).Value = "ID"
    wb.Worksheets(1).Range("B" & idCount).Value = "lat"
    wb.Worksheets(1).Range("C" & idCount).Value = "lon"
    wb.Worksheets(1).Range("D" & idCount).Value = "wcomp"

    clon = 2

    ' loop for lon values
    Do While clon <= rlon 'rlon

        ' get the first longitude value
        lon = basebook.Worksheets(wkCurr).Cells(1, clon).Value

        cCount = 3

        ' loop for lat values
        Do While cCount <= rCount

            ' get the latitude value (always in col A)
            cValue = "A" & cCount
            strLat = basebook.Worksheets(wkCurr).Range(cValue).Value
            lat = CSng(Mid(strLat, 1, 5))

            ' get the mean wind comp value
            wcomp = CSng(basebook.Worksheets(wkCurr).Cells(cCount, clon).Value)

            ' write values to first worksheet in new workbook
            ' idCount will keep track of rows

            wb.Worksheets(1).Range("A" & idCount + 1).Value = idCount
            wb.Worksheets(1).Range("B" & idCount + 1).Value = lat
            wb.Worksheets(1).Range("C" & idCount + 1).Value = lon
            wb.Worksheets(1).Range("D" & idCount + 1).Value = wcomp

            'MsgBox "ID: " & idCount & "   lat: " & lat & "   lon: " & lon & "  wcomp: "
& wcomp

            cCount = cCount + 1
            idCount = idCount + 1
        Loop
        clon = clon + 1
    Loop
    wkCurr = wkCurr + 1
Loop

MsgBox "Format of wind comp data is complete. Please save the new workbook as a CSV."

End Sub
```

H.3. SAS scripts to format tree-ring data

These scripts format the tree ring data, which allow the data to be imported into a database. First, ensure that all tree ring data is downloaded and contained in the proper directories. The files should be in text format and have a .crn extension. Then, edit treering_list.sas to change the directory names (if necessary). Finally, run treering_list.sas to create the list of tree ring files then run treering_mult_final.sas to output the data to the required format.

Script 1:

```
/*********************************************************
Filename: treering_list.sas
Author: Matthew Ladd, Laboratory for Paleoclimatology and Climatology
Last modified: March 22, 2007
Description: This program creates an output file with a list of the tree ring files
(.crn) in a directory
*********************************************************/

/* paths to the tree ring file directories - modify if necessary  */
FILENAME dirlist1 PIPE 'dir
L:\LPC_PCSN\DAVEA_STUFF\SLP_RECON\treeringcd\canada_chronologies /b' ;
FILENAME dirlist2 PIPE 'dir
L:\LPC_PCSN\DAVEA_STUFF\SLP_RECON\treeringcd\east_us_chronologies /b' ;
FILENAME dirlist3 PIPE 'dir
L:\LPC_PCSN\DAVEA_STUFF\SLP_RECON\treeringcd\europe_chronologies /b' ;
FILENAME dirlist4 PIPE 'dir
L:\LPC_PCSN\DAVEA_STUFF\SLP_RECON\treeringcd\world_chronologies /b' ;
FILENAME dirlist5 PIPE 'dir
L:\LPC_PCSN\DAVEA_STUFF\SLP_RECON\treeringcd\west_us_chronologies /b' ;

DATA dirlist1 ;

       /* length of each file no longer than 256 chars */
       LENGTH filename $256 ;

       /* should match filename where dir lists were piped to above */
    INFILE dirlist1 LENGTH=reclen ;

    INPUT filename $varying256. reclen ; /* record length can vary */

       /* output file path - modify if necessary */
       FILE "C:\MattL\filelist_can.txt";

       /* make sure only .CRN files are included in file list */
       ind = INDEX(filename,'.CRN');
       IF (ind > 0) THEN DO;
               PUT 'L:\LPC_PCSN\DAVEA_STUFF\SLP_RECON\treeringcd\canada_chronologies\'
filename ;
       END;

RUN ;

DATA dirlist2 ;
       /* length of each file no longer than 256 chars */
       LENGTH filename $256 ;
       /* should match filename where dir lists were piped to above */
```

```
    INFILE dirlist2 LENGTH=reclen ;
    INPUT filename $varying256. reclen ; /* record length can vary */
        /* output file path - modify if necessary */
        FILE "C:\MattL\filelist_eastus.txt" MOD;
        /* make sure only .CRN files are included in file list */
        ind = INDEX(filename,'.CRN');
        IF (ind > 0) THEN DO;
                PUT 'L:\LPC_PCSN\DAVEA_STUFF\SLP_RECON\treeringcd\east_us_chronologies\'
filename ;      END;
RUN ;

DATA dirlist3 ;

        /* length of each file no longer than 256 chars */
        LENGTH filename $256 ;

        /* should match filename where dir lists were piped to above */
    INFILE dirlist3 LENGTH=reclen ;

    INPUT filename $varying256. reclen ; /* record length can vary */

        /* output file path - modify if necessary */
        FILE "C:\MattL\filelist_eur.txt" MOD;

        /* make sure only .CRN files are included in file list */
        ind = INDEX(filename,'.CRN');
        IF (ind > 0) THEN DO;
                PUT 'L:\LPC_PCSN\DAVEA_STUFF\SLP_RECON\treeringcd\europe_chronologies\'
filename ;
        END;

RUN ;

DATA dirlist4 ;

        /* length of each file no longer than 256 chars */
        LENGTH filename $256 ;

        /* should match filename where dir lists were piped to above */
    INFILE dirlist4 LENGTH=reclen ;

    INPUT filename $varying256. reclen ; /* record length can vary */

        /* output file path - modify if necessary */
        FILE "C:\MattL\filelist_world.txt" MOD;

        /* make sure only .CRN files are included in file list */
        ind = INDEX(filename,'.CRN');
        IF (ind > 0) THEN DO;
                PUT 'L:\LPC_PCSN\DAVEA_STUFF\SLP_RECON\treeringcd\world_chronologies\'
filename ;
        END;

RUN ;

DATA dirlist5 ;

        /* length of each file no longer than 256 chars */
        LENGTH filename $256 ;

        /* should match filename where dir lists were piped to above */
    INFILE dirlist5 LENGTH=reclen ;

    INPUT filename $varying256. reclen ; /* record length can vary */

        /* output file path - modify if necessary */
        FILE "C:\MattL\filelist_westus.txt" MOD;

        /* make sure only .CRN files are included in file list */
        ind = INDEX(filename,'.CRN');
        IF (ind > 0) THEN DO;
```

```
               PUT 'L:\LPC_PCSN\DAVEA_STUFF\SLP_RECON\treeringcd\west_us_chronologies\'
filename ;
       END;

RUN ;
```

Script 2:

```
/*********************************************************************
Filename: treering_mult_final.sas

Author: Matthew Ladd, Laboratory for Paleoclimatology and Climatology

Last modified: April 2, 2007

Description: This program reads in .crn files and creates a properly formatted csv file
with al .crn files.

To ensure that all files are read properly make sure that outfile is either not too big
or split into 2 files.

Note: It is neccessary to run this script on each chronology file (e.g. -
filelist_can.txt, filelist_eur.txt,

filelist_world.txt, filelist_eastus.txt, filelist_westus.txt, etc.

*********************************************************************/

/* then we need to read in and display the site location, tree species, elevation,
latitude, longitude, and start/end years */

DATA tr_data ;
/* starting a new file so line count must be reset */
count = 1 ;
/* need to retain idcount on each iteration of the DATA step */
RETAIN idcount 0 ;
/* this is the file we are reading from - generated by running treering_list.sas */

INFILE "C:\MattL\SAS_treering\filelists\filelist_world.txt" LENGTH=reclen ;


/* this is the file we are generating - can change the path and filename if necessary */

FILE "C:\MattL\SAS_treering\treering_world.txt" ;



/* first we need to read in and display the site name */

IF (idcount = 0) THEN DO ;

       PUT
'ID,SiteName,Location,Species,Elevation,Latitude,Longitude,Year,GrowthRate,Samples' ;

END ;


/* Ensure fully qualified path will fit in FIL2READ */

LENGTH fil2read $300 ;


/* Input path of file to be read from outfile.txt */

/* INPUT fil2read $varying256. reclen ; record length can vary */

INPUT fil2read ;
```

```
/* set up a dummy infile since each file path is being read from filevar */

INFILE dummy FILEVAR=fil2read END=done TRUNCOVER;


/* for testing - will output the filename (with path) */

/*PUT fil2read ;*/


idcount = idcount + 1 ;



/* this is the file we are appending to - can change the path and filename if necessary
*/

/*FILE "C:\MattL\treering.txt" MOD;*/


/* need to check the line counts since lines 1-3 have a different format that lines 4 and
beyond */

DO WHILE(not done) ;

   IF count = 1 THEN DO ;

      /* Input statement for files to be read */

         INPUT siteName $ 10-61 ;

         /*PUT "Site Name: " siteName; */

         count = count + 1 ;

   END ;

   IF count = 2 THEN DO ;

      /* Input statement for files to be read */

         INPUT siteLoc $ 10-20  treeSpecies $ 23-40  elevation $ 43-46 latitude 47-51
longitude 53-58 startYear 68-71 endYear 73-76 ;



         /* lat/lon is in the following format: e.g 5113 rep 51.13 and 7805 rep 78.05 or
sometimes 78043 rep 78.043*/

         /* NOTE: only 2 sig figs are needed for lat/lon values */


         IF latitude >= 1000 THEN DO ;

         latitude = latitude / 100 ;

         END ;



         IF longitude >= 1000 THEN DO ;

            longitude = longitude / 100 ;

         END ;

         IF latitude <= -1000 THEN DO ;
         latitude = latitude / 100 ;
         END ;
```

```
         IF longitude <= -1000 THEN DO ;
            longitude = longitude / 100 ;
         END ;

         /* fix lat & lon values that are incorrect */

         IF latitude >= 90 THEN DO ;
            latitude = latitude / 10 ;
         END ;

         IF longitude >= 180 THEN DO ;
            longitude = longitude / 10 ;
         END ;

         IF latitude <= -90 THEN DO ;
            latitude = latitude / 10 ;
         END ;

         IF longitude <= -180 THEN DO ;
            longitude = longitude / 10 ;
         END ;


         /* --- for testing --- */

         /*PUT "Site location: " siteLoc ;

      PUT "Tree Species: " treeSpecies ;

         PUT "Elevation: " elevation ;

         PUT "Latitude: " latitude "Longitude: " longitude ;

         PUT "Record Length: " startYear " - " endYear ;*/

         count = count + 2 ;

   END ;

   IF count >= 4 THEN DO ;

      /* Input statement for files to be read */

         INPUT yrDecade 7-10 yr0growth 11-14 yr1samp 16-17 yr1growth 18-21 yr2samp 23-24
yr2growth 25-28 yr3samp 30-31 yr3growth 32-35 yr4samp 37-38 yr4growth 39-42 yr5samp 44-45
yr5growth 46-49 yr6samp 51-52 yr6growth 53-56 yr7samp 58-59 yr7growth 60-63 yr8samp 65-66
yr8growth 67-70 yr9samp 72-73 yr9growth 74-77 ;


         /* ensure that last line is not read in since it is simply chronology statistics
- No years older than 1000 AD*/

         IF yrDecade >= 1000 THEN DO;

            /* start with first year in decade (e.g. - 1930) */

            /* quotes are required for siteName field since some values for the field
contain commas */

               PUT  idcount ',' '"'siteName'"' ',' siteLoc ',' treeSpecies ',' elevation
',' latitude ',' longitude ',' yrDecade ',' yr0growth ',' ' ' ;

               /* this is the next year (e.g. - 1931) */

               yrDecade = yrDecade + 1 ;

               PUT idcount ',' '"'siteName'"' ',' siteLoc ',' treeSpecies ',' elevation
',' latitude ',' longitude ',' yrDecade ',' yr1growth ',' yr1samp ;

               yrDecade = yrDecade + 1 ;
```

```
                PUT idcount ',' '"'siteName'"' ',' siteLoc ',' treeSpecies ',' elevation
',' latitude ',' longitude ',' yrDecade ',' yr2growth ',' yr2samp ;

                yrDecade = yrDecade + 1 ;

                PUT idcount ',' '"'siteName'"' ',' siteLoc ',' treeSpecies ',' elevation
',' latitude ',' longitude ',' yrDecade ',' yr3growth ',' yr3samp ;

                yrDecade = yrDecade + 1 ;

                PUT idcount ',' '"'siteName'"' ',' siteLoc ',' treeSpecies ',' elevation
',' latitude ',' longitude ',' yrDecade ',' yr4growth ',' yr4samp ;

                yrDecade = yrDecade + 1 ;

                PUT idcount ',' '"'siteName'"' ',' siteLoc ',' treeSpecies ',' elevation
',' latitude ',' longitude ',' yrDecade ',' yr5growth ',' yr5samp ;

                yrDecade = yrDecade + 1 ;

                PUT idcount ',' '"'siteName'"' ',' siteLoc ',' treeSpecies ',' elevation
',' latitude ',' longitude ',' yrDecade ',' yr6growth ',' yr6samp ;

                yrDecade = yrDecade + 1 ;

                PUT idcount ',' '"'siteName'"' ',' siteLoc ',' treeSpecies ',' elevation
',' latitude ',' longitude ',' yrDecade ',' yr7growth ',' yr7samp ;

                yrDecade = yrDecade + 1 ;

                PUT idcount ',' '"'siteName'"' ',' siteLoc ',' treeSpecies ',' elevation
',' latitude ',' longitude ',' yrDecade ',' yr8growth ',' yr8samp ;

                yrDecade = yrDecade + 1 ;

                PUT idcount ',' '"'siteName'"' ',' siteLoc ',' treeSpecies ',' elevation
',' latitude ',' longitude ',' yrDecade ',' yr9growth ',' yr9samp ;

                yrDecade = yrDecade + 1 ;

         END ;

   END ;

END ;


/* for a blank line in between site records uncomment the next line */

/* PUT " "; */


RUN ;

/* output results to log window */

PROC PRINT DATA = tr_data ;

RUN ;
```

H.3.1. Sample output from script 2: treering_mult_final.sas

```
ID,SiteName,Location,Species,Elevation,Latitude,Longitude,Year,GrowthRate,Samples
1 ,"FORT CHIMO  (MERGED) ",CANADA ,TAMARCK ,46M ,58.22 ,68.23 ,1650 ,1315 ,
1 ,"FORT CHIMO  (MERGED) ",CANADA ,TAMARCK ,46M ,58.22 ,68.23 ,1651 ,1177 ,8
1 ,"FORT CHIMO  (MERGED) ",CANADA ,TAMARCK ,46M ,58.22 ,68.23 ,1652 ,1030 ,8
1 ,"FORT CHIMO  (MERGED) ",CANADA ,TAMARCK ,46M ,58.22 ,68.23 ,1653 ,1103 ,8
1 ,"FORT CHIMO  (MERGED) ",CANADA ,TAMARCK ,46M ,58.22 ,68.23 ,1654 ,1252 ,8
1 ,"FORT CHIMO  (MERGED) ",CANADA ,TAMARCK ,46M ,58.22 ,68.23 ,1655 ,1641 ,8
1 ,"FORT CHIMO  (MERGED) ",CANADA ,TAMARCK ,46M ,58.22 ,68.23 ,1656 ,1744 ,8
1 ,"FORT CHIMO  (MERGED) ",CANADA ,TAMARCK ,46M ,58.22 ,68.23 ,1657 ,1288 ,9
1 ,"FORT CHIMO  (MERGED) ",CANADA ,TAMARCK ,46M ,58.22 ,68.23 ,1658 ,913 ,10
1 ,"FORT CHIMO  (MERGED) ",CANADA ,TAMARCK ,46M ,58.22 ,68.23 ,1659 ,1765 ,11
1 ,"FORT CHIMO  (MERGED) ",CANADA ,TAMARCK ,46M ,58.22 ,68.23 ,1660 ,1559 ,
```

H.4. Software and additional scripts used

(1) The Visual Climate Data Analysis and Tools (VCDAT) is part of the Program for Climate Model Diagnostics and Intercomparison (PCMDI) available from http://badc.nerc.ac.uk/help/software/cdat/

(2) NOAA GRIB decoder converts GRIB data to CSV, NetCDF, Shapefile, or Raster and is available from http://www.nws.noaa.gov/mdl/NDFD_GRIB2Decoder/

(3) GRADS (Grid Analysis and Display System including gribmap) available from http://www.iges.org/GRADS

(4) NCL (National Center For Atmospheric Research [NCAR] command language) and NCAR graphics available from http://www.ncl.ucar.edu/index.shtml

(5) Climate data operators (CDO) available from http://www.mpimet.mpg.de/fileadmin/software/cdo/

(6) Xconv available from http://badc.nerc.ac.uk/help/software/xconv/

(7) Unidata integrated data viewer (IDV) available from http://www.unidata.ucar.edu/software/idv/

(8) NOAA grib2ctl available from http://www.cpc.ncep.noaa.gov/products/wesley/grib2ctl.html

(9) Hawth's Analysis Tools for ArcGIS available from http://www.spatialecology.com/htools/tooldesc.php

(10) Wind Speed Tools Toolbox (for ESRI ArcGIS 9.2) available from http://support.esri.com/index.cfm?fa=downloads.geoprocessing.filteredGateway&GPID=19

Appendix I – Additional methods for climate data analysis

I.1. Creation of July mean temperature anomaly maps using ERA-40 reanalysis

The purpose of this method is to examine the mean July temperature trends for the reanalysis period. After the data is acquired from the ECMWF data server at http://data.ecmwf.int/data/d/era40_daily/ the first step is to select the years from the ERA-40 July 1958-2002 2m temperature file. The next step is to run a monthly mean calculation on each file using CDO (or use ArcGIS). Each monthly mean file can be opened using Xconv. The data is then copied to an Excel workbook with each year on a separate worksheet. A formula is set up on the 46th worksheet to calculate the long term mean from the data on all 45 worksheets. A custom excel macro converts the temperature values from K to C and reformats the data so that it can be x-y mapped in ArcGIS. The output format is lat, lon, and mean July temperature value at that gridpoint for 1958, 1959,…2002, LT mean July temperature (1958-2002), and then the temperature anomaly value for 1958, 1959,…2002 (using a formula). The anomaly data is then interpolated using Kriging to create the difference surface then the anomaly maps are reclassified with a custom colour ramp. A screenshot of the Excel spreadsheet showing data for June 2002 is shown in Appendix G.

I.2. Creation of July mean wind direction anomaly contour maps using NCEP/NCAR reanalysis in ArcGIS

The first step was to download the U (zonal) and V (meridional) wind component data (July monthly means for each year of the reanalysis) from the NCEP/NCAR reanalysis page at http://www.cdc.noaa.gov/cdc/reanalysis/reanalysis.shtml. The U and V wind component files for July of a given year were merged using XConv software (Appendix H). The files can also be merged using CDO software (Appendix H - Linux only).

Start ESRI ArcGIS 9.2 software with a new blank map and make sure the list of toolboxes is visible. Under Multidimension Tools open the ‘Make NetCDF feature layer’ tool.

For input NetCDF file select the NCEP July monthly mean file with the merged wind components. Start with the long term monthly mean file then do each year individually. Select the appropriate variables and choose lon for x-var and lat for y-var. Select an output feature layer and for row dimensions, choose lat and lon. The other fields can be left with the default values.

The next step is to use the Windspeed Tools (figure below), an extension for ArcGIS 9.2 (Appendix H) to create a feature class with the wind direction in compass degrees. The function used is ‘UV to Speed Direction’ and the input shapefile will be each of the files created in the previous step. Select the variables U and V for the U and V fields and select an output feature class. The script should take less than a minute to run.

The next step is to interpolate each point shapefile to a raster. This can be done using the Geostatistical Wizard (use kriging) or the ‘interpolate to raster’ function (on the Spatial Analyst toolbar) in ArcGIS. This is repeated for July of each year in the reanalysis.

The final step is to subtract the July long term mean wind direction raster from the July mean wind direction of each year in order to produce the wind direction anomaly raster. Sample plots are shown in Appendix C.

I.3. Creating a July long term mean temperature map using North American Regional Reanalysis (NARR)

The first step is to acquire the data from the NARR website at http://www.cdc.noaa.gov/cdc/data.narr.html. The data can also be acquired using the script developed by the author (for a Linux system only) in Appendix H. The sample file is the long term mean (1979 to 2003) for July 2m (surface) temperature. NARR has a resolution of 32 km (0.3 deg) and is based on the ETA numerical weather prediction model.

Start ESRI ArcGIS 9.2 software with a new blank map and make sure the list of toolboxes is visible. Under multidimension tools open the ‘Make NetCDF raster layer’ tool. Only use the ‘Make NetCDF feature layer’ tool if you need a table of values for the data.

The parameters for the tool are as follows:

The variable selected was “air” (2m air temperature).
For x dim, select “x”. For y dim, select “y”.

NOTE: Do not select “lon” for x dim or “lat” for y dim. Initially, this seems logical however, a “Make NetCDF Raster Layer” error will result with the following information: “One or both dimensions have variable spacing in their coordinate values.”

The sample map (figure I1) is the July long term mean in raster format. Table I1 below clearly shows the grid spacing between points varies.

Table I1. Data values for NARR July LT mean 2m temperature file.

FID_	x	y	air	lat	lon
	1	1	298.87600000000	1.00000000000	-145.50000000000
	2	1	298.86500000000	1.10431000000	-145.31500000000
	3	1	298.86500000000	1.20829000000	-145.13000000000
	4	1	298.84600000000	1.31196000000	-144.94300000000
	5	1	298.84600000000	1.41530000000	-144.75700000000
	6	1	298.82300000000	1.51831000000	-144.57000000000
	7	1	298.81200000000	1.62099000000	-144.38200000000
	8	1	298.80400000000	1.72333000000	-144.19400000000
	9	1	298.80000000000	1.82534000000	-144.00600000000
	10	1	298.79600000000	1.92700000000	-143.81700000000
	11	1	298.79300000000	2.02831000000	-143.62700000000
	12	1	298.78500000000	2.12927000000	-143.43700000000
	13	1	298.77700000000	2.22988000000	-143.24600000000
	14	1	298.77000000000	2.33013000000	-143.05500000000
	15	1	298.76200000000	2.43001000000	-142.86300000000
	16	1	298.75100000000	2.52953000000	-142.67100000000
	17	1	298.75100000000	2.62868000000	-142.47900000000
	18	1	298.73600000000	2.72746000000	-142.28500000000
	19	1	298.72000000000	2.82586000000	-142.09200000000

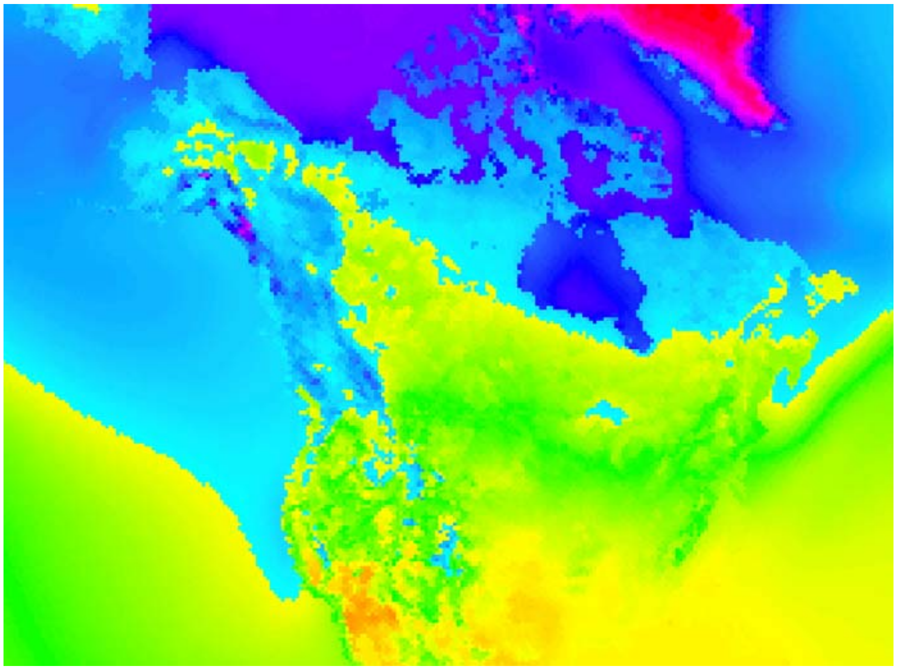

Figure I1. July mean temperature map for 1979 to 2003 using NARR.

I.4. Preparation of National Climatic Data Center (NCDC) data

The climate station data was acquired for Canada, USA, and Mexico. The station details are contained in separate file. This file was joined to each of the large station data files using a SAS script. Data for a specific month such as July could be extracted using a SAS script similar to the one used for Environment Canada data.

I.5. Read GRIB data into GRADS

For this study, it was necessary to load wind component data into GRADS. This requires a basic method to display a GRIB file (either .grib or .grb) in GRADS. It requires creating a control file that describes the grib file and then associating the control file with the grib file. It may be necessary to create a control file if the original control file has errors. If a large number of control files are to be created, then several Unix scripts should be used as shown in Appendix A. It should be noted that not all programs require a control file to open a grib file. One example is the Integrated Data Viewer (IDV) by Unidata.

1. Download GRADS and install it (see references for links). Download the wgrib program and compile it using cc wgrib.c command. Ensure the wgrib program (included with GRADS) is in your unix/linux path. For example, in the c shell (csh), the command would be set path=(/usr/local/bin $path) assuming that wgrib program is located in the /usr/local/bin directory.

2. Download grib data files from a climate data website (see references for links)

3. Download grib2ctl.pl program and place in an easy to locate directory. Ensure that the script is executable. The grib2ctl program creates a control file (.ctl) based on a grib file.

4. Run grib2ctl.pl on selected grib file to create a ctl file. The command is grib2ctl.pl tempsfc.grib -> tempsfc.ctl where tempsfc.grib is the input file and tempsfc.ctl is the output file.

5. Run gribmap or gribscan to create an index file (.idx) that associates the ctl file with the grib file. The command is gribmap -v -i tempsfc.ctl where tempsfc is the file to be processed.

6. If there were no errors, you should be able to open the ctl file in GRADS and view the data for any of the variables. If there are errors (e.g. - undefined parameter table), it is possible that GRADS will not be able to read the grib file because of the errors in the control file. If this is the case, try reading the grib file into another program such as NCL, VCDAT, or IDV (see programs sections).

I.6. Read GRIB data into ArcGIS with the use of Grib decoder

1. Start the program Tkdegrib (a grib file decoder), locate the directory with the Browse button select the grib file to view by double clicking it.

2. Select the variable, level, and time period desired. For example, choose Geopotential height for variable (Long name), 500 mb for level and January 2001 for time period (Ref Date). The reference date is given in the format MM/DD/YYYY thus the date selected in this case would be 01/01/2001.

3. Ensure the output location for the file is set properly by clicking the recommend button or manually entering a location.

4. For "Choose File Type" select SHP. Ensure that "Point" and "Verbose .shp file" options are selected.

5. Click the "Generate .shp file" button and a message should appear indicating the process is done.

6. Start ArcGIS and click the add data button. Locate the shape file and click OK. You may want to add a background map and set the projection of the data frame first.

7. Now adjust the symbology so there is a legend with different classes and an appropriate color ramp. For example with geopotential heights there are standard classes such as 5280, 5340, 5400, etc. The colour ramp should go from warm to cool colours with progressively lower heights. This is done by editing the layer properties. The symbology tab is selected where categories can be generated and the colour ramp changed.

8. There are many other possibilities for customization such as making the world map slightly transparent, adding topography, locations, etc.

It should be noted that NetCDF data can be read directly into ArcGIS 9.2 using the NetCDF to Raster tool.